АСТРОНОМИЧЕСКИЙ
ЖУРНАЛ

SOVIET ASTRONOMY

AJ

VOLUME 1 NUMBER 6

A Translation
of the
Astronomical Journal
of the
Academy of Sciences of the USSR

(RUSSIAN ORIGINAL VOL. 34, NO. 6)

Published by the
AMERICAN INSTITUTE OF PHYSICS
INCORPORATED

SOVIET ASTRONOMY

AJ

A translation of the "Astronomical Journal" of the Academy of Sciences of the USSR

A publication of the
AMERICAN INSTITUTE OF PHYSICS

Governing Board

FREDERICK SEITZ, *Chairman*

Members

WALTER S. BAIRD
JESSE W. BEAMS
RAYMOND T. BIRGE
R. H. BOLT
J. W. BUCHTA
J. H. DILLON
VERNET E. EATON
HERBERT A. ERF
IRVINE C. GARDNER
S. A. GOUDSMIT
C. KITTEL
WINSTON E. KOCK
R. BRUCE LINDSAY
WALTER C. MICHELS
G. E. PAKE
R. RONALD PALMER
JOSEPH B. PLATT
RALPH A. SAWYER
H. D. SMYTH
JOHN STRONG
GEORGE E. UHLENBECK

Officers and Staff

ELMER HUTCHISSON
Director
HENRY A. BARTON
Associate Director
WALLACE WATERFALL
Secretary and Treasurer
EDWARD P. TOBER
Mgr., Production and Distribution
THEODORE VORBURGER
Advertising Manager
RUTH F. BRYANS
Publication Manager
KATHRYN SETZE
Assistant Treasurer
ALICE MASTROPIETRO
Circulation Manager
EUGENE H. KONE
Director of Public Relations
WILLIAM C. KELLY
Director of Education Projects

American Institute of Physics Advisory Board of Russian Translations

ROBERT T. BEYER, *Chairman*

FREEMAN DYSON, DWIGHT GRAY, MORTON HAMMERMESH,
DAVID HARKER, VLADIMIR ROJANSKY, HAROLD F. WEAVER

Advisory Editor, Soviet Astronomy—AJ: HAROLD F. WEAVER,
Leuschner Observatory, University of California, Berkley 4, California

"Soviet Astronomy—AJ" is published by the American Institute of Physics, with the cooperation of the American Astronomical Society, for the purpose of making available in English reports of current Soviet research in astronomy as contained in the "Astronomical Journal" of the Academy of Sciences of the USSR. The translation begins with the 1957 issues.

Transliteration of the names of Russian authors follows the system employed by the Library of Congress.

This translating and publishing project was undertaken by the Institute in the conviction that dissemination of the results of research everywhere in the world is invaluable to the advancement of science. The National Science Foundation of the United States encouraged the project initially and is supporting it in large part by a grant. Translation and printing are being handled by Consultants Bureau, Inc.

The American Institute of Physics and its translators propose to translate faithfully all of the scientific material in the "Astronomical Journal" of the Academy of Sciences of the USSR appearing after January 1, 1957. The views expressed in the translated material, therefore, are intended to be those expressed by the original authors, and not those of the translators nor of the American Institute of Physics.

One volume is published annually. Volume 1 will contain all of the scientific material published in the original Russian Volume 34 for 1957.

Subscription Prices:

Per year (6 issues), starting with Vol. 1, No. 1

General:	*United States and Canada*	*$25.00*
	Elsewhere	*27.00*
Libraries of non-profit academic institutions:		
	United States and Canada	*10.00*
	Elsewhere	*12.00*
Back numbers, all issues		5.00

Subscriptions should be addressed to the American Institute of Physics, 335 East 45th Street, New York 17, New York.

Copyright American Institute of Physics Incorporated, 1959

SOVIET ASTRONOMY

AJ

VOLUME 1, NUMBER 6 NOVEMBER-DECEMBER 1957

ON THE PRINCIPLES OF STATISTICAL MECHANICS OF STELLAR SYSTEMS

K. F. Ogorodnikov

Reasons are given in favor of the possibility of developing a statistical mechanics of extragalactic stellar systems. Two principal difficulties met with in modern stellar dynamics are considered. 1) The problem of the relaxation time-scale. This problem is connected with the problem of the origin of the Schwarzschild ellipsoidal law of velocity distribution. There exist no known statistical mechanisms of smoothing out stellar velocities, necessary to make them agree with any statistical distribution law. It is pointed out that the true time of relaxation in the galaxies must be much shorter than its classical value 10^{13}-10^{14} years, deduced from the theory of stellar-stellar encounters. As a matter of fact it must be of the order of 10^7-10^{10} years, i.e., comparable with the periods of their rotation. The uniform rotation of galaxies of all types (in the case of S-galaxies in their inner parts) may be regarded as an indication in favor of the short relaxation time-scale. Theoretically, the short relaxation time-scale is obtained if it is assumed that at least 10 per cent of matter within the galaxies is accumulated into condensations of 10^5-10^6 solar masses on the average. 2) The question of the possibility of assigning any definite outer boundary to stellar systems is another major problem of modern stellar dynamics. It is obviously connected with the well-known paradox of the infinite mass usually obtained for steady stellar systems. As a counterpart it is shown that the phase (velocity-coordinate) distribution function can be defined only when a suitable elementary-macroscopic volume (EMV) around the point of space considered can be constructed. The EMV's are well-known in physics, EMV being a volume which is sufficiently small in order to represent local properties of the stellar medium and at the same time sufficiently large to contain within it a very large number of stars. In any stellar system this can be realized within its inner and denser part, which we may call the main body. The main body coincides approximately with the bar in the case of SB spirals, with the visible contours in the case of E-galaxies and with the confines of uninterrupted spiral arms in the case of S spirals. The main

body is the bearer of the structural features of any particular galaxy. Only within it is the Boltzmann equation valid, as well as all theorems deduced from it.

All that lies outside the main body of the galaxy consitutes its corona. The corona surrounds the main body of the galaxy as a kind of diffuse stellar cloud, the equidensity surfaces of which are in most cases concentric ellipsoids (e.g., the well-known photograph taken by Baade of NGC 4594 in three colors). The corona exerts practically no gravitational action on the main body and plays a role very similar to that of the walls of the container in the theory of gases. Indeed the corona ensures that in the place of a star that has just escaped from the main body there will appear another star, which will fly from the corona into the main body with a velocity which is exactly necessary for maintaining a steady phase distribution. The only difference is that while the walls send back the same star, the corona sends back another one.

In a subsequent paper the above principles will be applied to the dynamics of some types of galaxies.

1. Introduction

In the last 30-40 years, considerable progress has been made in the dynamics of stellar systems. Through the development of the theory of galactic rotation, the introduction of Schwarzschild's law, and the use of the Boltzmann equation, Jeans, Eddington, Oort, Lindblad, Charlier, Chandrasekhar, Ambartsumian, and others were able to formulate the bases of the modern theory of stellar systems. At the present time, however, it must be admitted that in the further development of the theory we encounter a number of fundamental difficulties which lead some authors to deny completely the possibility of applying the methods of statistical mechanics to stellar systems (for example, see references [1], [2]).

This is not the point, however, as it must be realized that the methods of statistical mechanics developed to describe events on a laboratory scale are not applicable, of course, to objects on a cosmical scale without the appropriate generalizations and some changes. The author's opinion is that the methods of statistical mechanics are so powerful that, with a suitable alteration, they can be applied to any system of interacting similar particles. In particular, they can also be applied to the types of stellar systems observed by us.

The present work is a further development of some ideas which were first proposed by the author in 1948 [3]. Galaxies of the type S, SB and E are considered first of all.

We will here consider two problems: 1) the problem of relaxation time, and 2) the problem of the dynamical boundaries of stellar systems. Both of these problems lead to the occurrence of the fundamental difficulties in the stellar-system dynamics which we have mentioned at the beginning.

The calculated magnitude of the relaxation time, which is of the order of 10^{13}-10^{14} years, for all practical purposes is infinitely large. Therefore, at the present time it is considered that the stars in a galaxy describe regular orbits for an indefinitely long period of time under the influence of the regular force of attraction of the stellar system as a whole.

Using this approach, B. Lindblad and S. Chandrasekhar [4] were able to describe the formation of small and thin branches in some types of galaxies with a large and massive central nucleus (of the type of M81). However, it is perfectly clear that this method will never lead to a theory which can describe the structural features of galaxies in general, particularly if we consider the large variety in their shapes.* Let us recall that in the Lindblad-Chandrasekhar theory of instability of circular orbits, leading to the motion of stars along spiral orbits, arises only outside the main body of the galaxy. It is even more hopeless to attempt a solution of the problem of galactic evolution by the method of regular orbits, in particular, the problem of the evolutionary transitions of galaxies from one form into another.

---

* In connection with the publication of the Palomar Atlas of the sky in which there are thousands of photographs of galaxies, it becomes apparent how primitive were our ideas about the variety and typicalness of the forms of the galaxies, since our ideas were obtained in most cases from a study of several "classical" galaxies which, in the last thirty years, have passed through the pages of all the text books. The publication of a special atlas of galaxies has become necessary.

2. The Relaxation Time in Real Stellar Systems

The relaxation time for a stallar system is usually defined as the interval of time in which the mathematical expectation of the square of the velocity change becomes equal to the square of the mean velocity of a star:

$$T = \frac{v^2\bar{v}}{8\pi G^2 m^2 \nu \ln (R / P)}, \tag{1}$$

where v is the mean peculiar velocity of the stars, $\bar{v}$ the mean relative velocity of the stars when they approach each other, m the mean mass of the perturbing stars, ν the density of their distribution in space, G the gravitational constant, R the radius of the stellar system; and P is the "distance of approach", defined as the distance at which the irregular forces, arising as the result of an encounter, are of the same order of magnitude as the regular forces.

For the neighborhood of the sun, the calculated value of T is found to be 10^{13}-10^{14} years, i.e., five orders of magnitude greater than the period of rotation of the Galaxy. This value is considerably greater than any imaginable value for the age of both the stars and of the Galaxy as a whole and, therefore, this is usually accepted as showing that in our Galaxy star-star encounters and the resulting irregular forces for all practical purposes are not important. This idea became so customary that it was taken as a basic assumption in the later development of the dynamics of stellar systems, which can be called stellar dynamics without encounters.

However, if we examine the problem more closely we find that the assumption of the absence of irregular forces is highly questionable.

It is known that Schwarzschild's law of the ellipsoidal distribution of stellar velocities is an important part of modern stellar dynamics. Already in 1907, K. Schwarzschild himself showed that the law was in satisfactory agreement with observational data. The acceptance of the fact that Schwarzschild's law is strictly obeyed at all points of the Galaxy served as the basis for the classical investigations of Jeans, Eddington, Oort, Chandrasekhar and, at least to some extent, of Lindblad. The results obtained from this theory on the relation between the velocity-ellipsoid semiaxes and Oort's constants A and B (Lindblad's equation), and also the results on the relation between the circular velocity of the centroid and the distance from the center, are in satisfactory agreement with observations made on our Galaxy as well as on the other galaxies (in the case of the latter relation).

At the same time we do not know of any process which in stellar systems would lead to a distribution of peculiar velocities of the type of Schwarzschild's law.

This circumstance is the reason for the unusual situation in stellar dynamics, which we can call the paradox of Schwarzschild's law. Schwarzschild's law exists and leads to the formulation of stellar dynamics, but the way in which it was established is unknown.

We can doubt, of course, that Schwarzschild's law holds exactly at all points in a stellar system. We can see that it does not hold exactly simply from the fact that in stellar systems the velocity distribution is cut off as a result of the existence of a finite escape velocity. However, at the present time we do not have enough grounds for dismissing it as a valid approximation.

In what way does one or another form of the stellar-velocity distribution get established in a stellar system? To this question only two, fundamentally different, answers are possible. First, irregular forces are absent and the distribution of velocities reflects the law for the distributuion of regular-orbit elements which was established at the time of formation of the given stellar system; we can call this the "cosmogonical" law of velocities. Alternatively, there are random irregular forces acting in the stellar system which establish in a sufficiently short time (for example, comparable with the period of rotation of the given stellar system) the statistically most probable velocity distribution, at least within the densest inner region of the stellar system. In this case we can call the law of velocities "statistical."

Is it possible for us to make a choice between these two alternatives? Undoubtedly it is. We have already mentioned that from the theory of the regular stellar motions it is impossible to arrive at a theory of the equilibrium figures, i.e., the structure of stellar systems, as well as of their evolutionary changes.

However, the second (statistical) approach requires a short relaxation time. This is not supported by direct calculation. But, on the other hand, we have a number of observations which indicate indirectly that the relaxation time in galaxies is less than the period of their rotation.

First of all, we must consider the observed character of the rotation of galaxies which in practically all of the cases is rigid-body rotation, as we can easily show.

Rigid-body rotation by itself is quite convincing evidence of the presence of operative interaction forces between the individual particles — the stars — analogous to the presence of viscosity in physical media. In addition, it makes any theory that neglects the action of irregular forces even more unrealistic since it is very hard, if not impossible, to conceive of any cosmogonical process which secures for the regular orbits of all the stars the same angular velocity of rotation of their lines of apsides.

Let us first consider the nuclei of normal spirals. In all eight cases for which observational data exist: M31, NGC 4594, 4559, 3556, 3034, 7640, 6015 and 4244, there is rigid-body rotation within the limits of observational error.

In so far as the nuclei of the spiral galaxies are dynamically isolated systems, the question inevitably arises: what are the forces which initiate and then maintain this type of rotation? The only answer possible is that in these systems there must exist forces, analogous to the forces of internal friction, i.e., forces of the irregular type. To determine the nature of rotation of elliptical galaxies, at the present time we are forced to use the single example of the galaxy NGC 3115, of type E7; as the result of measurements made at Mt. Wilson Observatory rigid-body rotation was also found for the case of this galaxy.

We can determine the nature of the rotation of normal-spiral galaxies from two examples: M31 and M33, for which Babcock, Mayall and Aller have obtained the radial velocities at various distances from the center. In both cases there is agreement with the following equation which is derived theoretically from the Schwarzschild law:

$$v_c = \frac{k_1 R}{1 + k_2 R^2}, \tag{2}$$

where v_c is the circular velocity of the centroid and $\underline{R}$ the distance from the axis of rotation. However, within the observed boundaries of the galaxies which are determined by the condition

$$R < k_2^{-1/2}, \tag{3}$$

Equation (2) yields approximately

$$v_c \approx k_1 R,$$

i.e., once again a rigid-body rotation. Finally, we have to consider barred spirals. In this case, unfortunately, there are no spectroscopic measurements available from which we can determine the law of variation of velocity with distance from the axis. This is at least partially explained by the fact that when a galaxy is seen "edge-on" it is hard to classify it as belonging to a definite type. However, even without measurements it is obvious that if the barred spirals rotate at all, then their rotation must be of the rigid-body type, as otherwise their elongated body would be completely deformed after the first turn.

Thus, with the reservations noted above, all the galaxies exhibit rigid-body rotation. But, as we have seen, this means that in them there must exist a statistical mechanism for smoothing out the stellar velocities, analogous to internal friction or viscosity.

In addition to this evidence, we also have direct indications that even in our Galaxy the relaxation time is considerably shorter than its "classical" value, 10^{13} years. In one of my earlier papers, I showed, using the short-period cepheids as an example, that considering the number of stars of a given type which have velocities greater than the escape velocity (30 km/sec), the relaxation time cannot be longer than 10^9 years, i.e., at least four orders of magnitude smaller than the "classical" value [5].

Finally, from Equation (1) we see that the value of the relaxation time is strongly dependent on the mass of the perturbing bodies. To calculate this more accurately, let us assume for the time being that all the stars of the Galaxy form condensations of the type of stellar clusters. Let the average mass of each cluster be $M = n \cdot m$, where n is the average number of stars in a cluster. In doing this, instead of the stellar density ν in Equation (1) we have to use the density of the spatial distribution of stellar condensations which is clearly equal to ν / n. We will show that the other factors remain practically unchanged. In fact, the initial velocity of a star relative to the centroid (peculiar velocity) must remain unchanged, the mean velocity $\bar{v}$ of the perturbed star relative to the perturbing body will be decreased in the ratio $1 : \sqrt{2}$ if we assume that the peculiar velocities of the condensations are very small. Finally, the radius of approach p will be increased by the factor $\sqrt{n}$. If we neglect, in the first approximation, the changes in $\bar{v}$ and p, then relaxation time T_1 in the case of condensations will be given in terms of T by the relation:

$$\frac{T_1}{T} \approx \frac{1}{n}. \tag{4}$$

Taking $n = 10^5$, i.e., the average mass of the condensations to be of the same order of magnitude as that of the globular clusters, we obtain

$$T_1 \approx 10^8 \text{ years} \tag{5}$$

i.e., a value of the same order of magnitude as the period of rotation of the Galaxy. Even if, to be on the safe side, we consider that only a tenth of all the stars in the Galaxy belong to the condensations, we still obtain $T_1 \sim 10^9$ years, which is less than the time necessary, on the average, for a star to move through a distance equal to the diameter of the Galaxy with an average peculiar velocity of 20 km/sec. To this we can also add that we have completely neglected the possibility of the condensation of diffuse matter, which, as a rule, has a tufty structure. For further details, we refer the reader to another of our papers [5] where there are references to independent investigations of other authors who conclude that condensations of diffuse matter exist with masses from 10^2 to $10^6 m_\odot$.

3. Outer Boundaries of Stellar Systems.

The question of the outer boundaries of stellar systems arose after it was shown with the help of recording microphotometers that the blackening in photographs of galaxies extends considerably beyond their visible boundaries, gradually decreasing to zero at distances several times greater than the visible diameter.

On the other hand, the hydrodynamical theory of stellar systems based on the hypothesis of the universal applicability of Schwarzschild's law leads to an "isothermal" model of a stellar system (i.e, to a constant dispersion of the velocities parallel to the radius vector) and to a stellar density decreasing with distance as R^{-1} (R is the radius vector) [3], which results in an infinite radius and an infinite mass.

Thus in the last ten years, it has become widely accepted in stellar dynamics that the dimensions of stellar systems are indeterminate and, if models are considered, then an adequate model would be one in which the stellar density tends asymptotically to zero with increasing distance, i.e., a model with an infinite radius and a finite mass. Unfortunately, up to the present time all attempts to set up this model theoretically have failed.

Therefore, there is a fundamental contradication also in the problem of the external boundaries in stellar dynamics: observations indicate the absence of a definite boundary in stellar systems and, in effect, an infinite radius, but then the theory leads to an infinite mass, which is obviously without any physical meaning.

However, is it really so?

Firstly, that which we call the visible boundary of a galaxy must undoubtedly have a definite objective meaning, since the diameters are uniquely related to the integral visual magnitude of the galaxy, m_T, through the well-known Hubble relation (for example, see reference [4], p. 318):

$$m_T + 5 \log d = C,$$

and they can be used to determine the mean distances to the galaxies.

If we take a closer look at the photographs of galaxies (a good example is the well-known series of photographs in three colors of the galaxy NGC 4594), we see that the spherical component appears to be in the form of a halo in which the disc component, the main body of the galaxy, is embedded. Only the disc component possesses any structural features. The halo, on the other hand, is structureless. Therefore, if we speak of the structural differences between galaxies of various types, S, SB, or E, then we can only refer to the main body of the galaxy. In the case of spirals the main body will be the same as the disc component, in other cases with the mass enclosed by the visible boundaries of the galaxies.

In stellar dynamics the halo has a role analogous to that of the container walls in the theory of gases. In fact, in the theory of gases a molecule which hits the wall recoils with a velocity whose magnitude and direction is determined from the condition for maintaining a stationary phase distribution. But this is exactly the role played by the halo. In place of a star which leaves the main body and moves into the halo, another star moves back into the main body after describing in the region of the halo an appropriate segment of its Keppler orbit. If the phase distribution is stationary, then the exchange of stars between the main body and the halo will maintain it in exactly the same way as in the case of a wall. The only difference between the case of a gas and a stellar system is that in the former case the same molecule will move back after reaching the external boundary, while in the case of the stellar system in place of the escaping star another star will enter the main body from the opposite direction.

However, as we have seen above, the stars inside the main body are indistinguishable, in the sense that in the dynamics of stellar systems the only meaningful quantities are the distribution of phase trajectories and the distribution of stars among the trajectories. From the point of view of stellar dynamics, it does not matter which individual star is at any given moment in a specified trajectory. The stars also lose their identity because under the action of the irregular forces they keep jumping from one orbit to another.

It is also important to note that the level surfaces of stellar density in the halo are in the form of concentric ellipsoids (for example, see the well-known photographs of NGC 4594 taken by Baade in three colors), as the result of which the attraction of the halo at points inside the main body, generally small because of the small mass of the halo, becomes completely negligible.

We can therefore assume that the galaxies behave as if enclosed in a hard adiabatic envelope which can only be penetrated by stars whose velocities exceed the escape velocity.

We will show that from the point of view of stellar dynamics also, the mass of any stellar system can be naturally divided into two qualitatively different parts: the inner (dense) part, or the main body, and the halo (the external, rarefied part).

In fact, the basic equation in stellar dynamics is the Boltzmann equation:

$$\frac{Df}{Dt} = 0, \tag{6}$$

where D/ Dt is the Stokes derivative in the phase space of the coordinates and the velocities, and f if the phase density. As is known, if for any system the phase density satisfies Equation (6), then for the system, by simply averaging Equation (6), we can obtain the usual hydrodynamical equations, i.e., we can consider any such system as a continuous medium.

We will show that for only some of the stellar systems can the phase density be determined. To do this, the stellar system must obey certain conditions which depend on its dimensions (the scale of its structural shape) and the stellar density. For this purpose we will use the concept of an elementary macroscopic volume (or the ν-volume, as it was called in our 1948 paper [3]).

Let us consider an arbitrary stellar system containing a large number $N \gg 1$ of stars and occupying a sufficiently large volume of space V, which can also be infinitely large. Let us take an arbitrary point in space $X \subset V$ and surround it by an elementary macroscopic volume dX. By dX we will mean a volume which satisfies simultaneously two contradictory requirements:

1. Its dimensions must be small by comparison with the characteristic dimensions of the structural features of the galaxy in the neighborhood of the point X. If dX satisfies this condition, then inside this volume we can consider the stellar density $\nu(X)$ to be quasi-constant, while we can take the volume dX to determine the local

properties of the stellar system in the vicinity of the point X.

2. On the other hand, dX must be large enough so that the number of stars in it at any given time

$$dN = \nu(X)\,dX \tag{7}$$

must itself be large enough in order that we can determine the distribution function of the stellar velocities.

This procedure, for example, we can think of as follows: knowing the velocity components for each star, we can represent a star by a point in an arbitrary stationary coordinate system. Repeating this for each of the $dN \gg 1$ stars, we will construct a cloud of representative points. Taking an arbitrary point Y inside the volume occupied by the cluster (in this case its volume will obviously be finite), we again enclose it in a volume element dY, which in some respects will be similar to the elementary macroscopic volume dX mentioned above [Equation (7)], since dY must also characterize the local structural features of the cluster. However, there is a fundamental distinction between dX and dY, since the minimum dimensions of dY will only be determined by the necessity for smoothing out the inherent fluctuations in the velocity distribution.

Repeating for all points the reasoning given above, we obtain the distribution function for the velocities and the coordinates, i.e., the phase density.

We can estimate approximately the necessary number of stars dN in the volume dX from the following considerations. To determine the distribution function of one characteristic X, the number of determinations of the value of X necessary is, at least, of the order of a hundred. To obtain the distribution function of three characteristics (velocity components), n^3 observed values are necessary, which we can conservatively take to lie between 10^5 and 10^6.*

From this we can conclude that the Boltzmann equation and all the deductions following from it (including hydrodynamical equations) can be applied only to those stellar systems, or their internal regions, where at every point we can determine the elementary macroscopic volume.

Only with the help of the elementary macroscopic volume are we able to determine such "macroscopic" quantities as the velocity of the centroid, which is the analog of the hydrodynamical flow velocity, or the dispersion of peculiar velocities, which is the analog of the viscosity component of the stress tensor in a liquid.

To determine the velocity of the centroid at a given point X in space (irrespective of whether there is a particle, a star, at this point or not), we enclose it by a small volume and determine the mean value of the vector sum of the velocities of all stars whose centers lie inside the volume dX. Formally, to determine the mean velocity it is necessary to have only a small number of particles. However, in order that the centroid velocity obtained should actually represent a hydrodynamical velocity, it is necessary that it be independent of both the shape and the size of the volume dX. It is obvious that in stellar dynamics (as in any dynamics of rarefied media) it is meaningless to make dX contract to the point X, as is usually done in hydrodynamics, since the diameter of the volume dX must be large compared to the mean distance between the particles or stars.

If the number of stars contained in the volume dX is very large then, as its size and shape is changed, the mean value of the velocity will remain practically constant because of the law of stability of the mean value for an arbitrary selection from the given ensemble which, for example, can mean the ensemble of stars situated inside the sphere with center at the point X and whose radius is equal to the upper limit of the dimaters of all the volumes dX.

The same is obviously true for all the other macroscopic quantities (second-order moments of the peculiar velocities, etc.), independently of whether we take the masses of the stars to be equal or not. The introduction of a mass distribution for the stars is very unimportant and will only slightly modify our discussion; therefore, we will not consider this question here.

It is obvious that for any stellar system with a finite mass, the region in which the concept of an elementary macroscopic volume can be applied has a finite diameter. In the case when the density gradually decreases to zero, there must be a distance beyond which the determination of this volume becomes impossible. Outside this limit the phase density will also lose its meaning.

---

*For systems with spherically symmetrical distributions of velocities and coordinates (of the type of globular clusters) the conditions for determining the elementary macroscopic volume appear to be less strict because of the absence of appreciable structure. However, to be certain that a given system is indeed spherically symmetrical, it is necessary to obtain a six-dimensional phase distribution.

4. Summary

Thus, in any stellar system we can identify two qualitatively different parts: the inner part—the main body of the galaxy, where its structure is determined by the Boltzmann equation and where the stellar system can be considered to be continuous medium, and the outer part — the halo, where the stellar system can be considered to be essentially discrete. Within the boundary of the main body the separate orbits of the individual stars are practically of no importance, just as in a laboratory gas the trajectories of the individual molecules are not important. On the other hand, in the halo, the individual orbits of the stars are of primary importance and all the internal parameters of the halo (stellar density, velocity ellipsoid, etc) are determined by the distribution function of orbit elements of the individual stars. In general, the motion of stars in the halo will be determined by the gravitational field produced by the main body of the galaxy.

From what has been said above, it does not follow that the trajectories of the individual stars do not exist within the main body. This may be seen from the fact that in a stationary system any phase point uniquely determines an orbit. Therefore, the phase density uniquely determines the distribution of the orbits (of their elements). Because of stationarity (the phase density is independent of the time), the distribution of orbits remains unknown and, consequently, as the result of the action of the irregular forces, the stars can only jump from one orbit to another, while the number of stars in each orbit at each instant of time remains constant. Therefore, it is possible to investigate the individual orbits inside the main body. However, as we have pointed out above, this is insufficient for the solution of the principal problem in stellar dynamics: the finding of the theoretical equilibrium figures of stellar systems.

It is clear that the determination of a concrete boundary between the main body and the halo is associated with the well-known uncertainty. However, from the point of view of observation, there are no difficulties involved in determining the external boundaries of galaxies. As regards theory, its aim should therefore be the description of the shape and sizes of the galaxies of various types if their dynamical parameters are specified: mass, energy, moment of momentum, etc.

Thus, the development of a theory of galactic structure into two associated, but fundamentally different problems: the investigation of the internal structure of the galaxies (of the main bodies), where the main method of approach should be hydrodynamical, and the investigation of the structure of the halo, where the methods of the statistics of discrete ensembles should have the main role. The aim of the investigations of the internal structure is the development of a theory of the equilibrium figures and of the evolution of the central regions of the galaxies which are enclosed, in all probability, by what we have called the visible boundaries of the galaxies. The aim of the investigations of the halo is to determine the distribution of the individual stellar orbits. The common boundary between the main body and the halo, which we can call the effective surface of the galaxy, serves to connect the solutions of the two problems.

In this respect, the dynamics of galaxies is analogous to the theory of stellar structures which can be divided into a theory of internal structure and a theory of stellar atmospheres. In stars these regions are qualitatively different and therefore two different methods of investigation are required. In the dynamics of galaxies, as in stellar physics, it is incorrect to attempt an investigation by the one method of the structure in the whole region from the center to the outermost layers. Many of the fundamental difficulties which are now in the way of the development of the dynamics of stellar systems can be explained as arising from just the underestimation of the latter circumstance.

From the above it follows that in principle it is possible to apply the methods of statistical mechanics to the problems of stellar dynamics.

In conclusion, as an example, we will consider the problem of determining the elementary macroscopic volume in the vicinity of the sun in the Galaxy. As is known, the density of stars at the point at which the sun is situated is equal to 0.1 stars per ps^3. Therefore, a cube of side 100 ps will contain 10^5 stars and in this respect it would be suitable as the volume we are looking for. However, it is too large to characterize the local properties of the Galaxy, since in the direction of the z-coordinate the stellar density decreases according to the barometric law.

$$\nu(z) = \nu_0 e^{-z/\beta}, \tag{8}$$

in which $\beta = 380$ ps on the average. From this we conclude that at a distance of 100 ps from the galactic plane, the stellar density changes by 40%. Therefore, we can say that the point where the sun is situated, i.e., at a distance 7.2 kps (see reference [4], p. 286) from the center, the elementary macroscopic volume is already fairly difficult to determine. This is in good agreement, on the one hand, with the fact that the maximum of the circular velocity of the centroid of our Galaxy is at a distance of 6.5 kps from the center (see reference [4], p. 389), i.e., nearer to it than the sun. From this follows that the sun is situated outside the main body of the Galaxy, although close to its edge. On the other hand, this also agrees with the conclusion, obtained by V. A. Ambartsumian [6] from an analysis of the surface brightness of our Galaxy, that for an observer placed at a great distance outside the limits of our Galaxy the point where the sun is situated must be outside the visible boundary of the Galaxy.

Finally, one more remark on the application of the Boltzmann equation to the problems of dynamics of stellar systems. In the most general case, when in addition to the regular forces the irregular forces are also taken into account, this equation, as is well known, takes the form

$$\frac{Df}{Dt} = \left(\frac{\partial f}{\partial t}\right)_i, \tag{9}$$

which differs from the homogeneous equation (6) by the presence of the right-hand side, where $(\partial f/\partial t)_i$ denotes the rate of change of the phase density produced by the presence of irregular forces. It is usually neglected because in stellar systems these forces have a negligible effect on the phase density. Can we apply the homogeneous equation (6) also to the internal regions of galaxies if we use the converse hypothesis, i.e., if we consider that the action of irregular forces is very effective? Undoubtedly we can, if the phase distribution that has become established is the most probable one among all the possible distributions, since in this case the irregular forces will not only not disrupt the distribution, but will also tend to maintain it indefinitely.

Astronomical Observatory
Leningrad State University

Received April 6, 1957

LITERATURE CITED

[1] R. Kurth, Z. angew. Math. u. Phys. 6, 115 (1955).

[2] E. Finlay – Freundlich and R. Kurth, Naturwiss. 42, 7, 167 (1954).

[3] K. F. Ogorodnikov, Usp. Astron. Nauk 4, 3 (1948).

[4] P. P. Parenago, A Course of Stellar Astronomy [In Russian] (GITTL, Moscow, 1954), 3rd ed.

[5] K. F. Ogorodnikov, Peremennye Zvezdy 10, 3, 135 (1955).

[6] V. A. Ambartsumian, Doklady Akad. Nauk Armyan SSR 10, 4, 149 (1949).

PLANETARY RING NEBULAE

G. A. Gurzadian

It is shown that planetary nebulae are not isothermal throughout the whole volume of the gaseous sphere but consist of two parts – the central region, where the electron temperature depends on the temperature of the nucleus and is of the order of 30,000-60,000°, and an outer region which is cooler. The usually accepted value of the electron temperature of planetary nebulae, on the average equal to 10,000°K and independent of the temperature of the nucleus, is that of the temperature of this outer, cooler, and denser part of the nebula.

It is widely accepted that the planetary ring nebulae are not uniform gaseous spheres but have a rarefied region in the interior. Curtis, from a study of over forty photographs of planetary nebulae, estimates the thickness of their shells to be of the order 0.1-0.5 of the external radius of the nebula [1]. Since it is very improbable that the internal region of the nebula is completely empty, we have there a medium whose density is to some degree less than the density of the shell itself. Because of projection, the nebula can sometimes appear as a ring, if the difference of the densities in the two regions is sufficiently large. In this case we will have a ring nebula.

On the other hand, as we will see below, the existence of planetary ring nebulae, i.e., formations with a rarefied inner region, is incompatible with the fact of their comparatively slow expansion, as well as with the assumption that they are isothermal throughout the whole of their volume.

For the investigation that follows it is necessary to estimate in some way the degree of rarefaction of the central regions of these nebulae, i.e., the relative density of matter in them. This can be made fairly simply and it is sufficient to have observational data on the ratio of the radii of the external and internal boundaries of the visible "ring," as well as the ratio of the surface brightness at the center of the "ring" and the surface brightness at its internal boundary.

Let us agree to call the inner rarefied part of a ring nebula the "region A" to distinguish it from the shell which surrounds this region.

Let us consider a ring nebula with an inner rarefied region whose external and internal radii are equal to r_2 and r_1, respectively. Let the average hydrogen-ion concentration be n_1 in region A and n_2 in the shell. It is obvious that I_1, the surface brightness of the nebula in hydrogen lines in the direction passing through the center of the nebula (along the line 1-1 in Fig. 1), will be the sum of the radiation from region A, corresponding to an ion concentration n_1, and the radiation from the front and rear regions of the shell, corresponding to an ion concentration n_2. In the direction 2-2, however, which passes through the inner boundary of the shell, at a distance r_1 from the center, the surface brightness I_2 will be determined by the ion concentration n_2. Taking into account that the amount of energy radiated by a unit volume of the nebula is proportional to the square of the ion concentration (provided that the ion concentration is equal to the free-electron concentration) and also that the nebula is transparent to radiation in the optical region, we can easily deduce the following expression for finding the ratio of the concentrations n_1/n_2:

$$\frac{n_1}{n_2} = \left\{\delta\left[\left(\frac{r_2}{r_1}\right)^2 - 1\right]^{1/2} - \left(\frac{r_2}{r_1} - 1\right)\right\}^{1/2}, \tag{1}$$

where δ is the ratio of the surface brightness at the center of the ring nebula to the surface brightness at the inner edge (or at a distance r_1 from the center), i.e.,

$$\delta = \frac{I_1}{I_2} \tag{2}$$

and is found from observation. For typical ring nebulae δ must be less than unity.

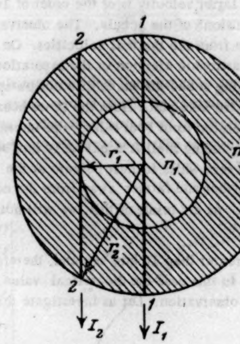

Fig. 1.

Let us consider the following limiting cases. Suppose that the region A is completely empty, i.e., $n_1 = 0$. Then the theoretical value of δ will be a minimum and equal to

$$\delta_{\min} = \frac{(r_2/r_1) - 1}{[(r_2/r_1)^2 - 1]^{1/2}}. \tag{3}$$

In the case when there is no rarefaction, i.e., $n_1 = n_2$, the theoretical value of δ will be a maximum and equal to

$$\delta_{\max} = \frac{r_2/r_1}{[(r_2/r_1)^2 - 1]^{1/2}}. \tag{4}$$

Since in typical ring nebulae the condition that $0 < n_1 < n_2$ holds, the observed value of δ must be less than $\delta_{\max}$, but greater than $\delta_{\min}$, i.e.,

$$\delta_{\min} < \delta < \delta_{\max}. \tag{5}$$

Let us apply the above considerations to the well-known ring nebula NGC 6720 in Lyra for which there are available the isophotes of surface brightness obtained by Aller for the line H_γ λ4340 [2]. From these isophotes we find that I_1, the brightness of the nebula NGC 6720 at its center, is equal to about 63, in arbitrary units, while at the inner edge of the ring I_2 is equal to about 100. This yields $\delta = 0.63$. Curtis finds that the relative thickness of the shell in NGC 6720 is 0.4. This gives $r_2/r_1 = 1.7$. Using these data, we find from Equations (3) and (4) that $\delta_{\min} = 0.5$ and $\delta_{\max} = 1.2$, i.e., the observed value of δ ($\delta = 0.63$) satisfies the Relation (5) and, consequently, the internal region of the nebula is not completely empty.

Substituting $\delta = 0.63$, $r_2/r_1 = 1.7$ into Equation (1), we find

$$\frac{n_1}{n_2} = 0.37.$$

From our measurements we have $r_2/r_1 = 2$, which gives

$$\frac{n_1}{n_2} = 0.30,$$

i.e., the ion concentration in the central rarefied region of the nebula NGC 6720 is approximately one-third of the concentration in the shell. This, at first sight, small difference leads to a decrease of the coefficient of emission from the center of the nebula by approximately a factor of ten.

NGC 7293 is also a typical example of a ring nebula. In the case of this nebula we have:* the brightness at the center in arbitrary units is approximately 1.20; near the inner boundary it is 2.10. From this we find that $\delta = 0.57$. For the ratio of the external and internal radii we have $r_2/r_1 \approx 1.7$. Using these data we find from (1) that

---

* The measurements were made by E. S. Parsamian on a photograph in red light taken with the 700 mm telescope of the Abastuman Astrophysical Observatory.

$$\frac{n_1}{n_2} \approx 0.3,$$

which indicates that the nebula NGC 7293 is to some extent similar to nebula NGC 6720, in the sense that their internal structures are the same.

Let us now go back to our basic problem. We have remarked above that the fact of existence of planetary ring nebulae appears to be incompatible with their low rate of expansion. The point is that even a static nonexpanding nebula will gradually increase in size as the result of the diffusion of gaseous matter into space with a velocity of the order of the thermal velocity of the hydrogen atoms. The latter velocity is of the order of 10 km/sec. Therefore, $v_0 = 10$ km/sec will be the smallest possible velocity of "expansion" of the nebula. The observed velocities of expansion are of the order of 20 km/sec., i.e., they differ little from the thermal velocities. On the other hand, if we assume that the nebula was formed as the result of a catastrophic ejection or the separation of a mass of gas from the central nucleus and that right from the very beginning it had the shape of a hollow sphere, then there are no reasons for assuming that the thermal expansion cannot also take place from the inner boundary of the nebula. As a result, the thickness of the shell must increase by expansion from both sides – the internal as well as the external surface. If, for example, the proper velocity of the expanding shell is equal to 10 km/sec., then the actual velocity at the outer layers of such a shell must be 20 km/sec, while it must be zero at the inner layers. In other words, during the time that the outer surface will move farther and farther away from the center, the inner surface will remain motionless and will always be at the center. As the result of this, we will not have a ring nebula, but a nebula which is uniform throughout its whole volume.

Actually, the velocities of expansion of the planetary nebulae are greater than 10 km/sec and, therefore, a "cavity" must anyway be formed at the center of the nebula. However, in this case the theoretical value of r_2/r_1 is found to be considerably less than the value which we obtain from observation. Let us investigate this problem in some detail.

Let v_0 denote the observed velocity of expansion of a "hollow" nebula. Obviously, v_0 represents the sum of the true velocity of expansion of the nebula $\underline{v}$ and the thermal velocity of the hydrogen atoms (forming the main body of the nebula) $\underline{u}$. We take $\underline{v}$ and $\underline{u}$ to be constant within a certain interval of time. Then we will have the following equations of motion for the external and internal surfaces of the nebula, relative to the center:

$$\begin{aligned} r_2 &= (v+u)\,t + h = v_0 t + h, \\ r_1 &= (v-u)\,t = (v_0 - 2u)\,t, \end{aligned} \tag{6}$$

where $\underline{h}$ is the initial thickness of the nebula. For a sufficiently large value of $\underline{t}$, from (6) we will approximately have

$$\frac{r_1}{r_2} = \frac{v_0 - 2u}{v_0}. \tag{7}$$

It is usually considered that the electron temperature T_e and, consequently, the thermal velocity of the hydrogen atoms $\underline{u}$ do not vary appreciably from one planetary nebula to another. T_e is taken to be, on the average, equal to 10,000°K which corresponds to a thermal velocity $u = 13$ km/sec. The expansion velocities $\underline{v}$ can be different fro the various nebulae. As a result of this we can obtain a theoretical dependence of r_2/r_1 on v_0 from the Equation (7). Fig. 2 gives the curve of this dependence for the case $u = 10$ km/sec. In Fig. 2, the points give the observational data on the 13 planetary nebulae for which the velocity of expansion v_0 and the ratio of the radii r_2/r_1 are known (Table 1). The former are taken from the paper of Wilson [3], the latter from the estimates of Curtis [1] and Wilson's measurements [3] (these are indicated by an asterisk in Table 1).

From the figure given, it follows that, as a rule, the observations give considerably greater values for the ratio of the radii r_2/r_1 and, consequently, considerably smaller values for the relative thickness of the nebulae, than the values which follow from a "normal" expansion of the nebulae; almost all of the points are above the theoretical curve. Further, the nebulae which have an expansion velocity less than 20 km/sec should not have a central "cavity" at all. At the same time they represent nearly one-half of the nebulae given in Table 1.

TABLE 1

NGC	r_1/r_2	v_0, km/sec	NGC	r_1/r_2	v_0, km/sec
1535	0.7	19.8	6720	0.6	24.5
1418	0.6*	25	6741	0.4	20.7
2165	0.4	20	6818	0.7	24.8
J900	0.6	17.8	7009	0.7	17.8
2392	0.5*	53.3	7026	0.6	40.8
3242	0.6*	15	7662	0.6*	25
6543	0.8	12			

It is apparent that there must be some reason for the formation of a central "cavity" in planetary nebulae in those cases when it should be completely absent, i.e., when $v_0 < 20$ km/sec, as well as some reason for the expansion of the inner surface of the shell with a velocity considerably in excess of the value $v_0 - 2u$ in those cases when $v_0 > 20$ km/sec. The reason for the above phenomena must lie in the fact that in the central regions of the planetary nebulae there are high electron temperatures, several times higher in magnitude than the usually accepted value $T_e = 10{,}000$°K which, strictly speaking, only refers to the shell, i.e., to the dense outer region of the nebula.

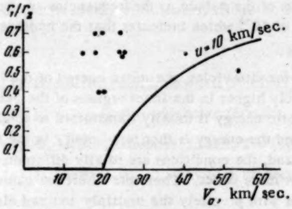

Fig. 2.

Let us assume that the boundary separating the shell from the region of the "cavity" is in a state of equilibrium, i.e., the relative velocity (with respect to the shell) of this boundary is equal to zero. This is only possible when the pressures on this boundary from both sides – from the direction of the shell and of the "cavity" – are equal. Neglecting the radiation pressure produced by the L_α radiation of the nebula itself, the attraction of the central star, and only taking the gas pressure into consideration, at this boundary we will have

$$n_1 T_{e1} = n_2 T_{e2}, \tag{8}$$

where T_{e1} and T_{e2} are the electron temperatures of the central region ("cavity") and the shell, respectively. The latter is $T_{e2} = 10{,}000$°K.

However, all of the data, in particular, the increase of brightness and, consequently, the increase of the density at this boundary which is frequently observed in planetary nebulae, indicate that this boundary is not in a state of equilibirum but, on the contrary, that it moves outwards with some acceleration. In other words, on this boundary we have the following condition;

$$n_1 T_{e1} > n_2 T_{e2}. \tag{9}$$

From this we obtain for the temperature of the central region ("cavity") of the nebula

$$T_{e1} > \frac{n_2}{n_1} T_{e2}. \tag{10}$$

Above we found $n_2/n_1 \sim 3$ in the case of the nebulae NGC 6720 and NGC 7293. Therefore, the electron temperatures in the central regions of these nebulae are

$$T_{e1} > 30000^\circ \text{K}. \tag{11}$$

Thus, although in principle from these observational data we can obtain the hydrogen-ion concentrations in both regions of the nebula, we can only obtain the lower limit to the electron temperature.

In what way can such a high electron temperature arise in the central regions of the planetary nebulae? To answer this question, let us first of all refer to the data given by observation. Curtis and, particularly, Wilson have measured the dimensions of the monochromatic photographs of several planetary ring nebulae. They found the well-known law governing the sizes of the images, according to which the dimensions of a monochromatic photograph usually decrease with the increase of the ionization potential of the element producing the given line. Of particular interest are the photographs in the light of the lines λ 3426 [Ne V] and λ4686 [He II]. It is found that the external radii of these photographs almost coincide with the radius of the "cavity." This fact deserves special attention. More often the following occurs: the nebula in the hydrogen lines has a ring-like shape, while in the line λ 3426 [Ne V] it has the shape of an exact disc (but not a ring!) with a diameter approximately equal to the diameter of the "cavity" (for example, in the nebulae NGC 2165, 7662, and others). In other words, the monochromatic photograph in λ 3426 [Ne V] can "fit in" almost completely into the central "cavity" of the ring nebula.

Normally, the λ 4686 [He II] line arises from cascade transitions, the start of which corresponds to the doubly ionized state of helium. On the other hand, the forbidden line λ 3426 [Ne V] arises in nebulae from the transitions of the type $2p^2$. In other words, for the excitation of these lines it is necessary that the helium is ionized twice and the neon four times. Doubly ionized helium and quadruply ionized neon, among the ions observed in planetary nebulae, have the highest ionisation potentials, equal to 54.2 ev and 96 ev, respectively, which correspond to ionization-producing wavelengths of less than 240 and 130 A, respectively. This means that the optical thickness of the "cavity" (up to the inner boundary of the nebula) for waves with $\lambda < 130$ A is of the order of unity. From this we can estimate the upper limit to the optical thickness of this region of the nebula at the frequencies of the Lyman continuum of hydrogen ($\lambda < 912$ A). It is found to be of the order of 10^{-3}, which indicates that the hydrogen in this region is almost completely ionized.

Further, because the radiation density is relatively high in the far ultraviolet, the mean energy of the electrons removed from the hydrogen by the photoionization will be considerably higher in the inner regions of the nebual than in the outer regions (in the shell). In nebulae, the electron kinetic energy is usually transmitted to singly and doubly ionized oxygen, nitrogen and other easily excited ions and the energy is then reradiated in the form of forbidden lines. In the inner regions of the nebula, on the other hand, the conditions are totally different: here the oxygen, nitrogen, and the other elements will be ionized three or more times. Therefore here we can only consider the emission of forbidden lines excited by electron collisions with precisely the multiply ionized elements. Unfortunately, as yet we do not know many of the physical parameters concerning the forbidden lines of most of these elements. However, starting from the observation that usually the excitation potential for exciting a metastable level rises with increasing degree of ionization of a given element, we can conclude that even after an electron loses its kinetic energy in a collision with these ions its residual "unutilized" kinetic energy will correspond to a temperature considerably higher than 10,000°K. In other words, the higher the degree of ionization of the nebula, or of any region of it, the smaller is the degree of cooling.

TABLE 2

NGC	T_*	T_{el}	NGC	T_*	T_{el}
1535	37000°	32000°	6720	75000°	55000°
1418	40000	34000	6741	84000	59000
2165	84000	59000	6818	55000	43000
2392	40000	34000	7009	83000	58000
3242	76000	55000	7026	64000	48000
6543	58000	45000	7662	88000	61000

We can try and estimate the upper limit to the electron temperature in the central region of the nebula in the absence of cooling, i.e., if we assume that the electrons retain all of the energy they acquire. It is clear that the electron temperature estimated in this way will already depend on the temperature of the nucleus. Similar calculations were carried out in Reference [4] for the case of an optically thin nebula which corresponds to our case and the magnitudes of the electron temperatures were obtained for various values of the temperatures in the nucleus (with the assumption that the electron-velocity distribution is Maxwellian). Using the results of these calculations, we have estimated the upper limits to the electron temperatures in the region of the "cavity" for the planetary nebulae listed in Table 1. The results are given in Table 2. The nuclear temperatures T_* are taken from Reference [5], with the exception of the nebulae NGC 1535 and NGC 2392, where the temperatures of the nuclei have been taken from Reference [6].

From the data of this table, we see that the upper limits to the electron temperatures in the central regions of the planetary nebulae can be as high as 50,000-60,000°K. The actual values of these temperatures must be somewhat lower, if we take into account the possibility of some cooling in the nebulae.

The astrophysical methods of determining the electron temperatures in nebulae are based on the investigation of certain spectral lines which are usually emitted by the bright, i.e., more dense regions of the planetary nebulae. The result obtained was then extended, although without any foundation, to all of the other regions of the nebula. We now see that this idea of a planetary nebula, isothermal throughout its volume, appears to be incorrect; each ring nebula consists of two parts: a central, high-temperature region and an outer, cooler region. The ratio of the temperatures in these two regions can be as high as 4-5. Under certain conditions it is possible that this temperature difference leads to the appearance and propagation of a shock wave through the nebula which is analogous to the occurrence of shock waves in ionized (H II) and un-ionized (H I) regions of interstellar hydrogen [7].

Biurakan Astrophysical Observatory
of the Academy of Sciences, Armenian SSR

Received January 16, 1957

LITERATURE CITED

[1] H. Curtis, Publ. Lick Obs., 13 (1917).

[2] L. Aller, Gaseous Nebulae (London, 1956).

[3] O. Wilson, Astrophys. J. 111, 279 (1950).

[4] D. Menzel et al., Physical Processes in Gaseous Nebulae [Russian Translation] (IL, Moscow, 1948), p. 40.

[5] G. A. Gurzadian, Biurakan Astrophys. Obs. Report, vol. 18 (1956)

[6] H. Zanstra, Z. Astrophys. 2, 1, (1930).

[7] M. Savedoff and J. Greene, Astrophys. J. 122, 477 (1955).

THE SPATIAL STRUCTURE OF SOME PLANETARY NEBULAE

Iu. K. Gulak

A numerical method is given for determining the spatial distribution of brightness in a nebula, the layers of equal brightness of which can be represented as some figures of rotation. The observed distribution of brightness in the photographs of NGC 6720, 7009 and 7662 is interpreted from the point of view of a possible spatial distribution of radiating atoms OIII. The latter is given in Figs. 2,3 and Table 1. The population of the $^1D_2$ level of the OII ion in these nebulae lies within the limits: $0.50 \cdot 10^{-7}$ - $1.25 \cdot 10^{-5}$, $1.30 \cdot 10^{-5}$ - $9.90 \cdot 10^{-4}$ and $0.43 \cdot 10^{-4}$ - $2.27 \cdot 10^{-4}$ cm^{-3}, respectively.

On the basis of L. Berman's data on the distribution of brightness in the $H\delta$-concentration image of NGC 7009, the distribution of electron density and then the concentration of the ion OIII in the ^3P level were calculated. The values of the former vary from $2.2 \cdot 10^2$ to $8.9 \cdot 10^3$ cm^{-3}, of the latter – from 0.28 to 3.1. The distribution of N_e and N_p is given in Figs. 4, 5.

The density maximum of the hydrogen envelope is twice as far from the center of the nebula as that of the radiating atoms OIII, which probably points to different velocities of expansion.

In the investigation of radiation transport in planetary nebulae the geometrical model taken for the nebula is of considerable importance. The nebula is usually considered to be a hollow spherical shell of gas whose thickness is considerably smaller than the radius of the sphere. This idealization of the structure has undoubtedly led to the discovery of the general physical processes taking place in the nebula, but in most cases this model is far from being correct [1].

In the present paper the observed distribution of brightness in the photographs of the nebulae NGC 6720, 7009, and 7662 [2] is interpreted as the result of a distribution of radiating atoms.

A study of the brightness distribution in the photographs of the nebulae NGC 6720 and 7009, the investigation of the shape of the isophotes, and of the total radiation from the various regions of the nebulae lead us to consider, with some justification, that the shapes of the nebulae can be represented by figures of revolution. If we assume that the axis of rotation lies in the image plane,* then in the plane AA' which cuts the nebula at right angles to the axis of rotation the contours of constant density will be in the form of concentric circles (Fig. 1). The brightness i_1 of a unit area on the edge of the image of the nebula is the result of the emission from the matter contained in a cylinder of length l_{11} whose axis coincides with the line of sight. Since in this position the line of sight passes through the layer of constant density, it is clear that in the direction of the observer the emission from a unit volume situated inside this layer will be given by

$$\rho_1 = \frac{i_1}{l_{11}}. \qquad (1)$$

---

*From an analysis of the isophotes and the statistical data we can sometimes obtain the limiting values of the angle between the rotation axis and the image plane and from this, in turn, we can make the appropriate correction to the structure of the layers of equal emission.

B. A. Vorontsov-Vel'iaminov has called this quantity "the spatial luminous density."

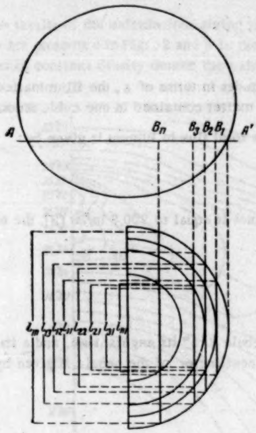

Fig. 1.

The luminous density of the second layer of constant emission is given by the equation

$$\rho_2 = \frac{i_2 - \rho_1 [l_{12} - l_{21}]}{l_{21}},$$

where i_2 is the brightness of a unit area of the image in the region B_2, $\rho_1 [l_{12} - l_{21}]$ is the contribution to i_2 from the first layer, l_{12} is the length of the line of sight in the whole of the nebula, and l_{21} is the length of the same line in the second layer.*

Similarly, for the n-th layer we obtain

$$\rho_n = \frac{i_n - \sum_{i=1}^{n-1} \rho_i [l_{i,\, n+1-i} - l_{i+1,\, n-i}]}{l_n}. \quad (2)$$

Thus, Equations (1) and (2) determine the relation between the brightness of the image of the nebula and its spatial luminous density. To be able to apply them, we must know the distribution of brightness along the line corresponding to the projection of the plane AA' and the distances along the line of sight through the various layers of constant emission.

From the assumed conditions we have that

$$l_{ni} = 2\sqrt{r_n^2 - a_i^2},$$

where r_n is the radius of the circular contour of constant density which passes through the middle of the layer of constant emission and a_i is the distance of the chord l_{ni} from the center.

By traversing the image of the nebula in such a way that the planes of section are sufficiently close together, it is possible to determine the manner of the variation of the constant-emission layers.

The advantage of the proposed method for determining the spatial structure of the nebulae is that when we apply it to objects possessing axial symmetry, we do not have to assume a priori the form of the constant-emission layers since we are able to trace them out in the course of the investigation. In addition, it is suitable for an attempt to investigate quantitatively such remarkable and interesting objects as the Z-shaped nebula NGC 6778, the spiral-shaped nebula NGC 4361, and other similar nebulae.

The distributions of brightness along the chords symmetrically situated with respect to the major axis in the nebulae NGC 6720 and 7009 are found to be quantitatively as well as qualitatively very similar. On the other hand, the variation of brightness along each chord occurs in a symmetrical manner with respect to the center, i.e., with respect to the minor axis of the nebula. Thus, without an appreciable loss of accuracy, we were able to determine the luminous density for the nebulae by using a somewhat idealized model which was smoothed out in each particular case.

The values of the brightness at four symmetrically situated points were averaged and the average was plotted on a graph. Through these points we drew the curves of the variation of brightness along the chords parallel to the major axis. The values of the brightness obtained from the graph were used to calculate the spatial luminous density.

---

* The first subscript to l denotes the number of the layer corresponding to the given chord, the second subscript the serial number of the chord in the given layer, where the subscript 1 corresponds to the outermost chord formed by the intersection of the line of sight and the layer determined by the first subscript.

Using the well-known relation

$$M = -14\overset{m}{.}18 - 2.5 \log \epsilon,$$

we expressed the luminous density M obtained in visual stellar magnitudes in terms of ϵ, the illumination in luxes produced at the earth's surface by the light emitted from the nebular matter contained in one cubic second of arc.

If we denote by R the distance to the nebula in meters, then the total flux in lumens is given by

$$F_{\text{lu}} = 4\pi R^2 \varepsilon.$$

Since the coefficient of visibility at the wavelengths of the nebular lines is equal to 200.3 lu/ w [3], the energy flux in ergs emitted by a cubic second of nebular matter will be

$$F = \frac{4\pi R^2 \varepsilon \cdot 10^7}{200.3}. \tag{3}$$

Taking into account the relation between the distance to the nebula R, a" its angular size, and a its linear size, we find from (3) that the energy radiated per second by a cubic centimeter of the nebula is given by

$$E = \frac{4\pi\varepsilon \cdot 10^9}{200.3\, R \sin^3 1''}, \tag{4}$$

where R is expressed in centimeters.

On the other hand,

$$E = (A_{N_1} \nu_{N_1} + A_{N_2} \nu_{N_2})\, h n_D. \tag{5}$$

A_{N_1} and A_{N_2} are the probability coefficients for the spontaneous transitions from the $^1D_2$ level of OIII into the states $^3P_2$ and $^3P_1$. ν_{N_1} and ν_{N_2} are frequencies of the nebular lines, and n_D is the number of atoms in the state $^1D_2$.

Substituting the values of the constants [4] and the distances to the nebulae NGC 6720, 7009, and 7662 [1] into these equations, from (4) and (5) we obtain

$$n_D = 2.423 \cdot 10^9 \varepsilon, \quad n_D = 3.634 \cdot 10^9 \varepsilon, \quad n_D = 2.907 \cdot 10^9 \varepsilon, \tag{6}$$

respectively, from which we are able to calculate the distribution of OIII atoms in the state $^1D_2$ from the known distribution of the luminous density in the nebulae being investigated.

The distribution of luminous density in the nebula NGC 7662 was determined along a radius, on the assumption that the nebula is spherically symmetrical. The results are given in Table 1. The first column gives the distances from the center, the second the brightness in visual stellar magnitudes per square second of arc, the third the luminous density (per cubic second of arc, and the fourth the number of OIII atoms per cubic centimeter in the state $^1D_2$.

TABLE 1

r''	$M\,(1'')^{-2}$	$M\,(1'')^{-3}$	$n_D \cdot 10^4$ cm^{-3}
	m	m	
0.0	15.31	19.85	0.71
1.5	15.28	19.49	0.99
3.0	15.22	18.81	1.85
4.5	15.22	18.82	1.83
6.0	15.22	18.59	2.27
7.5	15.36	18.61	2.23
9.0	15.64	18.90	1.70
10.5	15.98	19.25	1.23
12.0	16.45	19.87	0.70
13.5	16.89	20.39	0.43
15.0	17.69	—	—

The assumption of spherical symmetry is admissible only for the outer regions of the nebula where the contours of equal brightness are almost circular [2]. In the central region ($r < 7''.5$) this assumption is found to be invalid; therefore, the estimates obtained for this region are very approximate and from them we can only obtain a general picture of the structural features. In particular, we can assert that there is a region of reduced density inside the nebula NGC 7662. Taking into account the shape of the isophotes, we can assume that this region is ellipsoidal in shape.

The results of the calculations giving the numbers of OIII ions in the $^1D_2$ level for the nebulae NGC 6720 and 7009 are presented in Figs. 2 and 3 in the form of contours of constant density. The numbers which label the curves of constant density denote the value of n_D, the number of particles per cubic centimeter.

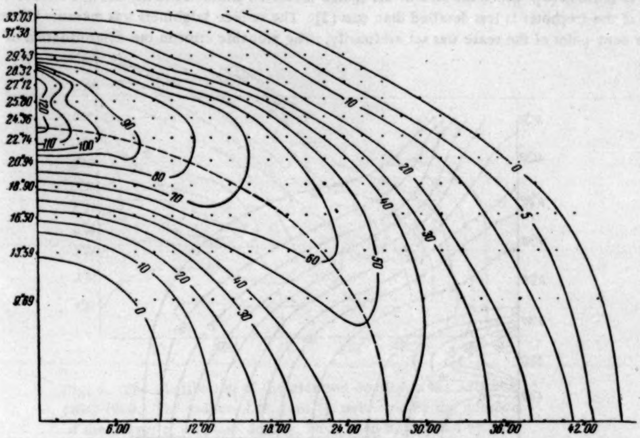

Fig. 2. The distribution of the concentration of OIII ions in the level $^1D_2$ in the nebula NGC 6720. The numbers on the curves of constant density indicate the number n_D of OIII ions per cm^3 (n_D has been multiplied by 10^7).

An analysis of the constant-density contours indicates that inside the nebulae NGC 6720 there is an ellipsoidal cavity; the eccentricity of the corresponding ellipse is equal to 0.67 (b = 9".75, a = 13".20). The major axis of the cavity lies in the direction of the minor axis of the nebula. The locus of the density maxima along any line drawn through the center of the nebula is a curve which is very nearly an ellipse with eccentricity of 0.54. Further, along any line through the center the density reaches its maximum value exactly halfway between the external boundary of the nebula and the boundary of the inner cavity. In spite of the fact that in the nebula NGC 7009 a continuous increase of the brightness is observed along the major axis towards the center, the density reaches its maximum value at a distance of 4".20 from the center and then decreases by more than a factor of two at the center. As in the case of the previous nebula, the density maxima lie on an ellipse with an eccentricity of 0.58. It is surprising that the eccentricities of the "ellipses of maxima" are found to be almost the same for both nebulae.[*] Therefore, there is a region with reduced density inside NGC 7009; it appears that the shape of this region is also ellipsoidal. It is characteristic that in this case the "ellipse of maxima" also passes halfway between the inner and outer density contours with the same value.

The number of OIII ions in the level $^1D_2$ for the various regions of the nebula NGC 6720 lies between $0.50 \cdot 10^{-7}$ and $1.25 \cdot 10^{-5}$ cm^{-3}, which, on the average, is almost two orders of magnitude lower than for the nebula NGC 7009 where this quantity varies from $1.30 \cdot 10^{-5}$ to $9.91 \cdot 10^{-4}$. It is possible that the density of radiating atoms in the brightest regions of the nebula NGC 7662 is somewhat higher than the calculated value assuming spherical symmetry, however, it is unlikely to exceed the value of the maximum density in the nebula NGC 7009. The range of the variation of the concentration in these nebulae differs little from that in the spherical nebula NGC 6572 ($4.1 \cdot 10^{-5}$-$-9.8 \cdot 10^{-4}$ cm^{-3}), the density distribution in which was studied by B. A. Vorontsov-Vel'iaminov [5].

---

[*] We cannot consider this result to be of great importance, since in both cases the calculations were carried out with the assumption that the axis of rotation lies in the image plane.

It is of great interest to estimate the density N_p of OIII atoms which are in the sub-levels $^3P_{012}$. We cannot conveniently calculate N_p for the various regions of a nebula using the mean value of the electron density. Taking into consideration that the distribution of electron density is known only for NGC 6572 [5], we were able to carry out the calculations in the case of NGC 7009 only, using for this nebula the picture of isophotes in the H_δ line reproduced by L. Berman [6]. Since the size of the image measured photometrically did not exceed 0.4 mm, Berman's map of the isophotes is less detailed than ours [2]. The surface brightness was measured in stellar magnitudes, but the zero point of the scale was set arbitrarily. The probable error in the determination of brightness is about $0^m.2$.

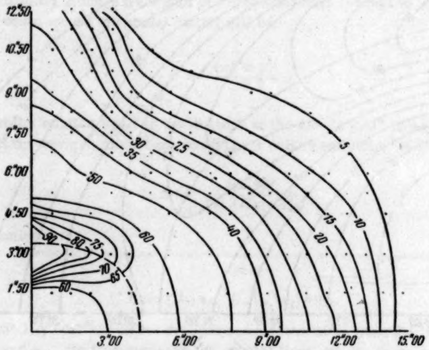

Fig. 3. The distribution of the concentration of OIII ions in the level $^1D_2$ in the nebula NGC 7009. The numbers on the curves of constant density indicate the number n_D of OIII ions per cm^3 (n_D has been multiplied by 10^5).

The conversion to absolute units was carried out by us in the following manner. The image intensities of NGC 7009 in N_1, N_2, and H_δ are in the ratio 96 : 34 : 2.49 [7]. Therefore

$$\frac{\varepsilon_{N_1+N_2}}{\varepsilon_H} = 52.21. \qquad (7)$$

From the known total visual stellar magnitude of the nebula in the nebular lines [2], we can find the corresponding magnitude $(\varepsilon_{N_1+N_2})_a$ in absolute energy units. From (7), taking into account that the coefficient of visibility in the H_δ line is equal to 0.8 lu/w, we find that

$$(\varepsilon_H)_a = 9.194 \cdot 10^{-14} \text{ lux}.$$

On a magnified reproduction of the isophote map, we used a planimeter to measure the relative areas S_n enclosed by each pair of neighboring contours of brightness; we then converted these areas into square seconds of arc. The product of the illumination ε_{no}, corresponding to the stellar magnitude given by Berman for each region, and the area S_n represents the contribution of the ring to the total energy radiated by the nebula. The sum of the contributions $\varepsilon_{no}S_n$ from all the regions gives the total illumination ε_{Ho}, in arbitrary units, produced by the image in Hδ. Therefore

$$(\epsilon_n S_n)_a = 9.194 \cdot 10^{-14} \left(\frac{\epsilon_n S_n}{\epsilon_H}\right)_o. \qquad (8)$$

If we divide (8) by s_n in square seconds, we obtain ϵ_n in luxes per square second. The first column of Table 2 gives the brightness of the isophots according to Berman, and the second column gives the corresponding illumination.

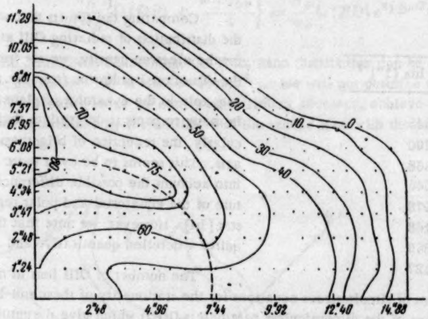

Fig. 4. The distribution of the electron density in the nebula NGC 7009. The values of N_e (cm^{-3}), indicated by the numbers of the curves of constant density, have been multiplied by 10^2.

The method used in determining the spatial distribution of the Hδ-radiation was the same as that used in determining the density of the radiating OIII atoms in this nebula. The values of the specific luminosity obtained in this way were used to calculate the electron density. The calculations were carried out using the results of D. Menzel [8], who found that the total amount of energy emitted by a unit volume of the nebula in the line Hδ is equal to*

$$E_{62} = \frac{2{,}509 \cdot 10^{-38} b_6 g_{62} R}{T_e^{3/2}} N_e N^+ e^{hR/36kT_e}. \qquad (9)$$

Numerous estimates made of the electron temperature in NGC 7009 vary between 8900°K and 20,000°K. We have taken the value of T_e to be 13,900°K, the value given in Reference [9] where the calculations were carried out on the basis of photoelectric measurements, taking into account the new values of the probability coefficients for the spontaneous transitions [4] and the effective cross sections [10].

The Kramers-Gaunt coefficient g_{62} was taken equal to 0.855 from the data of Reference [11]; the value of the quantity b_6, describing the departure from thermodynamic equilibrium, was taken equal to 0.381 from the same paper.

The calculations have been carried out on the assumption that hydrogen is the main source of free electrons in planetary nebulae, i.e., $N_e = N^+$.

In the observed part of the nebula the electron density varies within the range $2.2 \cdot 10^2 - 8.9 \cdot 10^3$ cm^{-3}, which is in good agreement with the determinations of the average electron density in this nebula ($6.3 \cdot 10^3 \text{cm}^{-3}$)[9]. The contours of constant density are presented in Fig. 4. As was to be expected, the general appearance of the diagram is the same as that giving the distribution of OIII ions emitting the nebular lines (Fig. 3). The eccentricity of the "ellipse of maxima" is equal to 0.63, but its semiaxes are almost twice as long as those in the case of OIII. This probalby indicates that the volocity of expansion of the hydrogen shell is greater than that of the OIII shell. It appears that the decrease of the expansion velocity as the ionization potential increases is not a feature of NGC 3242 [12] alone, but is characteristic of most of the planetary nebulae. In this connection the results of an analysis of the slit spectrograms of IC 418 are very representative [13]. In particular, the linear expansion velocity of this nebula obtained from an analysis of hydrogen lines is found to be 31 km/sec, while the velocity calculated from the OIII lines is 15 km/sec.

---

* It should be noted that in this reference out-of-date results were apparently used in the calculation of Kh (and not K as stated in the paper). In fact, $Kh = 2.168 \cdot 10^{-32}$.

Comparing the results that we have obtained for the distribution of radiating OIII atoms with those obtained for the electron density, we are inclined to think that the directional radiation from the nucleus plays a significant role in the dynamics of planetary nebulae and that in many respects it determines their appearance, particularly, the reduction of brightness along the major axis. This seems to be even more probable, if we take into account the possible difference in the surface temperature of the equatorial and polar regions of the central star [14]. However, we note that this assumption requires a detailed quantitative and qualitative verification.

TABLE 2

m_{rel}	$\epsilon_n \cdot 10^{-16}$ lux $(1")^{-2}$
m	
0.0	0.545
−0.4	0.790
−1.0	1.368
−1.2	1.645
−1.4	1.978
−1.5	2.168
−1.8	2.850
−1.9	3.127

The number of OIII ions in the sub-levels ^3P_i can be calculated by solving a system of simultaneous equations for the stationarity of these sub-levels. To do this, however, we must know the values of the dimensionless parameters $\Omega(iD)$ which give the number of induced transitions from an individual sub-level to the levels of higher energy. Since we do not have information on the values of the corresponding effective cross sections, the calculations were performed for the combined level ^3P and the value of $\Omega(PD)$ was taken equal to 1.73 [10].

If we neglect the transitions to levels with higher energy than the energy of the $^1D_2$ level, we can easily obtain the equation for the stationary state of this level from the equations given in Reference [15]. This equation will be of the form

$$\frac{n_D}{\omega_D}\left\{\Omega(PD) + \frac{\omega_D A_{DP}}{\alpha}\right\} = \sum_{i=0}^{2} \frac{N_i}{\omega_i}\,\Omega(iD)\, e^{\chi_{PiD}/kT_e}, \tag{10}$$

where n_D is the number of atoms in the level $^1D_2$, ω_D, ω_i are the statistical weights of the sub-levels ^3P_i, χ_{PiD} is the difference in energy between these levels and the level $^1D_2$, A_{DP} is the sum of the probability coefficients for spontaneous transitions from $^1D_2$ level to the sub-levels ^3P_i (which was calculated by R. Garstang [4]), and $\alpha = 8.54 \cdot 10^{-6}\, N_e T_e^{1/2}$.

Using the equations for the calculation of the energies of the p^2-configuration levels [4], we can easily show that we can neglect the differences in the energy of the ^3P_i sub-levels ($\nu_{02} = 9.402 \cdot 10^{12}$), i.e., $\chi_{PiD} \simeq \chi_{PD}$. In addition we can assume that

$$e^{-\chi_{01}/kT_e} \approx e^{-\chi_{02}/kT_e} \approx e^{-\chi_{12}/kT_e}.$$

Consequently, with a Boltzmann distribution of OIII ions in the sub-levels ^3P_i, we have

$$\frac{N_0}{\omega_0} = \frac{N_1}{\omega_1} = \frac{N_2}{\omega_2} = \frac{N_i}{\omega_i} = \gamma,$$

which gives

$$N_0 + N_1 + N_2 = \gamma(\omega_0 + \omega_1 + \omega_2)$$

or

$$\frac{N_i}{\omega_i} = \frac{N_P}{\omega_P}.$$

Then (10) can be written in the following form:

$$\frac{n_D}{\omega_D}\left\{\Omega(DP) + \frac{\omega_D A_{DP}}{\alpha}\right\} = \frac{N_P}{\omega_P}\Omega(PD)\, e^{\chi_{PD}/kT_e}. \tag{11}$$

The validity of the assumption concerning, the Boltzmann distribution can be checked by an analysis of the system of equations for the stationarity of the sub-levels $^3P_1$. We will not describe this method here because it is too complicated and, in particular, since we can, with sufficient accuracy, achieve the same results by comparing the number of transitions determined by the collisions of the second kind with the number of spontaneous transitions.

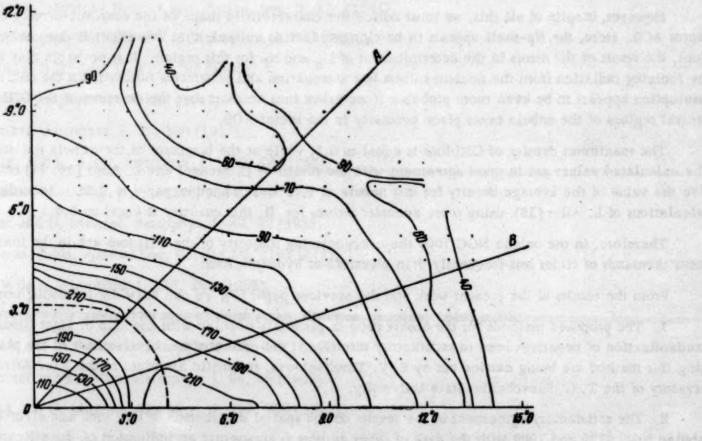

Fig. 5. The distribution of the OIII ions in the state ^3P in the nebula NGC 7009. The numbers on the constant-density contours indicate the number N_P of OIII ions per cm^3 (N_P has been multiplied by 10^2).

If we denote by N_{P_2} the number of atoms in the sub-levels $^3P_2$, then according to Reference [15] the number of collisions that transfer an atom from the state $^3P_2$ into the states $^3P_1$ and $^3P_0$ will be

$$\frac{\alpha N_{P_2}}{\omega_2}[\Omega(21) + \Omega(20)].$$

The number of spontaneous transitions will be given by the quantity

$$N_{P_2}(A_{21} + A_{20}).$$

The Boltzmann distribution will hold if

$$\frac{8.54 \cdot 10^{-6} N_e}{T_e^{1/2}\omega_2}\{\Omega(21) + \Omega(20)\} > A_{21} + A_{20}. \tag{12}$$

With the adopted values of the constants [4, 10] and of the temperature, the electron density must be higher than $5.77 \cdot 10^3$. Similarly, for the $^3P_1$ level we obtain $N_e > 4.90 \cdot 10^3$. Therefore, our calculations can be correct only for the inner,densest regions of the nebula.

The equation which we obtained from (11) after substituting the values of the constants and which we used in the calculations was the of the form

$$N_P = n_D \left\{14.51 + \frac{16.37 \cdot 10^6}{N_e}\right\}. \tag{13}$$

The results of the calculations are presented in Fig. 5 in the form of a map of the constant-density contours which is somewhat different than that obtained in the case of the distribution of OIII atoms in the $^1D_2$ state (Fig. 3). The "ellipse of maxima" has a smaller eccentricity (0.49). Along the major axis there is a relatively large region of increased density which is very prominent. The increase of the number of OIII ions near the boundary of the nebula, apparently, is the result of the errors in the determination of the electron density. It can be easily seen that for these regions of the nebula a small error in the value of N_e leads to a large change in N_P. On the other hand, with such low values of the electron density the assumption concerning the Boltzmann distribution is no longer correct.

However, inspite of all this, we must notice the characteristic shape of the constant-density contours in the sector AOB. Here, the N_P-shell appears to be elongated. It is unlikely that this effect is due only to the calculations, the result of the errors in the determination of N_e and N_P for this region. It is probable that in this direction the ionizing radiation from the nucleus suffers less attenuation and penetrates farther from the nucleus. This assumption appears to be even more probable if we taken into account that the decrease of the OIII density in the central regions of the nebula takes place precisely in the sector AOB.

The maximum density of OIII ions is equal to 3.1, while at the boundary of the nebula the density is 0.28. The calculated values are in good agreement with the results of D. Menzel and L. Aller [16, 17] who in one paper give the value of the average density for this nebula as 0.73 and in another paper as 1.28. According to the latest calculations of L. Aller [18], using more accurate values for Ω, this quantity is equal to 3.4.

Therefore, in the nebula NGC 7009 the overwhelming majority of the OIII ions are in the main level ^3P and occur thousands of times less frequently than electrons or hydrogen ions.

From the results of the present work and the previous paper [2], we can draw the following conclusions:

1. The proposed methods for the observation of planetary nebulae with the help of light filters and the standardization of negatives lead to satisfactory results. At the present time, observations of the planetary nebulae using this method are being carried out by E. V. Turchaninova, scientific associate at the Kiev Astronomical Observatory of the T. G. Shevchenko State University.

2. The satisfactory agreement of the results on the spatial distribution of OIII ions and electrons in the nebulae NGC 6720 and 7009 with the data of other authors is apparently an indication of the efficiency of the method used for the determination of the spatial luminous density. We consider that it is desirable to employ it in the investigation of other objects possessing axial symmetry.

3. In the investigation of planetary nebulae using the theory of radiation equilibrium and dynamics, we must keep in mind the fact that most of these objects depart from the usually adopted model of a nebula: a thin spherical shell of constant density. A more realistic model is one in which the nebula is considered as an ellipsoidal shell with the density increasing uniformly and symmetrically from the equator to the poles. We must also take into account that this variation of the density does not take place because of an increase of the total amount of matter in a given direction, but is the result of a variation of the linear dimensions of the nebula. In other words, the variation of density in various directions does not affect the optical thickness of the layer, which remains constant everywhere. This fact, by itself, requires a theoretical interpretation.

It is obvious that the dynamics and the equilibrium conditions in such a nebula will be considerably different from those in spherical nebulae with constant density. Further, they will be different within the nebula itself, in the regions of the equator and of the poles.

4. At the present time, when the basic physical processes occurring in gaseous nebulae have been explained

sufficiently well, it is desirable to make an attempt to develop a theory of the radiation balance for a concrete example of a planetary nebula, taking into account the actual distribution of radiating matter in it. The subject of these investigations can be the typical ring nebula NGC 6720 or NGC 7009.

The author is grateful to A. F. Bogorodskii for supervision during the course of the present work and also to N. A. Iakovkin for a number of extensive discussions.

A. S. Makarenko Sumsk State
Pedagogical Institute

Received September 24, 1956

LITERATURE CITED

[1] B. A. Vorontsov-Vel'iaminov, Novae and Gaseous Nebulae [In Russian] (Izd AN SSSR, Moscow-Leningrad, 1948).

[2] Iu. K. Gulak, Astron. J. (USSR) 34, 516 (1957).*

[3] S. V. Kravkov, The Eye and Its Operation [In Russian]. (Izd. AN SSSR, Moscow-Leningrad, 1950).

[4] R. Garstang, Monthly Notices Roy. Astron. Soc. 3, 115 (1951).

[5] B. A. Vorontsov-Vel'iaminov, Z. Astrophys. 12, 247 (1936).

[6] L. Berman, Bull. Obs. Lick 15, 86 (1930).

[7] L. Aller, Astrophys. J. 93, 236 (1941).

[8] D. Menzel, Astrophys. J. 85, 330 (1937).

[9] W. Liller and L. Aller, Astrophys. J. 120, 48 (1954).

[10] M. Seaton, Proc. Roy. Soc. A 218, 1134, 400 (1953).

[11] J. Baker and D. Menzel, Astrophys. J. 88, 52 (1938).

[12] O. Wilson, Publs. Astron. Soc. Pacific 58, 210 (1946).

[13] O. C. Wilson, Astrophys. J. 117, 264 (1953).

[14] P. Proisy and J. Cauzit, The Sun, (Comité franc. d'Astron. reunion, 1946) p. 59.

[15] M. Hebb and D. Menzel, Astrophys. J. 92, 408 (1940).

[16] D. Menzel and L. Aller, Astrophys. J. 94, 30 (1941).

[17] L. Aller and D. Menzel, Astrophys. J. 102, 239 (1945).

[18] L. Aller, Astrophys. J. 3, 609 (1950).

---

*See Soviet Astronomy — AJ.

THE KINEMATIC PECULIARITIES OF B STARS AND THE ROTATION OF THE LOCAL SYSTEM

A. Ia. Filin

The problem of explaining the kinematic peculiarities of B stars is considered. It is shown that the alteration of the galactic rotation constants can be explained quantitatively by the rotation of the Local System. In this case the unusual behavior of the Kamm function can also be explained. However, a complete explanation of the kinematic peculiarities can be obtained only if the dynamic characteristics of the Local System are known. An analysis of the behavior of the Kamm function for Bn, Bs, and Be stars leads to the conclusion that the structure of the Local System is complicated.

1. General Considerations

The present paper is the second part of a work on the kinematic peculiarities of B stars. In the first part [1] it was shown that the peculiarities of the motion of B stars are associated with the Local System. The idea that the kinematic peculiarities of B stars are associated with the Local System is not new. It was first proposed by K. F. Ogorodnikov [2] in the form that all of the peculiarities of stellar motions inside the Local System could be explained by its rotation.

From the point of view of kinematics, the problem of the rotation of the Local System was investigated by R. B. Shatsova [3, 4]. The successful explanation of the north-south asymmetries in the proper motions and the radial velocities that was given in these papers can be considered to be sufficiently reliable evidence in favor of the existence of the Local-System rotation. The possibility of the occurrence of this rotation can also be shown from purely dynamical considerations.

In the present paper the influence of the rotation of the Local System on the galactic rotation constants A and B and the Kamm function is investigated.

The following remarks can be made concerning the velocity dispersion, which is not considered in this paper. The Local System represents a group of stars which have, in all probability, a common origin and which are linked by a definite gravitational interaction, thus weakening the action of the tidal forces which arise as the result of galactic rotation. Therefore, the velocity distribution for the stars of the Local System must be different from that for the stars of the general galactic field. The velocity distribution in the Local System must be closer to a spherical distribution.

2. The Influence of the Local-System Rotation on the Radial Velocities

We will assume that the axis of rotation of the Local System is perpendicular to the galactic plane and that the rotation is in the same direction as the galactic rotation. The sun does not belong to the Local System and does not participate in this rotation.

According to R. B. Shatsova [3], the influence of the galactic rotation on the radial velocities can be separated from that of the Local-System rotation, i.e., the latter will contribute a separate term to the expression for the radial velocity:

$$\Delta V_r = \omega\rho_0 \sin(l - l_*) \cos b, \qquad (1)$$

where $l_\bullet$ is the longitude of center of rotation of the Local System, ω is the angular velocity at a distance ρ from the rotation center, and ρ_0 is the distance of the sun from the rotation center. Let us express ω as a power series in $\underline{r}$ (the distance of the star from the sun), leaving only the terms up to the second order:

$$\omega = \omega_0 + \left(\frac{d\omega}{dr}\right)_0 r + \frac{1}{2}\left(\frac{d^2\omega}{dr^2}\right)_0 r^2.$$

Substituting this expression into (1), we obtain

$$\Delta V_r = \omega_0\rho_0 \sin(l - l_\bullet)\cos b + \left(\frac{d\omega}{dr}\right)_0 \rho_0 \sin(l - l_\bullet)\cos b \cdot r + \\ + \frac{1}{2}\left(\frac{d^2\omega}{dr^2}\right)_0 \sin(l - l_\bullet)\cos b \cdot r^2. \tag{2}$$

But

$$\left(\frac{d\omega}{dr}\right)_0 = \omega_0'\left(\frac{d\rho}{dr}\right)_0, \\ \left(\frac{d^2\omega}{dr^2}\right)_0 = \omega_0''\left(\frac{d\rho}{dr}\right)_0 + \omega_0'\left(\frac{d^2\rho}{dr^2}\right)_0, \tag{3}$$

where

$$\omega_0' = \left(\frac{d\omega}{d\rho}\right)_0, \quad \omega_0'' = \left(\frac{d^2\omega}{d\rho^2}\right)_0.$$

ρ is determined from the relation

$$\rho^2 = \rho_0^2 + (r\cos b)^2 - 2\rho_0 r\cos(l - l_\bullet)\cos b,$$

from which we obtain

$$\left(\frac{d\rho}{dr}\right)_0 = -\cos(l - l_\bullet)\cos b, \quad \left(\frac{d^2\rho}{dr^2}\right)_0 = \frac{1}{\rho_0}\sin^2(l - l_\bullet)\cos^2 b.$$

Substituting these expressions into (3), we obtain

$$\left(\frac{d\omega}{dr}\right)_0 = -\omega_0'\cos(l - l_\bullet)\cos b, \\ \left(\frac{d^2\omega}{dr^2}\right)_0 = \omega_0''\cos^2(l - l_\bullet)\cos^2 b + \frac{1}{\rho_0}\omega_0'\sin^2(l - l_\bullet)\cos^2 b.$$

We transform Equation (2) with the help of these relations. The first term becomes

$$(\omega_0\rho_0\cos l_\bullet)\sin l\cos b - (\omega_0\rho_0\sin l_\bullet)\cos l\cos b.$$

Taking $l - l_\bullet = l - l_0 + \alpha$, where α is a constant, we obtain for the second term

$$-\frac{1}{2}\omega_0'\rho_0\cos 2\alpha\sin 2(l - l_0)\cos^2 b\cdot r - \frac{1}{2}\omega_0'\rho_0\sin 2\alpha\cos 2(l - l_0)\cos^2 b\cdot r = \\ = A_1 r\sin 2(l - l_0)\cos^2 b + C_1 r\cos 2(l - l_0)\cos^2 b,$$

where

$$A_1 = -\frac{1}{2}\omega_0'\rho_0\cos 2\alpha, \quad C_1 = -\frac{1}{2}\omega_0'\rho_0\sin 2\alpha.$$

The third term can be transformed into the form

$$\frac{1}{2}\left[(\dot{\omega}_0\rho_0 - \omega_0')\cos^2(l - l_*) + \omega_0'\right]\sin(l - l_*)\cos^2 b\cdot r^2.$$

The expression for the radial velocity now becomes

$$\begin{aligned} V_r = & -[X + \omega_0\rho_0 \sin l_*]\cos l\cos b - [Y - \omega_0\rho_0\cos l_*]\sin l\cos b - Z\sin b + \\ & + [A + A_1]\, r\sin 2(l - l_0)\cos^2 b + C_1 r\cos 2(l - l_0')\cos^2 b + \\ & + \frac{1}{2}\left[(\dot{\omega}_0\rho_0 - \omega_0')\cos^2(l - l_*) + \omega_0'\right]\sin(l - l_*)\cos^3 b r^2. \end{aligned} \tag{4}$$

The other two velocity components can be treated similarly, in particular, with the same assumptions as before, the influence of the Local-System rotation on the component V_l will be given by

$$\Delta V_l = \omega\rho_0\cos(l - l_*) - \omega r\cos b.$$

After the same transformations as above we obtain

$$\begin{aligned} V_l = & [X + \omega_0\rho_0\sin l_*]\sin l - [Y - \omega_0\rho_0\cos l_*]\cos l + \\ & + [A + A_1]\, r\cos 2(l - l_0)\cos b - \left[B - \omega_0 - \frac{1}{2}\omega_0'\rho_0\right] r\cos b - C_1 r\sin 2(l - l_0)\cos b + \\ & + \frac{1}{2}\left[(\dot{\omega}_0\rho_0 - \omega_0')\cos^2(l - l_*) + 2\omega_0'\right]\cos(l - l_*)\cos^2 b\cdot r^2, \end{aligned} \tag{5}$$

where A_1 and C_1 have the same meaning as in Equation (4).

Equations (4) and (5) lead to the following conclusions:

1) All of the kinematic constants are altered by the rotation of the Local System. 2) Comparing the solution of the usual equations with the last term in both of the above equations, we see the latter is identical with the expression for a constant K-effect which is not completely written down here. Actually, it is the sum of an infinite series. Its numerical value is mainly determined by the relations between the derivatives, but it also strongly depends on the nonuniformity of the distribution of stars according to longitude and in some complicated manner on the distance. 3) Since X and Y are close to the standard values, $\omega_0\rho_0$ must be small, perhaps of the order of 2 km/sec. 4) Both equations are completely analogous to the kinematic equations of Ogorodnikov and Milne [5]. However, the latter do not yield any results without a preliminary investigation since the Ogorodnikov-Milne kinematics represents only a mathematical description of the influence of all the conceivable types of motion in a stellar system on the velocity components and cannot lead to the discovery of the real reasons for this influence in any particular case.

TABLE 1

	ρ_0, ps	l_*	ω_0	$\omega_0\rho_0$ km/sec
Shatsova	150	253°	0".0163	–
Karpovich	288	–	–	2.3 ± 4.5

At the present time, unfortunately, it is impossible to carry out a quantitative verification of the derived equations since the necessary geometrical and kinematic features of the Local System are known rather approximately, while the existing determinations of them are very inconsistent. The values of several parameters of the Local System, obtained by R. B. Shatsova [3, 4] and M. Karpovich [6], are given in Table 1.

In addition, for a complete solution of the problem we must know the dynamic parameters of the Local System (mass, density distribution) which at the present time are unknown.

3. The Kamm Function and the Local-System Rotation

Let V_2^1 be the radial velocity of a star corrected for the solar motion and the K-effect. Then

$$V'_r = R_0\,[\Omega - \Omega_0] \sin(l - l_0) \cos b + \omega\rho_0 \sin(l - l_*) \cos b.$$

Dividing this expression by $\sin(l - l_0)\cos b$, we obtain the following expression for the Kamm function:

$$f(R, R_0) = R_0\,[\Omega - \Omega_0] + \omega\rho_0 \frac{\sin(l - l_*)}{\sin(l - l_0)},$$

which, when multiplied by a weight factor $w = |\sin(l - l_0)\cos b|$, gives the weighted value of $f(R, R_0)$

$$f(R, R_0)\,w = R_0\,[\Omega - \Omega_0]\,|\sin(l - l_0)\cos b| + \omega\rho_0 \sin(l - l_*) \frac{|\sin(l - l_0)|}{\sin(l - l_0)} \cos b. \qquad (\bullet)$$

Let us consider the second term of this equation which expresses the influence of the Local-System rotation on the Kamm function. Let us take cos b = 1 and let us assume that the Local System has the shape of a highly oblate ellipsoid rotating about its minor axis which is perpendicular to the galactic plane. Let the circle of radius ρ_2 in Fig. 1 represent the boundary of the Local System near the galactic plane, S represent the position of the sun, and C_1 the position of center of rotation of the Local System which is situated in the direction l_*. The galactic center lies in the direction l_0. For simplicity we further assume that $l_0 - l_* = 90°$. We construct a plane, perpendicular to the galactic radius of the sun, at a distance ρ_1 from the center of rotation of the Local System. This plane will intersect the galactic plane along the line EF. Let us investigate the part of the Local System that lies to the left of the galactic radius of the sun, since it is here that the usual behavior of the Kamm function is altered [1]. We will calculate the mean values of the second term in Equation ($\bullet$) for intervals of ρ_1, and not of R, in the case of stars lying near the galactic plane in a layer of thickness dz. The angle φ determines the limiting value of the weights of the Kamm function which were not used in obtaining the mean values. The remaining symbols can be understood from the figure.

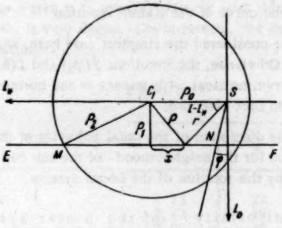

Fig. 1.

The weighted mean value of the second term in Equation ($\bullet$) for the interval $d\rho_1$ can be written as

$$f(\rho_1) = \rho_0\omega \sin(l - l_*) = \frac{\int_M^N \rho_0\omega(\rho) \sin(l - l_*)\, D(\rho)\, dx\, d\rho_1\, dZ}{\int_M^N |\sin(l - l_0)|\, D(\rho)\, dx\, d\rho_1\, dZ}, \qquad (\bullet\bullet)$$

where $D(\rho)$ and $\omega(\rho)$ are the stellar density and the angular velocity of the Local System at a distance ρ from the center of rotation. Since both $\omega(\rho)$ and $D(\rho)$ are unknown, for an approximate calculation we can assume that

$$\omega(\rho) = Ce^{-m\rho}, \quad D(\rho) = D(0)\, e^{-n\rho},$$

where D(0) is the stellar density for $\rho = 0$, and C = 190, m = 15, n = 10 are constants chosen in such a way that at $\rho = \rho_0 = 0.15$ kps, $\omega = \omega_0 = 20$ km/sec/kps (this gives a linear velocity of 3 km/sec), while $D(\rho) \approx 0$ at $\rho = \rho_2 = 0.5$ kps; $D(\rho)$ and $\omega(\rho)$ must decrease with increasing ρ. The above equations describe this behavior. The adoption of any other suitable expression will not change the behavior of the function $f(\rho_1)$.

From Fig. 1 we find

$$\sin(l - l_*) = \frac{\rho_1}{\sqrt{\rho_1^2 + (\rho_0 - x)^2}}, \quad \rho = \sqrt{\rho_1^2 + x^2}, \quad \sin(l - l_0) = \frac{\rho_0 - x}{\sqrt{\rho_1^2 + (\rho_0 - x)^2}}.$$

Equation (**) can now be written in the following form (we integrate only with respect to x):

$$f(\rho_1) = \frac{C\rho_1\rho_2 \int\limits_p^q \frac{1}{\sqrt{\rho_1^2 + (\rho_0 - x)^2}} e^{-(m+n)\sqrt{\rho_1^2+x^2}}\, dx}{\int\limits_p^q \frac{\rho_0 - x}{\sqrt{\rho_1^2 + (\rho_0 + x)^2}} e^{-n\sqrt{\rho_1^2+x^2}}\, dx},$$

where

$$p = -\sqrt{\rho_2^2 - \rho_1^2},\ q = \rho_0 - \rho_1 \tan\varphi.$$

The values of the integrals were obtained by a numerical integration. The results are given in Table 2 and presented graphically in Fig. 2 by the dotted curve. The dashed line shows schematically the behavior of the Kamm function in the absence of the Local-System rotation. The resultant curve, shown by the full line, represents well the characteristic bend in the curve of the Kamm function.

TABLE 2

ρ_1,kps	R,kps	$f(\rho_1)$ km/sec.
−0.40	6.80	−0.1
−0.30	6.90	0.3
−0.20	7.00	1.1
−0.10	7.10	3.2
−0.05	7.15	−2.7
0.00	7.20	0.0
+0.05	7.25	+2.7
+0.10	7.30	3.2
+0.20	7.40	1.1
+0.30	7.50	0.3
+0.40	7.60	+0.1

We have considered the simplest case here, when $l - l_* = 90°$. Otherwise, the functions $f(\rho_1)$ and $f(R, R_0)$ are no longer symmetrical with respect to the horizontal axis. This is in fact observed.

Thus, the disruption of the usual behavior of the Kamm function for the neighborhood of the sun can be explained by the rotation of the Local System.

4. Nonuniformity of the B-star System

The individual values of the Kamm function for B2-B5 stars show a very large dispersion when they are plotted in Fig. 2. At the same time, the dispersion is within the normal limits for the B0-B1 stars. Two factors could be operating here. 1) A slight differential effect due to galactic rotation. For stars belonging to the Local System, this effect is in fact reduced and for relatively small weights the dispersion of the values of the Kamm function can be large. This can serve as an indication of whether stars belong to the Local System. 2) A possible nonuniformity of B2-B5 stars.

TABLE 3

	Bn	Bs	Be		B
X	+15.7±0.9	+11.8±0.9	+13.6±1.7	+13.1±1.8	+17.3±0.2
Y	+ 8.5±1.2	+ 8.0±1.2	+11.8±3.2	+ 8.8±3.1	+ 7.0±0.3
Z	(+7.0)	(+7.0)	(+7.0)	(+7.0)	(+7.0)
A	+ 9.3±1.8	+18.8±2.2	+13.2±2.9	+15.1±3.0	+11.8±0.5
K	− 2.6±0.8	− 2.5±0.8	− 2.2±1.9	− 4.0±1.8	− 1.9±0.2
C_1	+ 2.1±1.9	+ 1.5±2.6	− 6.5±2.6	—	+ 0.7±0.2
'	570	471	882		548
n	166	133	64		685

In order to establish how real the second of these reasons is, the motion of stars with n, s, and e characteristics was investigated. The B emission stars were chosen from the catalogues of Merrill and Burwell [7]. The number of such stars with known radial velocities was found to be only 64. The fourth group consisted of the stars left after the Bn, Bs, and Be stars were excluded. In the following we will denote this group simply by B. The calculations using radial velocities were carried out for all the four groups. The results are given in Table 3. In the case of Be stars we carried out two versions of the calculations: with and without a constant C_1. Both versions, while they agree with each other within the limits of error, are too inaccurate. Z was taken equal to +7.0 km/sec. K was found from the coefficient of $\bar{r}\cos^2 b$.

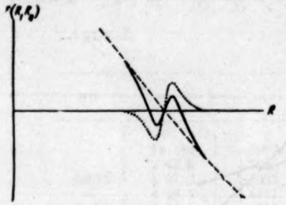

Fig. 2.

Figs. 3-6 give the Kamm function for the four groups. On the left of the figures the individual values are plotted; the mean values, which are also given in Table 4, are plotted on the right.

The theoretical curve is indicated by the crosses. The values of $f(R_1, R_0)$ which fell outside the limits ± 100 km/sec were not used to calculate the mean values. In addition, the points indicated by the circles in Fig. 4 were not included in the average for the B stars. From these figures it can be seen that the dispersion is less for Bs and Be stars, but for Bn and B stars the scatter of points is as large as before.

The large scatter of the points for the group Bn (Fig. 3) indicates a small influence of the differential effect of galactic rotation. The general behavior of the average curve is in good agreement with this. Its inflection at about R_0, characterizing a participation in the local rotation, is very slight. Consequently, the Bn stars belong to the Local System but almost do not participiate in its rotation.

TABLE 4

$\bar{R}$	n	$f(R, R_0)$	Σw	σ_l
6.72	22	+6.1	13.65	±1.4
7.13	46	−1.2	38.20	0.8
7.37	28	−1.1	21.65	1.1
7.62	22	−4.6	14.22	1.3
7.90	18	−6.5	13.14	1.4
8.17	9	−9.5	5.96	2.0
6.86	25	+10.9	15.96	1.2
7.15	25	+ 0.8	21.59	1.1
7.38	36	− 3.8	27.42	1.0
7.60	25	− 8.3	13.40	1.4
7;93	12	−12.8	7.66	1.8
6 .70	9	+21.3	5.12	2.2
.26	13	+ 6.1	10.85	1.5
.79	14	− 0.5	10.48	1.5
.35	6	−23.6	3.95	2.5
6.53	13	+23.6	7.33	1.8
6.88	41	+10.7	30.52	0.9
7.14	127	− 0.2	113.40	0.5
7.36	184	− 2.1	139.81	0.4
7.63	71	− 7.6	42.03	0.8
7.85	32	−20.8	19.56	1.1
8.24	22	−34.7	15.33	±1.3

On the other hand, for the group of B stars (Fig. 4) the characteristic inflection of the curve is quite prominent, so that in their case the rotation of the Local System shows up quite definitely. The region where this rotation is important lies between R = 7.0 kps and R = 7.8 kps. Outside these limits, for all practical purposes, the stellar motion is determined by the galactic rotation. The dispersion of the points is also large here, which within the above limits of the distance can be considered to be the result of a small differential effect of galactic rotation.

However, outside these limits there are also very large deviations. It is possible that these stars belong to the Bn group. These stars have been excluded from Table 5 and in Fig. 4 they are marked by circles.

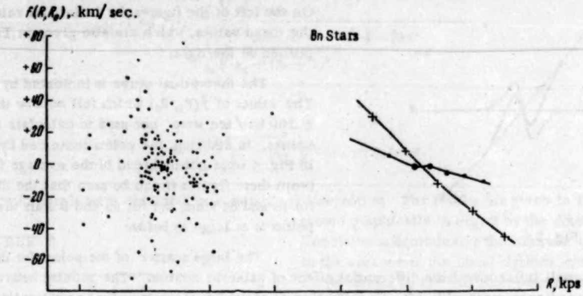

Fig. 3.

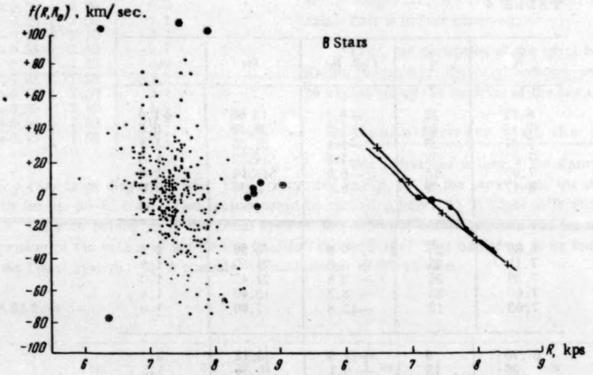

Fig. 4.

The Kamm function for the Bs stars (Fig. 5) varies smoothly throughout its range, without any hint of an inflection, and consequently indicates that these stars do not participate in the local rotation. However, they have a connection with the Local System since the observed curve is different from the theoretical.

The mean curve for the Be group (Fig. 6) is the least certain of the curves. However, these stars show the influence of the Local System since the observed curve differs from the theoretical one. It is possible that there is also an inflection in the observed curve. According to the investigations of Tai Wên-sai into the spatial distribution of Be stars [8], the latter are not influenced by the Local System. The same conclusion was also reached by Shnirel'man [9]. If Fig. 6 is even partially correct, then this would mean that the spatial distribution of stars can not always be used as a reliable criterion for classifying the stars as belonging to the Local System. In Fig. 6 there is a further curve which is shown as a dashed line. The nine points determining this curve were not taken into account in the calculation of the averages. All of these stars have been excluded from Table 6. The point marked by a circle was also excluded. It is the point for HD 232534, which has a radial velocity of 106 km/sec and also a large Z-coordinate, equal to 266 ps. The second curve is displaced very much from the normal position, but its behavior is in good agreement with that of the theoretical curve.

TABLE 5

HD	α		l	b		R	R, R
—	1h 4m.8	−59°7	93°.2	−2°.7	2200	8.6	+ 3
—	2 42.8	+5959	104.8	+1.5	1000	7.9	−126
29866	4 37.3	+4036	130.7	−2.1	240	7.4	+108
—	4 48.1	+4447	128.8	+2.1	1500	8.6	+ 1
45789	6 24.4	+ 712	171.8	0.0	750	7.9	+105
258982	6 26.2	+ 614	172.9	−0.2	1500	8.6	−135
259828	6 28.8	+ 811	171.4	+1.4	1600	8.7	+ 7
236775	6 41.5	+ 542	175.1	+3.0	2000	9.0	+ 6
—	6 44.2	+ 050	179.8	+1.2	1450	8.5	− 2
—	7 2.1	− 430	186.3	+2.3	1700	8.6	− 9
—	17 31.2	−3520	321.4	−3.3	800	6.4	− 57
172275	18 34.2	− 727	352.7	−2.2	1000	6.3	+105

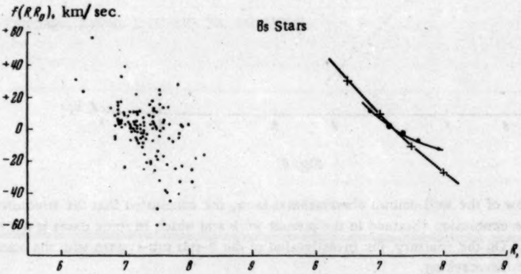

Fig. 5.

TABLE 6

HD	α	δ	l	b	r	R	f (R, R0)
—	1 8.4	+61°.25	93°.4	−0°.4	1400	8.1	− 69
—	4 47.8	+45 53	127.9	+2.8	1750	8.8	−113
259597	6 28.1	+ 8 24	171.2	+1.3	1000	8.1	− 72
51193	6 51.3	− 3 40	184.6	+0.8	1000	8.0	− 82
—	7 2.4	− 5 4	187.1	+2.6	1100	8.0	− 93
—	7 2.6	− 3 56	186.2	+3.1	1400	8.4	− 91
55885	7 9.8	−15 13	196.8	−0.7	800	7.8	− 57
173948	18 43.0	−62 18	300.9	−24.9	210	7.0	− 42
230780	19 4.7	+14 58	16.1	+1.6	1250	6.4	− 5

Thus, the analysis of the behavior of the Kamm function leads to the assumption that the Local System is not uniform. In spite of its unexpected nature, this conclusion probably reflects a real situation, because it seems that the structure of various aggregates of cosmic objects, which at first sight appear to be uniform, is as a rule complex. Thus, for example, the investigations of B. V. Kukarkin [10] established the complex structure of the Galaxy. The main result of this work is the discovery of the various sub-systems in the Galaxy and the establishing of the relations between the physical characteristics, the spatial distributions, and the kinematics of the objects forming the sub-systems. The investigation of the stellar motions has led P. P. Parenago [11] to discover the separation of the main sequence into two parts and P. G. Kulikovskii to conclude that the sub-system of the long-period variable stars of the type Mira Ceti is not homogeneous [12]. An analogous conclusion was reached by P. N. Kholopov [13] who investigated the visible distribution of stars in the globular clusters. Namely, "...the globular clusters can be considered as systems which consist of a large number of interpenetrating sub-systems of various types." In a paper which has recently appeared, P. P. Parenago [14] presents some arguments that make the earlier assumptions of the separation of the white dwarfs into two groups even more probable.

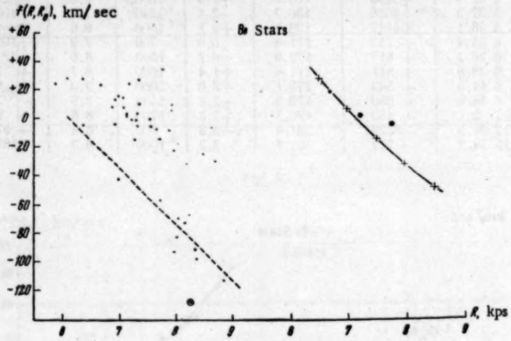

Fig. 6.

Consequently, in view of the well-known observational facts, the conclusion that the structure of the B-star sub-system is complex, the conclusion obtained in the present work and which in some cases is not completely certain, is not unexpected. On the contrary, the investigation of the B-star sub-system with the assumption that it is not homogeneous can be far-reaching.

5. Summary

1. Attempts to explain the separate peculiarities of the B stars without relating them to other peculiarities, ignoring the main observational fact — the presence of the Local System — did not lead to satisfactory results because of the methodologically inaccurate formulation of the problem [1].

2. The possible general reasons, for example, the motion along a spiral arm, the admixture of stars belonging to the spherical component, the wrong value of the mean absolute magnitude, and the errors in the evaluation of the absorption, also do not explain the observed peculiarities of the B-star motion [1].

3. All of the peculiarities of B stars can be satisfactorily explained quantitatively as the result of the existence of the Local System, which is one of the aggregates of hot giants determining the spiral structure of the Galaxy.

4. Another peculiarity, previously unknown, is also explained: the inflection on the curve $f(R, R_0)$ in the case of B2-B5 stars.

5. The existence of a difference in the behavior of the Kamm function between the B, Bn, Bs, and Be stars is evidence for the assumption that the B-star sub-system has a complicated structure.

In conclusion, I express my gratitude to Prof. P. P. Parenago for his supervision of the present work.

Stalinabad Astronomical Observatory
of the Tadzhik SSR Academy of Sciences

Received December 7, 1956

LITERATURE CITED

[1] A. Ia. Filin, Astron. J. (USSR) 34, No. 4 (1957).*

[2] K. F. Ogorodnikov, Uchenye Zapiski LGU** 15, 22, 3 (1950).

[3] R. B. Shatsova, Uchenye Zapiski LGU** 15, 22, 113 (1950).

[4] R. B. Shatsova, Uchenye Zapiski LGU** 16, 25, 67 (1952).

[5] P. P. Parenago, A Course in Stellar Astronomy [In Russian] (GITTL, Moscow, 1954), p. 409, 3rd ed.

[6] M. Karpovich, Referat. Zhur. 2, 1112 (1956).

[7] P. W. Merrill and C. G. Burwell, Astrophys. J. 98, 153 (1943); 110, 387 (1949); 112, 72 (1950).

[8] Tai Wên-sai, Referat. Zhur. 3, 1870 (1957).

[9] P. G. Shnirel'man, Astron. J. (USSR) 29, 179 (1952).

[10] B. V. Kukarkin, The Investigation of the Structure and Evolution of Stellar Systems on the Basis of a Study of Variable Stars [In Russian] (GITTL, Moscow-Leningrad, 1949).

[11] P. P. Parenago, Trudy GAISh , 20, 26 (1951).

[12] P. G. Kulikovskii, P. 3, 6, 225 (1948).

[13] P. N. Kholopov, Trudy GAISh, 23, 250 (1953).

[14] P. P. Parenago, Astron. J. (USSR), 33, 340 (1956).

---

*See Soviet Astronomy — AJ.

**Leningrad State University.

THE OPEN STELLAR CLUSTERS NGC 6823 AND NGC 6830

K. A. Barkhatova

The open stellar clusters NGC 6823 and NGC 6830 were investigated. The distance to NGC 6823 is 1800 ps, to NGC 6830 1680 ps, their linear diameters are 7.9 ps and 9.7 ps, respectively. It is surmised that NGC 6830 and NGC 6823 are members of an association of high-luminosity stars, studied by Morgan, Whitford and Code [7].

During the summer and autumn of 1954 photographs were obtained at the Engel'gardt Astronomical Observatory of the clusters NGC 6823 and NGC 6830 with KSA 40 stars used as standards. During this period, eight photographs were obtained on Ilford Zenith plates and ten photographs on Agfa ISS plates with a yellow filter. The photographs were taken along the meridian, always in the same order: cluster – standard. The average photographic magnitudes obtained from four plates had a mean square error of $\pm 0^m.06$. The photovisual magnitudes were obtained from four plates with a mean error of $\pm 0^m.05$. The mean square error of the color indices was $\pm 0^m.07$. The photographic magnitudes obtained in the case of the cluster NGC 6823 were in good agreement with the data of Becker and Stock [1], after the latter were reduced to the international system.

a) The Cluster NGC 6823

The cluster NGC 6823 is situated in the Vulpecula constellation and has the following equatorial and galactic coordinates:

$$\left.\begin{aligned} \alpha &= 19^h38^m.9, & l &= 27^\circ, \\ \delta &= +23^\circ4', & b &= -1^\circ.3 \end{aligned}\right| \; 1900.$$

This cluster has been studied by many investigators. According to Trumpler [2], the cluster is of class IV 3 p. Its distance from the sun, determined by the method of diameters, is equal to 3890 ps. Zug [3] was the first to construct the color index – apparent magnitude diagram for the stars of the cluster; the diagram did not have any sufficiently marked outlines (the stellar magnitudes were determined from the diameters), but it was possible to use it to make a more reliable estimate of the distance to the cluster and of the light absorption in the direction of the cluster.

The apparent magnitudes of the stars in the cluster were obtained for three regions of the spectrum by Becker and Osvalds [4]. At a later date Becker and Stock [1] again investigated the cluster using the method of three-color photometery. Additional photographic and photoelectric observations were carried out in order to determine the stellar magnitudes. From the results of the latter investigation the distance to NGC 6823 was found to be 3700 ps, while the first investigation gave the distance as 2400 ps. Therefore, the cluster NGC 6823 is among the most distant objects in our Galaxy. However, the results of Markarian [5] and the author [6] lead to a considerably smaller distance to the cluster, namely, 1800-2000 ps, while at the same time the distance determined photometrically is in good agreement with the distance obtained from the method of diameters. An association of high-luminosity stars, situated at a distance of 1800 ps from the sun, has been discovered in the region of the cluster [7].

In the present work photographic and photovisual magnitudes were obtained for 212 stars in the region of the cluster. So that the boundary of the cluster could be determined, the whole region was divided into eight concentric zones and the number of stars of a given magnitude was found for each zone. From the stellar counts it has been found that the cluster contains about 40 stars with $m_{pg} < 15^m$. As can be seen from Fig. 1, a, the stars with $m_{pg} < 13^m$ are markedly concentrated towards the center and the angular dimensions of the cluster found from these stars is 8-10'. The same sharp concentration towards the center is exhibited by the stars with $14^m < m_{pg} < 15^m$ (Fig. 1, b).

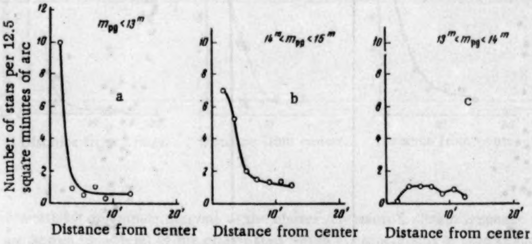

Fig. 1

The angular diameter determined from the distribution of faint stars is approximately equal to 13-15'. It is interesting to note that the stars with $13^m < m_{pg} < 14^m$ (Fig. 1, c) do not show any concentration towards the center; their density at the center is actually lower than that near the boundaries of the cluster. The angular diameter of the cluster determined from the distribution of stars of all magnitudes can be taken to be 13-15'. The angular diameter, obtained by the method of stellar counts, is larger than that usually found by various authors from direct measurements. From the stellar counts it has been found that the cluster occupies the region of the first four zones.

TABLE 1

Zone	m_{pg}	CI	n
1a	10.88	0.47	4
1	13.00	0.58	12
2	14.20	0.73	20
3	13.84	0.65	15
4	13.55	0.65	20
5	13.70	0.72	12
6	13.60	0.64	26

TABLE 2

№	m_{pg}	m_{pv}	CI	Sp (HDE)
4	9.56	9.35	0.21	A0
5	11.56	11.09	0.57	
6	11.05	10.48	0.57	
7	10.14	9.59	0.55	B
8	10.70	10.36	0.34	A
9	12.90	12.35	0.55	
10	11.66	11.12	0.54	
11	11.76	11.13	0.63	
12	12.30	11.85	0.45	
13	11.32	10.95	0.37	B2
14	12.64	12.27	0.37	A

The study of the stellar distribution inside the cluster shows that the bright stars are more concentrated towards the center than the fainter ones. Their density at the center is 15 times as high as the density at the boundary, the density of stars with $14^m < m_{pg} < 15^m$ is only 7 times as high at the center as it is on the boundary, while the stars with $13^m < m_{pg} < 14^m$ are uniformly distributed near the boundary. This conclusion is confirmed by the data given in Table 1, where the average photographic magnitudes and color indices are given for the separate concentric zones and the stars that belong to the cluster have been identified by means of the color index — apparent magnitude diagram.

A subgroup 1a, containing the central stars, has been taken separately from the stars found in zone 1.

From the table given above it can be seen that the brightest stars of the cluster are concentrated at the center. From the known photographic magnitudes and color indices, the color index — apparent magnitude diagram was constructed. As can be seen from Fig. 2, the stars situated in the first three zones show a sharply defined main sequence. However, the stars in zones 4-8 also form a similar sequence in the diagram, but with a considerably larger dispersion of the points (Fig. 3). It is quite possible that part of the stars in the outer regions are physically linked to the cluster NGC 6823, forming together with it a stellar association.

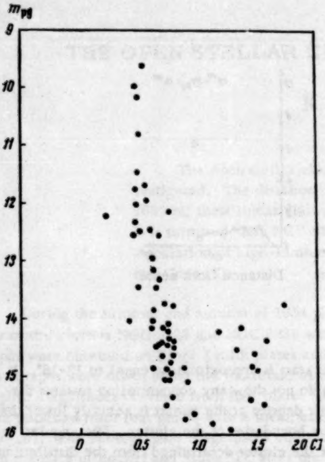

Fig. 2

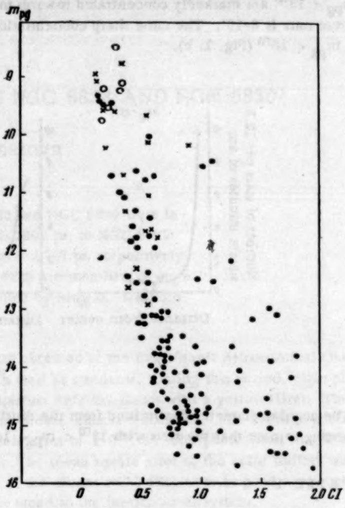

Fig. 3

As was mentioned above, the cluster NGC 6823 is part of a stellar association or an aggregate of high-luminosity stars in Vulpecula and, probably, it is one of the more condensed nuclei of this association. In Fig. 3, the high-luminosity stars taken from Reference [7] are indicated by the open circles, while the crosses denote the stars situated near to BD + 23° 3760 (Fig. 4). Table 2 gives the photographic and photovisual magnitudes, as well as the color indices of the stars lying in the vicinity of BD + 23° 3760.

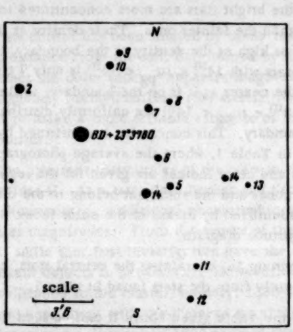

Fig. 4

On the color index – apparent magnitude diagram, all of the above stars lie within the limits of the main sequence, and on this basis it is possible to assume that in addition to the high-luminosity stars, the association contains stars with a large range of luminosities.

Crosses are also used to indicate the BD stars, situated in the vicinity of the cluster, which are possibly also members of the association.

Data concerning several possible members of the association are given in Table 3; Morgan, Whitford, and Code [8] have listed some of them. The first column gives the BD number, the second – HDE spectral classes, the third – spectra according to References [8] and [9], the fourth – photographic magnitudes, the fifth – color indices according to the international system obtained from References [8], [9], and [10]. The sixth and seventh columns give the proper motions taken from Reference [10].

From Table 3 it can be seen that the proper motions of the stars are very close to one another and the average for the whole group is $\mu_\alpha = -0''.007$ and $\mu_\delta = -0''.007$.

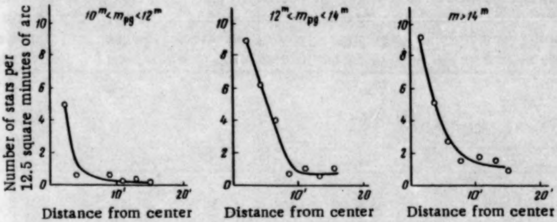

Fig. 5

The color index–stellar magnitude diagram of the cluster represents the main sequence which rises steeply upwards. Spectra are known for several of the cluster stars which are supergiants of type O and B. The nucleus of the cluster consists of several bright O9 and B0 stars forming an almost linear chain [5].

TABLE 3

BD	Sp (HDE)	Sp [8, 9]	m_{pg}	CI	μ_α	μ_δ
+23°3761	B	B0 II	9.22	0.32	—0".003	—0".005
+23 3767	G5	B1 Ia	--	—	—0.007	—0.011
+23 3762	B	B0.5 IIInn	9.72	0.42	—	—
+23 3759	B	B0 II	9.22	0.42	—0.004	—0.010
+23 3760		B8 Ia	7.66	0.65	—0.014	—0.013
+23 3747	B	B1 III	10.58	0.28	—	—
+23 3745	B	B0.5 Ib	9.12	0.32	—0.003	—0.002
+22 3782	B	O7	9.53	0.23	—0.006	—0.003
+22 3781	B	B0 IV	9.05	0.30	—	—
+23 3730	B	B8 Ib	10.17	0.90	—0.011	+0.001
+23 3752	K5		10.64	0.44	—0.017	—0.013
+22 3766	B9		9.47	0.17	0	—0.004
+23 3706		B9	8.79	0.59	—	—
+22 3778		B2 V : nne	10.22	0.22	—	—
+28 3728	F2		8.98	0.13	—0.005	—0.020
+22 3808	A2		9.10	0.12	—0.007	—0.001
+23 3756	A3		9.65	0.55	—0.006	—0.001
+22 3800	B5	B2 III : n	9.62	0.30	—0.006	—0.009

The cluster NGC 6823 and the stars of the association are apparently linked physically with the diffuse nebulae S199, S200, and S201 [11].

The average color excess for the stars of the cluster is CE = $0^m.95$. The total light absorption in the photographic region of the spectrum is therefore $A_{pg} = 4^m.45$. The apparent distance modulus is $m - M = 15^m.75$, while the true modulus is $m_0 - M = 11^m.30$ or r = 1800 ps. If the angular diameter of the cluster is taken as 15', the linear diameter is found to be equal to 7.9 ps. The linear diameter of the association is approximately equal to 50 ps (d ~ 100').

b) The Cluster NGC 6830

The cluster NGC 6830 has remained almost uninvestigated up to the present time. It is situated in the constellation Vulpecula, at a distance of 2° from NGC 6823 (Fig. 8), and has the following coordinates:

$$\alpha = 19^h46^m.8, \quad l = 27^\circ.5, \qquad \delta = +22^\circ50', \quad b = -3^\circ.0 \quad \Big| \; 1900.$$

According to Raab's description [12], the cluster is very irregular and does not contain many stars. The bright stars are situated eccentrically, without any appreciable concentration towards the center. According to Trumpler [2], the cluster is of type IV 2 p. The distance to the cluster has been measured many times by the method of diameters [2, 6]. In the present work, the photographic and photovisual magnitudes of 146 stars of the cluster were obtained. The plates used for the study of the cluster NGC 6823 were also used for the investigation of NGC 6830.

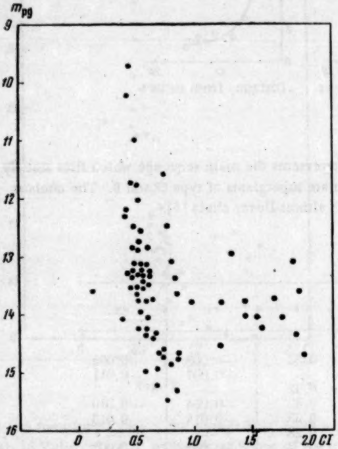

Fig. 6

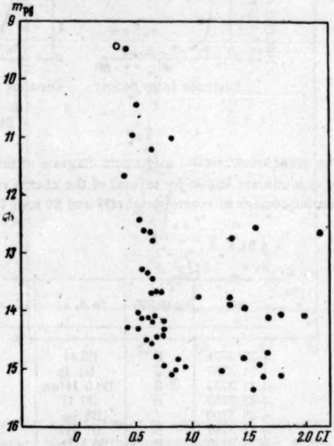

Fig. 7

The number of stars of given magnitudes were obtained for seven annular zones. On the basis of the stellar counts it has been established that the cluster contains about 70 stars brighter than the 15th magnitude.

TABLE 4

Zone	m_{pg}	CI	n
1	12.34	0.56	12
2	13.54	0.61	21
3	13.64	0.64	19
4	13.64	0.68	15
5	13.55	0.65	10
6	13.80	0.72	9

Fig. 5 gives the radial distribution of the stars of various magnitudes. The diameter of the cluster, determined from the stars with $10^m < m_{pg} < 12^m$, is 13', while from stars with $12^m < m_{pg} < 14^m$ it is larger, namely, 18-20'. It is possible that the dimensions of the cluster are even larger than this, but the density of stars in the outermost regions of the cluster is very small. Using the method of stellar counts, Raab [12] found the angular diameter of the cluster to be 15-18'. The diameter of the cluster, corrected for light absorption in the Galaxy, is 21' [6]. Other investigators have determined the angular diameter of the central, brightest region of the cluster, which is equal to 8-10'. Although there is no appreciable concentration of stars towards the center of the cluster, a study of the distribution of stars in the cluster shows that the concentration of bright stars towards the center is more pronounced than that of the faint ones. This is also shown by the average photographic magnitudes determined separately for each of the concentric zones (Table 4).

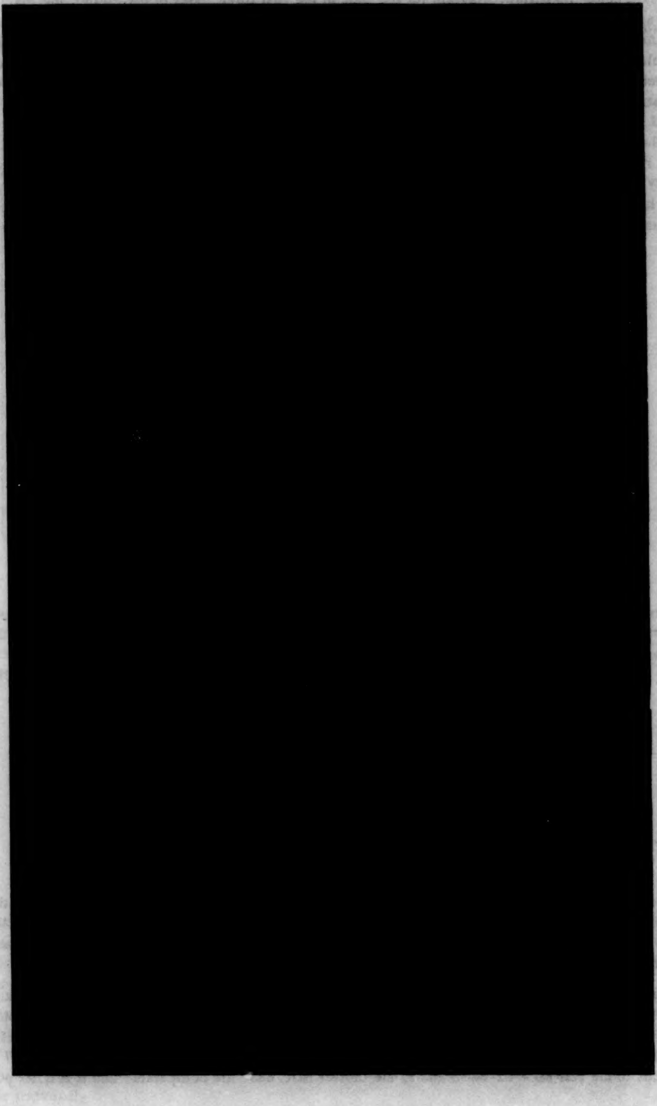

Fig. 8

The color index–apparent magnitude diagrams were constructed for each zone separately. In Fig. 6, which represents the color–magnitude diagram for the stars in the first three zones of the cluster, the main sequence is fairly clearly marked. The scatter of points in the diagram is possibly due to an irregular distribution of absorbing matter. According to Collinder [13], there is a dark nebula projected against the cluster. This is also shown by the irregularities of the background in the central part of the cluster. A large part of the stars situated in the outer zones also lie on the main sequence (Fig. 7) and, apparently, some of them are members of the cluster. A group of stars on the color index–stellar magnitude diagram with apparent magnitudes of about 14^m and color indices CI > $0^m.75$ are of interest. These stars are situated mainly in the first four zones. Their concentration is particularly high in the third zone. Their position on the diagram corresponds to the region of bright giants. It should be noted that the main sequence has the form which is characteristic of the stellar clusters that contain high-luminosity stars. The vertical end of the main sequence extends to $4^m.5$; therefore it would be expected that there are high-luminosity stars in the cluster under investigation. However, available information on the spectra of the stars does not as yet support this hypothesis. The spectra of the stars according to the HDE system are given below.

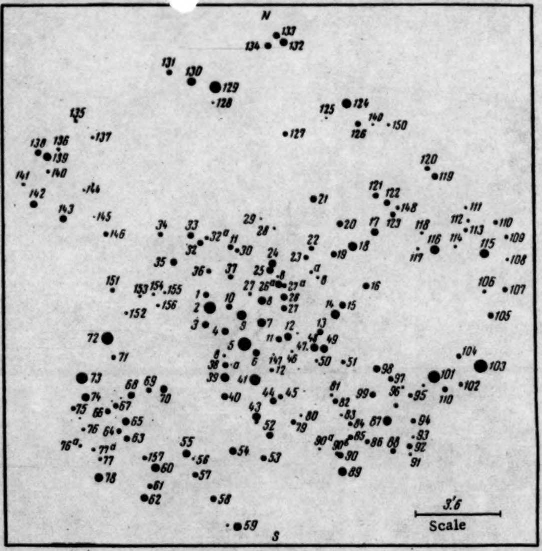
N
133
134
132
131
130
129
128
125
124
140
150
126
127
135
138
136
137
139
140
141
142
144
143
145
146
120
119
21
121
122
148
111
110
20
17
123
118
112
113
109
116
114
115
18
19
117
108
34
33
32a
11
31
30
29
28
22
23
24
25
26
8
a
35
36
37
27
26a
27a
28
27
16
106
107
151
153
154
155
1
10
8
2
156
152
14
15
105
3
4
9
7
12
13
72
5
11
47
48
49
71
6
147
46
50
51
104
103
38
a
12
98
97
101
102
73
68
69
39
41
81
99
96
95
110
74
70
40
44
45
82
75
66
67
43
80
83
84
87
94
65
52
79
76
64
63
93
76a
77a
55
90a
90b
85
86
88
92
77
157
56
54
53
90
91
60
57
89
78
61
62
58
3'.6
Scale
59
S

Fig. 9. NGC 6823

The average color excess of the stars of the cluster is CE = $0^m.72$. The absorption of light in the direction of of the cluster is $A_{pg} = 3^m.38$. The apparent distance modulus, determined from the color index–stellar magnitude diagram is $m - M = 14^m.50$. The true distance modulus is $m_0 - M = 11^m.12$ or r = 1680 ps. If the angular diameter of the cluster is 20', then this corresponds to a linear diameter of 9.7 ps.

The star BD + 22° 3836 is situated at a distance of 15' from the center of the cluster. According to the data of the HDE catalog its spectrum is B3, according to Reference [8] its spectral class is B1 II. The photographic magnitude of the star is $m_{pg} = 9^m.40$, the photovisual magnitude is $m_{pv} = 9^m.02$, and the color excess is CE = $= 0^m.88$. The apparent distance modulus is $m - M = 15^m.30$ and the true modulus $m_0 - M = 11^m.17$ or r = 1710 ps. The distances to the star BD + 22° 3836 and to the cluster NGC 6830 are comparable and it is quite possible that this star is a member of the cluster. It should be pointed out that, according to Reference [8], in addition to BD + 22° 3836, several stars of early spectral classes have been discovered in the vicinity of the cluster. According to the list of Merrill and Burwell [14], there is an 11^m star with an emission spectrum B(5) e at a distance of 22' from the center of the cluster. The coordinates of the star are: $\alpha_{1900} = 19^h48^m.2$; $\delta_{1900} = +22°26'$.

The proper motion of some stars in the cluster and in its vicinity has been determined [10]; the list of the stars is given below.

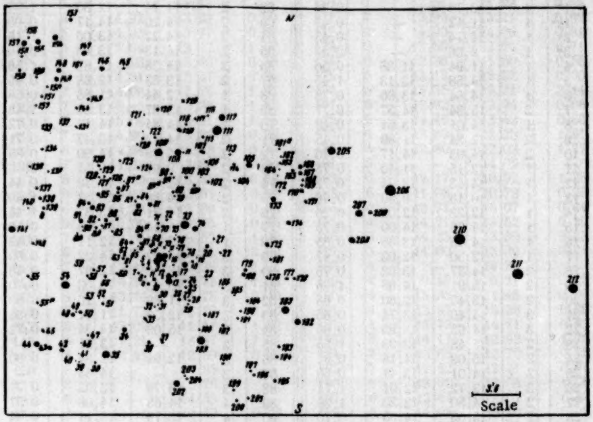

Fig. 10. NGC 6823

The average proper motion of these stars ($\mu_\alpha = -0''.008$, $\mu_\delta = -0''.003$) is almost the same as that of the cluster NGC 6823. The distances to the clusters NGC 6830 and NGC 6823 are also comparable. It is interesting to note that the radial velocity of the star BD + 22° 3836 (V_r = +4 km/sec) is equal to the radial velocity of the star BD + 22° 3781 which is a member of the cluster NGC 6823 [15].

TABLE 5

№	BD	Sp (HDE)
103	+22°3829	A2
116	—	A5
72	+22°3837	B8
73	+22°3837	B9
2	—	B9
5	—	B8

TABLE 6

BD	Sp (HDE)	μ_α	μ_δ
+22°3837	B8	−0".009	+0".004
+22°3837	B9	−0.009	+0.003
+22°3825	B3	−0.004	−0.007
+22°3829	A2	−0.012	−0.012

On the basis that the distances, radial velocities, and the proper motions of the clusters NGC 6823 and NGC 6830 are almost the same, it may be surmised that the two clusters are linked physically and are the most concentrated nuclei of an association in Vulpecula. However, it should be pointed out that as yet the information on the radial velocities of the stars in these clusters is very meager.

If the cluster NGC 6830 does belong to the association, then the angular dimensions of the latter can be taken to be 200'; this corresponds to linear dimensions of 100 ps.

A. M. Gor'kii
Ural State University

Received December 23, 1956

CATALOG OF STARS

Cluster NGC 6823

№	Zone	m_{pg}	m_{pv}	CI	№	Zone	m_{pg}	m_{pv}	CI
1*	1	10.70	—	0.48	62	2	14.14	12.80	1.34
1a*	1	11.42	—	0.47	63	2	14.20	14.17	0.03
2*	1	11.74	—	0.45	64	2	14.22	13.06	1.16
3*	1	9.66	—	0.52	65	2	14.13	13.43	0.70
4	1	11.94	11.38	0.56	66	2	14.38	12.82	1.56
5	1	14.58	13.13	1.45	67	2	13.33	12.68	0.65
6	1	14.64	13.86	0.78	68	1	12.44	11.86	0.58
7	2	15.34	14,57	0.77	69	1	15.37	13.94	1.43
8	1	14.01	13.61	0.40	70	2	14.84	14.12	0.72
9	2	12.34	11.89	0.45	71	2	14.13	13.42	0.71
10	2	14.93	14.17	0.76	72	2	15.78	14.90	0.88
11	1	12.15	11.40	0.75	73	2	9.97	9,51	0.46
12	1	14.46	13.74	0.72	74	2	12.02	11.58	0.44
13	1	10.15	9.69	0.46	75	2	14.86	13.37	1.49
14	1	12.22	12.02	0.20	76	2	14.81	13.37	1.44
15	1	14.76	14.00	0.76	77	1	14.14	13.55	0.59
16	1	14.45	13.80	0.65	78	1	12.54	12.11	0.43
17	1	12.50	12.03	0.47	79	3	14.82	14.22	0.60
18	2	14.37	13.62	0.75	80	3	13.45	12.97	0.48
19	2	15.91	14.66	1.25	81	3	13.73	13.03	0.70
20	2	13.45	12.80	0.65	82	3	11.69	11.16	0.53
21	3	14.40	13.74	0.66	83	3	12.56	11.91	0.65
22	3	14.63	13.95	0.68	84	3	15.06	14.34	0.72
23	2	15.48	13.93	1.55	85	3	—	13.61	—
24	2	15.09	14.18	0.91	86	3	12.94	12.34	0.60
25	2	14.01	13.41	0.60	87	3	—	14.63	—
26	2	13.72	12.01	1.71	88	3	13.79	13.02	0.77
27	2	14.50	13.20	1.30	89	4	14.65	14.08	0.57
28	2	15.05	14.35	0.70	90	4	13.78	13.14	0.64
29	3	14.64	14.14	0.50	91	4	11.31	10.86	0.45
30	2	15.63	14.69	0.94	92	1	—	14.42	—
31	2	15.43	14.72	0.71	93	4	11.00	10.68	0.32
32	2	15.80	14.70	1.10	94	4	13.50	13.01	0.49
33	3	13.16	12.56	0.60	95	4	13.49	12.74	0.75
34	4	12.44	11.46	0.98	96	4	14.75	13.85	0.90
35	5	10.46	9.37	1.09	97	4	12.49	11.39	1.10
36	4	14.46	13.46	1.00	98	4	14.13	13.13	1.00
37	4	15.48	14.65	0.83	99	4	15.56	14.59	0.97
38	5	15.08	14.09	0.99	100	4	14.82	13.26	1,56
39	6	14.25	13.65	0.60	101	4	15.39	13.55	1.84
40	6	14.55	13.84	0.71	102	4	14.10	13.23	0.87
41	5	14.85	14.18	0.67	103	4	15.75	13.82	1.93
42	6	13.16	11.73	1.43	104	5	14.23	12.63	0.60
43	6	11.91	11.47	0.44	105	6	11.94	11.33	0.61
44	7	11,58	9.51	2.07	106	5	14.77	13.81	0.96
45	6	13.54	12.85	0.69	107	5	—	12.16	—
46	5	—	14.37	—	108	5	11.59	11.17	0.42
47	5	—	15.17	—	109	5	10.73	10.14	0.59
48	5	14.21	12.90	1.31	110	6	13.45	11.21	2.24
49	5	14.56	13.03	1.54	111	6	9.12	8.80	0.32
50	4	12.11	11.95	0.16	112	7	12.56	12.11	0.45
51	3	14.36	13.58	0.78	113	6	14.48	13.56	0.92
52	3	14.44	13.57	0.78	114	5	15.49	13.82	1.67
53	4	14.41	13.75	0.66	115	6	14.76	13.95	0.81
54	4	10.64	10.20	0.44	116	7	14.86	13.08	1.78
55	6	13.14	12.51	0.63	117	6	15.23	14.29	0.94
56	3	13.84	13.23	0.61	118	6	—	14.42	—
57	3	—	14.96	—	119	7	—	13.75	—
58	4	—	14.37	—	120	7	12.20	10,10	2.10
59	4	—	14.80	—	121	7	14.88	12.85	2.03
60	2	14.83	13.96	0.87	122	6	14.88	14.07	0.81
61	2	14.10	13.38	0.72	123	6	13.65	12.92	0.72

Remarks (to pp. 830 and 831). For the stars marked (*), the photographic magnitudes and color indices have been taken from Becker [1].

(continued)

№	Zone	m_{pg}	m_{pv}	CI	№	Zone	m_{gp}	m_{pv}	CI
124	4	14.73	13.35	1.38	169	7	14.71	13.65	1.06
125	5	—	14,57	—	170	7	12.54	11.99	0.55
126	4	14.92	13.93	0.99	171	7	13.90	13.21	0.69
127	5	14.63	13.77	0.87	172	6	14.90	14.09	0.81
128	5	15.04	13.47	1.57	173	6	13.55	12.84	0.71
129	5	13.98	13.40	0.58	174	6	12.36	11.80	0.56
130	5	14.31	13.47	0.84	175	5	13.12	12.52	0.60
131	7	14.06	12.74	1.32	176	5	15.35	13.21	2.14
132	7	15.15	13.33	1.82	177	6	13.62	12.94	0.68
133	7	15.06	13.91	1.15	178	6	14.10	13.42	0.68
134	7	14.90	14.08	0.82	179	4	13.89	12.28	1.61
135	6	14.96	14.18	0.78	180	4	13.80	12.03	1.77
136	7	14.78	13.83	0.95	181	5	—	14.62	—
137	6	14.09	13.47	0.62	182	6	12.17	10.92	1.25
138	6	13.15	12.64	0.51	183	6	11.08	10.73	0.35
139	6	14.82	13.89	0.93	184.	4	13.71	13.07	0.64
140	6	15.00	14.25	0.75	185	4	14.21	13.52	0.69
141	7	10.55	9.53	1.02	186	3	14.33	13.80	0.53
142	6	13.84	13.25	0.69	187	3	14.00	13.39	0.61
143	7	13.62	12.38	1.24	188	4	—	14.30	—
144	7	14.76	13.72	1.04	189	4	9.46	9.21	0.25
145	8	13.24	12.75	0.49	190	4	15.35	14.45	0.90
146	8	11.75	11.29	0.46	191	4	13.97	13.28	0.69
147	8	13.09	11.47	1.62	182	4	14.73	14.11	0.62
148	8	15.21	13.47	1.74	193	6	14.17	12.42	1.75
149	8	13.45	12.60	0.85	194	7	13.65	12.70	0.95
150	8	—	14.35	—	195	7	12.82	12.21	0.61
151	8	—	13.76	—	196	6	13.90	12.84	1.06
152	8	—	14.53	—	197	6	12.44	12.07	0.37
153	8	10.76	10.49	0.27	198	5	14.08	13.30	0.78
154	8	11.43	10.85	0.58	199	6	13.23	12.75	0.48
155	8	11.72	11.16	0.56	200	7	11.80	11.38	0.42
156	8	15.68	14.39	1.29	201	7	12.76	12.24	0.52
157	8	14.41	12.12	2,29	202	5	13.06	12.34	0.72
158	8	15.12	14.38	0.74	203	5	—	14.07	—
159	8	14.80	13.30	1.50	204	5	—	14.19	—
160	8	14.91	13.62	1.29	205	8	10.05	9.47	0.56
161	8	—	14.53	—	206	8	9.40	9.00	0.40
162	8	—	13.77	—	207	8	10.92	10.59	0.33
163	8	—	13.91	—	208	8	10.80	10.27	0.53
164	7	—	14.11	—	209	8	13.78	13.15	0.63
165	7	13.85	13.10	0.75	210	8	9.47	9.28	0.19
166	7	12.98	11.41	1.57	211	8	9.47	9.30	0.17
167	7	13.10	12.42	0.68	212	8	9.26	9.10	0.16
168	7	15.45	13.82	1.63					

Spectra

№	Sp	№	Sp	№	Sp
1*	09	111	B0,5 I b	206	G0
1a*	B0	183	A3	207	A2
2*	B2	189	G0	210	A3
3*	09	35	K0	211	B9
13	09	54	F0	212	A0
73	K0	141	K5		

Cluster NGC 6830

№	Zone	m_{pg}	m_{pv}	CI	№	Zone	m_{pg}	m_{pv}	CI
1	2	13.30	12.86	0.44	66	3	13.62	12.74	0.86
2	1	10.96	10.45	0.51	67	3	12.66	12.01	0.55
3	1	15.14	12.50	2.64	68	3	13.34	12.72	0.62
4	1	13.37	12.52	0.85	69	2	—	13.93	—
5	1	10.25	9.83	0.42	70	2	—	12.73	—
6	1	13.54	13.06	0.48	71	3	14.38	13.80	0.58
7	1	11.72	11.25	0.47	72	3	9.74	9.30	0.44
8	1	12.01	11.50	0.52	73	4	10.41	9.90	0.51
9	1	—	11.63	—	74	4	12.65	12.07	0.58
10	1	13.45	12.87	0.58	75	4	14.12	13.57	0.55
11	1	13.79	12.78	0.99	76	4	15.13	13.52	1.61
12	1	12.74	12.22	0.52	77	4	15.05	13.78	1.25
13	2	13.79	12.54	1.25	78	2	11.60	10.85	0.75
14	2	12.46	11.98	0.48	79	2	14.60	13.86	0.74
15	2	13.14	12.64	0.50	80	2	14.86	14.05	0.81
16	3	13.14	12.54	0.60	81	2	14.98	14.40	0.58
17	4	14.13	12.13	2.00	82	2	13.35	13.78	0,57
18	3	12.48	11.70	0.78	83	3	14.92	14.23	0.69
19	3	13.20	12.65	0.55	84	3	14.70	13.83	0.87
20	3	13.72	12.00	1.72	85	3	13.74	13.12	0.62
21	3	14.01	12.56	1.45	86	3	14.08	13.47	0.61
22	3	13.75	13.11	0.64	87	3	12.92	11.58	1.34
23	2	13.74	13.23	0.51	88	4	13.93	12.49	1.44
24	2	12.20	11.77	0.43	89	3	12.83	12.23	0.60
25	2	12.27	11.87	0.40	90	3	13.60	13.48	0.12
26	2	13.08	12.27	0.81	91	4	14.95	13.38	1.57
27	1	14.70	13.08	1.62	92	4	15.12	12.85	2.27
28	3	14.73	14.00	0.73	93	4	14.06	13.55	0.51
29	2	15.48	14.70	0.78	94	4	14.14	13.55	0.59
30	2	14.09	13.71	0.38	95	4	14.57	13.95	0.62
31	2	13.29	12.84	0.45	96	4	—	14.72	—
32	3	14.04	12.46	1.56	97	3	15.30	14.45	0.85
33	3	13.53	13.02	0.51	98	3	12.88	12.35	0.53
34	3	13.71	13.20	0.51	99	3	—	13.07	—
35	2	13.53	12.96	0.57	100	2	14.24	12.65	1.59
36	2	14.54	13.30	1.24	101	4	11.04	10.22	0.82
37	2	14.40	13.75	0.65	102	5	15.16	13.38	1.78
38	1	13.44	12.85	0.59	103	5	9.48	9.05	0.43
39	1	11.74	11.23	0.51	104	5	14.52	13.92	0.60
40	2	13.20	12.66	0.54	105	5	14.74	13.10	1.64
41	1	—	11.45	—	106	5	14.33	13.59	0.74
42	1	14.26	13.66	0.60	107	6	13.81	12.75	1.06
43	2	—	12.35	—	108	6	14.89	13.96	0.93
44	2	13.34	12.84	0.50	109	6	14.84	13.96	0.88
45	2	14.26	13.75	0.51	110	4	13.68	13.00	0.68
46	1	13.96	13.44	0.55	111	5	14.27	13.85	0.42
47	2	—	14.03	—	112	5	—	13.41	—
48	2	13.25	12.62	0.63	113	5	—	13.92	—
49	2	12.85	12.37	0.48	114	5	14.18	13.52	0.64
50	2	14.63	13.76	0.87	115	5	10.97	10.50	0.47
51	2	14.66	13.96	0.70	116	4	11.67	11.27	0.40
52	2	13.35	12.89	0.46	117	4	15.02	14.17	0.85
53	3	—	11.94	—	118	5	—	14.11	—
54	3	13.75	12.31	1.44	119	5	12.76	12.11	0.65
55	3	13.57	11.65	1.92	120	5	15.10	14.27	0.83
56	3	—	13.75	—	121	4	14.31	13.80	0.51
57	3	15.20	14.51	0.69	122	4	14.37	13.63	0.74
58	3	14.70	12.75	1.95	123	4	13.36	12.59	0.77
59	4	12.53	10.99	1.54	124	5	12.65	10.52	2.13
60	3	13.08	11.20	1.88	125	5	14.44	13.75	0.69
61	4	14.20	13.45	0.75	126	5	13.30	12.75	0.55
62	4	14.05	12.27	1.78	127	5	13.56	12.66	0.80
63	3	14.37	12.47	1.90	128	5	—	13.97	—
64	3	14.38	13.70	0.68	129	5	11.26	10.62	0.64
65	3	—	12.24	—	130	6	12.75	11.41	1.34

(continued)

№	Zone	m_{pg}	m_{pv}	CI	№	Zone	m_{pg}	m_{pv}	CI
131	6	13.27	12.68	0.59	139	6	12.42	11.90	0.52
132	6	12.65	12.02	0.63	140	5	15.35	13.84	1.51
133	6	14.12	12.45	1.67	141	6	14.77	14.10	0.67
134	6	13.62	12.91	0.71	142	5	14.08	12.11	1.97
135	6	13.69	13.05	0.64	143	5	13.85	12.52	1.33
136	6	14.11	13.45	0.66	144	5	14.84	13.40	1.44
137	6	—	13.88	—	145	4	14.94	14.17	0.77
138	6	13.80	12.47	1.33	146	4	13.46	12.81	0.65

LITERATURE CITED

[1] W. Becker and J. Stock, Z. Astrophys. 34, 1 (1954).

[2] R. Trumpler, Lick Observatory Bull. 14, 154 (1930).

[3] R. Zug. Lick Observatory Bull. 16, 119 (1935).

[4] W. Becker and V. Osvalds, Astronomische Nachrichten 227, 4 (1949).

[5] V. E. Markarian, Soobshch. Biurak. Obs. 11, 34 (1951).

[6] K. A. Barkhatova, Astron. J. (USSR), 27, 180 (1950).

[7] W. W. Morgan, A. E. Whitford and A. D. Code, Astrophys. J. 118, 318 (1953).

[8] W. W. Morgan, A. D. Code and A. E. Whitford, Astrophys. J. , Suppl. 14, 11, 41 (1955).

[9] W. A. Hiltner, Braulio Jriarte, Astrophys. J. 122, 185 (1955).

[10] Trans. Astr. Obs. Yale University 25 (1954).

[11] V. F. Gaze and G. A. Shain, Izv. Krymsk. Astrofiz. Obs. 9, 123, (1952).

[12] S. Raab, Lund. Medd. 2, No. 28 (1922).

[13] P. Collinder, Lund. Ann. 2 (1931).

[14] P. W. Merrill and C. G. Burwell, Astrophys. J. 110, 387 (1949).

[15] D. Popper, Astrophys. J. 111, 495 (1950).

ON THE INTERPRETATION OF THE EMISSION SPECTRUM OF LONG-PERIOD VARIABLE STARS. I.

V. G. Gorbatskii

The emission in lines of hydrogen from long-period variable stars for the post-maximum time is due to recombination in the inner layers of atmosphere, where the hydrogen was initially ionized. The effect of L_α-radiation, which escapes from these layers, on the state of the upper layer of the atmosphere is considered. It is shown that the atoms of neutral metals in the outer layers of the atmosphere of the star are ionized by the L_α-radiation and thus the opacity of the upper layers decreases. The appearance of bright lines belonging to neutral metals in the post-maximum spectrum of long-period variable stars is the result of the recombination of ionized metal atoms.

At the present time, the following facts concerning the line-emission spectrum of the long-period variables are firmly established [1].

1. At the time near the maximum of luminosity, absorption lines of neutral metals are superimposed on the bright hydrogen lines, while most of the H_α and H_β emission is screened by molecular absorption bands. Therefore, at this time there is a layer, which contains un-ionized metals, above the atmospheric layer producing the emission of the bright hydrogen lines.

2. When the luminosity of the star decreases the screening of the bright lines by molecular bands decreases; the absorption lines due to the neutral metals weaken and disappear. Consequently, the concentration of neutral metals above the hydrogen-line emitting layer decreases and the optical thickness of the absorbing layers, determined by the presence of metals and molecules (TiO, ZrO, etc.), correspondingly decreases.

3. Simultaneously with the disappearance of the absorption lines of the metals, in the spectrum of the star there appear bright lines of neutral metals whose intensity reaches a maximum approximately halfway along the falling branch of the light curve.

In this work it is shown that the appearance of the bright lines of the metals in the spectrum of the star and the decrease of the optical thickness of the absorbing layers can be explained by the ionization of the metal atoms in this layer by the L_α-line radiation emerging from the deeper layers of the atmosphere. The L_α-line quanta are produced in the same layer as the quanta of the Balmer-series lines as the result of the recombination of ionized hydrogen atoms, and some of the L_α-line quanta come out to the surface because of the Doppler effect. In the first section the number of L_α-quanta emerging from the layer is estimated and the dependence on the time of the number of emerging L_α-quanta is approximately determined. In the second section the ionization of metals in the outer layers of the atmosphere of a long-period variable is investigated and it is established that the number of L_α-quanta entering these layers is sufficient to keep the metals there in an ionized state for a period of the order of 10^7 sec. In the third section the theoretical intensity of the bright metal lines and the time during which they should be observed are estimated.

1. The Hydrogen-Line Emission After the Maximum of Luminosity of the Star

The presence of the bright lines of the hydrogen Balmer series in the spectra of the long-period variable stars was explained by V. V. Sobolev [2] from a theory of moving stellar envelopes. The basis of this explanation was the hypothesis that the long-period variables are hot stars surrounded by envelopes with a large optical thickness. The high-frequency radiation of the hot star ionizes the hydrogen in the inner layers of the envelope, which emit the bright hydrogen lines, while it does not reach the outer layers and a low-temperature spectrum with metallic-absorption lines and molecular-absorption bands is formed in these layers. This model agrees well with observations in the period up to the maximum of the light curve. However, it cannot be be used for investigating the emission of hydrogen lines by the star after the maximum. During this period the bright hydrogen lines, partially screened by the outer layers of the atmosphere (the absorbing power of which gradually decreases, as was indicated above), are themselves superimposed on the molecular-absorption bands originating in the deeper layers [3]. Therefore, during this time the ionizing radiation from the hot star cannot ionize the hydrogen in the layer where the bright hydrogen lines are produced. Moreover, since the bright lines are still observed after the luminosity maximum (they are produced as the result of recombination), the degree of ionization must decrease, i.e., the layer producing the hydrogen-emission lines will "decay." This conclusion is also supported by the fact that after the maximum the bright lines rapidly weaken, although the absorption of the line radiation by the outer atmospheric layers decreases.

On the basis of the above fact, we will assume that the emission of hydrogen lines after the maximum of luminosity of the star occurs as the result of recombination in the layer of the atmosphere where the hydrogen was highly ionized before the maximum. On the other hand, the problem of why the ionizing radiation becomes ineffective and the problem of the way in which the emission from the atmosphere is related to the variation of the luminosity of the star are outside the scope of this paper and will be considered separately.

The problem of the "decay" of a hydrogen envelope was investigated earlier [4]. As can be shown, the "decaying" layer in the atmosphere of a long-period variable is optically thick, i.e., its optical thickness in the Balmer continuum during the process of recombination becomes greater than unity. For such an envelope T, the lifetime for recombination, is given by the expression

$$T \approx 10^{-17} nz, \tag{1}$$

where z is the thickness of the layer and n the number of hydrogen atoms in 1 cm^3. From observation it is known that $T = 10^7$ to $2 \cdot 10^7$ sec. From (1), with this value of T, we have that $nz \approx 10^{24}$; assuming that the thickness of the "decaying" layer is of the order of 10^{13} cm, we find that the total number of atoms in it is $N \approx 10^{51}$. Let us note that N can be estimated by other methods and, in particular, if we take into account that the number of atoms in the layer above the photosphere of the star is usually of the order of 10^{24}, we also obtain the same value of N.

During the "decay" of an optically thick ionized envelope each quantum of the Lyman continuum (L_C) produces one quantum of the Balmer series or of the Balmer continuum. Therefore, the number of Balmer-series quanta emitted by the medium must be of the same order of magnitude as the number of L_C-quanta present in the medium at the beginning of the "decay." If the medium originally was in a highly ionized state, then the number of Balmer-series quanta emitted will be of the order of N.

Unfortunately, we do not possess accurate photometric data on the emission of the Balmer-series lines by the long-period variables after the maximum of luminosity. According to Joy [5], the emission in the bright lines during the maximum of luminosity of the star o Ceti is about one per cent of the total radiation of the star in the visible part of the spectrum. Consequently, we can assume that $H_{Ba} = 10^{32}-10^{33}$ ergs/sec. Taking into account the reduction of the intensity of the bright lines after the maximum, we find that during the total time from the luminosity maximum to the disappearance of the emission lines 10^{50}-10^{51} Balmer-series quanta are emitted. This number agrees with the value of N found above.

As the ionized layer "decays" one L_α-quantum is produced from each L_C-quantum. A considerable number of these quanta escape from the medium because of the Doppler effect and, having penetrated into the outer unionized layer of the stellar atmosphere, have a substantial influence on its state. In particular, the L_α-quanta ionize the metal atoms, thereby decreasing the transparency of the outer layers of the atmosphere. In considering the processes taking place in the outer layers of the atmosphere, we will use the asymptotic expression for κN_α, the number of L_α-quanta escaping from the "decaying" medium in 1 sec. From the equations given in Reference [4] which describe the emission in the line L_α during "decay," for a sufficiently large t ($t > t_0$, where $t_0 \gg 1/\kappa$) we can find that

$$\varkappa N_\alpha \approx N^+(t_0)\sqrt{q\varkappa}\, e^{-\sqrt{q\varkappa}(t-t_0)}. \tag{2}$$

Here t is the time from the instant when the medium began to "decay," $N^+(t_0)$ the number of ionized atoms in the medium at time t_0, $q = \frac{10^{17}}{nz}$ and $\kappa = \frac{c}{2u}\frac{dv}{dz}$, where u is the mean thermal velocity of the atoms and $\frac{dv}{dz}$ is the velocity gradient in the medium. In the conditions for the "decay" of the atmospheres of the long-period variables $\kappa > 10^{-5}$ and, consequently, Equation (2) is already valid when $t \geq 10^6$ sec. For t between 10^5 and 10^6 sec, a relatively small number of quanta escape from the envelope. It must be noted that of all the L_α-quanta produced in the medium, only about 10% escape, while the rest are destroyed in collisions of the second kind or in the ionization of hydrogen atoms from excited states. Keeping this circumstance in mind and also taking into account the uncertainty in the values of the parameters q and κ, we will assume that (2) is valid for $t > 0$ $(t_0 = 0)$; taking $\sqrt{q\kappa} \approx 10^{-6}$, from (2) we find that

$$\varkappa N_\alpha \approx 10^{44} e^{-10^{-6}t}. \tag{3}$$

Equation (3) will be used in the following during the the investigation of the ionization of metals in the outer layers of the atmosphere of the star.

2. Ionization of Metals in the Outer Layers of the Atmospheres of Long-Period Variable Stars

Let us investigate the influence of the L_α-quanta on the state of the outer layers of the atmosphere in which the hydrogen is neutral.

An L_α-quantum entering the outer layer of the atmosphere is scattered by the hydrogen atoms. The optical thickness of these layers for the L_α lines is very large and the quantum experiences a very large number of scatterings. However, the scattering of the quantum will be interrupted by one of the following processes which lead to the disappearance of the L_α-quantum:

a) the absorption by neutral metal atoms whose ionization energy is less than the L_α-quantum energy,

b) the absorption of the L_α-quantum by a hydrogen atom which is in an excited state,

c) the collision of excited hydrogen atoms with electrons in which the excitation energy of the atom is transformed into the kinetic energy of the electron (collision of the second kind).

Since the optical thickness of the atmosphere, determined by the absorption by metal atoms and excited hydrogen atoms, is large compared to unity, the L_α-quantum cannot escape from the atmosphere without going through one of the processes listed above, even if a velocity gradient exists. Let us find the number of L_α-quanta destroyed through these processes in 1 cm³ in 1 sec. The number of quanta destroyed is

$$\begin{aligned} &\text{a) } s n_m n_\alpha, \\ &\text{b) } p n n_\alpha^2, \\ &\text{c) } l\, n n_e n_\alpha, \end{aligned} \tag{4}$$

where n_α, n, n_m, and n_e are the numbers of L_α-quanta, hydrogen atoms, neutral metal atoms, and free electrons, respectively. The quantities l, p, and s are given by the expressions

$$l = \frac{g_2}{g_1}\frac{h\nu_{12}}{\sigma_{12}\Delta\nu_{12}} v_e \sigma, \quad p = \frac{g_2}{g_1}\alpha'_{2c}\frac{ch\nu_{12}}{\sigma_{12}\Delta\nu_{12}}, \quad s = \alpha c, \tag{5}$$

where ν_{12} is the frequency of the L_α-line, $\Delta\nu_{12}$ is the width of this line, v_e is the mean thermal velocity of the electrons, σ is the effective cross section for the collisions of the second kind, α'_{2c} and α are the absorption coefficients for the absorption of L_α-quanta by excited hydrogen atoms and by neutral metal atoms, respectively, and $\sigma_{12} = \frac{8\pi h\nu_{12}^3}{c^3}$.

Using fixed values and assuming $\Delta\nu_{12}/\nu_{12} \approx 10^{-3}$, then from (5) we get

$$l \approx 3\cdot 10^{-21}, \quad p \approx 2.5\cdot 10^{-21}, \quad s \approx 3\cdot 10^{9}. \tag{6}$$

In order to evaluate the branching ratios for the processes leading to the destruction of L_α-quanta in the outer layers of the atmosphere, we will determine the density of hydrogen atoms in this region. We will use the few results available on the photometery of the spectra of the long-period variables. According to Scott [6], the number of CaI and CaII atoms which take part in the formation of the absorption lines at the brightness maximum in a column with a cross-sectional area of 1 cm^2 in the atmosphere of ο Ceti is $N_{Ca} = 10^{18}$. On the other hand, from the work of Fujita [7] it follows that the relative abundances of the elements in the atmosphere of another long-period variable χ Cygni are of the same order of magnitude as the cosmic abundances. Assuming that in the atmosphere of ο Ceti the ratio N_{Ca}/N_H is 10^{-6}-10^{-7}, we find that $N_H = 10^{24}$-10^{25}.

From the data on the translational velocity of the atmosphere in long-period variables, as well as the data on their radii supported by interferometric measurements, we can conclude that the thickness of the atmsophere of long-period variables is 10^{13}-10^{14} cm. There is no evidence of a large density gradient in the atmosphere. Therefore, for the average concentration of hydrogen atoms in the atmosphere of ο Ceti we have the value $n \approx 10^{11}$ and taking into account that $n_m/n \approx 10^{-4}$, we obtain for the concentration of metal atoms $n_m \approx 10^7$. It appears that these values of $\underline{n}$ and n_m are characteristic of most of the long-period variables since ο Ceti is a star which is representative of the stellar type under consideration.

Using the values of the coefficients $\underline{l}$, $\underline{p}$, and $\underline{s}$ found above, we see that for each L_α-quantum destroyed through the ionization of a metal atom there are $10^{-12}\, nn_e/n_m$ quanta destroyed by the collisions of the second kind and $10^{-12}\, nn_\alpha/n_m$ quanta absorbed by the excited hydrogen atoms. Since originally $n/n_m \approx 10^4$, $n_e \ll n_m$, and $n_\alpha \ll 10^8$, then the most important process is the absorption of the L_α-quanta by the metal atoms. As the degree of ionization of the metals increases, the other processes become more and more important.

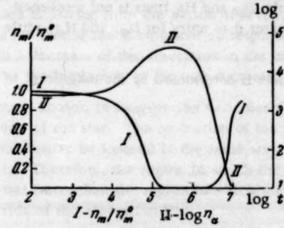

Fig. 1. The variation of the relative concentration of metals and of the concentration of L_α-quanta in the atmosphere of the star with time (the time is reckoned from the maximum of brightness). I) n_m/n_m^0; II) log n_α

In the collisions of the second kind the energy of the quanta goes into the kinetic energy of the electrons. The excess energy of the L_α-quanta after the metal atoms and the excited hydrogen atoms have been ionized is also transformed into electron kinetic energy. As the result of this, the number of collisions of the first kind, which produce excitation in the hydrogen atoms, increases, and this leads to an increase in the number of L_α-quanta in the atmosphere. Inasmuch as the collisions of the first kind can only accelerate the ionization of metal atoms, we will not consider this factor further, since even without this process the degree of ionization of the metals in the atmosphere becomes high.

Let us determine the way in which n_m, the concentration of metal atoms, varies with the time. If we assume that all the metals have the same absorption coefficient of recombination C' and that the ionization of the metals is only due to L_α-quanta, then we obtain the following equation:

$$\frac{dn_m}{dt} = C' n_m^+ n_e - s n_m n_\alpha. \tag{7}$$

The variation of the concentration of L_α-quanta, n_α, is given by the equation:

$$\frac{dn_\alpha}{dt} = \frac{F_\alpha}{V} - s n_m n_\alpha - p n_\alpha^2 \cdot n - l n n_e \cdot n_\alpha. \tag{8}$$

Here F_α is the number of L_α-quanta entering the un-ionized layer per sec and V the volume of this layer. Since the hydrogen in this layer is not ionized, $n_e = n_m^+$. In addition, we have that

$$n_m^0 = n_m + n_m^+. \tag{9}$$

where n_m^0 is the density of the neutral metal atoms before the ionization process starts. The initial conditions for Equations (7) and (8) are as follows: at time $t = 0$

$$n_m = n_m^0, \quad n_\alpha = 0.$$

Equations (7) and (8) were solved numerically, taking (9) into account; the values of the coefficients $\underline{l}$, $\underline{p}$, and $\underline{s}$ found above were used in the calculation and the following values of the constants were adopted: $n = 10^{11}$, $n_m/n = 10^{-4}$; $V = 10^{42}$ cm^3, $C' = 10^{-14}$, while F_α was determined from (3). The solution of the equations is presented graphically in the figure. It is found that the metals in the outer layers of the atmosphere are rapidly ionized by the L_α-quanta. The concentration of the L_α-quanta even after the metals have been ionized remains low because of the collisions of the second kind and the ionization of hydrogen atoms from excited states. In a time of the order of 10^6 sec the magnitude of n_m/n_m^0 decreases to about 10^{-3} and n_α becomes approximately equal to 10^3. Because of this decrease of n_m, these layers become optically thin for the light of the metal lines.

The calculated value of the time in which the optical thickness of the outer atmospheric layers, determined by the absorption due to the metals and the molecular bands, changes appreciably was found for the case considered to be less than that observed. According to observation, the absorption lines of the metals disappear after $5 \cdot 10^6$ to -10^7 sec. However, taking into account the fact that the values of a number of quantities (V, n_m^0, C', etc.) which we have used are very approximate and also that Equation (3) is an approximation, we can consider that the agreement between theory and observation is satisfactory.

The magnitude of n_α can be determined independently. From observations [8] it is known that after the brightness maximum the intensity ratio $H_\gamma / H_\delta > 1$, but is considerably smaller than the theoretical value; the line H_α is considerably weaker than H_γ; the line H_α is not visible, while the higher members of the Balmer series are practically not absorbed. The continuous spectrum next to the H_α and H_β lines is not weakened. Thus, the optical thickness of the layer lying above the emitting layer is greater than unity for H_α and H_β, while it is of the order of unity for H_γ.

The optical thickness of the layer for the lines of the Balmer series is determined by the magnitude of n_α. The optical thickness for the line H_γ is given by the expression

$$\tau_{H_\gamma} = n_2 \alpha_{H_\gamma} \Delta r, \tag{10}$$

where Δr is the thickness of the layer and n_2 is found from the relation

$$\frac{n_2}{n} = \frac{g_2}{g_1} \frac{h\nu_{12}}{\sigma_{12}\Delta\nu_{12}} n_\alpha. \tag{11}$$

Substituting the values of the constants into (11), we find

$$n_2 \approx 10^{-13} n n_\alpha.$$

Since $\tau_{H_\gamma} \approx 1$, $\alpha_{H_\gamma} \approx 10^{-14}$, and $n \cdot \Delta r = 10^{24}$-$10^{25}$, from (10) and (11) we obtain $n_\alpha = 10^2$-10^3. Consequently, the magnitude of n_α found from the observations agrees with the magnitude calculated from the investigation of the ionization process taking place in the outer layers of the atmosphere. This is a confirmation of the ideas presented above concerning the influence of the L_α radiation on the state of the atmospheres of long-period variable stars.

3. The Formation and Development of the Line-Emission Spectrum of Low Excitation

As the luminosity of a long-period variable falls, bright lines belonging to the atoms of FeI, MgI, and other metals appear in the spectrum. It was shown above that the metal atoms in the outer layers of the atmosphere are ionized by the radiation emitted from the lower layers of the atmosphere. The metal ions when recombining with free electrons must produce emission in the metal lines. Thus, the appearance of the bright metal lines is the result of the existence of ionized metals in the atmosphere of the star.

Simultaneously with the bright lines of the neutral metals, bright lines of FeII and other doubly ionized atoms are observed for a considerable time after the brightness maximum. It appears that these lines are produced in the same regions of the atmosphere as the bright hydrogen lines because in the regions where the hydrogen is ionized, the iron is mainly in the doubly-ionized state (the FeII ionization potential is less than the energy of an L_α-quantum). In these layers the number of FeII atoms is small and therefore the number of FeII atoms recombining is also small. Consequently, the bright lines of the neutral metals are mainly produced in the outer layers of the atmosphere.*

The following features of the low-excitation emission spectrum (of the neutral metals) have been observed [1, 3]:

1. The intensity of the bright lines relative to that of the continuous spectrum is small and only the strongest of them have a relative intensity comparable to that of the bright hydrogen lines at the luminosity maximum. However, when the bright lines have the maximum intensity, the continuous spectrum of the star weakens considerably, so that the absolute intensities of the bright FeI, MgI, and other lines are considerably lower than the absolute intensities of the hydrogen lines at the luminosity maximum.

2. The bright line frequently arises on the violet side of the corresponding absorption line and gradually gets stronger. At the same time the absorption line weakens so that when the intensity of the bright line is at a maximum, the absorption line is no longer visible.

3. As the luminosity decreases, the number and the intensity of the bright lines increase and reach their maximum value approximately halfway along the descending branch of the light curve; after this, the bright lines gradually disappear and at the minimum of luminosity only the strongest lines remain.

The increase of the intensity and the number of bright metal lines after the luminosity maximum can be explained as arising from the action of several factors. Firstly, the degree of ionization of the metals increases and the number of recombinations correspondingly increases. Secondly, the increased ionization of the metals leads to a decrease of the absorption in the metal lines. Moreover, the relative intensities of the bright lines increase as the luminosity of the star decreases and the continuous spectrum gets correspondingly weaker.

As is known, in long-period variables the expansion velocity of the atmosphere decreases with distance from the center of the star. The ionization of the metals must proceed gradually, "layer by layer", the outer layers being the last to be ionized, in the same way as it took place, according to V. V. Sobolev, in the envelope of N Herculis. Therefore, the region in which the bright metal line is originally formed moves away from the center of the star faster than the region in which there is absorption by the metals, so that the bright line appears on the violet side of the absorption line.

Let us calculate approximately the energy E_m emitted in the bright metal lines after the degree of ionization of the metals has reached its maximum value, from the following equation:

$$E_m = C' n_m^+ N_m^+ h\nu. \tag{12}$$

Taking $C' = 10^{-14}$, $n_m^+ = 10^7$, $N_m^+ = 10^{49}$, and $h\nu \approx 10^{-11}$, we find $E_m \simeq 10^{31}$ ergs/sec. From this it follows that the energy radiated in all the bright lines is of the same order of magnitude as the energy radiated at the luminosity maximum in the hydrogen line H_δ alone. This energy is distributed among hundreds of metal lines. Therefore, at the time of the maximum, most of the bright metal lines are imperceptible, but as the luminosity falls, their relative intensities increase.

During the period of approximately 10^7 sec, the energy emitted in a 1 A interval of the continuous spectrum of o Ceti, at about λ 4150, decreases by a factor of 30 [6] (at longer wavelengths it decreases by a factor of 100 or more) and is equal to 10^{28}-10^{29} ergs/sec, while at the maximum the energy radiated in the same interval is 10^{30}-10^{31} ergs/sec. Since the energy radiated in a bright metal line is 10^{29}-10^{30} ergs/sec and the width of the line is 0.1-0.3 A, this line must be well marked after the decrease of the luminosity.

When the flux of L_α-radiation is sufficiently low, the recombination of the metal ions will no longer be compensated by ionization and the radiation from the atmosphere in the metal lines weakens. The lifetime T_1

---

* The problem of the origin of the FeII lines is investigated in the second part of this paper.

for the decay of the radiation in the metal lines is given by the expression

$$T_1 \cong \frac{1}{C' n_e^0}. \qquad (13)$$

Since $C' \approx 10^{-14}$ and $n_e^0 \approx n_m^0 = 10^7$, T_1 is found to be of the order of 10^7 sec which is in complete agreement with observation. The coefficients of recombination are not equal for the various metals. Because of this, the bright lines of the metals with small recombination coefficients must be observed longer than the lines of the metals with large recombination coefficients.

Thus, the main features of the line-emission spectrum of low excitation are explained if we assume that the metal atoms in the atmospheres of the long-period variables are ionized by the L_α-radiation escaping from the lower layers of the atmosphere.

SUMMARY

1. The emission in the bright hydrogen lines after the luminosity maximum of a long-period variable occurs as the result of recombination taking place in the lower layers of the atmsophere of the star where the hydrogen was initially ionized.

2. A fraction of the number of L_α-quanta produced during recombination, because of the Doppler effect, escapes from the "decaying" region into the outer layers of the atmosphere of the star and by ionizing the metal atoms decreases the optical thickness of these layers.

3. The ionized metal atoms on recombining emit line radiation, thus producing the line-emission spectrum of low excitation.

Received February 11, 1957

LITERATURE CITED

[1] P. Merrill, The Spectra of L-P Variable Stars (Chicago, 1940).

[2] V. V. Sobolev, Moving Stellar Envelopes [In Russian] (Leningrad State University Press , Leningrad, 1940).

[3] A. Joy, Astrophys. J., Suppl. 1, 2, 39 (1954).

[4] V. G. Gorbatskii, Vestnik LGU (Leningrad State Univ.) 13, 178 (1957).

[5] A. Joy, Astrophys. J. 63, 281 (1926).

[6] R. M. Scott, Astrophys. J. 101, 71 (1945).

[7] J. Fujita, Trans. International Astron. Union (1952).

[8] G. A. Shain, Doklady Akad.Nauk SSSR 44, 293 (1944).

VARIATION OF THE COEFFICIENT OF TRANSPARENCY OF THE ATMOSPHERE DURING THE TOTAL SOLAR ECLIPSE OF JUNE 30, 1954

B. D. Fomenko

The variation of the coefficient of transparency of the atmosphere has been investigated in the case of the integral flux and in the spectral regions 2900-5250 A, 5250-6250 A, and 6250-20,000 A during the total solar eclipse of June 30, 1954 and also investigated with the help of actinometric data obtained during other eclipses. Some features of the variation of the coefficient of transparency during the eclipse have been obtained. An estimate has been made of the variation of the thickness of the ozone layer as the result of its destruction at large eclipse phases. The influence of water vapor on the variation of the coefficient of transparency of the atmosphere has been evaluated.

In the course of the processing of observational data obtained during a total eclipse of the sun, it is very important for the astrophysicist to know the value of the coefficient of transparency of the atmosphere. For the absolute photometry of the solar corona, for the absolute photographic photometry, for the photometry in the various regions of the spectrum, and for a number of other problems, it is necessary to know the total coefficient of transparency of the atmosphere, as well as the coefficients of transparency for various spectral regions.

In practice, the coefficient of atmospheric transparency is usually determined from observations made before and after the eclipse [1, 2]. The same values are also used at the moment of the total phase; at best, a few observations are made during the partial phase of the eclipse. This approach to the determination of the coefficient of atmospheric transparency cannot be considered acceptable. During the course of an eclipse, the coefficient of atmospheric transparency must vary and this variation must proceed regularly, inasmuch as the spectral energy distribution in the solar radiation flux changes as the sun is being screened. In addition to these variations, there will be others due to local meteorological conditions. The detailed variation can only be found by means of special investigations. In these observations the transparency coefficient must be determined, not from the slope of the Bouguer line, but from one measurement made at a definite time. Up to the present time, such investigations during an eclipse have not been carried out.

The aim of the present work is to make up to some extent for the lack of such investigations; the contribution is limited because we restricted ourselves to the investigation of the variation of the transparency coefficient in the case of the integral flux and in the case of three spectral regions (2900-5250 A, 5250-6250 A, 6250-20,000 A) using actinometric and not spectrographic observations.

In order to carry out the actinometric observations, the author organized an expedition of the Stalingrad Pedagogical Institute to the area of the total solar eclipse. The expedition was situated on the territory of the kolkhoz "Red October" ($\varphi = 45° 48$, $\lambda = 40° 06$) near Tikhoretsk Actinometric and meteorological observations were made. Fourth-year students of the physico-mathematical faculty: L. Makeeva, T. Bakumova, I. Gerasimenko, V. Matveev, L. Val'dman, I. Sadovova, took part in the investigations.

In addition to our measurements, actinometric measurements carried out at our request at the agricultural meteorological station "Giant" (near Sal'sk) were used in the present work. The observations were made under the direction of B. A. Klepatskii; besides there, the data obtained during the eclipse of June 9, 1945, observed in Karadag (Crimea) [3], the eclipse of May 9, 1948, observed in Tartu [4] and near Vladivostok [5], and the observational data on the eclipse of June 19, 1936, obtained at Ak-Bulak by the geophysical expedition of the Kazakh University [6] were used.

To determine the variation of the coefficient of atmospheric transparency, we had to calculate the intensity of the direct solar radiation at the top of the atmosphere in the case of the integral flux and three regions of the spectrum for different phases of the eclipse, taking into account the effect of solar limb darkening, to compare our results with the results obtained from the processing of the data of other eclipses, and to estimate the influence of meteorological factors on the variation of the coefficient of atmospheric transparency. In addition, an estimate of the variation of the thickness of the ozone layer and of the absorption of long-wave radiation by water vapor were made.

Results of Observation

The direct solar radiation in the region of the kolkhoz "Red October" was measured by us with the help of a Savinov-Ianishevskii actinometer No. 2, both without filters and with yellow OQ_1 and red RQ_2 Schott filters.

The sensitive element of the actinometer was a blackened (on the side facing the sun) disc which had 36 thermocouple junctions attached to it; the disc was fixed into a tube with a number of diaphragms. A detailed description of the Savinov-Ianishevskii actinometer is given in the monograph of V. N. Kedrolivanskii and M. S. Sternzat [7].

The current from the thermopile was measured by means of a needle galvanometer (φ) No. 55751 with a sensitivity of $1.5 \cdot 10^{-6}$ amp. The galvanometer deflection is proportional to the intensity of solar radiation. The instrument is sensitive to the wavelength interval 2900-20,000 A.

The actinometer was calibrated at the Stalingrad geophysical observatory on October 17, 1954, and once again on October 7, 1955, after the observatory actinometer had been calibrated by the State Actinometric Inspection Office. For the comparison of our actinometer with the observatory standard, we adhered to the general specifications recommended for the calibration of actinometric instruments [8].

The sensitivity of the actinometer was found to be equal to 6.305 $\frac{\text{mv} \cdot \text{cm}^2/\text{min}}{\text{cal}}$; the conversion factor is 0.0134 $\frac{\text{cal}}{\mu\text{a} \cdot \text{cm}^2 \cdot \text{min}}$. The results of the 1954 and 1955 calibrations differ by 0.2%. The error with which the full intensity of the solar radiation can be measured is 1.3%.

Glass Schott filters OQ_1 and RQ_2 were used for the measurement of radiation intensity in separate regions of the spectrum. As has been shown by A. Gordov [9], the optical properties of these filters (coefficients of transmission and reflection) are unaffected by a high intensity of radiation. Moreover, their cut-off is very sharply defined, at λ 5250 A in the case of the yellow filter and λ 6250 in the case of the red [10].

According to K. Feussner [11], a variation of temperature by 60° produces a shift of the spectral curve by 10 $m\mu$ and a decrease of the transparency of the filter by 3%.

In the case of a layer $\underline{x}$ mm thick, the amount of radiation transmitted, V_λ, is given by the expression

$$V_\lambda = f_\lambda^x,$$

where f_λ is the amount transmitted by a layer 1 mm thick. It is necessary to take into account the reflection at both surfaces of the filter. It has been shown by A Gordov [9] that the reflection coefficient R is practically the same for different wavelengths: R = 0.913. The total transmission coefficients of the filters OQ_1 and RQ_2 were determined by graphical integration. The areas s_1, bounded by the ordinates λ_1 and λ_2 and the curve of the spectral intensity of the solar radiation falling on the filter,

$$s_1 = \int_{\lambda_1}^{\lambda_2} I(\lambda) P^m(\lambda) \, d\lambda,$$

and s_2, bounded by the ordinates λ_1 and λ_2 and the curve of the spectral intensity of the radiation transmitted through the filter,

$$s_2 = R \int_{\lambda_1}^{\lambda_2} I(\lambda)\, P^m(\lambda)\, d\lambda,$$

were measured; in the above expressions I (λ) is in arbitrary units and has been taken according to the data of Abbot , P(λ) is the coefficient of atmospheric transparency [12], and m is the mass of the atmosphere; m has been taken for the mid-point of the eclipse and is equal to 1.7. $D = s_1/s_2$, the filter transmission coefficient, is equal to 0.810 for OQ_1 and 0.848 for RQ_2. The thickness of OQ_1 is 2.11 mm, that of RQ_2 is 1.80 mm.

From the filter transmission coefficients obtained, it was possible to find the losses in the filters. The results of the measurement of the direct solar radiation are given in Table 1.

TABLE 1

Time	n	S	n_1	S_1	n_2	S_l	S_i	S_s
14 hr 00 m	93.5	1.252	61.0	1.010	52.2	0.824	0.186	0.242
10	93.4	1.250	61.0	1.010	52.2	0.824	0.181	0.245
20	93.2	1.248	60.9—61.0	1.005	52.2	0.824	0.181	0.243
30	93.0	1.246	60.6	0.998	52.2	0.824	0.174	0.248
40	92.7	1.240	60.6	1.000	52.0	0.823	0.167	0.240
50	92.0	1.230	60.5	0.996	52.0	0.823	0.173	0.234
15 hr 00 m	91.0	1.216	60.0	0.985	52.0	0.823	0.162	0.231
10	89.0	1.189	56.5	0.931	48.5	0.766	0.165	0.258
20	85.1	1.136	54.7	0.901	46.0	0.726	0.175	0.235
30	81.0	1.082	52.5	0.864	43.2	0.684	0.180	0.218
40	69.9—70.0	0.948	46.5	0.766	38.0	0.602	0.164	0.183
45	64.0	0.855	42.0	0.693	34.7	0.550	0.144	0.162
50	57.5	0.770	38.4	0.634	31.6	0.500	0.134	0.136
55	51.0	0.680	34.2	0.563	28.2	0.443	0.120	0.117
16 hr 00 m	42.0	0.561	27.8	0.459	23.6	0.374	0.105	0.102
05	33.0—33.1	0.441	22.0	0.364	18.5	0.293	0.070	0.078
10	24.0	0.320	15.6	0.257	14.2—14.3	0.225	0.050	0.045
15	16.0	0.213	11.3	0.186	10.2	0.162	0.024	0.027
20	6.8	0.095	5.0	0.083	4.5—4.6	0.072	0.011	0.017
22	4.9	0.066	3.5	0.059	3.1	0.050	0.009	0.007
25	2.0	0.0268	1.5	0.025	1.4	0.022	0.003	0.0016
28	0.0	0.0	0.0	0.0	0.0	0.0	0.0	0.0
30.5	0.8—0.9	0.0114	0.6	0.0098	0.5—0.6	0.0092	0.0016	0.0014
35	6.9—7.0	0.087	4.8	0.080	4.3	0.069	0.011	0.006
37	10.0	0.134	7.0—7.1	0.117	6.4	0.101	0.016	0.017
40	15.0	0.200	10.4	0.173	9.7	0.153	0.020	0.027
45	22.5	0.300	15.7	0.258	14.5	0.228	0.030	0.042
50	31.0	0.414	20.5	0.336	18.5	0.293	0.043	0.078
17 hr 00 m	46.0	0.614	28.7	0.474	25.8	0.407	0.064	0.143
10	60.0	0.806	37.0	0.606	31.0	0.489	0.117	0.200
20	75.0	1.000	45.3	0.746	36.2	0.573	0.174	0.253
30	81.3	1.08	52.0	0.857	41.8	0.660	0.197	0.223
40	82.5	1.10	52.2	0.862	43.0	0.680	0.177	0.243

n, n_1, n_2 denote the galvanometer scale readings without a filter, and with the yellow and red filters, respectively; S, S_1, and S_l denote the radiation intensities in cal/ cm²·min without a filter, with a yellow filter, and with a red filter, respectively. Losses in the filters have been taken into account. The measurements made with the use of the filters lead to the selection of three spectral regions: 1) from 2900 to 5250 A, 2) from 5250 to 6250 A, and 3) from 6250 A to 20,000A. The first can be obtained as the difference $S - S_1$; we will call it the short-wave region and denote $S - S_1$ by S_s; the second, obtained as the difference $S_1 - S_l$, will be called the intermediate region and $S_1 - S_l$ will be denoted by S_i; the third region is directly selected by the filter RQ_2 and we will call it the long-wave region – S_l .

Variation of the Coefficient of Atmospheric Transparency During an Eclipse

The coefficients of atmospheric transparency for the partial phases of an eclipse were calculated from the formula

$$S_m = S_0 P_m^m,$$

where S_m is the intensity of the direct solar radiation at the earth's surface, S_0 is the intensity of the radiation at the top of the atmosphere (when there is no eclipse, S_0 is the solar constant, whose value was taken by us in accordance with the European scale, taking into account the distance between the earth and the sun); the noneclipse value of S_0 for July 1 was taken equal to 1.82 cal/ cm²·min; P_m is the coefficient of transparency; m is the "mass" of the atmosphere according to Bemparade.

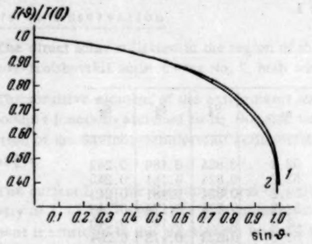

Fig. 1. Solar limb darkening in the case of the total flux. Curve 1 – from observation; curve 2 – from Chandrasekhar's exact solution.

It should be pointed out that the problem of the value of S_0 has not yet been settled as can be seen from the analysis of the latest results given by Waldmeier [13] in the second revised edition of his book "The Results and Problems of Solar Investigations."

The coefficients of atmospheric transparency for individual spectral regions were calculated from an analogous formula:

$$S_{\Delta\lambda} = S_{0,\Delta\lambda} \cdot P_{\Delta\lambda}^m,$$

where $S_{\Delta\lambda}$ is the radiation intensity at the surface of the earth and $S_{0,\Delta\lambda}$ that at the top of the atmosphere.

In order to determine P_m and $P_{\Delta\lambda}$ it is necessary to know S_0 and $S_{0,\Delta\lambda}$ for the partial phases of an eclipse. This quantity was calculated by a graphical integration with limb darkening of the sun taken into account. In the calculations we have used the data on limb darkening given by Allen [14] and Aller [15], inasmuch as their results are practically identical for $\sin\vartheta = 0.954$, where ϑ denotes in degrees the distance from the center of the solar disc. Curve 1 of Fig. 1 gives the limb darkening in the case of the itegral flux and curve 2 the limb darkening obtained from Chandrasekhar's exact solution. For the calculation of S_0 for different phases of an eclipse, the whole solar disc was subdivided into 12 zones, including the central one. The width of the first 8 inner zones corresponds to a change of 0.10 in $\sin\vartheta$, and that of the outer zones to a change of 0.05 in $\sin\vartheta$. The relative brightness of each zone was put equal to the relative brightness of the center of the corresponding zone. The values of $S_{0,\Delta\lambda}$ for the different eclipse phases and for the spectral regions at λ = 4330, 5900, and 7300 A were calculated in an analogous manner. The noneclipse values of $S_{0,\Delta\lambda}$ are 0.493 cal/ cm² min for the "short-wave" region, 0.245 cal/ cm² min for the "intermediate" region, and 1.082 cal/ cm²·min for the "long-wave" region. As has been pointed out by S. P. Popov [16], there are no generally accepted values of $S_{0,\Delta\lambda}$ for spectral regions selected by the OQ_1 and RQ_2 filters. Our values are different from those recommended by S. P. Popov by an insignificant amount: by 0.003, 0.004, and 0.001 absolute units, respectively.

The distribution of energy in absolute units in the solar spectrum was taken from a table given by K. Ia. Kondrat'ev [12]. The numerical data given by him are according to the 1948 U.S. pyroheliometric scale which is based on the Smithsonian measurements. Recently G. F. Sitnik [17] and E. A. Makarova [18] in the U.S.S.R. have measured the distribution of energy (in absolute units) in the spectrum of the center of the sun in the interval of 3500-8000 A.

The results of the calculation of S_0 and $S_{0,\Delta\lambda}$ for the different eclipse phases are given in Table 2.

In Fig. 2, curve 1 shows the variation of S_0 according to the data of Table 2; for comparison, curve 2 shows the variation of S_0 calculated without allowing for limb darkening.

If in the calculation of S_0 for the integral radiation flux, Chandrasekhar's results on limb darkening are used, then the value of S_0 at the phase 0.95 is 4% lower than that given by us in Table 2, while at phase 0.4 the discrepancy is 0.3%.

The calculated coefficients of atmospheric transparency for the integral radiation flux and for the "short-wave," "intermediate," and "long-wave" regions of the spectrum are presented in Table 3. In the course of the eclipse, the mass of the atmosphere in the region of the kolkhoz "Red October" changed from 1.350 to 2.2. The calculation of the coefficient of transparency for the second half of the eclipse was terminated at the phase 0.2, since the measurements made towards the end of the eclipse were vitiated by the appearance of clouds.

TABLE 2

Phase	$S_{\bullet}$	$S_{0}, \Delta\lambda$		
		2900–5250 A	5250–6250 A	6250–20000 A
0.0	1.820	0.493	0.245	1.082
0.1	1.762	0.479	0.237	1.045
0.2	1.651	0.450	0.222	0.998
0.3	1.491	0.406	0.202	0.883
0.4	1.3098	0.354	0.174	0.772
0.5	1.093	0.294	0.147	0.658
0.6	0.865	0.231	0.115	0.524
0.7	0.615	0.162	0.082	0.374
0.8	0.389	0.1045	0.0521	0.2345
0.85	0.270	0.0742	0.0365	0.1603
0.9	0.1413	0.0340	0.0184	0.0893
0.93	0.0775	0.0175	0,0100	0.0502
0.95	0.0482	0.0102	0.0055	0.0323
0.97	0.0222	0.0043	0.0024	0.0152

TABLE 3

Phase	Integral flux	2900–5250 A	5250–6252 A	6250–20000 A	Phase	Integral flux	2900–5250 A	5250–6250 A	6250–200000 A
0.0	0.725	0.575	0.754	0.798	0.95	0.746	0.485	0.700	0.859
0.1	0.716	0.580	0.803	0.750	0.95	0.731	0.465	0.635	0.822
0.2	0.713	0.581	0.844	0.761	0.9	0.701	0.442	0.579	0.761
0.3	0.736	0.583	0.868	0.777	0.85	0.695	0.421	0.580	0.753
0.4	0.741	0.574	0.890	0.788	0.8	0.687	0.467	0.583	0.786
0.5	0.747	0.569	0.898	0.795	0.7	0.711	0.588	0.661	0.812
0.6	0.755	0.588	0.892	0.803	0.6	0.726	0.627	0.625	0.777
0.7	0.753	0.557	0.817	0.812	0.5	0.744	0.689	0.649	0.778
0.8	0.723	0.445	0.668	0.790	0.4	0.753	0.711	0.745	0.775
0.85	0.725	0.423	0.633	0.790	0.3	0.770	0.731	0.808	0.768
0.9	0.736	0.449	0.606	0.788	0.2	0.778	0.743	0.867	0.775

The behavior of the total transparency coefficient for the kolkhoz "Red October" is given in Fig. 3; in the same figure the variation of the transparency coefficient calculated without allowing for the solar limb darkining is also shown. We have also calculated the total coefficients of atmospheric transparency for the eclipses observed at the Agricultural Meteorological Station "Giant," in Ak-Bulak, Vladivostok, and Karadag. Numerical data are not given here for lack of space, but the curves for the variation of the total coefficient of atmospheric transparency are given in Fig. 4.

From Fig. 4 it can be seen that there is a similarity between the curves for the various eclipses which were observed at different places under different meteorological conditions: the coefficient of transparency decreases during the first half of the eclipse up to phase 0.75-0.8; then it increases considerably; after the total phase it decreases (up to phase 0.8-0.75), and then in the second half of the eclipse it begins to increase with decreasing phase of the eclipse. Variations arising out of meteorological conditions at the point of observation (kolkhoz "Red October" – first half of the eclipse, Ak-Bulak, AMS "Giant" – second half of the eclipse) are superposed on this regular variation. The symmetry of the curves can therefore be seriously distorted.

The curves for the coefficients of transparency calculated on the assumption that there is no solar limb darkening are markedly different from the curves calculated with the limb darkening taken into account. The eclipse itself results in a considerable decrease in the total coefficient of transparency (because of a lowered radiation flux), while the reddening of the radiation (because of the effect of limb darkening) acts in the opposite direction. The second effect counterbalances the first, and close to totality there is even an increase of the coefficient of transparency. At eclipse phases of 0.95, the total coefficient of transparency is on the average 3-5% higher than its value before the eclipse and, possibly, it increases even more as the phase increases further.

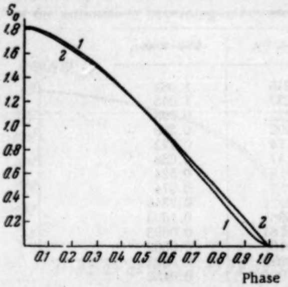

Fig. 2. The intensity of the direct solar radiation at the top of the atmosphere. Curve 1 – solar limb darkening taken into account; curve 2 – solar limb darkening not taken into account.

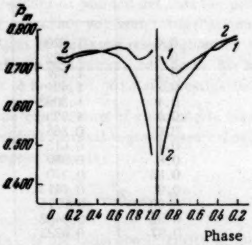

Fig. 3. The coefficient of atmospheric transparency for the integral flux (kolkhoz "Red October"). Curve 1 – solar limb darkening taken into account; curve 2 – solar limb darkening not taken into account.

The main atmospheric factors which influence the transparency of the atmosphere are ozone and water vapor. Therefore it is of interest to investigate the variations of the coefficients of transparency for the "short-wave" and "long-wave" regions of the spectrum. Fig. 5 shows the variation of the coefficient of transparency for the "long-wave" region, and Fig. 6 that for the "short-wave" region. The curves for Ak-Bulak, Karadag, and Tartu are given in the same figures. The numerical values of the coefficients which we have calculated are not given here for lack of space. In the case of Tartu, only the behavior of the curve is shown since absolute measurements of the radiation were not made.

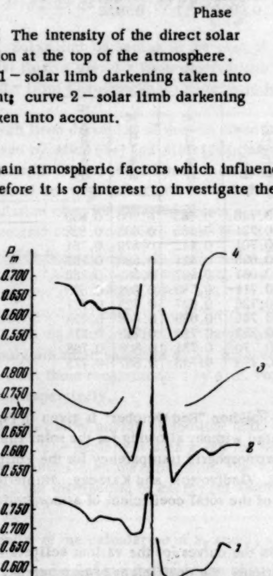

Fig. 4. The coefficient of atmospheric transparency for the integral radiation flux. 1) Ak-Bulak, 2) Vladivostok, 3) Karadag, 4) Agricultural Meteorological Station "Giant."

The values of $P_{\Delta\lambda}$ are not affected by the Forbes effect, since all the observations were made with the sun situated at zenith angles less than 68°. As has been shown by E. V. Piaskovskaia-Fesenkova [19], in the case of observations made with filters, as a rule, the relation between the logarithm of the intensity and the atmospheric mass remains linear up to a zenith distance of 81-83°. In another paper [20], E. V. Piaskovskaia-Fesenkova shows that for a blue filter (transmission-band width 200 mμ) $P_{\Delta\lambda}$ changes by 1% for a variation of the atmospheric mass from 2 to 6, while the change in the case of a red filter is only 0.1%. In our case the atmospheric mass did not exceed 3 and, consequently, the errors in $P_{\Delta\lambda}$ are less than 0.5% in the case of the "short-wave" region and less than 0.1% in the case of the "long-wave" region.

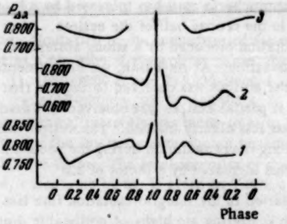

Fig. 5. The coefficient of atmospheric transparency for the spectral region 6250-20,000 A; 1) kolkhoz "Red October;" 2) Ak-Bulak; 3) Karadag.

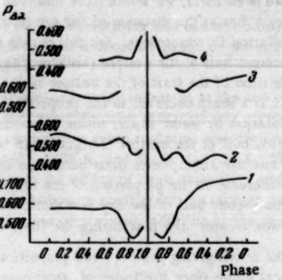

Fig. 6. The coefficient of atmospheric transparency for the spectral region 2900-5250 A; 1) kolkhoz "Red October;" 2) Ak-Bulak; 3) Karadag; 4) Tartu.

From the curves of the coefficient of transparency for the "long-wave" spectral region (Fig. 5) we see that there is a general tendency for the coefficient to increase towards the middle of the eclipse. The dips in the curves and the decrease of the coefficient during the second half of the eclipse and the dip in the curves constructed for the kolkhoz "Red October" are caused by an appreciable absorption of the radiation by water vapor.

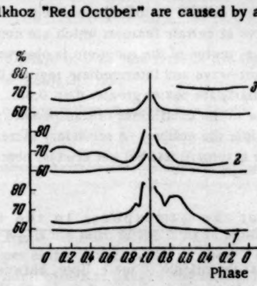

Fig. 7. The proportion of "long-wave" radiation in the integral flux at the top of of the atmosphere and at the surface of the earth; 1) kolkhoz "Red October;" 2) Ak-Bulak; 3) Karadag.

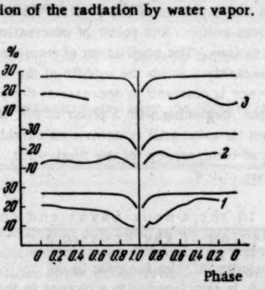

Fig. 8. The proportion of "short-wave" radiation in the integral flux at the top of the atmosphere and at the surface of the earth; 1) kolkhoz "Red October;" 2) Ak-Bulak; 4) Karadag.

In the case of the "short-wave" region of the spectrum (Fig. 6), the coefficient of transparency at the beginning of the eclipse is seen to decrease with increasing phase and only for phases greater than 0.85 does it increase by 5-7%. During the second half of the eclipse, there is a decrease until the phase is 0.9-0.85. At about a phase of 0.4, the coefficient is observed to increase again by 12 and 3%, respectively.

In order to determine the role played by the atmosphere, we have calculated the proportion of the "long-wave" and "short-wave" radiation present in the integral flux at the top of the atmosphere and compared these values with the ones observed. In Fig. 7 this comparison has been made for all the observation points in the case of the "long-wave" radiation, and in Fig. 8 for the case of the "short-wave" radiation.

As the eclipse phase increases, the proportion of "long-wave" radiation increases particularly sharply after phase 0.8. The experimental curve follows the theoretical curve (for the top of the atmosphere) and if the atmosphere had been ideal, we would have observed a symmetrical picture relative to the instant of maximum phase. It is known that as the distance of the sun from the zenith increases, the proportion of long-wave radiation in the total radiation flux increases. For this reason the experimental curves lie above the theoretical ones at the beginning of the second half of the eclipse (kolkhoz "Red October"). The atmospheric mass has increased by a factor of 1.4 from the time of the start of the eclipse to the time of phase 0.6 in the second half of the eclipse. After the phase 0.6 there is a sharp decrease in the proportion of the long-wave radiation produced by a strong absorption of long-wave radiation by water vapor, whose concentration increased at that time. At Ak-Bulak, the experimental curve for the first half of the eclipse is higher than in the second since the eclipse was observed during the first half of the day and the atmospheric mass decreased by a factor of 1.55. A partial eclipse was observed in Karadag; therefore the increase in the proportion of the long-wave component was less clearly marked. The eclipse was observed during the second half of the day and therefore the proportion of long-wave radiation during the second half of the eclipse was greater than that during the first. The atmospheric mass increased by a factor of 2.2

The curve giving the observed proportion of short-wave radiation in the integral radiation flux lies below the theoretical curve since the losses of short-wave radiation through scattering are high. A noticeable drop begins after phase 0.75. Thus, as the eclipse phase increases, the proportion of long-wave radiation in the integral solar radiation flux at the top of the atmosphere increases by 10% to the time of phase 0.98, while the proportion of short- wave radiation decreases by 8%. The proportion of the radiation in the intermediate region of the spectrum falls by 2%. The earth's atmosphere produces a serious distortion in these changes, particularly in the long-wave region of the spectrum. The proportion of long-wave radiation can increase by 15-18% at the middle of the eclipse as compared to the beginning of the eclipse. An increase in the concentration of water vapor can lead to a considerable decrease in the proportion of long-wave radiation and the latter can become less than the value at the top of the atmosphere.

From a comparison of the coefficients of atmospheric transparency for the various spectral regions determined for the various eclipses and points of observation, it is possible to arrive at certain features which are common to these observations. The coefficient of transparency for the long-wave region of the spectrum is observed to increase appreciably towards the middle of the eclipse, while in the short-wave and intermediate regions the coefficient of transparency is observed to decrease as the phase increases, particularly for phases greater than 0.65. At the middle of the eclipse, beginning with a phase of 0.9, there is a slight increase in the coefficient of transparency; it increases by 5-7%, but its value still remains considerably smaller than that before the eclipse. A secondary increase in the coefficient of transparency for the short-wave region of the spectrum is sometimes, but not always, observed at about a phase of 0.4.

Changes in the Ozone Layer and the Transparency of the Atmosphere in the Short-Wave Region of the Spectrum

We assume that the increase in the coefficient of transparency at the middle of the eclipse, between the phases of 0.9, is associated with a change in the thickness of the ozone layer. It is obvious that, in the limiting case, actinometric measurements can lead to a determination of the variations in the intensity of the solar radiation in the short-wave region of the spectrum, although detailed spectrographic observations should be made in the future. According to Kawabata [21], who observed the eclipse of June 19, 1936 in Tokyo, there is evidence that the concentration of ozone changed during the eclipse. In a very short note he points out that the ozone concentration dropped between the first and second contacts. N. Gerlow, Ollson, and Schüep [22] have measured the direct solar radiation in the region of the Chappuis absorption band with a Molle thermopile during the eclipse of July 9, 1945, which was observed in Lovånger (Sweden). They observed a decrease in the amount of ozone present form 0.3 cm at the beginning of the eclipse to 0.2 cm at the end. The authors hesitate to ascribe these changes to the action of the eclipse itself.

We have carried out calculations to determine the ozone concentration in the ozone layer during an eclipse and to determine the variations in the thickness of the layer. In these calculations we have used the following assumptions:

1) The formation of ozone and its decomposition [23, 24] take place under the action of short-wave solar radiation. The ozone is formed as the result of a photochemical reaction when oxygen absorbs radiation in the

Schuman (1750-2100 A) and the Hertzberg (2400-2600 A) spectral regions. The decomposition of ozone takes place under the action of radiation of longer wavelengths in the Hartley (2400-3600 A) and Chappuis (4400-6500 A) bands.

2) As the eclipse phase increases, the ratio of the intensities of the ozone-forming and ozone-destroying radiation decreases because of the effect of limb darkening. This must lead to a decrease in the ozone concentration and, consequently, to a decrease in the thickness of the ozone layer.

In the calculation of the intensities of the ozone-forming and ozone-destroying radiation at the top of the atmosphere as a function of the eclipse phase, the spectral region of the ozone-forming radiation was divided into two parts: 1) 1850-2200 A and 2) 2200-2600 A, while the region of ozone-destroying radiation was divided into five parts: 1) 2400-2600 A, 2) 2600-3000 A, 3) 3000-3400 A, 4) 4400-5000 A, and 5) 5000-6500 A. This division into spectral intervals was made so as to take better into account the effect of limb darkening, while the above widths for the intervals were chosen because calculated average absorption coefficients for oxygen and ozone are available for them. The total intensity of the ozone-forming and ozone-destroying radiation at the top of the atmosphere, calculated by us, is given in Table 4.

TABLE 4

Phase	$S_{0}.\ \Delta\lambda$ in abs. units		Phase	$S_{0}.\ \Delta\lambda$ in abs. units	
	ozone-forming	ozone-destroying		ozone-forming	ozone-destroying
0.0	0.00420	0.5973	0.8	0.000782	0.1352
0.2	0.00379	0.5539	0.85	0.000530	0.0923
0.4	0.00293	0.4461	0.9	0.000241	0.04388
0.6	0.00188	0.2904	0.93	0.000122	0.02478
0.7	0.00132	0.2063	0.95	0.0000675	0.01437

At the phase of 0.95, the ratio of the intensities of ozone-destroying and ozone-forming radiation has increased by a factor of 1.55.

The concentration of ozone in a layer at a height of 20-25 km was estimated from the Nicolet formula:

$$n_3 = 3\,\frac{K_{12}}{K_{13}}\,n_2^2\,\frac{1}{\left(1+\frac{n_3}{n_2}\,\frac{\alpha_3 S_3}{\alpha_2 S_2}\right)},$$

where K_{12}/K_{13} is the ratio of the rates of ozone-forming and ozone-destroying reactions, n_2 the number of oxygen molecules per unit volume, n_3 the number of ozone molecules per unit volume at equilibrium, α_2 and α_3 are the absorption coefficients of oxygen and ozone, and S_2 and S_3 the intensities of the ozone-forming and ozone-destroying radiation. The height of the layer has been taken as 20-25 km because the center of mass of the ozone layer is situated at a height of 22-23 km. Allen [14] gives it as 21 km; according to the measurements of A. P. Kuznetsov [25] near Moscow, the center of mass is situated at a height of 23 km.

The concentration of oxygen molecules has been taken equal to $2.8 \cdot 10^{17}$ [24], the ratio K_{12}/K_{13} for this layer according to Schroer [23] is equal to $4 \cdot 10^{9}$. The average value of α_2, the oxygen absorption coefficient, is $8.34 \cdot 10^{-6}$ cm^{-1}, the average ozone absorption coefficient α_3 is equal to 1.43 cm^{-1} [23]. According to Mitra [24], at equilibirum the ratio n_3/n_2 does not exceed 10^{-3}.

The variation of the ozone concentration and the variation in the thickness d of the ozone layer, for initial thicknesses of 0.3 and 0.36 cm, as functions of the eclipse phase are given in Table 5.

The concentration of ozone in the 20-25 km layer when there is no eclipse is found to be in good agreement with Schroer's data. As can be seen from the table, when the phase is 0.95, the thickness of the ozone layer is $1/3$ of the original thickness; we should observe considerable changes in the thickness of the ozone layer during the last 10 minutes before the second contact and the first 10 minutes after the third contact. These variations should result in a considerable increase in the intensity of the solar radiation in the short-wave region since there is considerably less absorption in the ozone layer. At this moment we should observe an increase in the atmospheric transparency in the short-wave region of the spectrum.

TABLE 5

Phase	$n_3 \cdot 10^{18}$	d, cm		Phase	$n'_3 \cdot 10^{18}$	d, cm	
0.0	3.85	0.300	0.360	0.8	3,30	0.252	0.308
0.2	3.75	0.292	0.351	0.85	3.15	0.244	0.294
0.4	3.67	0.285	0.343	0.9	2.98	0.225	0.276
0.6	3.57	0.277	0.338	0.93	2.75	0.210	0.257
0.7	3.52	0.271	0.329	0.95	2.56	0.200	0.240

In order to determine the radiation-intensity variations that should be observed during an eclipse, we have calculated the intensity of the solar radiation after traversal of the ozone layer in the case when the thickness remains constant and when it changes. The calculations were made for two values of the initial thickness of the ozone layer; 0.3 cm and 0.36 cm. The calculations were carried out for the spectral region 2900-5250 A, both for the whole region with the use of the weighted-mean value of the ozone absorption coefficient, as well as for the separate narrow regions; the two results were then compared. The attenuation of the radiation in the ozone layer was determined from the formula

$$S_{\Delta\lambda} = S_{0,\Delta\lambda} \cdot 10^{-\alpha_3 dm},$$

where α_3 is the ozone absorption coefficient, d the thickness of the ozone layer, and m the atmospheric mass.

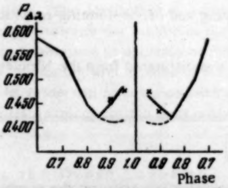

Fig. 9. Variation of the coefficient of atmospheric transparency produced by a change in the thickness of the ozone layer in the region of the kolkhoz "Red October."

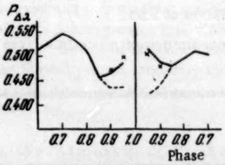

Fig. 10. Variation of the coefficient of atmospheric transparency produced by a change in the ozone-layer thickness in the case of Ak-Bulak.

The calculations have shown that by the time of phase 0.95 there has been an increase in the intensity of radiation by 4.5-4%. This increase is adequate to account for the increase of the coefficient of transparency for the short-wave region between the phases of 0.85.

Figures 9 and 10 show the observed variations of the coefficient of transparency during large phases (full line) and the variations which would have been observed at the kolkhoz "Red October" and Ak-Bulak if the ozone-layer thickness were constant (dotted line). The figures refer to the case d = 0.36. The crosses denote values of $P_{\Delta\lambda}$ calculated from the molecular scattering and the absorption by the ozone, with the variations of the ozone layer taken into account.

As was shown by G. M. Dobson, A. V. Brewer, and B. M. Cwilong [26], after the passage of a cold front a considerable increase in the amount of ozone present is observed; the increase is up to 13%, or more, of the average value which is equal to 0.3 cm. The kolkhoz "Red October" was at the rear of a cold front. G. M. Dobson points out that the region in which the amount of ozone increases is considerable and can be up to 1000 km long.

The calculations made show that the decrease in the thickness of the ozone layer by a third is completely adequate to account for the increased transparency of the atmosphere in the short-wave region by 5-7%. This effect can be observed, apparently up to a phase of 0.9, in a strip 200-350 km wide on either side of the central track of the eclipse.

The Absorption of Solar Radiation by Water Vapor and Atmospheric Transparency in the Long-Wave Region of the Spectrum

The water vapor in the atmosphere is the main factor responsible for the absorption of solar radiation. Its concentration in the atmosphere determines, not only the transparency of the atmosphere in the long-wave region of the spectrum, but also the atmospheric transparency for the integral flux.

It is known that the long-wave region of the spectrum contains a large number of water-vapor absorption bands, of which the main ones are : a, 0.8 μ, $\rho\sigma\tau$, Φ, Ψ, and Ω. The difficulty in evaluating the absorption of radiation in these bands (in addition to the complexity of the system) is also due to the fact that the experimental data on the radiation absorption have been obtained from laboratory measurements carried out at temperatures and pressures which are different from those observed in the actual atmosphere. Almost every investigation is based on the well-known measurements of Fowle [27], although they were obtained for low water-vapor concentrations, while the Mügge-Meller [28] formula is often used for the calculation of the total absorption.

Various methods for the calculation of the absorption of solar radiation have been reviewed by K. Ia. Kondrat'ev [29, 30]. All of the existing methods are applicable to actual conditions and special problems can be solved; as has been correctly pointed out by W. Godson [31], it is usually only possible to carry out an approximate calculation in the case of some simplified problem.

To determine the total absorption of long-wave radiation by water vapor it is useful to use, not the absorption coefficients, but the absorption function. E. S. Kuznetsov [32, 33] has recently developed an exact mathematical method for determining the coefficients of absorption when the experimental results are presented in the form of a transmission function. For each transmission band the function has been given as

$$P(W) = \gamma e^{-\alpha W} + (1 - \gamma) e^{-\beta W}.$$

Here W is the amount of water vapor present in a column of atmosphere 1 cm^2 in cross section. The parameters α and β can be considered as "average" absorption coefficients for the particular band; α refers to a number of nonoverlapping regions whose total width is γ, while β refers to all the other absorbing regions with a width of $(1-\gamma)$.

A generalized transmission function was introduced for the whole of the long-wave region:

$$P(W) = \frac{\int_a^b S_\lambda e^{-k_\lambda W} d\lambda}{\int_a^b S_\lambda d\lambda},$$

where k_λ is the absorption coefficient and S_λ is the radiation intensity.

From the Kuznetsov generalized transmission functions, we have calculated the absorption of radiation in absolute units for the kolkhoz "Red October" during the eclipse (Table 6, second column); for comparison, the observed values of the absorption ΔS are given in the third column of Table 6. From the observed values we have calculated the generalized transmission function P(W) (fourth column) and these values are compared in Fig. 11 with the theoretical values of P(W) given by E. S. Kuznetsov (curve 1); in the same figure, P(W) according to Meller is shown by curve 2. The total moisture content in a column of the atmosphere pointing in the direction of the sun is given in the fifth column of Table 6; the unit used is centimeters of condensed water. The total moisture content W was calculated from S. I. Sivkov's formula [34]

$$W = 3.8 e_0^{0.66},$$

which was checked by observations in the region of Krasnodar (about 100 km from our observation point). In the above formula, e_0 denotes the absolute humidity in millimeters at the surface of the earth. The measured values of of e_0 are given in the sixth column of Table 6.

TABLE 6

Phase	ΔS from [33]	ΔS obs.	P (W)	W	e_0
14 hr 50 m	0.278	0.259	0.760	3.10	13.3
15 hr 10 m	0.317	0.316	0.707	3.12	15.5
0.0	0.327	0.356	0.670	3.49	18.0
0.1	0.322	0.340	0.675	3.69	18.7
0.2	0.303	0.313	0.680	3.79	18.8
0.3	0.277	0.272	0.691	3.88	18.8
0.4	0.243	0.227	0.705	3.98	19.1
0.5	0.208	0.193	0.706	4.07	18.9
0.6	0.156	0.150	0.715	3.18	17.9
0.7	0.109	0.103	0.724	4.04	18.0
0.8	0.073	0.077	0.670	3.63	17.9
0.9	0.029	0.025	0.704	4.46	18.8
0.95	0.0101	0.0092	0.671	4.71	19.1
0.9	0.0312	0.0302	0.645	4.81	19.1
0.8	0.079	0.0815	0.652	5.00	19.4
0.7	0.126	0.121	0.678	5.10	19.3
0.6	0.178	0.199	0.621	5.25	19.6
0.5	0.228	0.258	0.610	5.49	19.4
0.4	0.268	0.315	0.592	5.70	19.6
0.3	0.309	0.372	0.579	5.86	19.8
0.2	0.348	0.422	0.568	6.21	20.0

From the data given in the table it can be seen that up to values of 5 cm for the moisture content in the atmosphere, there is good agreement between the observed values for the absorption and those calculated by E. S. Kuznetsov's method; the discrepancy between the two does not exceed 2%, while the mean error is 1.6%; however, for a higher moisture content, there is a systematic deviation from the values of P(W) given by Kuznetsov, the deviation becomes larger with increasing W and reaches a value of 7.6% for W = 6.2 cm. This depends, not so much on the increase of W as the result of the increase of the optical thickness of the atmosphere, as on the increase of the absolute humidity of the atmosphere. This is seen from Fig. 12, where curve 1 shows the magnitude of radiation absorption during the eclipse if the humidity were constant (15.5 mm), while curve 2 shows the observed absorption in percent of the intensity of the long-wave radiation. It is seen that the relative absorption increases with increasing absolute humidity and is 9% higher at the end of the eclipse than at the beginning. It may be conjectured that for an absolute humidity of 19.5-20 mm and m = 2, there is an increase in the specific absorption

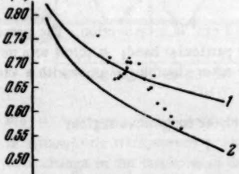

Fig. 11. The transmission function for water vapor; 1) according to E. S. Kuznetsov, and 2) according to F. Meller. The points denote values obtained from observation.

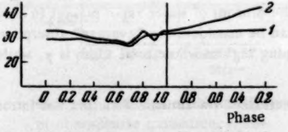

Fig. 12. The absorption of radiation by water vapor; 1) for constant humidity and 2) observed.

coefficient of water vapor. The existence of this effect in a laboratory experiment has recently been pointed out by A. M. Brounshtein [35]. For further verification of this, it is necessary to carry out special investigations for a real atmosphere.

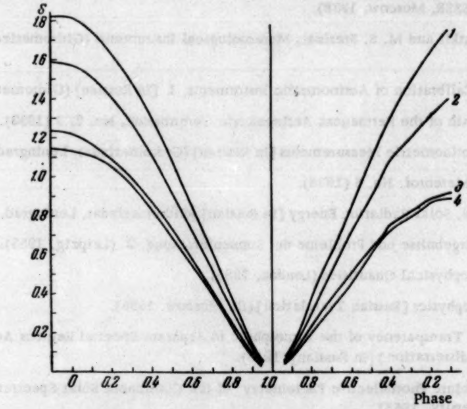

Fig. 13. The total variation in the direct solar-radiation flux; 1) at the top of the atmosphere; 2) after molecular scattering and absorption by ozone; 3) after absorption by water vapor; 4) observed at the surface of the earth.

The above calculations show that the variation of the transparency in the long-wave region of the spectrum and in the case of the integral radiation flux when the moisture content of the atmosphere increases, can be accounted for by an increased absorption by water vapor.

In conclusion, Fig. 13 shows the variations in the radiant flux that took place during the eclipse of June 30, 1954, as observed at the kolkhoz "Red October." Curve 1 denotes the intensity of the direct solar radiation at the top of the atmosphere, curve 2 the radiation intensity after scattering and ozone absorption, curve 3 that after absorption by water vapor, and curve 4 shows the observed intensity at the surface of the earth. The area between the curves represent the radiation losses,in absolute units,as the result of molecular scattering and ozone absorption, the absorption by water vapor, and the aerosol losses.

The work which we have carried out makes up to some extent for the lack of investigations of the variation of the coefficient of transparency of the atmosphere and the studies of the influence of atmospheric factors on these variations in the course of a solar eclipse.

Stalingrad Pedagogical Institute
P. K. Shtemberg
State Astronomical Institute

Received February 16, 1957.

LITERATURE CITED

[1] Report of the Expedition for the Observation of the Total Solar Eclipse of June 19, 1936. Vol. 1. [In Russian] (Izd. AN SSSR, Moscow, 1938).

[2] Report of the Expedition for the Observation of the Total Solar Eclipse of September 21, 1941 [In Russian] (Izd. AN SSSR, Moscow, 1949).

[3] S. I. Sivkov, "Actinometric and Meteorological Observation," Coll.: Solar Eclipses and Their Observation [In Russian] (GTTI, Moscow, 1954).

[4] Ia. E. Einasto, Biull. VAGO,* No. 15, (22) 10 (1954).

[5] V. V. Borisov, Biull. VAGO,* No. 6 (13), 28 (1949).

[6] V. F. Litvinov, Reports of the Expedition for the Observation of the Total Solar Eclipse of June 19, 1936, Vol. II [In Russian] (Izd AN SSSR, Moscow, 1938).

[7] V. N. Kedrolivanskii and M. S. Sterizat, Meteorological Instruments (Gidrometizdat, Moscow, 1953) [In Russian].

[8] Manual for the Calibration of Actinometric Instruments, 1 [In Russian] (Gidrometizdat, Leningrad, 1952).

[9] A. Gordov, Bulletin of the Permanent Actinometric Commission, No. 2, 3 (1933).

[10] N. N. Kalitin, Actinometric Measurements [In Russian] (Gidrometizdat, Leningrad, 1938).

[11] K. Feussner, Z. Meteorol. No. 6 (1936).

[12] K. Ia. Kondrat'ev, Solar Radiation Energy [In Russian] (Gidrometizdat, Leningrad, 1954).

[13] M. Waldmeier, Ergebnisse und Probleme der Sonnenforschung, 2 (Leipzig, 1955).

[14] C. W. Allen, Astophysical Quantities (London, 1955).

[15] L. H. Aller, Astrophysics [Russian Translation] (IL, Moscow, 1955).

[16] S. P. Popov, The Transparency of the Atmosphere in Separate Spectral Regions According to the Observations Made at Alma-Ate (dissertation) [In Russian] (1948).

[17] G. F. Sitnik, Absolute Photoelectric Photometry of the Continuous Solar Spectrum (dissertation) [In Russian] (Moscow State University, 1955).

[18] E. A. Makarova, The Investigation of the Energy Distribution at the Center of the Solar Disc in Absolute Units by a Photographic Method (Dissertation) [In Russian] (Moscow State University, 1956).

[19] E. V. Piaskovskaia-Fesenkova, Astronom. J. (USSR), 23, 49 (1946).

[20] E. V. Piaskovskaia-Fesenkova, Investigation of the Scattering of Light in the Atmosphere of the Earth (dissertation) [In Russian] (Astrofiz. Inst., AN Kaz. SSR, 1956).

[21] Y. Kawabata, Japn. J. Astron. Geophys. 14, 264 (1936-1937).

[22] N. Gerlow, H. Ollson and N. Schüep, Tellus 6, No. 1, 44 (1954).

[23] I. A. Prokof'eva, Atmospheric Ozone [In Russian] (Izd AN SSSR, Moscow-Leningrad, 1951).

[24] S. K. Mitra, The Upper Atmosphere [Russian Translation] (IL, Moscow, 1955).

[25] A. P. Kuznetsov, On the Vertical Distribution of Ozone in the Atmosphere (dissertation) [In Russian] (Moscow State University, 1956).

[26] G. M. Dobson, A. W. Brewer, B. M. Cwilong, Uspekhi Fiz. Nauk, 31, 96 (1947).

[27] F. Fowle, Astrophys. J. 42, 394, 1915.

[28] R. Mügge and F. Meller, Zs. f. Geophys. 8, 61 (1931).

[29] K. Ia. Kondrat'ev, The Transport of Long-Wave Radiation in the Atmosphere [In Russian] (GTTI, Moscow-Leningrad, 1950).

[30] K. Ia. Kondrat'ev, Radiant Heat Exchange in the Atmosphere, [In Russian] (Gidrometizdat, Leningrad, 1956).

[31] W. Z. Godson, Quart. Journ. Roy. Meteorol. Soc. 70, N341, 367 (1953).

[32] E. S. Kuznetsov, Trudy Geofiz. Inst. Akad. Nauk SSSR, Sbornik Statei 23, 150, 3 (1954).

[33] E. S. Kuznetsov, Trudy Geofiz. Inst. Akad. Nauk SSSR, Sbornik Statei. 23, 150, 26 (1954).

---

* VAGO = All-Union Astronomical and Geodetic Society.

[34] S. I. Sivkov, Trudy GGO* 14, 76 , 7 (1949).

[35] A. M. Brounshtein, Trudy GGO* 42, 104 , 5 (1953).

---

*GGO = Main Geophysical Observatory.

SOLAR LIMB DARKENING AT WAVELENGTHS OF 1-4 μ

N. I. Kozhevnikov

Solar limb darkening was investigated in the infrared region from 1.07 μ to 3.92 μ with the help of an infrared spectrograph IRS-11. The results obtained, on the whole, are in agreement with those of Pierce and Peyturaux.

There is an increase in the limb darkening at wavelengths of about 1.78 μ and 2.36 μ by comparsion with neighboring regions of the spectrum.

1. In 1954-1955 we investigated the phenomenon of limb darkening in the spectral region 1.07-3.92 μ. The work was carried out with the help of an infrared spectrograph IKS-11 in combination with the horizontal solar telescope of the Kuchinsk Astrophysical Observatory (focal distance 15 m, mirror diameter 0.3 m).

2. The infrared spectrograph (IKS-11) is intended for the investigation of infrared emission and absorption spectra of various substances. The instrument is mass-produced for the use of physico-chemical laboratories.

Its application to astrophysical measurements requires small alterations in the optical and electrical systems of the instrument. The spectrograph consists of a monochromator, an energy-sensitive device with an amplifier, and a recorder. The monochromator is constructed according to an autocollimating principle. The dispersing system consists of interchangeable alkali halide (KCl, KBr, NaCl, LiF) and glass (F-1) prisms. The linear dispersion of the prisms is variable between the limits 0.035 μ/mm (for the LiF prism) to 0.291 μ/mm (for the KBr prism).

The energy-sensitive device is a compensated vacuum radiation thermoelement. The thermocouple has two junctions (manganin and constantan are used in each junction) connected in opposition to one another. One of the junctions is used to measure the incident energy, while the other is used to compensate for the external influences on both junctions. The sensitivity of the thermoelement is 1.4 v/w.

The current from the thermoelement is used to operate Kozyrev a photoelectrooptical amplifier (FEOU-15). The principle of operation of the FEOU-15 is that of a photorelay. The signal from the FEOU-15 goes to a mirror galvanometer. The deflection of the galvanometer mirror is recorded on light-sensitive paper.

An energy of 10^{-9} w can be measured with this instrument.

3. In the autumn of 1954 the infrared region of the solar spectrum from 0.8 to 13.78 μ was obtained with the help of the instrument. It was not possible to go further because of low intensity of the observed solar spectrum and because of the inadequate sensitivity of IKS-11.

The main part of the work to record the intensity of the solar disc along a diameter was done during the summer of 1955. To obtain such a recording, the image of the sun in the plane of the entrance slit of the spectrograph was displaced relative to this slit by the diurnal motion of the sun.

The diameter of the solar image was 14 cm.

The dimensions of the entrance slit are: height (the side perpendicular to the diurnal motion of the sun) 0.8 cm, the width of the slit for the spectral region 1.07-2.12 μ was taken to be equal to 0.07 cm or 0.01 of the radius of the solar image; for the spectral region 1.07-2.12-3.94 μ, the width of the slit was 0.14 cm (0.02 of the radius of the solar image).

The observations were made when the sun was within 1^h of the meridian, on either side.

TABLE 1

sin θ λ (μ)	sin θ 0.00	0.40	0.50	0.60	0.70	0.80	0.85	0.90	0.92	0.92	0.94
1.07	1.00	0.975	0.055	0.940	0.910	0.870	0.845	0.810	0.790	0.790	0.750
1.29	1.00	0.98	0.965	0.945	0.920	0.885	0.860	0.825	0.805	0.785	0.770
1.50	1.00	0.98	0.970	0.950	0.930	0.900	0.875	0.835	0.815	0.795	0.780
1.56	1.00	0.985	0.975	0.960	0.935	0.910	0.885	0.830	0.850	0.810	0.795
1.65	1.00	0.990	0.980	0.965	0.940	0.910	0.885	0.855	0.835	0.820	0.800
1.74	1.00	0.985	0.975	0.960	0.940	0.910	0.890	0.870	0.850	0.835	0.825
1.80	1.00	0.990	0.980	0.970	0.950	0.920	0.900	0.870	0.850	0.830	0.820
1.90	1.00	0.985	0.975	0.960	0.940	0.915	0.890	0.865	0.845	0.820	0.800
2.08	1.00	0.990	0.980	0.970	0.955	0.925	0.905	0.875	0.755	0.835	0.820
2.12	1.00	0.990	0.980	0.970	0.955	0.925	0.900	0.870	0.845	0.820	0.800
2.18	1.00	0.990	0.980	0.965	0.945	0.915	0.895	0.865	0.850	0.830	0.820
2.26	1.00	0.990	0.975	0.960	0.945	0.920	0.900	0.875	0.860	0.840	0.830
2.32	1.00	0.990	0.980	0.970	0.955	0.930	0.910	0.880	0.865	0.850	0.840
2.38	1.00	0.990	0.980	0.965	0.945	0.920	0.900	0.870	0.875	0.845	0.835
2.40	1.00	0.990	0.980	0.970	0.950	0.920	0.900	0.875	0.860	0.845	0.835
3.46	1.00	0.990	0.980	0.970	0.950	0.925	0.905	0.880	0.870	0.855	0.845
3.61	1.00	0.990	0.980	0.965	0.950	0.925	0.910	0.890	0.880	0.870	0.865
3.80	1.00	0.995	0.990	0.985	0.970	0.945	0.930	0.910	0.895	0.880	0.875
3.94	1.00	0.995	0.990	0.980	0.970	0.950	0.935	0.915	0.900	0.890	0.885

Remarks. 1. The first column gives the wavelength in microns. The first row gives the value of sin θ. 2. The entries in the table give the ratio of the brightness of the solar disc at the given point to the brightness of the disc center for various wavelengths.

4. A few remarks on the analysis of the spectrograms are given below.

a) The scattering of light in the earth's atmosphere. The scattering of light changes the true ratio of the radiances at the center and the limb of the sun. The magnitude of this effect decreases with increasing wavelength of the scattered radiation.

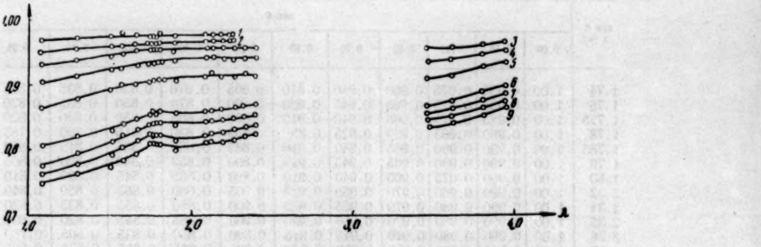

Fig. 1. 1) sin θ = 0.4; 2) sin θ = 0.5; 3) sin θ = 0.6; 4) sin θ = 0.7; 5) sin θ = 0.8; 6) sin θ = 0.9; 7) sin θ = 0.92; 8) sin θ = 0.94; 9) sin θ = 0.95.

According to Pierce [1, 4], the amount of scattered light for wavelengths greater than 1 μ is less than 0.5% of the central brightness of the disc. We have therefore compared directly the brightness of the center with that of the limb, without the introduction of any corrections for the scattered radiation. The agreement between our results with the data of Pierce [1, 4], Peyturaux [5], and Abbot [2, 3], at about 1 μ (when the scattering should have the largest effect in the region investigated by us) is evidence in favor of our assumption.

b) The scintillation of the solar limb. To overcome this effect, we only used those days when the solar image was stable. In addition, we rejected the points situated in the region 0.95-1.00 of the radius of the disc.

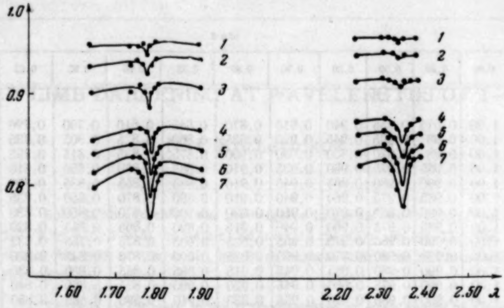

Fig. 2. 1) sin θ = 0.6; 2) sin θ = 0.7; 3) sin θ = 0.8; 4) sin θ = 0.9; 5) sin θ = 0.92; 6) sin θ = 0.94; 7) sin θ = 0.95.

c) The inertia of the detector and amplifier system. The analysis of the records showed that the maximum difference between the records obtained for the right and left sides of the solar disc (for the region 0 - 0.95 of the disc radius) is less than 1%. In the presence of such deviations, it is adequate to take a simple average of the recordings for the left and right halves of the disc.

5. The results of the measurements are given in Table 1. A comparison of our results with those obtained by Peyturaux and Pierce shows good agreement in the region 1.0-1.5 μ. For greater wavelengths, there exists a systematic deviation. The values measured by us are smaller than those of Peyturaux and, particularly, than those of Pierce. The discrepancy reaches a value of 2% of the central brightness of the disc (in the wavelength region of 2.4-μ wavelengths).

TABLE 2

sin θ λ (μ)	sin θ									
	0.00	0.40	0.50	0.60	0.70	0.80	0.85	0.90	0.92	0.94	0.95
1.74	1.00	0.985	0.975	0.960	0.940	0.910	0.895	0.870	0.850	0.835	0.825
1.76	1.00	0.985	0.975	0.965	0.945	0.920	0.900	0.870	0.850	0.835	0.820
1.775	1.00	0.985	0.975	0.965	0.940	0.910	0.890	0.865	0.850	0.830	0.820
1.78	1.00	0.980	0.965	0.950	0.925	0.890	0.865	0.830	0.815	0.790	0.785
1.785	1.00	0.990	0.980	0.965	0.940	0.910	0.885	0.850	0.835	0.815	0.800
1.79	1.00	0.990	0.980	0.965	0.945	0.910	0.890	0.853	0.840	0.820	0.805
1.80	1.00	0.990	0.975	0.960	0.940	0.910	0.890	0.865	0.845	0.825	0.810
2.32	1.00	0.990	0.980	0.970	0.955	0.925	0.905	0.880	0.865	0.850	0.840
2.34	1.00	0.990	0.980	0.970	0.955	0.925	0.900	0.870	0.855	0.835	0.820
2.35	1.00	0.990	0.980	0.970	0.950	0.920	0.900	0.865	0.845	0.820	0.800
2.36	1.00	0.990	0.980	0.970	0.945	0.915	0.890	0.850	0.835	0.805	0.780
2.37	1.00	0.990	0.980	0.970	0.950	0.920	0.895	0.865	0.855	0.835	0.825
2.38	1.00	0.985	0.975	0.970	0.950	0.920	0.900	0.870	0.860	0.840	0.830
2.40	1.00	0.985	0.980	0.965	0.950	0.920	0.900	0.880	0.865	0.845	0.835

Remarks. 1. The first column gives the wavelength in microns. The first row gives the value of sin θ. 2. The entries in the table give the value of $I_\lambda(\theta)/I_\lambda(0)$, the ratio of the brightness of the solar disc at the given point to the central brightness of the disc, as a function of the wavelength.

The ratio $I_\lambda(\theta)/I_\lambda(0)$ as a function of the wavelength λ is given in Fig. 1.

At about 1.6 μ there is a clearly marked "hump" which has been mentioned in Pierce's paper.

We have observed a marked increase in the limb darkening at wavelengths of 1.78 μ and 2.36 μ, by comparison with the neighboring regions of the spectrum. The observational results for these regions are given in Table 2. The width of these regions is of the order of 0.05 μ.

For the point $\lambda = 1.78\ \mu$ and $\sin\theta = 0.95$, the ratio of the brightness to the central brightness of the disc is is 0.77 instead of 0.83 which is to be expected from the general appearance of the curve of $I_\lambda(\theta)/I_\lambda(0)$.

For the point $\lambda = 2.36\ \mu$, $\sin\theta = 0.95$ we have 0.78 and 0.835, respectively (Fig. 2).

P. K. Shternberg
State Astronomical Institute

Received February 16, 1957

LITERATURE CITED

[1] A. K. Pierce, R. R. MacMath, L. Golderg and O. C. Mohler, Astrophys. J. 112, 289 (1950).

[2] C. J. Abbot, Smithonian Ann. 3, 157 (1913).

[3] C. J. Abbot, Smithsonian Ann. 4, 221 (1922).

[4] A. K. Pierce, Astrophys. J. 120, 221 (1954).

[5] R. Peyturaux, Ann. Astrophys. 18, 1 (1955).

APPLICATION OF SILVER SULFIDE PHOTOELECTRIC CELLS WITH A BARRIER LAYER TO ABSOLUTE SPECTROPHOTOMETRY AND PYROMETRY

II. METHOD OF USING SSBL FOR ABSOLUTE SPECTROPHOTOMETRIC AND PYROMETRIC MEASUREMENTS

G. F. Sitnik

The results of the investigation of silver sulfide barrier layer cells (SSBL*) are given. These were used to develop a method of application of the cells to absolute spectrophotometric and pyrometric measurements. This method is based on the control of the integrated sensitivity of the SSBL by means of constant luminous flux from a low-voltage incandescent lamp.

The method of controlling sensitivity and the measuring scheme described in Part I permitted the SSBL to be used for absolute measurements, which make high demands on the radiation receiver. The mean error of a single measurement of the small luminous fluxes with which one deals in spectrophotometry is on the average 0.5-0.8%, despite the inevitable variation in the sensitivity of SSBL during a long series of absolute measurements.

In absolute measurements special requirements are made with regard to the sensitivity stability of the measuring apparatus during the long series of observations which are characteristic of such measurements. Therefore for the successful use of a silver sulfide barrier layer cell (SSBL) in absolute measurements it was necessary to conduct a careful investigation of the photoelectric cell in this respect. This investigation enabled us to develop and test a method of controlling the sensitivity of SSBL during absolute measurements. The method and measuring setup described in the first part of this communication [1] enabled us to use SSBL successfully in absolute measurements. It was first necessary to investigate the time change of sensitivity since the literature [2] contains indications that there exists some change of sensitivity (of the order of a few per cent) during the first 20 minutes after the beginning of illumination, followed by stabilization of the sensitivity. It is stated in Ref. [2] that this effect is especially noticeable in freshly manufactured SSBL but that the operation of the cells is stabilized with aging.

We investigated the time change of sensitivity of SSBL as follows. A standard 1000-ohm resistance coil is connected in series with the cell. The voltage drop across this coil or the equal drop in the cell itself is measured by means of a potentiometer. The potentiometer was balanced exactly by changing the direction of current through a galvanometer [1]. The illuminating lamp was controlled by a potentiometer [3]. When the cell was illuminated the voltage drop across the resistance was measured at small intervals of time during a period of 3 hours, after which the cell was stored in darkness. The cell was placed in a small metal box within which the temperature was controlled.

Each cell was measured under different conditions.

1. Before the test, the cell, which had previously been stored in darkness was exposed for 1 hour to ordinary daylight from a window.

2. Before the next run, the same cell was illuminated by scattered daylight (from a window) for a longer period (about 2 days).

---

* Russian designation — FESS.

In addition, each cell that was investigated was, after 2 days of continuous illumination, studied by the method shown in the figure of Reference [1]. The method of measurement is described in Reference [1]. These measurements enabled us to study the effect on the sensitivity of an SSBL produced by a small external emf comparable with the photo-emf. Each cell in the balanced setup was investigated under different conditions.

1. The external emf acted continuously on the SSBL during all 3 hours of observation.

2. The external emf was switched off after each measurement. In other words, the switch S was used to open the circuit at each dark period (see the figure in Ref. [1]).

This method was used to study 8 cells, the data for which are given in Table 1 below and in Table 1 of Ref. [1]. Table 2 and Figs. 1 and 2 give the results for cells Nos. 550, 337, and 555.

TABLE 1

Ratings of Silver Sulfide Barrier Layer Cells

Designation	No. of cell	Integrated sensitivity μa /lumen	Photo-emf at 25 luxes, mv	Months of manufacture during 1949
FESS-U2	550	6500	46	XI
FESS-U2	560	6500	101	X
FESS-U3	548	6750	48	X
FESS-U3	628	6600	40	XI
FESS-U10	1102	6100	58	X
FESS-U10	1104	6100	58	X

In Figs. 1 and 2 the ordinate is the voltage drop across the load resistance or the resistance R_0 which is proportional to the photocurrents; the abscissa is computed from the beginning of measurements. An analysis of the results for the 8 cells enables us to draw some conclusions which are significant for the application of SSBL to absolute measurements.

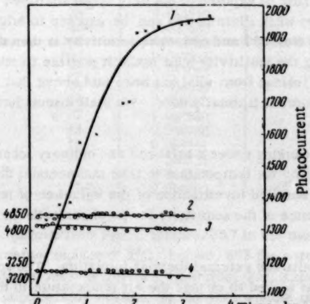

Fig. 1. Variation of sensitivity of SSBL cell No. 550 with time. 1) August 14, 1950 (after 1 hour of preillumination); 2) August 21, 1950 (external emf switched off after each measurement); 3) August 19, 1950 (continuous external emf); 4) August 17, 1950 (after 2 days of illumination).

1. Preillumination for 1 hour is not always sufficient, since after this period the sensitivity of the cell can change appreciably during the measurements. This refers especially to recently manufactured cells. The sensitivity of cell No. 550, when investigated in 1950, increased during the first 2.5 hours by a factor of about 1.5 (Fig. 1), although the temperature change (0.9° C) during this time should have reduced the sensitivity by only about 2%. Tests during 1956 showed that cell No. 550 was well stabilized. In 1950 cell No. 560 was unstable. During 2.5 hours of measurements its sensitivity changed by a factor of 4. In 1956 this same cell was found to be stabilized.

No. 337 (Fig. 2) was the most stable cell. On September 11, 1950 (Fig. 2, line 1), this cell showed only a small change of sensitivity with time (within 1%), which can be attributed to a change of temperature as well as to errors of measurements. This cell gave a a similar result in the balanced setup (Fig. 2, line 2).

For the other cells the changes of sensitivity during the first 3 hours of measurements were also small (about 1-2%). During this time the temperature change inside the metal box which held each cell did not exceed 0.4° C. However, for cells Nos. 628, 1102 and 1104, the character of the sensitivity change does not agree with the temperature change close to the cell (observations of 1950). From the data we infer that the operation of an SSBL is stabilized by aging. The aging period required for sensitivity stabilization varied with the cell. The average is about 2 years. After the required aging period a preilluminated cell when tested shows a change of sensitivity which results from the change of temperature of the cell.

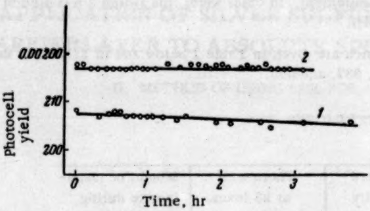

Fig. 2. Variation of sensitivity of SSBL cell No. 337 with time. 1) September 11, 1950 (without external emf); 2) September 12, 1950 (continuous external emf).

2. After prolonged preillumination the operation of all of the tested cells was well stabilized both with and without an external emf (Figs. 1 and 2). Certain peculiarities of the SSBL must be mentioned. Cell No. 548 showed good stability when investigated in 1950 (August 25, 1950). A different result was given by the same cell in 1951. On February 27, 1951, after weak illumination for 1 day the sensitivity showed a tendency to increase up to 10%. Cell No. 555 showed similar behavior on April 25, 1951, May 11, 1951, and September 4, 1956 (Table 2). Thus, on April 25th, after 3 days illumination by scattered light this cell showed a reduction of sensitivity which clearly exceeded the temperature-induced change. The same result was found on May 11th, before which the cell had been shielded for 3 days. On September 4, 1956, the sensitivity change of this cell also exceeded the temperature-induced change. The temperature-induced change of sensitivity of No. 555 does not exceed 2.5% for a temperature change of 1°C. Thus, there is evidently some uncertainty in the behavior of the sensitivity (especially of a freshly manufactured cell) which is associated with the conditions of its previous storage as well as with a temperature difference between the cell and surrounding air due to the thermal inertia of the cell. This characteristic of SSBL had to be taken into account in developing a method of absolute measurements. For relative measurements over small intervals of time this effect is not significant.

3. For the use of an SSBL in absolute measurements it must first be exposed to not very bright scattered light. In other words, between measurements the cell must be kept under weak illumination and be exposed to brighter light before operation. This method was fully tested using cells Nos. 337 and 555. The sensitivity is then shown to be quite stable (Figs. 1 and 2). Also, the method of controlling the sensitivity must make it possible to take into account the effect of sensitivity change on the measurements. It follows from what has been said above that the integrated sensitivity must be controlled rather than the temperature, as is usually done. We shall discuss further the method of controlling the integrated sensitivity of SSBL.

We shall first discuss the influence of temperature on SSBL working under a balanced and ordinary scheme of loading. Since in our work we did not use a method of controlling the temperature to take into account the sensitivity variation during measurements, we did not carry out a detailed investigation of the influence of temperature on cell sensitivity. We investigated the temperature dependence of the sensitivity for 2 of our cells (Ref.[1], Table 1) over a limited temperature range (15-45°C).

The tested cell was placed inside a reservoir with double walls and external thermal insulation. The space between the walls of the reservoir was filled with water, which was heated to change the air temperature in the interior of the reservoir, where the cell was placed. For more uniform temperature distribution of the air inside the reservoir a special device was used to keep the air in circulation. A thermometer was used to measure the temperature close to the cell. When the inside temperature reached 43-45°C heating was terminated and measurements were made during the period of gradual cooling which followed. Light from an electric lamp controlled by a high-resistance potentiometer [3] illuminated the cell through a glass window in the reservoir wall. The conditions of illumination were not changed during an entire run. Measurements of the cell performance were obtained under 2 setups: 1) A 1000-ohm load resistance was placed in series with the SSBL; the voltage drop across this load was measured by a low-resistance potentiometer; 2) the cell was connected according to the figure of Ref. [1]. The results are given in Fig. 3. The horizontal axis of Fig. 3 gives the cell temperature, while the vertical axis gives the voltage drop across the load resistance or the resistance R_{ob} (Ref.[1]) proportional to the photocurrent. The unit of the ordinate scale is the value at 20°C. Curves I and II of Fig. 3 refer to cells Nos. 337 and 555 in conjunction with the 1000-ohm load. Curve III refers to cell No. 337 in the balanced setup.

TABLE 2

Performance of Silver Sulfide Barrier Layer Cell FESS-U2 No. 555

April 25, 1951. After illumination of cell for 3 days			May 11, 1951. Cell covered prior to measurements		
Time from beginning of measurement	Voltage drop across load resistance of 1000 ohms	Temperature near cell, °C	Time from beginning of measurement	Voltage drop across load resistance of 1000 ohms	Temperature near cell, °C
0^h00m	0.061295		0^h00^m	0.001812	13.7
07	0.061170		05	0.001807	
21	0.060770	13.0	08	0.001795	
2^h17m	0.059010		17	0.001788	
20	0.058950		22	0.001782	
22	0.058931		32	0.001770	
23	0.058860		56	0.001756	13.7
25	0.058790		1^h43	0.001726	13.7
28	0.058726		46	0.001724	13.7
33	0.058665		51	0.001723	13.8
36	0.058585		59	0.001719	13.8
43	0.058466		2^h09	0.001715	13.8
48	0.058384		16	0.001711	13.8
59	0.057930				
3^h01	0.057900		September 4, 1956, Before measurements the cell was connected to the apparatus and illuminated by scattered light in the room		
03	0.058160		0^h00m	0.006791	16.2
43	0.057976		25	0.006685	16.4
54	0.057902		50	0.006665	16.4
4^h01	0.057864		1^h10	0.006651	16.4
05	0.057843		45	0.006580	16.5
09	0.057776		2^h03	0.006556	16.5
21	0.057710		20	0.006574	16.5
28	0.057646		45	0.006513	16.4
38	0.057540		3^h25	0.006546	16.5
42	0.057490				
54	0.057433				
5^h06	0.057335				
26	0.057095				
44	0.056930				
56	0.056880				
6^h07	0.056830				
13	0.056780				
16	0.056761				
22	0.056724				
42	0.056583				
57	0.056490	13.5			

It follows from Fig. 3 that No. 337 in the usual measuring setup reveals a change of sensitivity by 2.5% with a temperature change of 1°C. For No. 555 the corresponding sensitivity change is 2-2.5%. The cell behavior in the balanced setup is different from this. Fig. 3 shows that the temperature dependence of the sensitivity in this case is considerably weaker. In one temperature region there is no appreciable variation of sensitivity. This is another advantage of the setup described in Ref.[1], which is very important for the practical us of SSBL in absolute photoelectric measurements.

It is known that temperature affects the photocurrent of SSBL principally through resistance changes in the blocking layer. This resistance is an internal variable path of leakage. Complete elimination of the potential difference across the resistance of the blocking layer would have the result that the external current (photocurrent) would cease to depend on the variable magnitude of this resistance. However, in the balanced scheme (see the figure in Ref.[1])the voltage drop is reduced to zero only across the entire photocell. Therefore the effect of the blocking layer resistance on the external current is reduced but not eliminated. As a result the temperature dependence of the cell sensitivity is reduced but does not disappear completely. Observations confirm this (Fig. 3).

With incomplete balancing of the voltage drop across the resistance of the blocking layer the direct proportionality between the luminous flux and the photocurrent under strong illumination is destroyed. The effect of temperature on the sensitivity of blocking layer cells in practice is usually taken into account through temperature control and the introduction of suitable corrections. This procedure has been found to be entirely satisfactory for selenium cells.

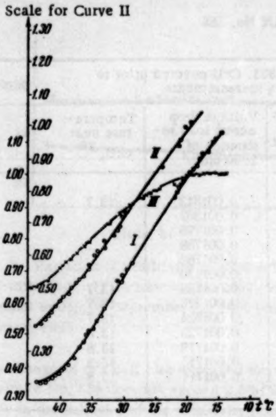

Fig. 3. Sensitivity of SSBL as a function of temperature.

TABLE 3

Observations of Reproducibility for Different Settings of the Control Lamp, November 23, 1951.

Observation time	Photocell Yield	Photocell temperature, °C
12^h41^m	0.039666	16°.4
45	0.039690	
49	0.039631	
53	0.039620	
58	0.039595	
13^h04	0.039648	
08	0.039671	
12	0.039601	
15	0.039584	
18	0.039656	
22	0.039632	16°.4
Average	0.039636	

Average error of one setting ± 0.000034 (± 0.09%).

However, our experiment has shown that this method of control is not satisfactory for SSBL. Because of a certain change of sensitivity during measurements, which depends on the thermal inertia of SSBL and on the degree of aging of the cell, temperature control alone does not insure correct results in absolute measurements. It is more satisfactory to control directly the integrated sensitivity of the SSBL. This method enables us to take into account simultaneously all factors which affect the sensitivity. Moreover, the control of the integrated sensitivity excludes possible errors of the temperature corrections. These errors result from a difference between the temperature of the cell and of the surrounding air. Due to the thermal inertia of the material of the cell this temperature difference always exists. This is the cause, in addition to errors of measurement, of the systematic difference of 1-2% which we observed between the measurements before heating of the reservoir containing the cell and after cooling, when the air surrounding the cell assumes room temperature.

Beginning in November, 1951 we controlled the integrated sensitivity of SSBL by means of a low-voltage lamp. The luminous emission of the lamp was controlled by a potentiometer [3]. The lamp was considerably underheated in order to insure stability. The light from the lamp was further weakened by blackened paper. The control lamp e was placed inside a metal tube which could be moved inside another tube that was fastened to a special head (Fig. 4). The entire device was placed directly in front of the photocell Ph back of the exit slit of the monochromator.

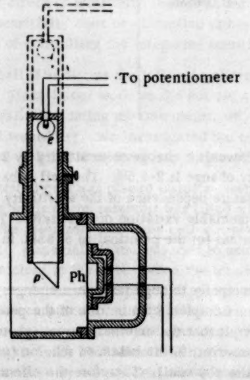

Fig. 4. Special head containing control lamp.

TABLE 4

Control of Sensitivity Variation in FESS No. 337, February 7, 1952

Time of observation	Yield of photocell for control lamp	Test source	
		Yield of cell	Yield reduced to identical sensitivity
10^h11^m	0.009388		
17		0.000423	0.000417
20		0.000418	0.000412
24		0.000425	0.000419
30		0.000427	0.000421
36		0.000425	0.000420
11 34	0.009329		
54		0.000425	0.000423
58		0.000419	0.000417
12 00		0.000420	0.000418
05		0.000420	0.000418
09		0.000419	0.000417
24	0.009253		
36		0.000417	0.000417
45		0.000415	0.000415
48		0.000419	0.000419
51		0.000419	0.000419
54		0.000418	0.000418
13 00	0.009228		
04		0.000417	0.000418
06		0.000417	0.000418
08		0.000419	0.000420
10		0.000420	0.000421
13		0.000419	0.000420
20	0.009234		
15 01	0.009216		
05		0.000421	0.000423
08		0.000417	0.000419
11		0.000419	0.000421
14		0.000419	0.000421
17		0.000421	0.000421
27	0.009191		
30		0.000419	0.000421
32		0.000419	0.000421
38		0.000419	0.000421
16 00		0.000419	0.000421
06	0.009230		
17 06	0.009245		
10		0.000419	0.000421
18		0.000419	0.000421
21		0.000419	0.000421
18 00		0.000419	0.000421
05		0.000419	0.000421
12		0.000419	0.000421
25	0.009197		
19 30	0.009195		
33		0.000419	0.000421
35		0.000418	0.000421
19 39		0.000418	0.000421
45	0.009199		
		Average	0.000420

Average error of a single measurement ± 0.0000023 (± 0.5%).

TABLE 5

Control of Sensitivity Variation of FESS No. 555

Date and time of observation	Yield of photocell for control lamp	Test source		Relative sensitivity
		Yield of photocell	Yield reduced to identical sensitivity of cell	
16.III.1955				
12^h40^m		0.000822	0.000822	1.000
51	0.007620			1.000
14^h28	0.007700			1.010
36		0.000831	0.000823	1.010
15^h40		0.000835	0.000827	1.010
45	0.007693			1.010
16^h55	0.007646			1.003
59		0.000831	0.000829	1.003
17^h55		0.000825	0.000818	1.008
58	0.007684			1.008
17.III.1955				
9^h53^m		0.000826	0.000814	1.004
58	0.007729			1.014
10^h57	0.007696			1.010
11^h02		0.000828	0.000820	1.010
53		0.000828	0.000818	1.012
56	0.007710			1.012
14^h19	0.007721			1.013
23		0.000826	0.000815	1.013
15^h02		0.000826	0.000812	1.017
06	0.007750			1.017
08	0.007746			1.017
16^h41	0.007756			1.018
45		0.000831	0.000816	1.018
17^h36		0.000838	0.000821	1.020
42	0.007776			1.020
18.III.1955				
10^h37^m		0.000869	0.000820	1.057
45	0.008058			1.057
11^h13	0.008047			1.056
15		0.000866	0.000818	1.055
12^h16		0.000866	0.000829	1.041
30	0.007933			1.041
14^h08	0.007864			1.032
15		0.000857	0.000829	1.032
15^h41		0.000855	0.000833	1.025
45	0.007812			1.025
16^h32	0.007812			1.025
41		0.000853	0.000832	1.025
19.III.1955				
10^h19^m		0.000821	0.000815	1.007
21	0.007677			1.007
		Average	0.000822	

Average error of a single measurement ± 0.0000064 (± 0.78%).

A total reflection prism P measuring 1 × 1 cm was rigidly fastened to the other end of the movable tube. During operation the lamp was 250 mm from the cell. This distance minimizes the possible errors in measurement of the luminous flux reaching the cell. Such errors result from a variation in the mounting of the tube. In our design the tube had an exactly fixed position with respect to the cell. A test of the control device showed that the performace of the cell during successive periods of illumination by the lamp agrees within 0.1% (Table 3).

The accurate mounting of the control lamp insures the control of sensitivity changes of the SSBL.

The accuracy of the control of the integrated sensitivity of the SSBL was investigated as follows. The cell together with the head for the control lamp was placed on a photometer bench. A light filter was placed in front of the cell. As a measurable light source another lamp (such as an illumination-measuring lamp) was placed at a fixed distance from the SSBL. The electrical operation of this lamp was controlled by a potentiometer. The distance of the measuring lamp from the cell and the filter were such that the yield of the cell was small. This was done in order to determine the accuracy of control and measurement under the most unfavorable conditions. Other than this,the conditions were similar to those under which absolute spectral photometric measurements were made. The cell was placed in a setup (see the figure inRef.[1]) where at several intervals of time the luminous flux from the control and test lamps was measured. The time of each measurement was noted and observations were continued during one or more days. During the observations which extended over a single day the lamps were not extinguished. Each day 30 minutes before the measurement began the control lamp was lit so that its emission would become stationary. The comparison lamp was also lit in advance; the warming-up time depended on the properties of the lamp which was used.

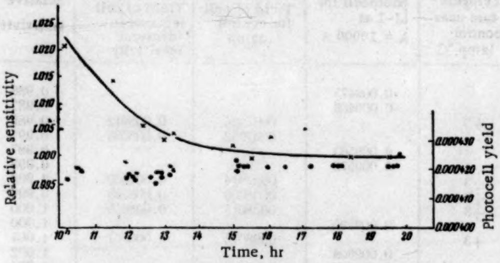

Fig. 5. Correction for sensitivity variation of radiation receiver.

The results for SSBL Nos. 337 and 555 are given inTables 4 and 5. The first column gives the date and time of measurement; the second and third columns give the yield of the cell when illuminated by the control lamp and the test source, respectively. The data for the control lamp in Table 4 permit us to infer that during the entire period of observation the sensitivity of the cell changed by approximately 2%. In order to take this change into account and to reduce all observations of the test source to a single sensitivity we plotted the time dependence of the measurements of the control lamp (Fig. 5). This is the upper curve of Fig. 5, where the crosses denote individual measurements of the control lamp. The horizontal axis gives the time of observation and the vertical axis gives the yield of the cell for relative sensitivity.

In order to allow for the sensitivity variation of SSBL we used a certain value of the cell yield when illuminated by the control lamp as unity. For observations with SSBL No. 337 on February 7, 1952,this value was 0.009250 and for SSBL No. 555 it was 0.007620. Then from the curve of sensitivity variation, for each observation time,we can obtain the relative sensitivity (column 5, Table 5).

Dividing the yield of the cell for the test source by the corresponding value of the relative sensitivity, we obtain the yield of the cell reduced to identical sensitivity (column 4, Table 4 and 5). From this column (Table 4) the lower part of Fig. 5 was plotted. Tables 4 and 5 show that the average error of a single measurement for small light flux is 0.5-0.8%. Large light flux is measured with an accuracy of 0.3-0.5%. With the integrated sensitivity of SSBL controlled in this way, we can obtain satisfactory reproducibility of the readings despite the sensitivity variation of the cell during long runs.

The sensitivity of SSBL was controlled by an incandescent lamp at different temperatures of the surrounding air. Change of the outside temperature can affect the constancy of light emission by the lamp. Reference [4]gives data on the influence of temperature on emission from an incandescent lamp. These data show that for a vacuum lamp beginning with luminous temperatures of the order of 1000°C the change of air temperature around the lamp has no appreciable effect on emission by the lamp. However, we regarded it as necessary to perform a direct investigation of the affect of the outside temperature on emission by the control lamp although the temperature of the filament exceeded 1000°C. The results of this investigation are given in Table 6. The light flux from the control lamp at outside temperatures of 3, 18.3 and 35°C was measured by an SSBL (Table 6, column 4). 18.3° was the room temperature. To control the sensitivity variation of the cell we used emission from a ribbon lamp (LT-1) at above 1800° for a wavelength of 10,000 A (column 3). The measurements of the light flux of the control lamp, reduced to identical sensitivity according to column 3, are contained in column 5 of Table 6. No evidence is found that light emission varies with the outside temperature. Random fluctuations must be attributed to errors of measurement. The average relative error of a single measurement is ± 0.48%.

TABLE 6

Investigation of the Effect of Outside Temperature on Emission From the Control Lamp (April 11, 1955).

Time of observation	Temperature near control lamp, °C	Yield of photocell for LI-1 at λ = 10000 A	Control lamp		Relative sensitivity
			Yield of cell for control lamp	Yield of cell reduced to identical sensitivity	
14^h10^m		0.009475			0.988
12		0.009466			0.987
14	+3		0007924	0.008012	0.989
17			0007963	0.008035	0.991
23		0.009563			0.997
25		0.009572			0.998
30	+3		0007914	0.007930	0.998
32	+3		0008000	0.008008	0.999
35	+3		0008015	0.008015	1.000
38		0.009590			1.000
40	+3		0008015	0.008007	1.001
43		0.009608			1.002
16^h45	+18.3	0.009432			0.984
48		0.009412			0.981
54	+18.3		0007878	0.008055	0.978
17^h05	+18.3		0007832	0.008049	0.973
08	+18.3		0007820	0.008070	0.969
14		0.009256			0.965
20		0.009232			0.963
24	+18.3		0007765	0.008072	0.962
29		0.009213			0.961
31	+18.3		0007770	0.008085	0.961
41		0.009226			0.962
47		0.008954			0.934
54		0.008735			0.911
18^h20	+35		0007158	0.008016	0.893
22			0007130	0.007993	0.892
25	+32.5		0007122	0.008002	0.890
37		0.008522			0.889
32	+31.5		0007112	0.008000	0.889
35		0.008520			0.888
			Average	0.008023	

Average error of a single measurement ± 0.0000392 (± 0.48%).

Thus, within the limits of experimental error (0.5-0.8%) light emission from a lamp does not vary with changes of the outside temperature; this is in agreement with the result given in Ref.[4].

In pyrometric and absolute spectrophotometeric measurements with SSBL, in accordance with this article, we periodically (every 20-30 minutes) measured the cell yield under illumination by the control lamp. As a result, all measurements of the spectrum from the investigated source (a perfect black body, ribbon lamp or the sun) could be reduced to identical sensitivity of the radiation receiver. This method of controlling the sensitivity variation of SSBL, which we have already used for a number of years, has given good results. Our method of controlling the sensitivity and the use of the measuring setup described in Ref.[1] have enabled us to use silver sulfide cells in absolute measurements, which require a receiver that can satisfy special requirements.

In conclusion I wish to thank D. L. Razumin-Astavin, E. A. Makarova, M. S. Murasheva and R. N. Khmeleva for their assistance with the numerous measurements.

P. K. Shternberg State Astronomical
Institute

Received November 12, 1956

LITERATURE CITED

[1] G. F. Sitnik, Astron. J. (USSR) 34, 3, 424 (1957).*

[2] V. E. Kosenko and E. G. Miseliuk, J. Tech. Phys. (USSR) 18, 1369 (1948).

[3] G. F. Sitnik, Trudy GAISh 22, 3 (1953).

[4] A. N. Gordov, Trudy VNIIM 5, 65, 66 (1949).*

---

* Soviet Astronomy — AJ, p. 416.

A NEW VALUE OF THE LIGHT CONSTANT OF THE MOON

N. N. Sytinskaia

The light constant of the moon is defined as the illumination E_0, by the light of the moon, of a plane at right angles to its rays at the phase angle 0° and the mean parallax of the sun and moon. The measurements of the light of the moon made in the USSR with visual photometers during 1932-1955 were used. Some of the results were recalculated. Bouguer's method was used for extrapolating to the edge of the earth's atmosphere, and Rougier's curve for extrapolating to phase 0°. The derived mean value was $E_0 = 0.342 \pm 0.011$ lux. This value, according to the method of its determination, is reduced to the day spectral sensitivity curve of the eye.

The light constant of the moon expressed in absolute photometric units (luxes or phots) is the illumination E_0, by the light of the moon, of a plane at right angles to its rays, at phase angle 0°, the distance between the center of the moon and the plane being equal to the major semiaxis of the lunar orbit. As we know, the latter corresponds to the horizontal equatorial parallax $p = 57'.0$. E_0 is understood to correspond to the mean solar parallax $8''.80$.

The light constant of the moon is of considerable interest for astrophotometry in general in connection with the study of the moon as a luminous heavenly body, and especially for some problems of illumination, since at night light from the moon is important in making objects of the landscape visible. Therefore a sufficiently reliable value of E_0 is necessary for the solution of very many theoretical and practical problems.

The determination of the moon's light constant has a long history. The founders of scientific photometry, Lambert and Bouguer, first concerned themselves with it. Later many other observers compared lunar light with the light of a normal candle. At present all of these determinations are principally of historical interest both because the technique of measurements and reductions was then comparatively primitive and because the modern system of light units did not yet exist.

Modern photometry was used to determine the light constant of the moon by Soviet scientists beginning in the fourth decade of the present century. In 1932 V. V. Sharonov measured the lunar light with a special luxmeter developed for this purpose by the VOOMP (All-Union Optical Equipment Industry Association) [1]; in 1936 L. N. Radlova performed measurements [2]. Some measurements of this type were performed in Alma-Ata by members of the team observing the solar eclipse of September 21, 1941, while working on the standardization of coronal observations [3]. The same was done by O. S. Vasil'ianovskaia while working up the data on the solar eclipse of July 9, 1945 [4]. A. K. Suslov made a special series of observations of lunar light by means of a visual photometer in 1950 at Stalinabad and in 1951 at Alma-Ata [5]. In connection with work on the standardization of the solar corona, observations which provide a new value of E_0 were performed in 1952 by T. A. Polozhentseva [6] and in 1954 by L. D. Petrenko and V. A. Ivanova [7]. In 1955 the same was done by M. V. Kodachenko and G. A. Iurov in connection with observations of a lunar eclipse [8].

On the other hand a few summaries of values have been published. Russell [9] in his well-known work on the photometric parameters of the planets and their satellites gives the value 0.241 lux for illumination by the moon at the zenith. If we take the value $p = 0.766$ for the transmission coefficient which is given at that place (zenithal absorption $0^{m}.29$), we obtain $E_0 = 0.314$ lux. If we take $0^{m}.25$ for the zenithal absorption (as was done by Bullrich [10]) we obtain E_0 = 0.283 lux. Sharonov [11] in compiling table of lunar illumination for purposes of illumination engineering took the value 0.250 lux for the illumination from the moon at the zenith.

In connection with tables of natural illumination [12] as well as in a review article on the photometry of bodies in the solar system [13] Sharanov gives E_0 = 0.291 lux, which corresponds to the zenithal value given above if we take the attenuation at the zenith as $0^m\!.20$. A practical check of Sharonov's tables by P. P. Feofilov [14] showed satisfactory agreement with reality. However, later measurements by A. K. Suslov [5] gave E_0 = 0.374 lux and Bullrich's observations [10] gave E_0 = 0.37 lux. In a later publication [15] Sharonov gives the mean value E_0 = 0.306 lux. From this we infer that the value of E_0 upon which the tables of lunar illumination are based is somewhat too low and the entire question must be reviewed.

In practice the determination of the light constant of the moon encounters a number of difficulties of which the most important are: 1) the necessity for extrapolating measurements of direct lunar illumination beyond the limits of the earth's atmosphere; 2) the necessity for extrapolating to phase 0°, because direct measurements at this phase are rendered impossible since the moon is in the earth's shadow; and 3) the still unsettled question of the photometric system to be used.

The following remarks must be made with regard to the last point. As we know, the system of visual light units,including the lux,assumes a spectral sensitivity of the radiation receiver which agrees exactly with the spectral sensitivity of the eye that has been adopted by international agreement for normal vision adapted to bright light. In the photometry of lunar light strict observance of this rule is very important since the illumination standards have a color temperature which is much lower than lunar light, so that we are concerned with heterochromatic photometry. However, in measuring lunar illumination we must deal with screen brightness which approaches the brightness of a moonlit landscape. Night vision functions at this level of brightness so that the Purkinje effect is involved in comparison of differently colored objects. This requires special agreement with regard to the significance of the lunar light constant. It is most reasonable to agree that the results should correspond to pure daylight vision, thus eliminating the Purkinje effect as much as possible.

This was the condition for all measurements performed in the USSR. In practice the comparison lamp of the visual photometer used in measuring lunar light was always preceded by a blue filter which would result in giving the two compared fields the same color. A similar filter was placed before the standard lamp during calibration of the photometer to provide the same coloration of the fields. Finally, the transmission of the blue filter for the standard lamp was obtained by a spectral computation using the standard visibility curve. This procedure theoretically eliminated the Purkinje effect, and the result referred to the standard curve of spectral sensitivity of the eye.

It is the purpose of the present article to review critically the different values of the lunar light constant which have been published by different authors,in order to arrive at the most probable value. In some instances this required complete reworking of the observations. Thus, in Ref.[1] Sharonov gave measurements at the edge of the atmosphere with the mean Potsdam value of atmospheric transmission; the result cannot, of course, be reliable. In many instances the observations of this author, which were performed at different zenith distances of the moon each night, provide a reliable value for atmospheric transmission for a given night by Bouguer's method. Whenever this was impossible the reduction was performed with the mean value of this coefficient for the given point of observation as derived from the entire series of lunar observations at the point. In those articles where the lunar light constant was obtained as an incidental result of photometry of the solar corona or lunar eclipses,the observers themselves made every effort to eliminate atmospheric effects from the measurements. The same refers to Suslov's measurements [5].

Different authors use different phase curves for the reduction to phase 0°. For the purpose of attaining consistency we recomputed all values using the Rougier curve [16]. There is little change in the final results because most observations were performed around full moon. We did not review the question of the photometric system determined, as was indicated above, by the light intensity from the standard lamps used in photometer calibration and by the transparency of the blue filters, because each observer used the light system which he himself obtained. We did not use the data of Bullrich [10] since the Purkinje effect was not excluded at all.

The final 36 values of E_0 are given in the table. If all of these values are given equal weight the average is E_0 = 0.342 ± 0.011 lux. This must be regarded at present as the most probable value. It is 1.18 times larger than E_0 = 0.291 lux, which was used in compiling the tables of lunar illumination mentioned above [11, 12].

We can see that the data in the table show considerable discrepancies, which in extreme cases amount to a factor of almost 2; this is also shown in the large root-mean-square deviation, which for a single value amounts to ± 0.062 lux or ± 18%. Such large discrepancies must be due primarily to the inaccuracy of the extrapolation to the boundary of the earth's atmosphere. This can be seen from the fact that the discrepancies are large in a single series of observations, in which case there are no differences in the photometric system. It follows that further increase in the amount of data obtained at the same level will not improve the accuracy of E_0. Therefore new determinations of E_0 will be necessary with absolute constancy of atmospheric transmission. A rapid and exact solution of this problem would come from measurements outside of the atmosphere as a result of advances in astronautics.

TABLE

No.	Date	Observer	Place	E_0	Reference
1	1932 Apr. 12	V. V. Sharonov	Nikol'sk	0.291	[1]
2	» » 13	»	»	0.318	»
3	» » 15	»	»	0.345	»
4	» » 16	»	»	0.390	»
5	» » 17	»	»	0.454	»
6	» » 21	»	»	0.438	»
7	» May 10	»	»	0.438	»
8	» » 12	»	»	0.358	»
9	» » 13	»	»	0.349	»
10	» » 18	»	»	0.356	»
11	» Sept. 14	»	Leningrad	0.338	»
12	» » 15	»	»	0.341	»
13	» » 16	»	»	0.298	»
14	» » 17	»	»	0.296	»
15	» Nov. 11	»	»	0.305	»
16	» » 12			0.352	»
17	1936 May 6	L. N. Radlova	»	0.232	[2]
18	1941 Sept. 10	I. A. Fogel'	Alma Ata	0.282	[3]
19	» » 11	»	»	0.302	»
20	» » 30	»	»	0.256	»
21	» Oct. 1	»	»	0.270	»
22	1945 Mar. 16	O. P. Vasil'ianovskaia	Leningrad	0.267	[4]
23	» » 17	»	»	0.372	»
24	1950 July 22	A. K. Suslov	Stalinabad	0.436	[5]
25	» » 23	»	»	0.357	»
26	» » 27	»	»	0.418	»
27	» » 28	»	»	0.363	»
28	» » 28	»	»	0.421	»
29	» » 29	»	»	0.361	»
30	» » 29	»	»	0.286	»
31	Aug. 3	»	»	0.404	»
32	1951 Aug. 17	»	Alma Ata	0.415	»
33	1952 Feb. 11	T. A. Polozhentseva	Pitniak	0.396	[6]
34	1954 July 12	V. A. Ivanova and L. D. Petrenko	Eisk	0.333	[7]
35	1955 Nov. 29	M. V. Kodachenko	Leningrad	0.237	[8]
36	» » 29	G. A. Iurov	»	0.235	»

P. F. Lesgaft Institute of Natural Sciences Received February 2, 1957

LITERATURE CITED

[1] V. V. Sharonov, Astron. J. (USSR) 11, 225 (1934).

[2] L. N. Radlova, Uch. Zp. LGU* 22, 132, (1938).

[3] V. V. Sharonov, Uch. Zap. LGU*132, 37 (1949).

[4] O. P. Vasil'ianovskaia, Uch. Zap. LGU 132, 159 (1949).

---

*Leningrad State University.

[5] A. K. Suslov, Biull. Stalinab. Obs. 2, 24 (1951).

[6] T. A. Polozhentseva, Uch. Zap. LGU*190, 113 (1957).

[7] V. V. Sharonov, Astr. Tsirkuliar Akad. Nauk SSSR 170, 4 (1956).

[8] M. V. Kodachenko and G. A. Iurov, Astro. Tsirkuliar Akad. Nauk SSSR 171, 10 (1956).

[9] H. N. Russell, Astrophys. J. 43, 103 (1916).

[10] Kurt Bullrich, Berichte des Deutschen Wetterdienstes in der US Zone No. 4 (1948).

[11] V. V. Sharonov, Astron. J. USSR 20, 21 (1943).

[12] Tables for the Calculation of Natural Luminance and Visibility [In Russian] (Izd. AN SSSR, 1945).

[13] V. V. Sharonov, Uch. Zap. LGU 53, 5 (1940).

[14] P. P. Feofilov, Doklady Akad. Nauk SSSR 34, 252 (1942); Izv. Akad. Nauk SSSR, Ser. Geograf. i Geofiz. 6, 290 (1942).

[15] V. V. Sharonov, Uspekhi Astron. Nauk 6, 181 (1954).

[16] G. Rougier, Ann. Observ. Strassbourg. 2, 3 (1933).

---

* Leningrad State University.

PHOTOELECTRIC PHOTOMETRY OF SECTIONS OF THE SURFACE OF MARS

V. I. Moroz and A. V. Kharitonov

In 1956, during the favorable opposition of Mars, measurements of the brightness of regions of the planet's surface were made with an electrophotometer and reflector, $f = 11.26$ m, $d = 50$ cm. In order to single out the regions, an approximately elliptical diaphragm, 0.12 × 0,17 mm, was used, the diameter of the image of Mars being ~ 1.3 mm. For photometry blue, yellow, and,in some cases, red color filters were used, the effective wavelengths of which, in combination with the spectral characteristic of the photomultiplier and the energy distribution curve of the spectrum of Mars, were 4495, 5450 and 6050 A,respectively. The recordings fof the photometer were read directly. Observations made during 6 nights (the end of August and September) of 37 different points of the surface of Mars were chosen for reduction. The observations were referred to a comparison star, sufficiently close to Mars. The stellar magnitude and color index in the international system of the two comparison stars used were determined in October with sufficient accuracy by referring them to six stars, included in Eggen's photoelectric catalog.

As a result the international photovisual and photographic magnitudes of the brightness (the brightness of 1 sec^2, expressed in stellar magnitudes) and the color indices of different points of the planet's surface were derived. The stellar magnitude of the brightness of each measured point was used for determining the albedo. The data are given in the form of tables and maps. The contrast between the maria and continents is comparatively small. For $\lambda_e =$ $= 5450$ A it does not as a rule exceed $0\overset{m}{.}1$, and usually equals only several hundredths. The contrast in blue light is less, but on the whole the color index of the maria differs little from that of the continents (the maria are a little "bluer"). Evidently the contrast between dark and light regions varies strongly with time, in particular from one opposition to another, in dependence on different factors. Of the regions measured, of special interest is that of the bright cloud which appeared at the end of August. The contrast between the cloud and the "undisturbed" surface was $0\overset{m}{.}07$ in photovisual and $0\overset{m}{.}01$ in photographic light. For one of the nights the radiometric luminous intensity from 1 sec^2 of the planet's surface in three wavelengths was calculated.

1. Introduction

Data on the brightness, color and contrast of light and dark regions on the surface of Mars, in spite of the exceptional interest centered on the study of that planet from several points of view, have been scarce and contradictory. It is sufficient to turn to the more extended and, apparently, up to date review by G. de Vaucouleurs [1]. Observations carried out at the time of various oppositions lead to different values for the contrast of dark and light regions. De Vaucouleurs was inclined to attribute this to some sort of systematic observational errors and to give greater weight to those observers obtaining higher contrast values. The weak contrast between light and dark regions, characteristic of the last opposition, has meanwhile been established as an indisputable fact flowing from observations performed using different procedures. Probably, changes in the Martian atmosphere as a whole and, possibly, other factors as well, may bring about certain significant changes in the albedo of the dark and light regions and in the contrast between them. Such phenomena as the disappearance, for a short time (three days), of the polar ice cap, the appearance of a large and bright cloud, have been duly noted by all who observed Mars during the time of the recent opposition, and much has been said on those points. As regards the color of the dark regions, de Vaucouleurs views the visually observed bluish hue of the maria as hardly acceptable proof for a growth of albedo of the maria with decrease in wavelength ([1], p. 261), giving no credence to the photometric data which are, besides, rather scanty.

Taking the above into account, it seemed to us of interest to carry out photoelectric measurements of the brightness and color of various sections of the surface of Mars with the intention of obtaining sufficiently accurate values for brightness, albedo, color and contrast between light and dark regions. The basic difficulty to be overcome in photoelectric observations of regions of the surface of planets appears to be flicker. To circumvent this difficulty is impossible without having recourse to very high-speed recording. There remained only the choice of selecting nights with rather little flicker. However, it must be noted that the same difficulty is associated with photographic photometry; in ordinary exposures of the order of a tenth of a second, the effect is almost of the same degree. Flicker interference effects are partially removed in visual observations, since the eye is capable of abstracting from the oscillations of the disk as a whole. Preliminary findings on special studies of flicker on the Kamensk plateau near Alma-Ata (where the Astrophysical Institute is located), carried out by L. N. Tulenkova, demonstrated that flicker is not very high and is less than a second of arc on good nights at a telescope aperture of 20 cm.

We were familiar with only one earlier attempt to perform electrophotometric measurements of sections of the surface of Mars, about which only one very brief communication has come to light [2]. A small diaphragm was used to scan the disk of Mars, photometric sections were recorded, and a chart giving the brightness distribution was drawn up on the basis of the records. We made use of a simpler approach. Below, we give a description of the equipment used (§ 2), the technique for observing Mars and the absolute reference (§ 3), and the findings which we obtained in the observations carried out during the time of opposition of Mars in 1956 (§ 4).

2. Photoelectric Photometer

The observations were performed using a photoelectric photometer, set at the Cassegrain focus of the 50 cm reflector of the Astrophysical Institute (f = 11.24 m). The photometer, in essence a stellar electrophotometer, was designed by V. I. Moroz and built in the mechanical workshop of the Astrophysical Institute. The optical arrangement of the photometer may be seen in Fig. 1. The 00' axis is the optical axis of the telescope. The diaphragm 1, a round orifice in a specular surface mounted on a revolving drum 2, is located on the 00' axis. Turning the drum and fixing it in corresponding positions, it is possible to set diaphragms of different diameters on the optical axis. Perpendicular to the latter and situated above the working diaphragm is the ocular 3. With the aid of this ocular, it is possible to observe the image in the focal plane and, by operating the proper keys, to fix a star, a section of the surface of a planet, etc, in the diaphragm. In observations of Mars, an ocular with a relatively small magnification (simple lens f = 90 mm) was used for zeroing in. For photometry of Mars, a diaphragm 0.171 mm in diameter was employed. It was projected onto the focal plane as an ellipse having axes 0.171 × 0.121 mm or $3''.15 \times 2''.24$. This diaphragm appeared on the disk of the planet as a black point. It was scratched into the film of an aluminized mirror by means of a needle and a foil stencil. Since remnants of the film inevitably remain when the diaphragm is prepared in that fashion, its effective area, necessary for calculating brightness, was measured by means of a photometric comparison with a hole drilled in metal, the area of which was later determined using a universal measuring microscope UIM-21. The comparison of the areas was carried out on an MF-2 microphotometer,

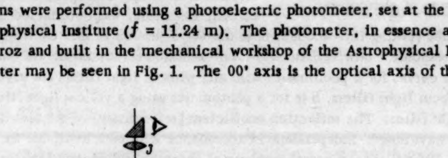

Fig. 1. Optical details of photoelectric photometer.

through the slit of which were passed alternately images of the diaphragm and of the hole in the metal plate. A portion of the mirror was freed entirely from the film, and, in the comparison, the plane of the hole through the metal was superposed onto the surface of glass on the portion completely freed from film. As a result, in passing from the diaphragm being used to the comparison hole, no refocusing of the microphotometer was required. Transmission of the mirror glass with the diaphragm was later measured on a monochromator and was found to be independent, in the region of the spectrum concerned, of the wavelength (of 9% losses in the glass, at least 8% were contributed by reflection and only the remainder by absorption). The effective area of the working diaphragm proved to be about half that of the geometrical area. The dimensions of the working diaphragm given above are the geometrical ones. They in fact determine what are the dimensions of that section of the planet encompassed in the diaphragm. The ratio of effective to geometrical area gives the total transmission of the remnants of the aluminum film. The wavelength dependence of the transmission of those remnants was not successfully revealed. For observations of comparison stars, a second diaphragm of considerably larger diameter (5 mm) is found on the diaphragm. This diaphragm is a hole drilled through a silver-coated glass plate.

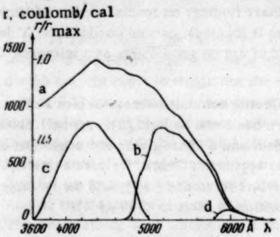

Fig. 2. Spectral response of photometer.

The optical arrangement of the photometer incorporates, as usual, a Fabry lens giving an image of the principal mirror on the cathode 5 of the photomultiplier. There are two measuring rules (6 and 7) serving the light filters. A continuously active phosphor is mounted on one of these bars (alpha-particle activation), the phosphor serving to monitor the sensitivity of the apparatus. An electromagnetic stop 9 is controlled by the observer taking notes and recording. The polarization analyzer 4 contained in the optical assemly of the photometer was removed during observations of Mars.

ZhS-17 and SS-5 light filters were used for observations of Mars. The spectral response of the photoelectric multiplier was determined by using a UM-2 monochromator and a standard tube (taking into account both the dispersion curve and the transmission properties of the monochromator), and the response characteristic was later corrected somewhat on the basis of the observation of comparison stars. Isoenergetic curves for a photometer with and without light filters are given in Fig. 2. Curve a is referred to a photometer without light filters, b is for a photometer using a yellow light filter, and curve c is for a photometer using a blue light filter. The reflection coefficient [reflectivity] of the aluminized mirrors of the telescope was assumed to be wavelength-independent in accordance with data available in the literature [3]. The effective wavelengths of the light filter – spectral response of photomultiplier – optical transmission – atmospheric transmission – energy distribution combination in the spectrum of Mars were equal to 5450 A for a ZhS-17 [yellow] filter and 4495 A for a SS-5 [blue] filter. The choice of filters was arrived at from considerations of adequately satisfactory approximation of the observational system of stellar magnitudes and color indices to the international system.

The electrical circuitry of the photometer is presented in Fig. 3. A photoelectronic multiplier of the FEU-19M type, with a planar semitransparent cathode acting as light receiver in the photometer, operated with voltage scaled down to 750 v during observations of Mars. The sensitivity of the tube at the spectral response peak (in the neighborhood of 4400 A) amounted to about 1420 coulombs/ cal. In observations on weak stars, the voltage may be increased on up to 1000 v, with the sensitivity increased 35 times in the process, but this also involves an increase in the dark current, whose oscillations set limits on the penetrating power of the photometer of magnitude 11^m (without a light filter, stars of such brilliance may be examined photometrically to an accuracy of ~ 3%).

The anode current of the photomultiplier is amplified by a simple dc vacuum tube amplifier. This amplifier consists of a differential cathode follower, whose tubes operate with reduced grid current. A similar circuit is given detailed description and discussion in [4, 5] . A variant of this circuit, employed in the photoelectric photometer in question, is characterized by the parameters tabulated in Table 1 below.

An M-25 galvanometer (sensitivity $2.1 \cdot 10^{-9}$ amp/mm/m, period of natural vibrations 6.8 sec., R_{cr} = 420 ohms, R_{int} = 87 ohms) functioned as recording instrument. The dependence of the amplifier output current on the input voltage was linear over a wide range. The gain varied by steps from 0.4 to 4000 with a variation of input impedance from 10^4 to 10^8 (using switch P). Brightness measurements of the sections of the surface of Mars were performed at an input impedance of 10^7 ohms. Since accurate input impedance values were not equal to rated values and may, generally speaking, vary with time, the ratio of gain at different ranges was determined empirically when using ranges in the measurements. These determinations were done in a very simple manner; the flux from the photometric standard (the phosphor) was measured over two comparable ranges at a certain definite photomultiplier supply voltage, which was chosen such that readings over both ranges could be made with sufficient accuracy. If it became necessary to compare a larger number of ranges, the photometric standard was measured at two or three different values for the photomultiplier supply voltage.

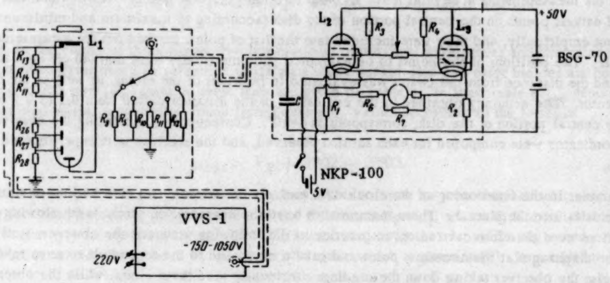

Fig. 3. Electrical circuitry of photometer.

The supply voltage source for the photoelectronic multiplier was a high-voltage stabilized rectifier VVS-1, the output voltage of which could be set within the range of 550 to 1050 v. As demonstrated by an experiment using this rectifier in electric photometric installations of the Astrophysical Institute, its stability was fully satisfactory.

TABLE 1

Tube grid current	$2 \cdot 10^{-11}$ amp
Slope of gain	40μa/v
Peak current gain	4000
Anode supply voltage	50 v
Tube filament voltage	4 v
Voltage fluctuation limit	$3 \cdot 10^{-5}$ v
Current fluctuation limit	$3 \cdot 10^{-13}$ amp

The accuracy of measurement of flux from a constant and sufficiently bright source, which could be provided by the photometer, was rather high; the average quadratic error of the arithmetic mean from four readings in measurements of such a source (and it was, in fact, a very quiet phosphor, free from spurious oscillations, which was at our disposal in testing the experiment) did not exceed $0\overset{\text{m}}{.}002$. The accuracy obtained in the photometry of astronomical objects was naturally lower, since it was restricted by the errors introduced by the earth's atmosphere.

3. Procedure for Observations of Mars and Reference to International System of Stellar Magnitudes and Color Indices

Photoelectric observations of Mars were carried out in the manner described below. The focal image of the planet was set on the optical axis of the telescope. The disk was viewed visually with the aim of clearing up characteristic details visible on the surface of the planet, and evaluating the extent of flicker. A certain amount of experience with preparatory test observations was required in order to gain the ability to determine at what point the flicker present would render photometry impossible, and up to what point it would not. However, a small amount of flicker was a necessary, but not a sufficient condition for the possibility of carrying out similar observations. Stable transparency was also required. It often happened that instants of exceptionally little flicker coincided with extreme instability with respect to transparency, and a certain impression of possible correlation between the two was even created. Usually, the second half of the night was more favorable for observations of Mars.

When the state of the atmosphere was acknowledged to be sufficiently good, several points were observed on the disk in a manner such that part of them were to be found in bright and others in dark regions. In order to minimize the effect of limb darkening on our results, we avoided carrying our observations too close to the limb. At first, a relatively large number of observation points (8 points, for instance, on August 28-29) were chosen, while, towards the end of the observation period, we preferred to measure a small number of points (e.g., 3 on Sept. 17-18), but repeated the measurements in several runs, in order to obtain the best possible verified contrast values. The brightest and darkest points on the central portion of the disk (according to maximum and minimum readings) were thus sought out empirically, and they were included into the list of points marked out for measurement in the original schedule. The positions of the points to be examined photometrically were marked off on a rough drawing of the disk and the distance from the center was evaluated in fractions of the radius, as well as the orientation of the radius vector. The accuracy obtained in the evaluation of the distance varied from 0.1 to 0.2 of the radius, which, in the central portion of the disk, corresponds to 5-10°. Consequently, in treating the observations, areographical coordinates were computed for each section observed, and the sections were superimposed onto a map of Mars (Fig. 6).

Inaccuracies in the functioning of the clockwork, entirely unnoticeable in observations of stars, introduced certain difficulties into the picture. These inaccuracies have the character of gentle jerks, slowing-downs, etc. The observations were therefore carried out in practice in the following manner: the observer, working at the ocular, set the diaphragm at the necessary point and gave a command to the second observer to take down the reading; or else the observer taking down the readings continually read them aloud, while the observer working at the ocular selected out those readings which coincided in time with the correct setting of the diaphragm, correcting the orientation with a fine movement of the key adjustments, when the diaphragm moved off the observed point. The inaccuracies alluded to in the functioning of the clockwork prevented us from trying out the method of recording sections. Besides, at conventional recording speeds, there is some basis for doubting the effectiveness of the last-mentioned technique for the task in question, since the technique must be more sensitive, if you please, to flicker than is the method of direct readings. The method of recording sections is an intriguing one in that it makes it possible to obtain data on limb darkening, which the method of obtaining direct readings is virtually incapable of providing. We were not in a position to measure limb darkening, since, at the peripheral parts of the disk, an accurate fix on the position of the diaphragm is required, and cannot be realized in practice owing to the difficulty of evaluating the distance by eye, and also because of the uneven behavior of the clockwork and flicker. In measurements of the central portion of the disk, all these factors acted essentially to a lesser degree, although even they were capable of causing a reduction in the measured values of contrast, compared with real values. Dark regions apparently suffered more from too high measured values for brightness, than did the light areas from reduced values (on account of the relatively smaller area presented by the former).

In measurements made with a yellow filter, readings on a half-meter galvanometer scale were of the order of 300 mm, while measurements made by the blue filter were of the order of 100 mm. The time required for each reading amounted to 5-10 sec.

The observations were carried out jointly by both authors in the course of a number of nights during August and September, six of those nights being selected for treatment of the data (August 28-29 and 30-31, September 1-2, 10-11, 11-12 and 17-18). Some additional material was obtained on October 5-6, whereby, to the two light filters in earlier use, a third red filter KS-10 was added (λ_e = 6050 A; isoenergetic curve of the photometer using this filter; curve d in Fig. 2).

The comparison star was subjected periodically to photoelectric measurement, the star chosen being sufficiently close to Mars, with AG 8421 serving exclusively as the reference star up until September 1-2, then to be replaced by 93 ψ_2 Aqr (Table 2).

The difference in the heights of the reference star and of Mars did not exceed 2°, and the correction for differential extinction arising on account of the difference in air masses was calculated on the basis of mean values of the coefficient of transparency. The question relating to the effect of the difference in the effective wavelengths when taking transparency into account will be discussed further below. In taking measurements of the reference stars, a diaphragm of 5 mm diameter was employed.

TABLE 2

	α_{1950}	δ_{1950}	m_{Ipv}	C_I
AG 8421	$23^h45^m08^s$	$-9°16'.5$	$5^m.77 \pm 0^m.015$	$+0^m.918 \pm 0^m.012$
$93\psi_2$ Aqr	23 15 18	-9 27.3	4.43 ± 0.01	-0.183 ± 0.007

In October, in the course of three nights, the international photovisual magnitudes and the color indices of the reference stars were determined by reference to six stars whose magnitudes and color indices are contained in Eggen's catalog of 833 stars [6]. Data on these stars are given in Table 3. In that table m_{Ipv} denote the international photovisual stellar magnitudes, found from Eggen's V_E values according to the formula

$$m_{I\,pv} = V_E + 0^m.02 \pm 0^m.03. \tag{1}$$

The error indicated is the probable error for one comparison. This formula may be obtained with ease by taking into account the fact that the systematic component of the difference $V_E - V_J$, where V_J is the stellar magnitude in the Morgan-Johnson system, equals, at most, $0^m.0015$, and consequently may be safely neglected. We determined $m_{Ipv} - V_J$ in accordance with the table of V_J values for NPS stars, which is given in [7]. It is equal to $0^m.02 \pm 0^m.02$

TABLE 3

Star	α_{1900}	δ_{1900}	m_{Ipv}	Spectrum	C_I	$(m_\psi - m)_A$	$0{,}12 \times (C_\psi - C)_I$	$(m_\psi - m)_{I\,pv}$	$m_{\psi I pv}$
δ Tri	$2^h10^m.8$	$+33°46'$	$4^m.90$	G 0V	$+0^m.497$	$-0^m.57$	$+0^m.08$	$-0^m.49$	$4^m.41$
γ Ceti	2 38.1	2 49	3.48	A2V	+0.035	+0.91	+0.03	+0.94	4.42
α Ceti	2 57.1	3 42	2.51	M2III	+1.519	+1.72	+0.20	+1.92	4.43
λ Aur	5 12.1	40 01	4.70	G0V	+0.512	−0.37	+0.08	−0.29	4.41
γ Aql	19 41.5	10 22	2.66	K3II	+1.392	+1.56	+0.19	+1.75	4.41
γ Aqr	22 16.5	1 53	3.89	A0V	−0.120	+0.57	+0.01	+0.58	4,47
						Mean			$4^m.43 \pm 0^m.01.$

and accordingly, taking into account the fact that the probable error of the one difference $V_E - V_J$ is equal to $\pm\ 0^m.017$, we obtain (1). The spectral classes in Table 3 are presented according to [6]. The color indices are obtained from the Eggen values according to the formula

$$C_I = \frac{(P-V)_E + 0^m.040}{1.065}. \tag{2}$$

In [6], that expression is derived for the association of C_p with $(P-V)_E$, where C_p is the color index in the system used in Eggen's earlier works. In conformity with [8], the mean difference $\overline{C_p - C_I} = \pm\ 0^m.019$, there is no systematic deviation and, consequently, we are justified in using (2). The probable error for the relationship between C_p and $(P-V)_E$ amounts to $\pm\ 0^m.011$, from which we get a probable error for (2) equal to $\pm\ 0^m.022$.

The seventh column in Table 3 gives the measured extra-atmospheric ratio in the brightness of the reference star No. 2 (93 ψ_2 Aqr), and the brightnesses of each of the Eggen stars. This ratio, expressed in stellar magnitudes in the observational and international systems of stellar magnitudes, was found on the basis of the same stars and six NPS stars (No. 1, 4, 5, 2r, 7, 9) in the form

$$\delta m_{Ipv} = \delta m_A - (0.12 \pm 0.01)\,\delta C_I, \tag{3}$$

where δm_{Ipv} is the difference in the stellar magnitudes of some pair of stars in the international system, δm_A is the same difference in the observational system, δC_I is the difference in the international color indices. The probable error for one comparison of δm_{Ipv} and δm_A is equal to $\pm\ 0^{m}03$. To obtain this relationship, the differences $\delta m_{Ipv} - \delta m_A$ were computed for each of the stars in Table 3 and for the stars of γ Ceti (class A2 V, $C_I = \pm\ 0^{m}035$) and in NPS between each of the observed stars and star No. 5 (class A2, $C_I = \pm\ 0^{m}00$), and all of these differences were laid out on the graph shown in Fig. 4 as a function of δC_I. The method of least squares was utilized to find the angular coefficient 0.12 ± 0.01.

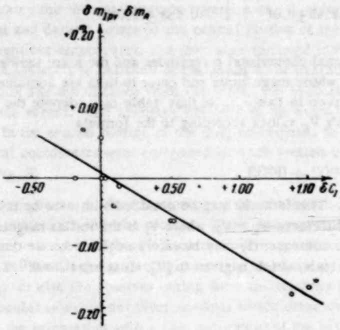

Fig. 4. Relation between observational system of stellar magnitudes and international system.

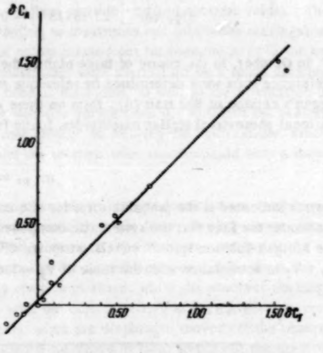

Fig. 5. Relationship between observational system and international system of color indices.

By means of relation (3), the differences of the stellar magnitudes $(m_\phi - m)_A$ in the observational system were converted to the differences $(m_\phi - m)_{Ipv}$, given in Table 3 in the ninth column. The differences $(C_\phi - C)_I$ needed to compute $(m_\phi - m)_{Ipv}$ were found from the measured differences $(C_\phi - C)$ on the basis of the relation

$$\delta C_I = (1.005 \pm 0.016)\, \delta C_A, \tag{4}$$

determined from the observations of the stars in Table 3, the same NPS stars, Capella and Vega in the same manner as was done in the case of the stellar magnitudes. A graphic representation of that relationship is given in Fig. 5. The probable error in one comparison of δC_I and δC_A amounts to $\pm\ 0^{m}04$. The extra-atmospheric magnitude of the reference star No. 2, determined on the basis of each of the stars appearing in Table 3, is given in the last column of that table. The color index given in Table 2 for star No. 2 was determined by comparison with the stars in Table 3 (adding Vega and Capella) and using relation (4).

$(m_\phi - m)_A$ and $(C_\phi - C)_A$ were determined by using the differential method, the procedure resorted to making it possible to circumvent determination of the coefficient of transparency. Attempts to use Bouguer's method, as might have been anticipated, led to the conclusion that is was impossible to adopt that method for purposes of accurate photometry, owing to the time variation of the coefficient of transparency. Nikonov's method [9], as in general any method requring the use of extra-atmospheric magnitudes and colors, calls for rather protracted preparatory work on the one hand, and on the other (in the case of stellar magnitudes), implies a high stability, of long duration, on the part of the control phosphor. We employed the following technique. All the stars to which $93\phi_2$ Aqr was compared were chosen with declinations exceeding the declination of the latter. Moments were computed for each star, when the given star and $93\phi_2$ Aqr reached the same height. $93\phi_2$ Aqr was scanned photometrically many times in the course of a night, and the dependence of the logarithm of the reading on the air mass for all the nights was obtained. Each star listed in Table 3 was scanned photometrically once in the vicinity of the moment when

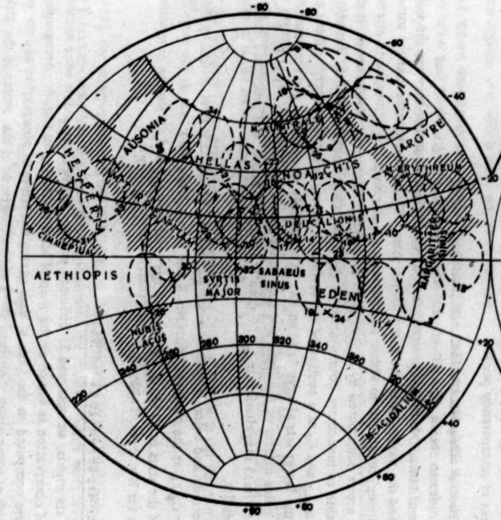
AUSONIA
HELLAS
NOACHIS
ARGYRE
M. AUSTRALE
M. ERYTHREUM
HESPERIA
M. CIMMERIUM
DEUCALIONIS
MARGARITIFER SINUS
AETHIOPIS
SYRTIS MAJOR
SABAEUS SINUS
EDEN
NUBIS LACUS
M. ACIDALIUM
OGIGIS
AONIS SINUS
THAUMASIA
M. CIMMERIUM
M. CIRRENIUM
MEMNONIA
NILOCERAS
TEMPE
-90
-80
-60
-40
-20
+20
+40
+60
+80
+90
220
240
260
280
300
320
340
360
20
40
60
80
100
120
140
160
180
200
220

Fig. 6. Chart of Mars showing areas observed.

it was found at the same height as $93\psi_2$ Aqr,and again once or twice after the same or some other interval of time had elapsed, so that the slope of the Bouguer straight line graph at about the moment indicated was determined for each such star. On the basis of those data, the difference in the observed stellar magnitudes of $93\psi_2$ Aqr and of the given star was computed with ease exactly at the moment they were found at the same elevation. Since, at that moment, the atmosphere attenuated the fluxes emanating from both stars to the same degree, this difference is precisely the extra-atmsopheric difference which it was required to find $(m_\psi - m)_A$. The latter is actually realized, true enough, only for the case of narrow light filters or for stars of closely related spectral classes, when the difference of the effective wavelengths for compared stars may be safely neglected. In the case of wide light filters and a large difference in spectral classes, it may not be neglected owing to the wavelength dependence of the coefficient of transparency. If we turn to the real form of this relation, which, for the Kamensk plateau, was determined by V. S. Sokolova [10] and T. P. Toropova [11], it is possible to arrive at the fact that, for a yellow filter (visual region), the effect under discussion is a slight one, and may be left out of consideration. However, with observations using a blue filter, the difference may be in excess of $0\overset{m}{.}1$ (if stars of classes B or M are compared). Thus, the color difference may be drastically affected by the difference in atmsopheric extinction (even in observations at different heights at the same moment, as was actually done in the present case), arising on account of the difference in effective wavelengths. A similar effect, with application to observations of variable stars, was discussed by V. B. Nikonov and E. K. Nikonova [12].

We emerge from the position outlined above in the following manner. Since, in the last analysis, we need the extra-atmsopheric values not of δC_A, but of δC_I, and the relationship between the catalog values of δC_I and the observational values of δC_A is determined to an appreciable extent from the observations made on the same stars with the same intervening atmospheric masses as were later used to determine the differences $(C_\psi - C)_A$, we may assume that, in employing this empirical relationship, the effect of the spectral class on transparency is automatically offset when we employ it for the purpose of finding $(C_\psi - C)_I$ on the basis of $(C_\psi - C)_A$. The error arising on account of the factor considered, in that operation, is roughly the same with respect to absolute magnitude as the one arising when the dependence of δC_A on δC_I is plotted, but is however of opposite sign. The essential of the matter is that the wavelength dependence of the coefficient of transparency is considerably more stable in time than the coefficient of transparency per se.

Since the comparison of $93\psi_2$ Aqr and Mars was performed at the same elevations we are in a position to employ relation (4) in order to obtain, in addition, the differences $(C_M - C_\psi)$, where C_M is the color index of segments of the surface of Mars. We failed to detect any appreciable correlation between the color variation of the segments scanned and the variation in the atmospheric mass. This demonstrates that the somewhat primitive (with respect to color index) technique to which we had recourse in computing atmospheric attenuation gives errors smaller than the errors contributed by flicker and inaccurate orientation. Furthermore, it should be noted that the errors attributable to inaccurate computation of the transparency have a slightly distorting effect only on the absolute values of m_{Ipg} and C_I of a section of the surface of Mars, being absolutely without effect on the contrast in m_{Ipg} and C_I, since the latter was always quite small. It is possible to evaluate the corresponding correction to the mean value of the color indices of the light and dark areas on all the nights, derived in § 4. This comes to $+ 0\overset{m}{.}02$. In the case of visual magnitudes m_{Ipv}, as already indicated above, the procedure under discussion gives completely accurate results.

The stellar magnitude and color of the reference star No. 1 (AG 8421) is determined by measuring $(m_{No.\,1} - m_\psi)_A$ and $(C_{No.\,1} - C_\psi)_A$ at the moment when No. 1 and No. 2 ($93\psi_2$ Aqr) are at the same height, rather than directly on the basis of the stars in Table 3. Therefore the error in m_{Ipv} and CI for the comparison star No. 1 is somewhat greater than for No. 2 (cf. Table 2).

4. Results of Observations of Mars

In the course of six nights, we observed 37 different points. All of those points were numbered in the approximate chronological order of observation as shown on the map of Mars appearing in Fig. 6. Areographic coordinates of the observed points were computed on the basis of data giving the times of observation and the coordinates of the visible center of the disk at some given moment. Data on the longitude of the center of the disk of Mars were taken from [13], and the latitude was numerically equal to the inclination of the earth as seen from Mars. This value was also given in [13]. Details given on the chart of the Martian hemispheres are taken from the chart compiled by D. P. Avigliano on observations of Mars made during the 1954 opposition [14]. The observed localities on the

Martian surface are indicated on the chart in the form of ellipses drawn by dashed lines, corresponding to our diaphragm with the orientation of the diaphragm at the moment of observation relative to the Martian meridians and parallels taken into account, and with the proper scale observed.

Some of the 37 points were observed several times each, and one point (No. 2) was subjected to observation during the course of two nights.

The brightness of segments of the Martian surface is expressed in terms of stellar magnitudes; with the effective area of our diaphragm known, computed, as mentioned earlier in the discussion, by taking into account absorption in the glass and in the film residues, and also taking into account the focal length of the telescope, equal to 11.24 ± 0.06 m (found by measuring the diameter of a plate of Mars taken on the night of September 15-16), it was possible to express the effective area of the diaphragm in square seconds, and then to refer the brightness found for segments of the surface of Mars to one square second. The characteristic so obtained is known as the stellar magnitude of luminosity, according to [15], for example.

The international photovisual m_{Ipv} and photographic m_{Ipg} stellar magnitudes of luminosity for the segments of the surface of Mars which we observed are given in columns 4 and 6, respectively, of Table 4. In the same columns are tabulated the number of independent measurements (in parentheses; each of the measurements consisted of several readings). Where a particular spot was observed several times, the arithmetic mean is given, and for point No. 2, observed over the course of two nights, the data obtained for each night are presented separately. The stellar luminosity magnitudes and color indices (column 8) are given to $0\overset{\mathrm{m}}{.}001$, although the magnitudes and color index of the reference stars are known only to $0\overset{\mathrm{m}}{.}01$. This is done in order to avoid blurring the limited, but real contrasts of detail.

In the first column of the table, we have the numbers of points as they are designated on the chart, and with them an indication as to just where on the disk of the planet the point in question was observed. The second column gives dates of observation and the world time, while, for points observed several times during a night, the average time of observation is given. In the third column, we have the areographic coordinates, and for some points the names of the Martian regions with which these points coincided.

The albdeo was also determined for each point. It was found on the basis of the following considerations. Let $E_e = a \cdot 10^{-0.4m_\odot}$ be the illumination of the earth from the sun, let a be some constant dependent on the system of units employed, $m_\odot$ the stellar magnitude of the sun. The amount of illumination falling on Mars will then be

$$E_M = a\left(\frac{\rho_e}{\rho_M}\right)^2 \cdot 10^{-0.4m_\odot},$$

where a is the same constant, and ρ_e and ρ_M are radius vectors of the earth and of Mars. The illumination occurring on the earth, associated with one square second of the surface of Mars, and in the same units, will be $e = a \cdot 10^{-0.4m}$, where m is the stellar magnitude (brightness of 1 sec²).

Since $B = de/d\omega$, where B is the brightness of an extended object, and de is the illumination coming from a segment $d\omega$, we have

$$B_M = \frac{e_0}{\omega} = (206265)^2\, a \cdot 10^{-0.4m}.$$

According to [17], the relative coefficient of brightness, i.e., the ratio of the brightness coefficient of the given surface to the brightness coefficient of an orthotropic-scattering absolute white surface, is equal to $r = B\pi/E$, accordingly

$$r = \frac{\pi B_M}{E_M} = (206265)^2 \pi \left(\frac{\rho_M}{\rho_3}\right)^2 \cdot 10^{0.4(m_\odot - m)}.$$

For an orthotropic-scattering surface, the albedo is equal to the relative coefficient of brightness, and we refer to this, as is usually done, as the magnitude r of the albedo.

TABLE 4

Position of observed point on disk	Date and world time	Areographic coordinates in φ в	φ	^{m}Ipv	^{r}Ipv	^{m}Ipg	^{r}Ipg	C_I	Remarks
1	2	3		4	5	6	7	9	9
1. center of disk	28 Aug. 21^h43^m	—19°	19°			5^m593 (1)	0.054		
2. center of disk	28 Aug. 22 28	—19	28	4^m125 (1)	0.115				Contrast between points 2 and 7 at its peak and equal to 0.13 in photo-visual beams
$\sim\frac{1}{2}R$ east of center	1 Sept. 22 43	M. Erytreum		4.037 (2)	0.124	5.436 (2)	0.063	$+1^m399$	
3. $\sim\frac{1}{2}R$ north of center	28 Aug. 21 43	+11	18		—	5.563 (1)	0.056		
4. $\sim\frac{1}{2}R$ south of center	28 Aug. 21 44	—49	19		—	5.539 (1)	0.057		
5. $\frac{3}{4}-\frac{4}{5}$ SSW of center	28 Aug. 22 16	—72	5	3.993 (3)	0.130	5.506 (1)	0.059	+1.513	
6. $\sim\frac{1}{2}R$ SE of center	28 Aug. 22 01	—43	54	4.027 (3)	0.126	5.609 (1)	0.053	+1.582	Points No. 6 and No. 7 on bright cloud
7. $\sim\frac{1}{2}R$ south of center	28 Aug. 22 12	—49	24	3.998 (1)	0.129				
8. $\frac{3}{4}-\frac{4}{5}R$ NNE of center	28 Aug. 23 52	+21	62	4.076 (2)	0.120	5.525 (2)	0.058	+1.449	Falls on cloud observed Aug. 28 and increasing in size
9. $\sim\frac{1}{2}R$ south of center	30 Aug. 22 21	—56	348	3.994 (4)	0.130	5.488 (2)	0.060	+1.494	
10. center of disk	30 Aug. 22 25	—19	11			5.509 (1)	0.058		
11. $\sim\frac{1}{2}R$ north of center	30 Aug. 22 26	+12 Gehon	10	4.067 (3)	0.121	5.519 (3)	0.058	$+1^m486$	
12. $\sim\frac{1}{2}R$ west of center	30 Aug. 22 26	—25 Noachis and Fretum Pandorae	345	4.087 (3)	0.119	5.518 (4)	0.058	1.431	
13. $\sim\frac{1}{2}R$ east of center	30 Aug. 22 29	— 8 M. Erytreum, Chrise	25	4.062 (1)	0.121	5.538 (2)	0.057	+1.476	
14. center	1 Sept. 21 04	—19 Near Deucalionis	333	3.985 (1)	0.131				

TABLE 4 (continued)

1	2	3	4	5	6	7	8	9
15. $\sim\frac{1}{2}R$ west of center	1 Sept. 22^h42^m	−19° 327° includes Sabaeus sinus	4^m027(2)	0.126	5^m371(2)	0.066	$+1^m344$	
16. center	1 Sept. 22 27	−19 351 Noachis a. Deucalionis	3.985 (1)	0.131	5.349 (1)	0.068	+1.334	
17. center	1 Sept. 21 02	−19 0	4.095 (1)	0.118				
18. $\sim\frac{2}{3}R$ south of center	1 Sept. 21 30	−60 340			5.399 (1)	0.065		
19. $\sim\frac{2}{3}R$ north of center	1 Sept. 21 26	+12 340			5.403 (1)	0.064		
20. $\sim\frac{2}{3}R$ west of center	1 Sept. 21^h15^m	−19° 300° near Syrtis Majoris	4^m062 (1)	0.121	5^m411 (1)	0.064	$+1^m349$	
21. $\sim\frac{2}{3}R$ SE of center	1 Sept. 21 47	−40 300 Hellas	3.968 (1)	0.133	5.386 (1)	0.065	+1.354	
22. $\sim\frac{3}{4}R$ SSW of center	1 Sept. 21 52	−56 315 M. Australe	4.018 (1)	0.127	5.440 (2)	0.062	+1.422	
23. $\sim\frac{1}{5}R$ NE of center	1 Sept. 22 04	−10 340	4.002 (1)	0.129	5.396 (1)	0.065	+1.394	
24. $\sim\frac{1}{2}R$ north of center	1 Sept. 22 33	+10 353	3.982 (2)	0.131	5.357 (2)	0.067	+1.375	
25. $\sim\frac{1}{2}R$ south of center	1 Sept. 22 40	−50 355	3.959 (2)	0.134	5.355 (2)	0.067	+1.396	
26. $\sim\frac{1}{2}R$ north of center	10 Sept. 21 20	+10 260	3.828 (2)	0.152	5.308 (2)	0.070	+1.480	
27. $\sim\frac{1}{2}R$ west of center	10 Sept. 21 18	−19 229 M. Cimmerium	3.808 (2)	0.155	5.281 (2)	0.072	+1.473	
28. $\sim\frac{1}{2}R$ south of center	10 Sept. 21 38	−49 262	3.789 (4)	0.158	5.266 (2)	0.073	+1.477	
29. $\sim\frac{1}{2}R$ east of center	10 Sept. 21 32	−19 287 M. Tyrrenium	3.805 (4)	0.155	5.288 (2)	0.072	+1.483	

TABLE 4 (continued)

30. $\sim \frac{1}{4}R$ south of center	10 Sept. $21^{h}47^{m}$	— 5° 265° Aethiopis	$3^{m}.765$(1)	0.161				
31. $\sim \frac{1}{2}R$ west of center	10 Sept. 21 49	—17 236 M. Cimmerium	3.824 (2)	0.153	$5^{m}.211$(1)	0.077	$+1^{m}.387$	
32. $\sim \frac{1}{2}R$ NW of center	11 Sept. 19 03	—14 305 Syrtis Majoris	3.890 (1)	0.144	5.398 (1)	0.065	+1.508	
33. $\sim \frac{1}{4}R$ WSW of center	11 Sept. 19 03	—25 240 Hesperia	3.845 (1)	0.150	5.376 (1)	0.006	+1.531	
34. $\sim \frac{1}{2}R$ south of center	11 Sept. 19 06	—49 280 Hellas	3.875 (1)	0.146	5.394 (1)	0.065	+1.519	
35. center	17 Sept. 19 05— 19 31	—20 148 Memnonia	3.918 (4)	0.141	5.456 (3)	0.062	+1.538	
36. $\sim \frac{1}{4}R$ west of center	17 Sept. 18 02— —20 18	—20 138	3.902+ 0.007 (10)	0.143	5.450± 0.007(10)	0.062	+1.548	
37. $\sim \frac{1}{2}R$ ESE of center	17 Sept. 18 06 — —20 17	—25 170	3.954± 0.014 (5)	0.137	5.468± 0.006 (6)	0.061	+1.514	

TABLE 5

	28–29 August		30–31 August		1–2 September		10–11 September		11–12 September		17–18 September	
	dark	bright	dark	bright	dark	bright	dark	bright	dark	bright	dark	bright
m_{Ipv}	$4^{m}.125$ (1) τ. 2	$3^{m}.993$ (3) τ. 5	$4^{m}.087$ (3) τ. 12	$3^{m}.994$ (4) τ. 9	$4^{m}.095$ (1) τ. 17	$3^{m}.959$ (2) τ. 25	$3^{m}.828$ (2) τ. 26	$3^{m}.789$ (4) τ. 28	$3^{m}.890$ (1) τ. 32	$3^{m}.845$ (1) τ. 33	$3^{m}.954$ (5) τ. 37	$3^{m}.902$ (10) τ. 36
r_{Ipv}	0.115	0.130	0.119	0.130	0.118	0.134	0.152	0.158	0.144	0.150	0.137	0.143
m_{Ipg}	$5^{m}.609$ (1) τ. 6	$5^{m}.506$ (1) τ. 5	$5^{m}.518$ (4) τ. 12	$5^{m}.488$ (2) τ. 9	$5^{m}.440$ (2) τ. 22	$5^{m}.355$ (2) τ. 25	$5^{m}.308$ (2) τ. 26	$5^{m}.266$ (2) τ. 28	$5^{m}.398$ (1) τ. 32	$5^{m}.376$ (1) τ. 33	$5^{m}.468$ (6) τ. 37	$5^{m}.450$ (10) τ. 36
r_{Ipg}	0.053	0.059	0.058	0.060	0.062	0.067	0.070	0.073	0.065	0.066	0.061	0.062
C_I	($1^{m}.582$) τ. 6	$1^{m}.513$ τ. 5	$0^{m}.431$ τ. 12	$1^{m}.494$ τ. 9	($1^{m}.422$) τ. 22	$1^{m}.396$ τ. 25	$1^{m}.480$ τ. 26	$1^{m}.477$ τ. 28	$1^{m}.508$ τ. 32	$1^{m}.531$ τ. 33	$1^{m}.514$ τ. 37	$1^{m}.548$ τ. 36
Δm_{Ipv}	$0^{m}.132$		$0^{m}.093$		$0^{m}.136$		$0^{m}.039$		$0^{m}.045$		$0^{m}.052$	
Δm_{Ipg}	$0^{m}.103$		$0^{m}.030$		$0^{m}.085$		$0^{m}.042$		$0^{m}.022$		$0^{m}.018$	
ΔC_I	($+0^{m}.059$)		$-0^{m}.063$		$+0^{m}.026$		$-0^{m}.003$		$-0^{m}.023$		$-0^{m}.034$	

The stellar brightness magnitude of Mars was obtained from our own observations, while ρ_M and ρ_e were taken from the "Astronomical Ephemeris." For the stellar magnitude of the sun, using the international photovisual scale, the value $m_{\odot Ipv} = -26^{\mathrm{m}}.72$ was taken in conformity with the review article by Z. V. Kariagina [16], and the photographic stellar magnitude of the sun was based on the color index, which was taken equal to $C_I = +0^{\mathrm{m}}.64$, according to a paper by E. K. Nikonova [17].

The value of the photovisual r_{Ipv} and photographic r_{Ipg} albedoes, computed for the points of Mars which we observed, are given in columns 5 and 7 in Table 4. Column 8 gives the color index for each point observed in double beams.

As a result of the fact that several points were observed only once, and several others a number of times, the accuracy of the values listed in Table 4 for magnitudes is different for particular points. The highest accuracy was evidently registered in measurements of segments observed on September 17-18. On this night, we observed no more than three points (Nos. 35, 36 and 37), but observed them many times. For these, we computed the mean quadratic error of the arithmetic mean of m_{Ipv} and m_{Ipg}, indicated in Table 4 for those points. The probable error in a single determination for those same points amounts to $0^{\mathrm{m}}\,015$-$0^{\mathrm{m}}.021$.

The main source for the spread in the brightness values obtained for the same point is the difficulty of directing the diaphragm accurately on the same point of the planet's image.

The data for each night, for the brightest and darkest points, taken from Table 4, are given in Table 5. Table 5 gives m_{Ipv}, m_{Ipg}, r_{Ipv}, r_{Ipg} and C_I for the brightest and darkest points, indicates the numbers of the latter and the number of observations carried out. The contrast registered in the photovisual Δm_{Ipv} and photographic Δm_{Ipg} beams and in the color index ΔC_I between the brightest and the darkest points for each night are also given. For two nights (August 28-29 and September 1-2), the darkest point in the photographic beams fails to coincide with its counterpart in photovisual beams.

The data in Table 5 are of special interest in connection with the fact that they are to a greater extent free from error. The effect of blurring the contrast, alluded to in §3, exerts its least effect on the data presented in Table 5, since the brightest and darkest points were selected expressly on the basis of the maximum and minimum readings.

Maximum and minimum magnitudes m_{Ipv}, r_{Ipv}, m_{Ipg}, r_{Ipg} and the contrasts vary in an erratic manner from night to night as a consequence of the fact that various details were scanned photometrically (owing to the rotation of Mars) and possibly also on account of random variations in the state of the Martian atmosphere. Values for r_{Ipv}, r_{Ipg}, and contrasts in m_{Ipv}, m_{Ipg} and C_I, averaged over six nights for points of maximum and minimum brightness, are listed in Table 6.

TABLE 6

	$\overline{r}_{Ipv}$	$\overline{r}_{Ipg}$	$\overline{C}_I$	$\overline{\Delta m}_{Ipv}$	$\overline{\Delta m}_{Ipg}$	$\overline{\Delta C}_I$
bright regions	0.143	0.063	1.513	0.083	0.050	—0.053
dark regions	0.133	0.061	1.460			

The difference between $\overline{\Delta m_{Ipv}}$ and $\overline{\Delta m_{Ipg}}$ and $\overline{\Delta C_I}$ does not coincide on account of the fact that, as we have already stated, the darkest points in photovisual beams sometimes failed to present the same aspect in photographic beams. In computing the values of $\overline{r_{Ipg}}$ and $\overline{C_I}$ listed in Table 6, a correction was introduced (alluded to in §3). for $\overline{C_I}$ and similar correction factor for r_{Ipg}:

Maximum contrast for Δm_{Ipv} was obtained on September 1-2, and amounted to $0^{\mathrm{m}}.136$, while maximum contrast Δm_{Ipg}, found on August 28-29, came to $0^{\mathrm{m}}.103$. The maximum contrast in color indices was on August 30-31, equal to $0^{\mathrm{m}}.061$ (cf. Table 5).

During the night of August 28-29, a bright cloud observed to the south of Noachis and Mare Erythreum (shown on the chart by dashed lines) was examined photometrically in a number of other regions. This detail was situated somewhat closer to the limb than the objects which we usually scanned, being despite that fact the brightest region appearing on the disk. A region located at the same distance from the limb, southwest of the continent Tempe, functioned as a comparison object. The contrast between the bright cloud and Tempe amounted to $0^{m}.08$ in photovisual beams and $0^{m}.01$ in photographic beams.

As may be seen from Table 5, the darkest spots in general appear to be a deeper blue as well. Furthermore, if all possible pairs of points observed in the two beams are taken for each night (the number of such pairs will be equal to the number of combinations of two each of the number of points observed each night), and differences ΔC_I and Δm_{Ipv} are formed for each pair, then the relationship between them will take on the form seen in Fig. 7. The correlation coefficient between ΔC_I and Δm_{Ipv} is − 0.13. The relationship finds a rather indeterminate expression, but it nevertheless really exists: 37 points lie above the abscissa, while 21 points are located below the abscissa.

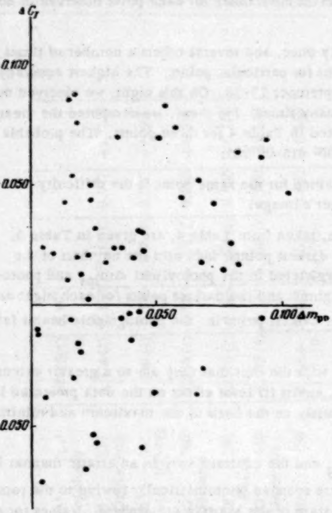

Fig. 7. ΔC_I as a function of Δm_{Ipv}.

In any case, the color difference in bright and dark regions is slight, which affords support to data obtained photographically by V. V. Sharonov [18]. Evidently, the apparent blue color of the maria as observed in visual observations is a phenomenon brought about by purely physiological effects. In observations made by eye (nonphotometrically), the contrast is very sharply enhanced, generally speaking.

From the data which we obtained, it follows naturally that the contrast of dark and light regions was of limited scope during the recent opposition. The variation in contrast from one opposition to the next is apparently quite real in nature. It may be explained by changes in the real properties of the Martian surface, possibly associated with climatic fluctuations. Additional observations were carried out on the night of October 5-6. The absence of phase angle from zero had already been readily noticed even a week before and up to a week after the opposition, and on October 6-7 the phase effect acted as a hindrance to photometric work. It is interesting to note that the maximum effect of the phase angle was exerted in the blue rays, and the minimum effect in the red (on that night, a red KS-10 filter, λ_e = 6050 A, was added to the SS-5 and ZhS-17 filters). The maximum contrast obtained with red filter was $0^{m}.18$.

According to data obtained on October 6-7, energetic illuminations from one square second of the surface of Mars (for medium-brightness points) were observed. They are tabulated in Table 7 and computed over a spectral interval of 500 A.

For that calculation, we utilized the radiometric stellar magnitude of the comparison star No. 2 ($93\phi_2$ Aqr), which we found, with the dependence of the heat index on stellar class already known [19]. $93\phi_2$ Aqr is of spectral class B5, according to [20], and its heat index is equal to $0^{m}.02$. According to the formula associating the radiometric stellar magnitude with radiometric irradiance [19], it may be reckoned that, for the star $93\phi_2$ Aqr, the latter is equal to $3 \cdot 10^{-13}$ cal/cm^2·min. This is the value referred to zenith under the transparency conditions prevailing at the Mount Wilson Observatory. Supposing the energy distribution in the stellar spectrum (in the working region) to correspond to Planckian distribution at a temperature of 18,000°, which is a rather good approximation [21], we obtained the radiometric irradiance E_λ^0 from the reference star in the spectral regions selected by our filters. This yielded the radiometric illuminances E_λ from 1 square second of arc of the surface of Mars (computed over a 500 A interval of the spectrum), given in Table 7. Correction factors were introduced to account for atmospheric extinction and for the difference in the effective wavelengths of the photometer with the same light filter for Mars and for the comparison star.

In view of the, to a certain extent, indeterminate character of the values for radiometric illuminance from the stars, it is not possible to vouch for the accuracy of the absolute values presented in Table 7, although the ratios of those values provide an idea of the energy distribution in the spectrum of Mars. The color temperature of the surface is about 3500°K.

TABLE 7

λ, A	6050	5450	4500
$E_\lambda \frac{\text{cal}}{\text{cm}^2 \cdot \text{min}} \cdot 10^{-14}$	5.06	4.16	1.49

TABLE 8

	m_{Ipv}	C_I
October 5-6	−2.41	1.417
October 7-8	−2.34	1.367

On October 5-6 and 7-8, the magnitudes and color indices of Mars as a whole were measured. The results of those measurements are to be found in Table 8.

In view of the fact that the limb darkening is weaker in blue light than in red, Mars is as a whole more blue than its central regions, where we took measurements in particular segments.

We feel ourselves obliged to express our gratitude to Academician V. G. Fesenkov, the initiator of this effort, for his constant kind attention to the endeavor and his critical judgment of the findings ensuing from it.

Astrophysical Institute of the Academy
of Sciences of the Kazakh SSR

Received December 15, 1956

LITERATURE CITED

[1] G. de Vaucouleurs, Physics of the Planet Mars [Russian translation] (Foreign Literature Press, Moscow, 1956).

[2] R. Hosfeld, Astron. J. 60, 3, 164 (1955).

[3] Strong, Techniques of Physical Experiments [In Russian] (Medical Press, Leningrad, 1948).

[4] V. I. Moroz, Pribory i Tekhnika Eksperimenta, No. 2, (1956).

[5] V. I. Moroz, Astron. J. (USSR) 33, 5 (1956).

[6] Olin J. Eggen, Lick Observatory Bulletin, 532, 131 (1955).

[7] H. L. Johnson, Ann. Astrophys. 19, 4, 292 (1955).

[8] J. Stebbins, A. E. Whitford and H. L. Johnson, Astrophys. J. 112, 3, 460 (1950).

[9] V. B. Nikonov, Doklady Akad. Nauk SSSR 14, 151 (1944).

[10] V. S. Sokolova, Vestnik Akad. Nauk Kaz. SSSR, 8 41 (1948).

[11] T. P. Toropova, Izvestiia Astrofiz. Institute Akad. Nauk Kaz. SSR 154 (1956).

[12] V. B. Nikonov and E. K. Nikonova, Izv. Krymsk. Astrofiz. Obs. 9, 41 (1952).

[13] Nautical Almanac (1956).

[14] Sky and Telescope 15, 11, 502 (1956).

[15] N. N. Sytinskaia, Absolute Photometery of Extended Celestrial Objects [in Russian] (Leningrad State University Press, 1948).

[16] Z. V. Kariagina, Izv. Astrofiz. Inst. Akad. Nauk Kaz. SSR 1, 1-2, 85 (1955).

[17] E. K. Nikonova, Izv. Krymsk. Astrofiz. Obs. 12, 56 (1954).

[18] V. V. Sharonov, Tsirkuliar GAO 3, 63 (1941).*

---

*GAO = Main Astronomical Observatory (in Pulkovo).

[19] J. A. Hynek (ed.), Astrophysics, a Topical Symposium (N.Y., 1952).

[20] A. Becvar, Atlas Coeli Skalnate Pleso 11, Katalog 1950 (Prague, 1951).

[21] E. R. Mustel'. Uspekhi Astronom. Nauk 3, 155 (1947).

PECULIARITIES OF THE MINERAL COMPOSITION AND STRUCTURE OF METEORITIC MATTER AND THE ORIGIN OF METEORITES

A. A. Iavnel'

The difference in the mineral contents of meteorites – the change of the composition of pyroxenes and the ratio of olivine to pyroxene in chondrites, the ratio of kamacite and taenite in iron meteorites, etc. – is explained by a regular change in their chemical composition.

The equilibrium diagram of the Fe–Ni system shows that the structure of iron meteorites was formed under very slow cooling of the iron-nickel alloys. The different structure of iron meteorites of identical composition is a result of the fixation of structures formed at different temperatures (lower than 450°C) and pressure (less than 10^5 atm).

The structures of meteorites, as well as their metamorphic variations, originated before the breaking up of asteroids, as a result of the complex thermal history of these cosmic bodies.

The essential mineralogical composition of meteorites is determined by their chemical composition and presents certain regularities [1].

Calcium-rich achondrites corresponding to the upper layers of asteroids are composed mainly of aluminosilicates in the form of plagioclase $m\mathrm{CaO} \cdot \mathrm{Al_2O_3} \cdot 2\mathrm{SiO_2} \cdot n\mathrm{Na_2O} \cdot \mathrm{Al_2O_3} \cdot 6\mathrm{SiO_2}$ and magnesian silicates such as pyroxene $(\mathrm{Mg, Fe})\,\mathrm{O} \cdot \mathrm{SiO_2}$ and, in part, olivine $2(\mathrm{Mg, Fe})\mathrm{O} \cdot \mathrm{SiO_2}$.

The silicate phase of calcium-poor achondrites, chondrites and other subclasses of meteorites from the deeper layers consists mainly of pyroxene and olivine, the latter increasing in amount (with increased MgO content) in pallasites. A regular change in the ratio of pyroxene to olivine and in the composition of these minerals is observed in passing from group I to group V of meteorites and is especially well shown by chondrites.

While the silicate phase of chondrites of group I consists entirely of pyroxene, the content of olivine increases gradually in the following groups, until in chondrites of group V (carbonaceous) it becomes an essential mineral. At the same time, the content of FeO increases in these minerals, the pyroxene of group I is almost pure enstatite ($\mathrm{MgO \cdot SiO_2}$) while that of group IV is hypersthene with over 20% FeO.

Thus, in chondrites the ratio of pyroxene to olivine and the content of iron in these minerals changes regularly over a considerable range. Therefore, calculations of averages of these characteristics and especially the attempts to to represent these averages in terms of definite molecular ratios are useless.

For this reason Chirvinskii's conclusions (his "laws" I and II) cited in a previous paper [1] do not in reality reflect any regularities in the chemical-mineralogical composition of chondrites.

The characteristics here are not the average ratio of pyroxene to olivine and the amount of iron in them but the systematic variation in these values. This regularity follows directly from the systematic increase of the FeO content in passing from group I to group V of meteorites [1].

As the result of increase in FeO, its content in the silicate minerals also increases, since Fe atoms replace those of Mg in the crystal lattices. This, however, is not all. As we have seen (Fig. 1 in [1]), the ratio of Mg to Si in different groups is sufficiently constant and computations of the molecular ratio MgO : SiO_2 in chondrites show that it is near unity. This was noticed by Brown and Patterson. Thus, in the absence of FeO the combination of these oxides should form pyroxene only, i.e., estatite, as in group I.

With increase in FeO, the molecular ratio (Mg,Fe)O : SiO_2 becomes greater than unity, and as the result, in addition to pyroxene, a certain amount of olivine forms, in which this ratio is two. The result of increase in the FeO content is the observed change of mineral composition of the chondrites.

The absence in the silicate minerals of meteorites of the higher oxides of elements and the presence of such minerals as schreibersite $(Fe, Ni)_3P$ indicate that the meteoritic matter was formed in an environment deficient in oxygen. This confirms the truth of our postulate advanced to explain the "primary" regularity of Prior.

The mineral composition of the metallic phase also varies systematically in passing from one group of meteorites to another and this is explained by the change in the content of nickel in the nickel-iron material.

In connection with this, it is advisable to review the related problem of formation of the iron meteorite structures.

Iron meteorites are alloys of iron with nickel and small amounts of cobalt, phosphorus and other elements. The atoms of nickel and cobalt replace iron atoms in the crystal lattice, forming two types of solid solutions with different lattices: the α-phase or kamacite has a body-centered cubic lattice (Fig. 1), while the γ-phase or taenite has a face-centered cubic lattice (Fig. 2). The parameters of the lattices depend on the content of nickel and cobalt in the alloy.

Most of the iron meteorites containing up to 6% of nickel consist of large crystals of the single-phase alloy and are called hexahedrites, while the rest contain two phases and exhibit either Widmanstatter (more correctly, Widmanstätten) structure with an octahedral pattern, and are called octahedrites or (a smaller part), a fine-grained structure and are called ataxites.

In order to explain the phase (mineralogical) composition of iron meteorites and their structures, it is necessary to refer to the phase diagram of the multicomponent system of the elements of which these meteorites are composed. As a first approximation the phase diagram of the system iron-nickel is usually taken.

This system investigated on artificial iron-nickel alloys with nickel concentration of about 30% and temperatures below 900°C exhibits allotropic change of the solid solution with the transformation from the gamma to the alpha phase. Artificial iron-nickel alloys containing up to 20% nickel consist of one phase only and differ in this from meteoritic iron, which with nickel content of only 6% is already composed of two phases (α and γ).

Another important difference is in the structure, which is microcrystalline in the artificial alloys but not in the meteorites. The hexahedrite structure shows very large crystals of the α-phase and the continuous Widmanstatten pattern in octahedrites also indicates a coarsely crystalline structure of the γ-phase. This is due most likely to the slow cooling of meteoritic iron both in the γ-phase at high temperatures and in the α-phase at low temperatures.

It should be noted that Perry's opinion [2] about separation of small crystals of iron-nickel phosphide along the boundaries of small γ-grains is erroneous. As has been shown by Uhlig, these crystals are concentrated along local deformations of the α-lattice and have no relation to the crystallization of the γ-phase. The author's conclusion [3] based on Perry's statement that the Sikhote-Alin meteorite cooled relatively rapidly at first was therefore incorrect.

It was supposed at one time that the meteoritic iron was formed under equilibrium conditions with a very slow rate of cooling and that its phase composition must be explained by the equilibirum diagram of the system Fe—Ni. For many years, attempts were made to construct an equilibrium diagram of this system with an eutectoid transformation of the solid γ-solution, i.e., a diagram different from the usual phase diagram of this system.

One of the latest diagrams of this type was a fairly complex one constructed by Bradley and Goldschmidt [4] in which the interval of the $\gamma \rightarrow \alpha$ transformation is only 230° (from 580 to 350°C). Accordingly, Bradley [5] expressed the opinion that a single cooling of the alloy in this narrow range could not lead to the formation of the coarsely crystalline Widmanstätten pattern and suggested that the structure of iron meteorites must have formed after repeated reheating of meteorites to a temperature not exceeding 580°C as the result of their approach to the sun and the subsequent sudden cooling to the temperature below 350°C.

Otherwise, had the alloy been raised even once to a temperature over 580°C or cooled slowly below 350°C, it would have lost, according to the Bradley-Goldschmidt diagram, the already acquired structure and the entire process of formation of Widmanstätten pattern would have had to start anew.

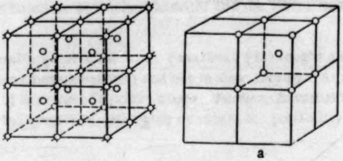

Fig. 1. Body-centered cubic lattice (a – unit cell).

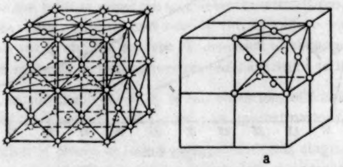

Fig. 2. Face-centered cubic lattice (a – unit cell).

This hypothesis is groundless from the astronomical point of view, as has already been pointed out by Watson [6]; moreover, the Bradley-Goldschmidt diagram has not been confirmed by later investigations.

Before proceeding with a discussion of these investigations, another unsupported view may be mentioned, namely, that the Widmanstätten figures in iron meteorites are due to some other cause than slow cooling. It was supposed by Slavinskii [7], for example, that this structure appears only in meteoritic iron and can be explained either by crystallization in the absence of nitrogen and oxygen of the air or by the presence in the iron of some minute admixtures which cannot be discovered. Widmanstätten structure, however, is well known in black and colored alloys and in Fe–Ni alloys among them, but is usually on a microscopic scale because of relatively rapid cooling of these alloys. Moreover, this structure appears whether melting was done in a vacuum or in the air.

It was believed by Owen [8] that meteorites falling through the earth's atmosphere are heated throughout to very high temperatures and that their characteristic structure could form only after they reach the earth. Everyone who is familiar with meteorites knows that they have a very thin fused crust and are heated during their fall to a very small depth from the surface. Therefore, Owen's hypothesis was immediately disproved [9].

Returning to the main problem, it must be mentioned that together with the diagrams of the eutectoid type many equilibrium diagrams were suggested of the same type as the nonequilibirium diagram of the system Fe–Ni. As a result of careful experimental work on iron-nickel alloys, Owen and Sully [10] obtained an equilibrium diagram for the system Fe–Ni which was later refined by Owen and Liu [11] and extended into the lower temperature region by Lihl [12].

This diagram, reproduced in Fig. 3, shows first of all that under equilibrium conditions there occurs only a shift in the lines of transformation of the solid solution without change in the type of transformation. Thus, different diagrams of the system Fe–Ni of the eutectoid type are not confirmed. In the lower part of Fig. 3 the distribution of iron meteorites according to the nickel content is shown, as well as their subdivision into groups.

An examination of this diagram gives an idea of the general features of formation of phases and structure of iron meteorites.

A slow cooling of an iron-nickel alloy leads to the formation of very large crystals of the γ-phase. When the temperature of the $\gamma \rightarrow \alpha$ transformation, corresponding to the upper line in Fig. 3, is reached, the α-phase appears whose crystal lattice is oriented in a definite way with respect to the lattice of the γ-phase, i.e., the plane (110) of the α-phase is parallel to the octahedral plane (111) of the γ-phase and the direction of (111) of the α-phase is parallel to (110) of the γ-phase. This orientation satisfies to the highest degree the conditions of structural and dimensional correspondence of both lattices at the moment of reconstruction. In this way the octahedral Widmanstätten structure of the alloy is formed.

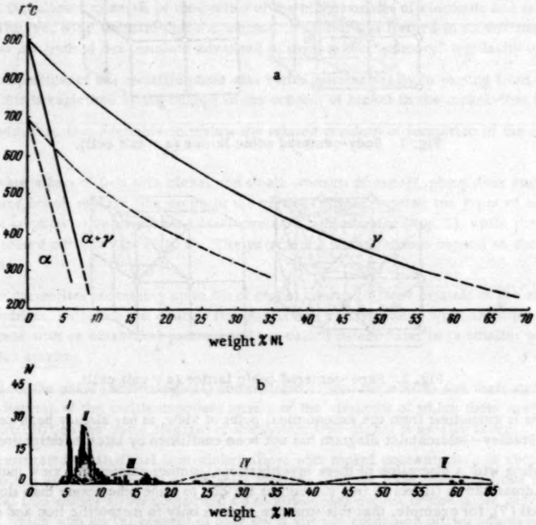

Fig. 3. a) Phase equilibrium diagram of the system Fe–Ni (at temperature below 900°C); solid line – Owen, Liu (1 atm); interrupted line – Lihl (1 atm); dotted line – Uhlig (10^5 atm – calculated).* b) Distribution of iron meteorites according to the nickel content.

The composition of the first nuclei of the α-phase is determined by the initial temperature of the $\gamma \rightarrow \alpha$ transformation (depending on the concentration of Ni in the alloy) and is found on the lower curve. With further lowering of the temperature and increase in the α-phase at the expense of the γ-phase, the composition of the phases changes, that of the γ-phase along the upper curve and of the α-phase along the lower curve.

It follows from this that the attempts to represent the composition of meteoritic iron by definite chemical formulas (by Buddhue, for example [13]) are without foundation, since Fe and Ni do not form either chemical compounds or definite solid solutions within the range of concentration below 75 % Ni. Nor is there basis to regard the hexahedrites [13] of group I as chemical compounds. As is shown in Fig. 3, the composition of iron meteorites of different groups is not based on any phase diagram of the system Fe–Ni, i.e., on the composition of the α- and γ-phases, but is determined by other causes cited earlier [1].

If the concentration of nickel in the alloy does not exceed a few percent, the entire alloy passes into the α-phase, which with slow cooling will form very large crystals. An alloy with a higher nickel content will consist of two phases and will preserve the Widmanstätten structure which will become more and more coarse with gradual cooling, due to the growth of crystals (rods) of the α-phase along the octahedral planes with simultaneous increase in nickel content in both phases.

---

* As in original – Publisher's note.

With rapid cooling the γ-phase changes into a metastable α_2-phase of the same composition as the γ-phase, but with a distortion of the body-centered cubic lattice. When heated, this phase breaks down into dispersed γ- and α-phases and acquires structure analogous to that of ataxites. No subsequent heating of the finely dispersed alloy in the $(\alpha + \gamma)$ region can bring on recrystallization with formation of Widmanstätten figures.

Thus, the coarsely crystalline structure of the hexahedrites and the Widmanstätten structure of the octahedrites are explained by slow cooling.

In spite of the convincing metallurgical data, A. N. Zavaritskii [14] sought an explanation of the structures of iron meteorites in recrystallization (metamorphism) and not in slow cooling. As a proof, he referred to the obviously erroneous ideas of Bradley [5] and Owen [8] cited above. Further, Zavaritskii, contradicting himself, gave an incorrect eutectoid diagram for the system Fe−Ni which admitted the possibility of formation of coarsely crystalline structure by slow cooling.

To explain the primary coarsely crystalline structure of the γ-phase, Zavaritskii proposed an entirely different mechanism − the growth of crystals of the γ-phase in a cloud of molten droplets of iron.

Thus, instead of one process of formation of iron meteorite structures which is explained by the phase diagram of the system Fe−Ni, constructed on the basis of experimental data, Zavaritskii proposed a very artificial scheme of this process without sufficient foundation. The main reason for this hypothesis was Zavaritskii's desire to reconcile the process of formation of iron meteorites with his concept of formation of chondrules; this will be discussed later. This approach to the problem of the structure of iron meteorites led Zavaritskii to incorrect conclusions.

It is more correct, evidently, to continue the study of the conditions of formation of iron meteorite structures on the basis of the phase diagrams of the system Fe−Ni (in the first approximation).

A comparison of the composition of phases of iron meteorites with this diagram (for pressure of one atmosphere) shows that the nickel content in kamacite (6.2%) and taenite (about 30% on average) is lower than the nickel content in the corresponding phases at low temperature.

To explain this discrepancy, Henderson and Perry [16] assumed that the iron-nickel alloy cooled slowly down to 450°C and then the rate of cooling increased rapidly so that the composition of each phase corresponding to this temperature became fixed, producing the kamacite and taenite of the meteorites.

A different explanation was given by Uhlig [17], who ascribed the discrepancy to the effect of high pressure, of the order of 10^5 atm. Under such pressure, according to Uhling's calculations, the temperatures of transformation in the iron-nickel alloy should be lowered by 200-300°C (Fig. 3). Therefore, the composition of the phases formed with slow cooling down to 300°C or even to lower temperatures, at which the rate of diffusion is extremely slow, would also correspond to the composition of kamacite and taenite.

Uhlig explained also a number of details in the structure of iron meteorites on the assumption of sudden release of pressure and the generation in the alloy of a shock wave.

These assumptions are justified by the authors with the explanation that iron meteorites were formed in a large body which was suddenly disrupted and this caused rapid cooling of the alloy (Henderson and Perry) or sudden release of pressure (Uhlig).

It should be noted that the process of formation of meteorites is probably more complex than this. In the author's opinion, the temperature of formation of structures is the same in all iron meteorites. According to Henderson and Perry it is 450°C (with pressure of 1 atm.); according to Uhlig, about 300°C (with pressure of the order of 10^5 atm.). In this case there should be a unique correspondence between the structure and nickel content in meteorites. In reality there are many meteorites with the same nickel content but different structures. This may be the result of fixation of structures formed at different temperatures and, evidently, at different pressures, namely (assuming intermediate conditions between those assumed by the authors) in the temperature interval below 450°C and pressure lower than 10^5 atm.

The fixation of structure may be explained by rapid cooling of the alloy form the given temperature. Thus, among iron meteorites of group I the hexahedral structure was evidently fixed at a lower temperature than in the coarse-grained octahedrites. In the latter, rapid cooling began before they passed into the one-phase region and this preserved the octahedral structure characteristic of higher temperature.

At the same time, the coarse-grained octahedrites of group II must have been at a lower temperature at the moment of fixation of their structure than the fine-grained octahedrites of the same composition, according to what was said earlier about the growth of the α-phase rods with decreasing temperature.

It follows from this that after a prolonged period of slow cooling the alloy was cooled suddenly. The differences in temperature in different parts of the alloy is most easily explained by assuming that the alloy had a large volume with a considerable temperature range through it. This confirms the conclusion that iron meteorites correspond to the central part of large bodies – asteroids. If the asteroids cooled from the surface towards the center, the coarse-grained octahedrites of group I (whose structures were fixed at a higher temperature) must correspond to the inner part of the central core, and the hexahedrites to the outer part. In group II very fine-grained octahedrites formed from the inner part of the core (possibly also nickel-rich ataxites) and coarse-grained octahedrites from the outer part, and so on.

What has been said of temperature applies also to pressure. As was shown above, an increase in pressure affects phase transformations just as increase in temperature, namely, it postpones the $\gamma \rightarrow \alpha$ transformation, i.e., the beginning of formation of octahedrite structure. But in the deeper parts of the iron core, increase in temperature should be accompanied by increase in pressure and their effect must be parallel.

It may be concluded that the structure of iron meteorites reflects the conditions which existed in the depths of the asteroids before their disruption, with which event the rapid decrease in temperature and pressure in the central part of these bodies must be connected.

Now the structures of the other types of meteorites will be briefly reviewed.

The structure of pallasites is a continuous net of iron-nickel alloy with Widmanstätten pattern and inclusions of olivine.

In mesosiderites nickel-iron is dispersed as inclusions in a holocrystalline silicate matrix.

Chondrites are characterized by the presence of minute globules – chondrules composed essentially of pure minerals – of olivine and pyroxene set in a fine-grained groundmass of the same composition as the chondrules. Nickel-iron occurs in small irregular grains and sometimes in globules (iron chondrules). The inner structure of the chondrules indicates that they are products of relatively rapid crystallization of molten mass [14].

The calcium-poor achondrites differ from the chondrites in the absence of chondrules.

The calcium-rich achondrites have structures similar to those of terrestrial basalts and diabases. Some have predominantly fine cataclastic structure.

There are transitional forms among these various meteorite structures.

Thus, the conclusion that the structure of iron meteorites was formed in the depths of asteroids must be extended to meteorites of other types. Observations show that there are gradual transitions from one meteorite type to another, not only so far as composition is concerned but also in relation to structure, and it must be admitted that the structures of iron-stone and stone meteorites were also formed essentially during the time when meteoritic matter was a part of asteroids. It follows, then, that chondrules which are found in the matrix of stony meteorites were formed during the formation of these cosmic bodies and were preserved during their later evolution.

This conclusion differs radically from the hypotheses of Zavaritskii and Urey and Craig concerning the conditions of formation of chondrules and chondrites.

According to Zavaritskii [14] chondrules were formed as the result of breakdown of the parent planet and formation of a cloud of fine dust-like particles of molten matter which later solidified into chondrules. As an alternative, Zavaritskii suggested that chondrules might be products of volcanic eruptions on the parent planet. In his latest work [18] he abandoned this idea because of the difficulties involved in it.

The structure of chondrites in Zavaritskii's opinion was formed after the disruption of the parent planet, and he extended this view to iron meteorites, considering their structure also as being the result of later recrystallization.

An analogous picture of formation of chondrules was suggested by Urey and Craig [19]. The main difference between the two conceptions is as follows: Zavaritskii, on the basis of the similar average composition of the chondrules and the rest of the chondrites, believed that chondrites were formed from the peridotitic layer of the parent planet.

According to Urey and Craig, chondrules were formed from the minerals of the outer shells of asteroids during collisions and later, mixing with the matter of the inner shells of each asteroid, became constituents of chondrites.

These ideas seem artificial to the author.

At the same time, the general conclusion concerning the formation of meteorite structure in large bodies is confirmed by the widespread phenomenon of metamorphism in iron and stone meteorites. In iron meteorites, structural metamorphism is evidently thermal and is found mainly in meteorites of group I – hexahedrites, some of which, because of heating, have a fine-grained structure. Such meteorites are called nickel-poor ataxites. In other groups the degree of metamorphism is lower [20].

The structural metamorphism of stone meteorites studied in detail by Zavaritskii [14] consists in recrystallization of chondrites (thermal metamorphism) and formation of hydrous silicates (hydrothermal metamorphism). The second type of metamorphism could have occurred at relatively low temperatures (300°-400°C) and is observed in carbonaceous meteorites.

If the chondrites are arranged in groups and the character of metamorphism in them is studied, it develops that the highest degree of metamorphism is found in chondrites of group I and the least, in chondrites of group V (carbonaceous), i.e., the same sequence in the degree of metamorphism as is observed in iron meteorites. It follows from this that the cause of metamorphism was general for whole groups of meteorites, i.e., for individual asteroids.

It may be concluded, therefore, that not only the formation of meteorite structures but also its metamorphism must have occurred before the disruption of the asteroids. For this reason the author some time ago advanced a hypothesis to the effect that a long period of time elapsed between the formation of asteroids and their disruption into meteorites, and that meteorites as such were formed relatively recently. This assumption is confirmed by the work of Singer [21] and other authors, who, on the basis of determination of He^3 content in meteorites, concluded that meteorites as fragments of matter have been in existence for only hundreds of millions of years.

The following general assumptions may be made on the basis of the data on the structure of meteorites concerning its origin.

After the formation of the silicate phase from the oxidized part of meteoritic matter and of the metallic phase from its unoxidized part, the material of these phases (or at least a part of it) acquired the shape of minute globules or chondrules. At the same time a differentiation of the phases (incomplete) took place during which the chondrules were preserved. The latter circumstance points to the fact, as was justly remarked by A. P. Vinogradov [22], that the differentiation of the phases did not consist in melting out of the metal from the initially homogeneous iron-silicate mass.

As the result of this differentiation, the main mass of asteroids consisting of the silicate phase with an admixture of nickel-iron acquired a chondrite structure, while its central part, containing the appropriate amount of nickel, acquired Widmanstätten structure. The presence of metamorphic structures in meteorites indicates, as has already been mentioned, that heating processes occurred in the asteroids before their disruption.

All this points to the complexity of the thermal history of the asteroids which has recently been reviewed in the work of Jacobs and Allen [23].

It should be recalled that some meteorites have cataclastic or brecciated structure. This indicates that during the process of formation of meteorites fragmentation and accretion took place.

In the present paper attention has been given to what the author regards as the main points, and many problems have not been touched upon.

An important role in the solution of the problem of origin of meteorites is played by the determination of the ages of different types of meteorites. However, at present we can speak definitely only of the maximum age of meteoritic matter which, according to the latest determinations, is about 4.8 billion years. Investigation of the physical properties of meteorites, their density, porosity, thermal conductivity, etc., is also of great importance for the general problem.

The content of minor constituents in meteorites was not touched upon because of the lack of systematic data on the subject, although it is clear that the distribution of different elements in meteorites may characterize different stages in the history of meteoritic matter. For example, the variable content of platinum in iron meteorites is determined, evidently, by the stage of differentiation of the proto-asteroidal matter (just as is the content of nickel). The content of gallium, on the other hand, is related in some way to the structure of iron meteorites, i.e., to the processes which had taken place within the asteroids, and the amount of helium in iron meteorites was determined to some extent by nuclear reactions initiated by cosmic radiation after the breaking up of the asteroids into small fragments.

The development of a final theory of the origin of meteorites requires not only the data on their composition, but also a consideration of the astronomical ideas on this subject – a problem for many investigators.

SUMMARY

A synthesis of data on the chemical composition of meteorites revealed a number of regularities leading to the separation of meteorites into five groups according to the composition of the metallic and silicate phases, and into six subclasses, according to the proportion of each phase in a given group, according to the relation between the composition and the amount of each phase in the individual subclasses of different groups (Prior's "group" regularity), according to the relation between composition and the content of each phase in different groups as a whole (Prior's "primary" regularity), and according to the regular variation of the elemental composition in different groups of meteorites.

An analysis of these regularities leads to the conclusion that meteoritic matter in its evolution underwent chemical differentiation, followed by separation into individual bodies (asteroids) and by further differentiation of the phases within each asteroid.

The mineralogical composition and structure of meteorites confirm the hypothesis of their formation from separate large layered bodies. Comparison of structural characteristics of different subclasses of meteorites has led to certain hypotheses concerning the thermal history of the asteroids which explain these characteristics.

The main results and conclusions of this work have been critically compared with the data obtained by other authors.

Committee on Meteorites
Academy of Science, USSR

Received December 3, 1956

LITERATURE CITED

[1] A. A. Iavnel', Astron. J. (USSR) 34, 445 (1957).*

[2] S. H. Perry, The Metallography of Meteoric Iron (Washington, 1944).

[3] A. A. Iavnel', Meteoritika 7, 141 (1950).

[4] A. J. Bradley and H. J. Goldschmidt, J. Iron Steel Inst. 139, 11 (1939).

[5] A. J. Bradley, Nature 143, 518 (1939).

[6] F. G. Watson, Between the Planets (1945) p. 188.

[7] M. P. Slivinskii, Metallurg No. 8, 7 (1932).

[8] E. A. Owen, Nature 142, 999 (1938).

[9] S. W. Smith and J. Young, Nature 142, 1162 (1938).

[10] E. A. Owen and A. H. Sully, Phil. Mag. 184, 614 (1939).

[11] E. A. Owen and Y. H. Liu, J. Iron Steel Inst. 163, 132 (1949).

[12] F. Lihl, Arch. Eisenhüttenw. 25, 475 (1954).

---

* Soviet Astronomy – AJ, p. 435.

[13] J. D. Buddhue, Meteoritics 1, No. 1, 97 (1935).

[14] A. N. Zavaritskii, Meteoritika 4, 50 (1948); 8, 100 (1950).

[15] A. N. Zavaritskii and L. G. Kvasha, Meteorites of the USSR [In Russian] (Izd. AN SSSR, 1952) part 1.

[16] E. P. Henderson and S. H. Perry, Geochim. et Cosmochim. Acta 6, No. 5/6, 221 (1954).

[17] H. H. Uhlig, Geochim. et Cosmochim. Acta 6, No. 5/6, 282 (1954); 7, No. 1/2, 34 (1955).

[18] A. N. Zavaritskii, Proc. of the First Conference on the Problems of Cosmogony, 1951 [In Russian] p. 191.

[19] H. C. Urey and H. Craig, Geochim. et Cosmochim. Acta. 4, No. 1/2, 36 (1953).

[20] A. A. Iavnel', Doklady Akad. Nauk SSSR 102, 3, 477 (1955).

[21] S. F. Singer, Scientific American, 191, No. 5, 36 (1954).

[22] A. P. Vinogradov, Vestnik MGU 4-5, 169 (1955).

[23] J. A. Jacobs and D. W. Allan, J. Roy. Astron. Soc. Can. 50, No. 3, 122 (1956).

A SUPPLEMENT TO THE GENERAL CATALOGUE OF ABSOLUTE BRIGHTNESSES OF COMETS. COMETS OF 1947-1954

T. V. Vodop'ianova

The absolute magnitudes H_{10} and photometric characteristics H_y and $y = 2.5\,n$ for 76 apparitions of comets during 1947-1954 are given (Table 1). These values were determined mainly by the method which S. K. Vsekhsviatskii and V. P. Konopleva used in the four earlier sections of the "General Catalogue of Absolute Brightnesses of Comets" [1, 2].

A general analysis is made of the collected estimates of cometary brightnesses. The determinations of the characteristic $y = 2.5n$ are compared with the mean law of cometary brightness $y = 10$, which was established by Vsekhsviatskii.

The absolute brightnesses of the last and first apparitions of 27 periodic comets in the list are compared; also those of the last two consecutive apparitions (Table 2). In the first case the absolute brightness of 23 comets decreased within the limits $6\overset{m}{.}9$ to $0\overset{m}{.}6$; in the second case that of 18 comets decreased by from $2^{m}6$ to $0.^{m}4$.

Cases are discussed in which the absolute brightness of individual comets increased; preliminary explanations are given, of which the most likely is a direct connection between a sudden increase of absolute cometary brightness and an increase of solar activity.

The mean decrease of absolute brightness, ΔH^1_{10}, per return of each comet of list 2 is given. The distribution of ΔH^1_{10} as a function of the inclination $\underline{i}$ and perihelion distance $\underline{q}$ shows that in general the disintegration of comets is not caused by proximity to the sun. The distribution of ΔH^1_{10} as a function of the number of returns shows that comets with this number not larger than 3 (i.e., discovered recently) have the highest value of ΔH^1_{10}.

The investigation of the absolute brightness of periodic comets confirms the fact, established by Vsekhsviatskii in 1933, that the absolute brightness of comets decreases at each successive return, which means that the comets are disintegrating.

1. The present article is supplement V to the "General Catalogue of Absolute Cometary Brightnesses" of Vsekhsviatskii [1] and is a direct continuation of supplement IV, which was compiled by A. P. Konopleva [2]. In order to obtain statistical data for all comets the method of determining their absolute brightnesses and photometric characteristics employed by earlier writers was followed without essential changes.

From 1947 to 1954, 76 apparitions of comets were studied. Preliminary results for their absolute brightness H_{10} and photometric characteristics H_y and $\underline{y}$ have already been published in brief summaries [3]. The data were published earlier only for the repeatedly observed comet of Oterma (1942 VII-1950 III) in connection with its perihelion passage in 1950.

Vsekhsviatskii began to collect observations of cometary brightnesses for the given period and this work was continued by the present author. Data on brightness and photometric observations were collected from circulars of the International Astronomical Union, from Astronomical Circulars of the Academy of Sciences of the USSR and from the following journals and publications of various observatories: M. N., Astr. J., Lick Obs. Bul., Obs., Pop. Astr.,

P. A. S. P., J. B. A. A., A.N., H. A. C., J. des Obs., B.A., B. S. A. F., T. A. B., Publ. Kiev Astr . Obs., etc.

As far as possible we used all published values of the integrated brightnesses of comets for a given apparition. The magnitudes of comparison stars whenever indicated by observers were reduced to the international scale of stellar magnitudes; we used the reduction tables given in Ref.[4].

2. The study of 20 comets of the last period, 1953-1954, as well as of Oterma's comet was begun two years after the publication of the absolute brightnesses of the comets in the period 1947-1952. It then appeared necessary to review the absolute brightnesses H_{10} and photometric characteristics H_y and $\underline{y}$ for 1947-1952, especially because during this period new observations were published for many comets (Beyer, van Biesbroeck and Boyer). We naturally included the new data together with previous observations in order to have a more complete picture of the variation of cometary brightness so as to provide a more exact determination of the absolute brightness H_{10} and characteristic $y = 2.5$ n. The characteristic H_y is fully reliable only when determined from values of the brightness obtained for $r \cong 1$ AU independently of their number.

In the course of the work it was found that the combination of photometric visual values obtained with weak magnification and photographic values, especially those obtained with large instruments, distorts the value $y = 2.5$ n and also increases the absolute brightness H_{10}.

The photographic brightness is usually below the visual value by $2\text{-}3^m$ since the photographic image of a comet contains mainly the central part of the head (central condenstion or nucleus) and does not include the entire radiation from the diffuse coma, whereas the extrafocal visual image of a comet combines the radiation from the entire head. Photographic values could not be reduced to visual values on the basis of simultaneous comparisons, with few exceptions, because of insufficient observations. The correspondence of these values depends generally on the degree of diffuseness and condensation of the coma, its size and its color.

For the majority of comets photographic observations with powerful instruments (Mount Hamilton, Mount Wilson, Mount Palomar, Mount Locke and Yerkes) usually include the initial and final (and sometimes both) periods of visibility of the comets before or after perihelion passage, when the comet becomes a telescopic object and can be observed only with large instruments. This excludes the possibility of reduction of observations of another period of the visibility even if this should appear desirable.

However these observations are extremely important since they increase the arc of the orbit which is spanned by the observations. Therefore these values, which were clearly too low, were used in some instances without introducing arbitrary corrections when they did not deviate too much from the curve of cometary brightness determined by visual observations. These deviations are smallest for the stellar appearance of a comet. The insufficient data for a number of comets, especially those of 1953-1954, limited the strict selection of observations, especially for the initial and final periods of visibility.

For telescopic comets we could only use photographic observations with large instruments; therefore, in view of the above, we can assume that for the majority the absolute brightness H_{10} was too large. In some instances, when comparable series of observations revealed a systematic divergence in the values given by two observers, these values were reduced to the observations of the observer whose data were in better agreement with the mean brightness curve.

3. The photometric characteristics for 76 apparitions are given in Table 1, which was compiled similarly to the tables in the earlier reports [3]. This table contains: 1) the serial number; 2) the name of the comet; 3) the number of observations included; 4) H_{10}, the absolute brightness for the apparition; 5) and 6) H_{10}^- and H_{10}^+, the absolute brightnesses before and after perihelion passage; 7) and 8) the photometric characteristics H_y and $\underline{y}$; 9) h_{10}, the average absolute brightness of the nucleus or condensation, $y = 2.5\ n = 10$; 10) log r_1 and log $\overline{r_2}$, the logarithms of the cometary radius vector for the intial and final dates of observation. The comets are placed in the order of their perihelion passage.

Of the 76 comets in the list, 45 are rediscovered comets. Of these 13 are short-period comets (with a period < 12 years) and 32 have almost parabolic orbits; in addition, two comets which were discovered as new, proved to be short-period comets that had been regarded as lost; these were the Tuttle-Giacobini comet redicovered by Kresak, which had not been observed since 1907, and Wolf 2, which had not been observed since its discovery in 1924 and was rediscovered by Harrington in 1951. 29 comets are second apparitions of periodic comets, including 27 of the short-period type (period < 12 years).

TABLE 1

№	Name of comet	No of obs.	H_{10}	H_{10}^-	H_{10}^+	H_y	y	h_{10}	log r_1, log r_2
1	1947 I Bester	41	$4^{\mathrm{m}}9$	$4^{\mathrm{m}}4$	$5^{\mathrm{m}}3$	$2^{\mathrm{m}}3$	15.9	—	0.421-0.381—0.800
2	1947 II (Grigg—Skjellerup)	21	13.4	13.8	13.2	13.4	13.3	—	0.013-9.931—0.176
3	1947 III Bečvar	15	10.5	10.5	—	10.6	3.7	—	0.063—9.986
4	1947 IV Rondonina—Bester	21	8.5	8.8	8.3	8.6	9.5	—	0.118—9.754—0.341
5	1947 V Bester	12	11.1	11.0	11.2	—	—	—	0.151—0.147—0.232
6	1947 VI Wirtanen	27	8.5	6.6	8.6	(4.7)	(16.4)	—	0.451—0.706
7	1947 VII (Reinmuth$_2$)	34	10.4	—	10.4	(8.2)	(17.5)	$11^{\mathrm{m}}7$	0.271—0.364
8	1947 VIII Wirtanen	12	4.3	—	4.3	4.4	9.9		0.690—0.980
9	1947 IX (Faye)	30	11.1	11.1	11.1	10.1	13.6	—	0.286—0.220—0.376
10	1947 X Honda	8	10.0	9.8	10.2	(10.5)	(16.4)	—	9.876—9.872—0.157
11	1947 XI (Encke)	98	10.3	10.3	—	10.3	9.9	14.6	0.266—9.545
12	1947 XII "Bright"	51	5.7	—	5.7	5.9	11.0		9.433—0.134
13	1947 XIII (Wirtanen)	9	14.4	—	14.4	—	—	—	0.231—0.308
14	1948 I Bester	223	6.7	5.6	6.8	6.6	8.3	10.0	0.398—9.876—0.689
15	1948 II Mrkos	31	7.4	7.3	7.5	8.3	6.9	9.3	0.232—0.176—0.644
16	1948 III Johnson	12	4.4	—	4.4	—	—		0.686—0.703
17	1948 IV Honda—Bernasconi	123	7.9	—	7.9	7.8	12.7	12.8	9.802—0.539
18	1948 V Pajdušakova—Mrkos	178	4.9	4.8	4.9	4.2	11.8	7.3	0.350—0.323—0.822
19	1948 VI (Whipple)	18	10.0	10.9	9.1	—	—	—	0.519—0.396—0.451
20	1948 VII (Schwassmann—Wachmann$_2$)	19	10.6	11.1	10.4	—	—	—	0.472—0.337—0.471
21	1948 VIII (Forbes)	10	13.3	13.8	12.1	—	—	—	0.296—0.190—0.191
22	1948 IX (Ashbrook-Jackson)	49	7.3	6.8	7.6	—	—	8.4	0.369—0.365—0.529
23	1948 X Bester	11	7.3	—	7.3	(5.4)	(17.9)	—	0.135—0.339
24	1948 XI "Southern"	63	4.7	—	4.7	4.8	9.5	—	9.606—0.486
25	1948 XII (Honda—Pajdušakova—Mrkos)	16	12.5	—	12.5	(13.7)	(21.1)	—	9.815—0.144
26	1948 XIII (Neujmin$_1$)	7	12.0	12.0	—	(13.3)	(5.4)	—	0.463—0.192
27	1949 I Wirtanen	21	6.0	5.7	6.2	5.8	10.3	—	0.596—0.401—0.833
28	1949 II (Johnson)	6	9.6	9.5	9.8	(7.9)	(14.8)	—	0.354—0.353—0.360
29	1949 III (Wilson—Harrington)	2	17.4	—	17.4	—	—	—	0.042—0.047
30	1949 IV Bappu—Bok—Newkirk)	82	7.0	7.0	7.2	6.7	11.0	8.9	0.393—0.314—0.743
31	1949 V (Väisälä$_1$)	6	13.4	—	13.4	(10.9)	(16.7)	—	0.254—0.436
32	1949 VI (Shajn—Shaldach)	33	7.9	7.9	8.4	—	—	—	0.375—0.362
33	1950 I Johnson	54	6.5	5.5	6.6	4.7	13.7	—	0.556—0.407—0.823
34	1950 II (D'Arrest)	23	11.7	14.8	11.4	10.3	15.0	—	0.170—0.140—0.443
35	1950 III (Oterma)	53	8.2	8.2	8.1	—	—	—	0.645—0.534—0.656
36	1950 IV (Reinmuth$_1$)	4	12.4	12.4	—	—	—	—	0.462—0.439
37	1950 V (Daniel)	16	12.8	12.8	12.8	11.2	16.6	—	0.166—0.383
38	1950 VI (Wolf$_1$)	7	13.2	13.2	13.2	—	—	—	0.411—0.398—0.407
39	1950 VII (Arend—Rigaux)	26	11.7	—	11.7	(6.5)	(35.6)	12.8	0.148—0.300
40	1951 I Minkovski	81	4.0	3.8	4.5	2.8	12.3	5.8	0.555—0.410—0.719
41	1951 II Pajdušakova	52	9.4	—	9.4	9.3	10.4	—	0.860—0.612
42	1951 III (Encke)	38	10.8	10.8	11.6	11.0	11.0	12.8	0.340—9.579—0.046
43	1951 IV (Tuttle—Giacobini—Kresak)	46	11.9	11.8	11.9	10.4	3.2	15.0	0.054—0.048—0.189
44	1951 V (Neujmin$_3$)	6	13.7	12.5	13.9	—	—	—	0.310—0.308—0.395
45	1951 VI (Pons—Winnecke)	7	14.1	14.2	13.2	12.6	15.1	—	0.417—0.065—0.123
46	1951 VII (Kopff)	15	10.6	11.9	8.0	(3.1)	(39.6)	—	0.374—0.175—0.186
47	1951 VIII (Tempel$_2$)	12	11.9	13.1	9.5	(8.0)	(25.4)	—	0.438—0.144—0.158
48	1951 IX (Harrington—Wilson)	11	12.7	—	12.7	—	—	—	0.273—0.356
49	1951 X (Arend)	24	11.8	11.6	12.2	—	—	—	0.269—0.260—0.356
50	1952 I Wilson—Harrington	36	9.0	9.0	9.0	9.0	10.4	10.5	0.428—9.871—0.142
51	1952 II (Wolf$_2$)	19	10.7	10.6	10.9	—	—	—	0.303—0.206—0.247
52	1952 III (Schaumasse)	85	8.8	9.7	8.3	(7.1)	(22.2)	13.2	0.251—0.078—0.284
53	1952 IV (Grigg—Skjellerup)	8	13.4	13.4	—	13.4	9.8	—	9.946—0.036
54	1952 V Mrkos	50	8.5	7.8	9.0	—	—	12.2	0.157—0.109—0.208
55	1952 VI Peltier	70	9.1	9.3	9.0	(8.6)	(19.5)	13.3	0.101—0.081—0.208
56	1952 VII (Camas—Solà)	37	8.8	9.3	8.7	8.6	12.5		0.587—0.248—0.496
57	1952 e Harrington	74	6.6	7.3	5.2	(2.1)	(27.0)		0.388—0.148—0.442
58	1952 f Mrkos	19	8.9	8.5	9.9	8.8	13.3		0.067—9.976—0.397
59	1953 a Mrkos—Honda	75	8.1	8.0	8.3	7.8	16.5		0.101—0.010—0.301
60	1954 b (Borrelly)	5	12.7	—	12.7	—	—		0.442—0.466

TABLE 1 (continued)

№	Name of comet	No. of obs	H_{10}	H_{10}^{-}	H_{10}^{+}	H_y	y	h_{10}	$\log r_1, \log r_2$
61	1953 b (Brooks$_2$)	15	13.7	13.5	13.7	13.6	10.3		0.283—0.272—0.381
62	1953 e (Harrington)	15	14.8	14.1	15.2	—	—		0.239—0.228—0.267
63	1953 i (Finlay)	10	11.6	12.7	11.3	(10.7)	(17.5)		0.020—0.016—0.217
64	1954 c Harrington	6	11.7	—	11.7	—	—		0.443—0.518
65	1953 h Pajdušakova	12	11.1	11.1	—	11.6	4.1		0.164—9.891
66	1954 a (Honda—Mrkos—Pajdušakova)	26	12.1	10.7	13.3	(15.4)	(28.7)		9.762—9.745—0.064
67	1954 i (Van Biesbroeck)	3	10.1	—	10.1	—	—		0.462—0.554
68	1953 d (Reinmuth$_2$)	6	12.2	12.2	—	13.0	8.3		0.445—0.357
69	1953 c (Pons—Brooks)	81	6.4	6.4	5.2	5.7	11.8	—	0.652—9.977—9.982
70	1954 f Vozarova	41	7.3	—	7.3	7.5	9.3	—	0.112—0.266
71	1955 b Abell	3	4.8	—	4.8	—	—	—	0.743—0.744
72	1953 f (Encke)	6	12.9	12.9	—	13.6	8.5	—	0.529—0.362
73	1953 g Abell	41	6.2	6.2	—	6.3	9.7	—	0.580—9.991
74	1954 j (Wirtanen)	3	15.0	—	15.0	—	—	—	0.226—0.252
75	1954 d (Kresak—Peltier)	18	9.3	9.2	11.0	8.6	17:7	—	0.145—9.985—0.107
76	1955 a (Harrington —Abell)	1	13.9	—	13.9	—	—	—	0.300

The absolute brightnesses H_{10} of all comets in Table 1 are within the limits $4^{m}0$ to $15^{m}0$. The largest absolute brightnesses are those of comets 1951 I (Minkovskii , $H_{10} = 4^{m}0$), 1947 VIII (Wirtanen, $H_{10} = 4^{m}3$), 1948 XI ("Southern", $H_{10} = 4^{m}7$), and the faintest comets are Wirtanen's periodic comet in both apparitions (for 1947 $H_{10} = 14^{m}4$ and for 1954 $H_{10} = 15^{m}0$) and Harrington's periodic comet of 1953e ($H_{10} = 14^{m}8$). The data for the Wilson-Harrington comet 1949 III, on the basis of which its absolute brightness was determined as $H_{10} = 17^{m}4$, cannot be regarded as reliable.

4. For 24 apparitions out of the observed 76 the characteristic of brightness variation $y = 2.5\ n$ could not be determined because of the small variation of log r.

For 16 apparitions y was determined with uncertainty or showed a large deviation from the average value $y = 10$. These deviations can be attributed to: 1) The small number of observations [1947 X (Honda), 1948 VIII (Forbes), 1948 X (Bester), 1948 XIII (Neujmin 1), 1949 V (Väisälä), 1951 VIII (Tempel 2)]; 2) insufficiently large variation of log r [1947 VII (Reinmuth 2), 1949 II (Johnson)]; 3) difference in the type of observation [1947 VI (Wirtanen), 1951 VIII (Tempel 2), 1950 VII (Arend-Rigaud), 1951 VII (Kopff)]; 4) nonuniformity of the values depending on the appearance of the comet, especially for comets with a large diffuse coma [1952 III (Schaumasse), 1952e (Harrington)] or pale nebulous spot, (both apparitions of the periodic comet of Honda-Mrkos-Pajdušakova). The large deviation of y from its average value $y = 10$ for 1952 VI (Peltier) evidently results from the observed fluctuations of brightness associated with changes of its appearance.

However, these four possible reasons for the large deviation of y from its average value are not strictly separated and the division of comets into four groups is only a rough approximation according to their principal characteristic.

The large deviation of y from the average ($y = 10$) for the Schaumasse comet, which can be attributed to nonuniform values resulting from its appearance, cannot be associated with the observed "flare-up" of its brightness which will be discussed below.

In our review of previously published characteristics y, H_y and H_{10} for some comets of 1947-1952 we used the visual observations of Beyer. These showed only poor agreement with photographic observations, especially with those obtained by means of powerful instruments. In some instances the discrepancy amounted to 4^{m}. In order to reduce the effect on H_{10} and y some of these observations were not used even at the expense of reducing the arc of the orbit which was spanned by observations. For the majority of cases under consideration these values were determined mainly from the extrafocal visual data of Beyer.

In general y deviated less from its average value $y = 10$ as less use was made of photographic observations obtained with large instruments. However, this does not mean that in each instance the deviation from the average results only from unreliability of the data.

The characteristic y which is determined from observations is an index of the state of a comet in the given segment of its orbit. Since a comet is usually observed in proximity to the sun, when we can expect the most intense solar influence on the processes in the comet itself, y can have different values in different comets. Therefore, when a comet is observed along a large arc of its orbit, as it recedes from the sun, the deviations of y from its average are smoothed out so that it approaches $y = 10$, as had been established for many comets. This mean law of cometary brightness was established by Vsekhsviatskii in 1925 and has been confirmed in a number of his later articles.

In the case of the 36 apparitions metnioned above for which the observations were reliable and for which the variation of log r is > 0.15, y assumes values from 3.2 (1951 IV) to 17.7 (1954d). For this group the average value is $y_{av} = 11.0 \pm 0.5$.

The average value of y for all periodic comets in the group under consideration is $y_{av} = 11.3$ and for parabolic comets $y_{av} = 10.8$.

5. Of the 44 apparitions of periodic comets in Table 1, 27 are returns. 25 out of the 27 are short-period comets with a period < 12 years and 2 are periodic with a period > 12 years; the latter are Neujmin 1 and the Pons-Brooks comet.

The study of the variation of absolute brightness H_{10} in different apparitions is not within the scope of the present investigation. However, it was of interest to determine this variation at least by comparison with the next-to-last and the first apparition. The results of these comparisons are given in Table 2, which contains: 1) the order of perihelion passage; 2) the name of the periodic comet; 3) and 4) the year of perihelion passage and the absolute brightness H_{10} for the last apparition, 5) and 6) the year of perihelion passage and the absolute brightness H_{10} for the preceding apparition, 7) the absolute brightness difference between the last and preceding apparitions, ΔH_{10}; 8) and 9) the year of passage through the perihelion and the absolute brightness H_{10} for the first apparition; 10) the absolute brightness difference between the last and first apparitions, $\Delta H_{10}{}^{n}$; 12) the period in years; 13) the number of observed returns; 14) the decrease of absolute brightness per cycle in stellar magnitudes, ΔH_{10}^{1}.

Comparison of absolute brightnesses in the last and first apparitions of 23 comets of the list showed a decrease of absolute brightness for individual comets varying from $6^{m}.9$ (the Faye comet) to $0^{m}6$ (the comets of Wirtanen and Tuttle-Giacobini-Kresak). Exceptions were the comets of Schaumasse, Honda-Mrkos-Pajdušakova, Wolf 2 and Comas-Solà.

In its last apparition, in 1952, the Schaumasse comet after its perihelion passage was in a state of heightened activity, as shown by observations of its brightness and appearance. Its absolute brightness increased by $1^{m}.5$ compared with its first apparition in 1911.

The comet of Honda-Mrkos-Pajdušakova, which has been observed only twice, revealed an increase of absolute brightness by $0^{m}4$ at its last apparition. However it must be noted that in the first apparition of 1948 the comet was observed two weaks after perihelion passage and its diffuse appearance must have affected the accuracy of observations of its brightness by different observers, of whom there were only a small number. During its second apparition, in 1954, it was observed at the time of perihelion passage and although it retained the appearance of a diffuse nebulosity, it was observed for four months during which its brightness was determined many times.

Comet Wolf 2 in its first apparition in 1924 was discovered by Wolf on a plate in the form of a small nebulous object, of 16^{m} according to Przhibilskii [5], 19 days before perihelion passage (T = 1925, Jan. 10.96). Becoming fainter rapidly, it was a difficult object to observe and was observed practically for only a month, up to January 23, 1925, although it was found for the last time by van Biesbroeck on a plate of February 14, 1925.

The comet was not found during its next three returns in 1931, 1938 and 1944. In 1951 it was discovered by Harrington as a new comet and only later was identified by Cunningham as the lost comet Wolf 2. In the last apparition the conditions for observation were more favorable than at the first apparition and it was observed for 6 ½ months before and after perihelion passage. At the beginning and end of its period of visibility it was observed with large instruments and, because of its diffuse appearance, the estimates of its brightness at those times are too low. Thus, the increase of absolute brightness of comet Wolf 2 at its last apparition can be regarded as real, at least in virtue of the very fact of its independent discovery.

The small increase of absolute brightness of comet Comas-Solà at its last apparition of 1952 ($0^{m}2$) can be most readily explained by the different kinds of measurements used at the two apparitions and also by the omission of a number of photographic measurements obtained with large instruments when H_{10} was determined at the last apparition.

TABLE 2

№	Name of comet	Last apparition		Preceding apparition			First apparition			Period (in years)	No. of returns	Decrease per cycle $\Delta H'_{10}$
		Year of perihelion passage	H_{10}	Year of perihelion passage	H_{10}	ΔH_{10}	Year of perihelion passage	H_{10}	ΔH^{n}_{10}			
1	Faye	1947	$11^{m}.1$	1940	$10^{m}.5$	$+0^{m}.6$	1843	$4^{m}.2$	$+6^{m}.9$	7.4	14	+0.49
2	Whipple	1948	10.0	1941	9.6	+0.4	1933	8.0	+2.0	7.5	2	+1.00
3	Schwassmann — Wachmann$_2$	1948	10.6	1942	8.9	+1.7	1929	7.5	+3.1	6.4	3	+1.03
4	Forbes	1948	13.3	1942	12.7	+0.6	1929	11.4	+1.9	6.4	3	+0.63
5	Neujmin$_1$	1948	12.0	1931	10.5	+1.5	1913	10.3	+1.7	17.7	2	+0.85
6	Väisälä	1949	13.4	1939	12.0	+1.4	1939	12.0	+1.4	10.6	1	+1.40
7	D'Arrest	1950	11.7	1943	11.3	+0.4	1851	9.5	+2.2	6.7	15	+0.15
8	Reinmuth$_1$	1950	12.4	1935	11.7	+0.7	1928	10.2	+2.2	7.2	3	+0.73
9	Daniel	1950	12.8	1943	13.7	—0.9	1909	9.5	+3.3	6.8	6	+0.55
10	Wolf$_1$	1950	13.2	1942	13.6	—0.4	1884	7.6	+5.6	8.3	9	+0.62
11	Tuttle—Giacobini—Kresak	1951	11.9	1907	12.3	—0.4	1858	11.3	+0.6	5.5	17	+0.04
12	Neujmin$_3$	1951	13.7	1929	10.8	+2.9	1929	10.8	+2.9	10.9	2	+1.45
13	Pons—Winnecke	1951	14.1	1945	12.7	+1.4	1819	8.6	+5.5	6.2	21	+0.26
14	Kopff	1951	10.6	1945	9.3	+1.3	1906	8.4	+2.2	6.6	7	+0.31
15	Tempel$_2$	1951	11.9	1946	10.7	+1.2	1873	9.1	+2.8	5.3	15	+0.19
16	Wolf$_2$	1952	10.7	1924	11	—0.3	1924	11	—0.3	6.5	4	—0.05
17	Schaumasse	1952	8.8	1943	12.0	—3.2	1911	10.3	—1.5	8.2	5	—0.30
18	Comas—Solà	1952	8.8	1944	9.3	—0.5	1927	9.0	—0.2	8.5	3	—0.07
19	Grigg—Skjellerup	1952	13.4	1947	13.7	—0.3	1902	9	+4.4	4.9	10	+0.44
20	Borrelly	1953	12.7	1932	9.2	+3.5	1905	9.0	+3.7	6.9	7	+0.53
21	Brooks$_2$	1953	13.7	1946	11.1	+2.6	1889	7.3	+6.4	7.0	9	+0.71
22	Finlay	1953	11.6	1926	12.7	—1.1	1886	9.2	+2.4	6.8	10	+0.24
23	Honda—Mrkos—Pajdušakova	1954	12.1	1948	12.5	—0.4	1948	12.5	—0.4	5.0	1	—0.40
24	Reinmuth$_2$	1954	12.2	1947	10.4	+1.8	1947	10.4	+1.8	6.6	1	+1.80
25	Pons— Brooks	1954	6.4	1883/84	4.9	+1.5	1812	4.2	+2.2	71.4	2	+1.10
26	Encke	1954	12.9	1951	11.3	+1.6	1786	9.9	+3.9	3.3	51	+0.00
27	Wirtanen	1954	15.0	1947	14.4	+0.6	1947	14.4	+0.6	7.2	1	+0.68

Table 2 also compares the absolute brightnesses for the last two apparitions of various comets. 18 comets revealed a decrease of absolute brightness varying from $2^{m}.6$ (comet Brooks 2) to $0^{m}.4$ (comets Whipple and D'Arrest). The Borrelly comet, which was not observed in its two previous returns of 1946 and 1939, decreased in absolute brightness by $3^{m}.5$ compared with 1932.

On the other hand, the following comets showed an increase of absolute brightness as against a general decrease from apparition to apparition: comets Schaumasse (by $3^{m}.2$), Daniel (by $0^{m}.9$), Comas-Solà (by $0^{m}.5$), Wolf 1 (by $0^{m}.4$) and Grigg-Skjellerup (by $0^{m}.3$).

The Finlay comet, which was not observed in three returns, showed an increase in absolute brightness by $1^{m}.1$ compared with 1926; the Tuttle-Giacobini comet, which was not observed since 1907 and was rediscovered by Kresak, increased in absolute brightness by $0^{m}.3$ compared with 1907; the Honda-Mrkos-Pajdušakova and Wolf 2 comets have been discussed above.

In this group special mention must be made of the Schaumasse comet. Its absolute brightness since its discovery in 1911 decreased in one cycle by $1^{m}.7$ (in 1943), but in its last apparition of 1952 increased by $3^{m}.2$, which was thus $1^{m}.5$ above the first apparition of 1911.

The observed fluctuations of brightness of the returning comet Schwassmann-Wachmann I, which were of varying duration and amounted to $3\text{-}5^{m}$, give an idea of the possible flare-up of comets in general. The extraordinary flare-up of the short-period Holmes comet was followed by its disappearance. Therefore the increase in absolute brightness of the comets mentioned above can be regarded as real for the majority of them, especially for the Schaumasse comet and for the three comets which can be regarded as lost: Comets Finlay, Tuttle-Giacobini and Wolf 2.

In general for cases of small variations of absolute brightness from apparition to apparition, attention must be paid to the effect of changes in the visibility conditions and in the relation of the period of observation to the perihelion passage, as well as to the effect of different kinds of measurements and their errors in determining H_{10} for individual apparitions, which especially affects a small number of observations.

6. In connection with the arguments of N. F. Bobrovnikov [6] against the reality of the decrease in absolute brightness of comet Wolf 1 as given by Vsekhsviatskii [7] the results for this comet in Table 2 require more careful study. From Vsekhsviatskii's comparison [7] of the absolute brightness of comet Wolf 1 at its tenth apparition in 1950 and first apparition in 1884, the decrease in absolute brightness in nine returns amounts to 5^m6. The average decrease per return is thus 0^m6.

However, from the absolute brightnesses in the last two returns, in 1950 and 1942, we obtain an increase of 0^m4 for 1950. Vsekhsviatskii [7] determined the absolute brightness in 1942. Cunningham [8] obtained the same results qualitatively. The increase in absolute brightness in the last (tenth) return can be regarded as a second "flare-up" within the pattern of general fading since the discovery of the comet in 1884. The first "flare-up" was noticed by Vsekhsviatskii during the sixth return in 1918 [7]. The decrease in the absolute brightness of comet Wolf 1 follows from the given comparison of the absolute brightness at the last and first apparition and from a comparison of the difference, ΔH_{10}^n, with the results obtained from the other 26 comets listed in Table 2. Comet Wolf 1 shows one of the largest values for this difference.

The attrition of the comet is also evident from a comparison of direct brightness observations and its superficial appearance at its first and last two apparitions [7, 9]. Therefore the observation of its appearance and the evaluation of its brightness during its next (eleventh) return in 1958 will be important in providing information regarding the evolution of this comet and regarding short-period comets generally. The same applies to the other short-period comets which showed increased absolute brightness at their last returns; these are the comets Schaumasse, Finlay, Daniel and Grigg-Skjellerup. Besides the causes mentioned above for the increased absolute brightness of short-period comets, solar corpuscular currents are evidently a cause of unexpected significant "flare-ups."

In any event, these sudden increases in brightness are most probably directly related to enhanced solar activity. S. V. Orlov [10] and S. K. Vsekhsviatskii [11] were among the first to note this fact, which was confirmed by the investigations of Hoffmeister [12], Martynov [13], Dobrovol'skii [14], Richter [15], Beyer [16], Konopleva [17], Cherednichenko [18] and others. Therefore the fact that the increased absolute brightness of comet Wolf 1 occurred at about the time of maximum solar activity in 1918 and 1950 is not a result of chance.

7. The average decrease of absolute brightness per return for each comet in the list, ΔH_{10}^1, was obtained by dividing ΔH_{10}^n, the absolute brightness decrease between the first and last apparitions, by the corresponding number of returns. Table 2 shows that for short-period comets ΔH_{10}^1 has values between 0^m04 (comet Tuttle-Giacobini-Kresak) and 0^m73 (comet Reinmuth 1). Larger values of ΔH_{10}^1, exceeding the upper limit of this distribution, are obtained for comets with a small number of returns: Comets Reinmuth 2 ($\Delta H_{10}^1 = 1^m8$), Väisälä ($\Delta H_{10}^1 = 1^m4$), Neujmin 3 ($\Delta H_{10}^1 = 1^m45$) and Whipple ($\Delta H_{10}^1 = 1^m0$).

For two periodic comets with a period > 12 years we have $\Delta H_{10}^1 = 0^m85$ for comet Neujmin 1 and 1^m1 for comet Pons-Brooks. The average decrease in absolute brightness per return for 21 short-period comets is $\Delta H_{10\,av}^1 = 0^m6 \pm 0^m1$.

The distribution of ΔH_{10}^1 as a function of inclination i did not reveal any dependence of ΔH_{10}^1 on i, that is, the passage of comets through regions closer to the ecliptic does not accelerate their disintegration.

The distribution of ΔH_{10}^1 as a function of perihelion distance q showed no increase of ΔH_{10}^1 with decreasing q. On the contrary, this distribution shows the probability of large ΔH_{10}^1 for large q, although for q from 1 to 2 AU equal values of ΔH_{10}^1 are generally probable.

Comet Encke is a special case; for the smallest distance, q = 0.3 AU, it shows one of the smallest values

$\Delta H_{10}^{1} = 0\overset{m}{.}08$. Comet Pons-Brooks at q = 0.77 has one of the largest values, $\Delta H_{10}^{1} = 1\overset{m}{.}1$.

The correlation coefficient which characterizes the relation between ΔH_{10}^{1} and perihelion distance is quite large: $r = 0.69 \pm 0.07$. However, the meagerness of the data prevents us from arriving at any definite conclusions.

There are thus indications that, in general, the disintegration of cometary matter is not caused by proximity to the sun, but can evidently be stimulated by corpuscular flux from the sun in the form of coronal rays [19]. According to the ideas of Vsekhsviatskii, which were confirmed by Nikol'skii [20], the density of the coronal rays can remain constant at a considerable distance from the sun and their direction is not affected by closeness to the ecliptic. This last fact can be related to the indicated absence of any dependence of brightness decrease per return, ΔH_{10}^{1}, on small values of i, the inclination of the cometary orbit to the plane of the ecliptic, as well as on small values of q, the perihelion distance, and thus confirms the important role of corpuscular activity on the sun for processes that take place in comets.

The distribution of ΔH_{10}^{1} with respect to the number of returns revealed clearly three groups of comets. The first group contains 8 short-period comets with not more than 3 returns (recently discovered). This group is characterized by the largest values of ΔH_{10}^{1}: from $0\overset{m}{.}6$ (comets Wirtanen and Forbes) to $1\overset{m}{.}8$. (comet Reinmuth 2). It also includes the periodic comets Neujmin 3 ($\Delta H_{10}^{1} = 0^{m}85$) and Pons-Brooks ($\Delta H_{10}^{1} = 1\overset{m}{.}1$).

From the fact that for the short-period comets discovered during the last two or three decades we find a predominantly greater decline of absolute brightness as compared with other comets observed at more than four returns, we can infer that the former are of recent origin. Their initially large quantities of matter were expended more rapidly during the first few cycles.

The second group contains 7 comets with from 6 to 10 returns. For 5 comets of this group ΔH_{10}^{1} ranges from $0\overset{m}{.}44$ (comet Grigg-Skjellerup) to $0\overset{m}{.}73$ (comet Brooks 2), this range being close to the average $\Delta H_{10_{av}}^{1} = 0\overset{m}{.}6$. The smallest values of ΔH_{10}^{1} for comets of this group were shown by comets Kopff ($\Delta H_{10}^{1} = 0\overset{m}{.}31$) and Finlay ($\Delta H_{10}^{1} = 0^{m}24$).

The third group contains 6 comets with 14 or more returns. For five of these comets the absolute brightness decrease per return, ΔH_{10}^{1}, did not exceed $0\overset{m}{.}26$ (comet Pons-Winnecke), which is below the average, ΔH_{10av}^{1}. This group is characterized by the smallest values of ΔH_{10}^{1} (comets Tuttle-Giacobini-Kresak, Encke, D'Arrest and Tempel 2). Comet Faye ($\Delta H_{10}^{1} = 0\overset{m}{.}49$) is an exception; its number of returns (14) observed up to 1947 is the smallest for this group.

Any investigation of the variation of absolute brightness of individual short-period comets from return to return is outside the scope of the present article. This has already been done for the majority of the comets by Vsekhsviatskii [7, 21, 22], Konopleva [17, 23] and Cherednichenko [24]. However, a quick review of the evolution of some short-period comets with a large number of returns generally indicates that the first few returns are usually characterized by steeper fluctuations of absolute brightness and for some comets by "flare-ups"; thereafter the decline of absolute brightness becomes more gradual. Observations confirm the exhaustion of short-period comets after a few returns, as revealed by the weaker development of the coma, tail and intensity of observed radiation (comet Wolf 1).

The brightness decrease of short-period comets depends not so much on their kinematic characteristics as on the individual peculiarities of their physical structure. In general this decrease is associated with the common features of the entire family of short-period comets.

The special position of comet Pons-Brooks in the given distributions distinguishes it from the short-period comet group with respect to both orbital and physical characteristics. The evolution of this comet since its discovery in 1812 shows features in common with Halley's comet, which also belongs to Neptune's family; their characteristics of brightness fluctuations, the ability to form halos, envelopes, considerable absolute brightness reduction per return — all indicate intensive processes in the cometary nucleus. Therefore periodic comets with a period longer than 30 years must occupy a special position among periodic comets with respect to their structure.

On the whole the study of the absolute brightnesses of periodic comets confirms Vsekhsviatskii's observation in 1933 that such comets disintegrate, showing a decrease in absolute brightness in successive returns.

I am deeply indebted to Professor S. K. Vsekhsviatskii for suggesting the subject of this article and for his continued interest, and also to G. M. Nikol'skii and E. A. Ponomarev for friendly criticisms and suggestions.

Astronomy Department, Kiev State University

Received January 10, 1957

LITERATURE CITED

[1] S. K. Vsekhsviatskii, Astron. J. (USSR) 10, 327 (1933); 12, 243 (1935); 19, 480 (1937); Publ. Kiev. Astr. Obs. No. 2 (1948).

[2] V. P. Konopleva, Publ. Kiev. Astr. Obs. No. 3 (1951).

[3] T. V. Vodop'ianova, Astr. Tsirk. 145 (1945); 147 (1954); 150 (1954); 169 (1956).

[4] P. P. Parenago, Uspekhi Astr. Nauk 4, 257 (1948).

[5] G. Merton, Monthly Notices Roy. Astron. Soc. 114, 368 (1954).

[6] N. T. Bobrovnikoff, Perkins Observatory Ohio Wesleyan Univ. and Ohio State Univ. Repreint No. 35 (1948).

[7] S. K. Vsekhsviatskii, Publ. Kiev Astr. Obs. No. 4 (1950).

[8] L. E. Cunningham, Un. Astr. Intern. Circ. No. 1284 (1950).

[9] S. K. Vsekhsviatskii, Physical Characteristics of Comets [In Russian] (GTTI, 1957).

[10] S. V. Orlov, Trudy GAFI 2, 150 (1923).

[11] S. K. Vsekhsviatskii, Astron. J. (USSR) 2, No. 3 (1925).

[12] C. Hoffmeister Z. Astrophys. 22, 265 (1941).

[13] D. Ia. Martynov, Astron. J. (USSR) 21, No. 6 (1944).

[14] O. V. Dobrovol'skii, Dissertation [In Russian](GAO, 1954); Bull. SAO No. 13 (1955).

[15] N. Richter, Astronomische Nachrichten 271, 207 (1940).

[16] M. Beyer, Berg. Mitt. 9, No. 72 (1950); Astronomische Nachrichten 282, No. 4 (1955).

[17] V. P. Konopleva, Trudy SAO No. 20 (1954).

[18] V. I. Cherednichenko, Dissertation, Kiev State Univ. 1956.

[19] S. K. Vsekhsviatskii, Astr. J. (USSR) 21, 149 (1944); Publ. Kiev. Astr. Obs. No. 1, 86 (1946).

[20] G. M. Nikol'skii, Dissertation [In Russian] (Kiev State Univ., 1955); Astron. J. (USSR) 33, No. 3 (1956).

[21] S. K. Vsekhsviatskii, Publ. Kiev Astr. Obs. No. 5 (1953).

[22] S. K. Vsekhsviatskii, Astron. J. (USSR) 29, No. 1 (1952).

[23] V. P. Konopleva, Publ. Kiev. Astr. Obs. No. 5 (1953).

[24] V. I. Cherednichenko, Publ. Kiev. Astr. Obs. No. 5 (1953).

A SPECIAL CASE OF THE GENERAL THREE-BODY PROBLEM

M. A. Dirikis

For a special case of the three-body problem, the nature of the motion is investigated by means of the numerical integration of the differential equations of motion. Initially, the three bodies (for example, three stars) are situated along a straight line. The values of the initial velocity are found for which 1) one star escapes from the system, 2) the system breaks up completely. The results are extended to the case where the masses and the initial separations can have any values.

There exist in the literature several examples of the solution of special cases of the general three-body problem, i.e., the problem in which the motion of three bodies with comparable masses under the action of mutual attraction is investigated [1-6]. Numerical methods of integration are used for solving the differential equations of motion.

E. Strömgren, K. Bohlin, and other authors [1-5] were mainly interested in such cases from the point of view of mathematics and mechanics. O. Iu. Shmidt [6] gave his example to prove the possibility of capture in the general three-body problem.

The aim of our paper is the investigation of the stability of multiple stellar systems. According to V. A. Ambartsumian's theory, stars originate in groups in extensive stellar aggregates – associations. It is assumed that such a group is unstable, i.e., it cannot exist for a long time. Such groups are observed as trapezoidal systems and as chains of stars [7, 8]. V. G. Fesenkov and D. A. Rozhkovskii [9] have proposed that the stellar chains are formed from nebular filaments consisting of gas and dust. At present, we cannot obtain sufficiently accurate information on the relative motions of the stars in these systems. To determine how these systems evolve, it is necessary to know extremely accurately the relative proper motions of the component stars. As yet, this is impossible in practice since the observations have been carried out during only a short interval of time. The radial velocities, also, are not always known. Only in the case of the Trapezium of Orion can we say with certainty that this system is actually breaking up [10].

Therefore, in order to determine the nature of the motion in multiple systems of the trapezium and chain types we have turned to simple artificial examples.

In the present paper we consider the case of a chain of three stars with equal masses. The initial conditions are chosen so that the separations (Fig. 1) r_{12} and r_{23} are equal. The initial velocity of one of the stars is zero, V_2 and V_3, the velocities of the remaining stars, are equal in magnitude but opposite in direction and are perpendicular to the line $m_1m_2m_3$.

At $t = 0$

$$V_2 = V_3 = V_0.$$

Thus, we obtain a system of equations with one parameter V_0. The system can also be described by the constant total energy $\underline{h}$:

$$h=\frac{1}{2}\left(m_1V_1^2+m_2V_2^2+m_3V_3^2\right)-\left(\frac{m_1m_2}{r_{12}}+\frac{m_2m_3}{r_{23}}+\frac{m_1m_3}{r_{13}}\right). \qquad (1)$$

In our examples the following values were taken:

$$\left.\begin{aligned} &\text{masses } m_1 = m_2 = m_3 = 1 \text{ (solar mass)} \\ &\text{separations } r_{12} = r_{23} = 5000 \text{ AU} \end{aligned}\right\} \qquad (2)$$

Substituting these values into (1), we have at t = 0

$$h = V_0^2 - 0.0005.$$

Differential equations of motion in an absolute coordinate system were used to find the trajectories and the other features of the motion of the three bodies considered. The origin of the coordinate system is at the center of mass of the system. In this case the equations of motion have the following form:

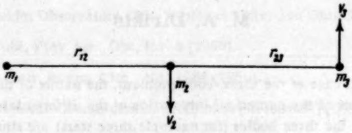

Fig. 1. Initial conditions.

$$\frac{d^2x_1}{dt^2} = \frac{x_2 - x_1}{r_{12}^3} + \frac{x_3 - x_1}{r_{13}^3}$$

$$\frac{d^2y_1}{dt^2} = \frac{y_2 - y_1}{r_{12}^3} + \frac{y_3 - y_1}{r_{13}^3};$$

$$\frac{d^2x_2}{dt^2} = \frac{x_3 - x_2}{r_{23}^3} + \frac{x_1 - x_2}{r_{12}^3};$$

$$\frac{d^2y_2}{dt^2} = \frac{y_3 - y_2}{r_{23}^3} + \frac{y_1 - y_2}{r_{12}^3};$$

$$\frac{d^2x_3}{dt^2} = \frac{x_1 - x_3}{r_{13}^3} + \frac{x_2 - x_3}{r_{23}^3};$$

$$\frac{d^2y_3}{dt^2} = \frac{y_1 - y_3}{r_{13}^3} + \frac{y_2 - y_3}{r_{23}^3}$$

We have taken the unit of time as year/ 2π, so that Gauss's constant is equal to unity.

This system of six differential equations of the second order has six unknowns: x_1, y_1, x_2, y_2, x_3, and y_3. To integrate the system we have used the method of quadratures. If we let

$$\frac{d^2x_i}{dt^2} = f_i,$$

$$\frac{d^2y_i}{dt^2} = g_i.$$

then

$$w\dot{x}_i(n) = \frac{1}{2}\left[w^{2\prime} f_i\left(n - \frac{1}{2}\right) + w^{2\prime} f_i\left(n + \frac{1}{2}\right)\right] - \frac{1}{24}\left[w^2 f_i'\left(n - \frac{1}{2}\right) + \right.$$

$$\left. + w^2 f_i'\left(n + \frac{1}{2}\right)\right] + \frac{11}{1440}\left[w^2 f_i'''\left(n - \frac{1}{2}\right) + w^2 f_i'''\left(n + \frac{1}{2}\right)\right] + \ldots,$$

$$x_i(n) = w^{2\prime\prime} f_i(n) + \frac{1}{12} w^2 f_i(n) - \frac{1}{240} w^2 f_i''(n) + \frac{1}{1951} w^2 f_i^{IV}(n) - \ldots,$$

where $\underline{w}$ is the interval of integration. We obtain analogous expressions for $\underline{y}$; we use the abbreviation $f_i^{(k)}(n)$ for the expression $f_i^{(k)}(t_0 + nw)$.

The integration interval w corresponding to the initial conditions (2) was usually taken equal to 20,000 time units (i.e., about 3183 years). Only when the velocities were high was the interval equal to 10,000 time units in order to decrease the influence of the high-order differences; on the other hand, when the separations of the bodies were large the interval was doubled, i.e., the value taken was w = 40,000.

To start the integration several values of x_i and y_i were calculated for the time close to t_0 with the help of the Taylor series

$$x_i = x_i(0) + \dot{x}_i(0)(t - t_0) + \frac{1}{2}\ddot{x}_i(0)(t - t_0)^2 + \ldots,$$

$$y_i = y_i(0) + \dot{y}_i(0)(t - t_0) + \frac{1}{2}\ddot{y}_i(0)(t - t_0)^2 + \ldots.$$

The first terms in the summation columns are the following:

$$w^{2\prime} f_i\left(\frac{1}{2}\right) = w\dot{x}_i(0) + \frac{1}{2}w^2 f_i(0) + \frac{1}{12}w^2 f'_{im}(0) - \frac{11}{720}w^2 f'''_{im}(0) + \ldots,$$

$$w^{2\prime\prime} f_i(0) = x_i(0) - \frac{1}{12}w^2 f_i(0) + \frac{1}{240}w^2 f_i^{\cdot}(0) - \frac{1}{1951}w^2 f_i^{\mathrm{IV}}(0) + \ldots,$$

where, for example, we have used the abbreviation

$$f_{im}(0) = f'_i\left(-\frac{1}{2}\right) + f'_i\left(+\frac{1}{2}\right).$$

The calculations can be checked to some extent by using the following equations:

$$x_1\dot{y}_1 - y_1\dot{x}_1 + x_2\dot{y}_2 - y_2\dot{x}_2 + x_3\dot{y}_3 - y_3\dot{x}_3 = C \quad \text{(angular momentum integral)},$$

$$\frac{1}{2}(V_1^2 + V_2^2 + V_3^2) - \left(\frac{1}{r_{12}} + \frac{1}{r_{13}} + \frac{1}{r_{23}}\right) = h \quad \text{(energy integral);}$$

moreover

$$x_1 + x_2 + x_3 = 0,$$

$$y_1 + y_2 + y_3 = 0,$$

etc., (we have similar expressions for the velocity components, as well as for the sums and differences of all orders).

Unfortunately, these equations are not sufficient to check the calculations.

From the start the calculations showed that the star m_3 is bound least to the system. Therefore, it is interesting to investigate the motion of star m_3 relative to the center of mass of the system $m_1 - m_2$. This motion can be conviently characterized by the quantity $1/a_{c3}$, where a_{c3} is the major semiaxis of the orbit about the center of mass of the system $m_1 - m_2$.

If $1/a_{c3} > 0$, then the star m_3 remains in the system and its orbit is somewhat similar to an ellipse.

If $1/a_{c3} \leq 0$, then the star m_3 escapes from the system and the orbit of the star as it moves away tends to a parabolic or hyperbolic shape.

The equation determining $1/a_{c3}$ is obtained from the well-known relation

$$V_{c3}^2 = k^2(m_c + m_3)\left(\frac{2}{r_{c3}} - \frac{1}{a_{c3}}\right),$$

where V_{c3} is the velocity of the star relative to the center of mass of the system $m_1 - m_2$, which is denoted by m_c.

and r_{c3} is the distance between the star m_3 and m_c. Since

$$V_{c3}=\frac{3}{2}V_3,\quad r_{c3}=\frac{3}{2}r_3,\quad k^2=1,\quad m_c=2,\quad m_3=1,$$

we find

$$\frac{1}{a_{c3}}=\frac{4}{3r_3}-\frac{3}{4w^2}\,(w^2V_3^2).$$

Thus, our first problem is as follows:

To determine the minimum value of the initial velocity V_0 for which the star m_3 escapes from the system of the stars m_1 and m_2. In other words, to determine the value of V_0 for which

$$\frac{1}{a_{c3}}=0,$$

when the distance r_{c3} becomes considerably greater than the distance r_{12} (approximately, $r_{c3} \geq 5r_{12}$).

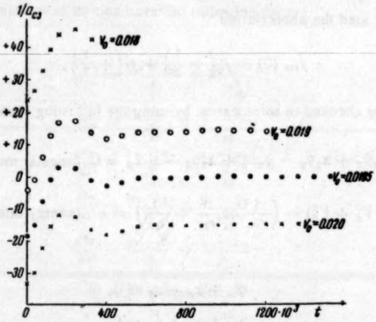

Fig. 2. The value of $1/a_{c3}$ for various initial velocities V_0. Along the abscissa the time is plotted in 1000 time units, along the ordinate the value of $1/a_{c3}\cdot 10^8$.

For the first example we have taken

$$\left.\begin{aligned} r_{12} = r_{23} &= 5000\ \text{AU}\\ m_1 = m_2 &= 1\ \text{solar mass,}\end{aligned}\right\}\qquad (2)$$

and $V_0 = 0.020$ AU per time unit, where 1 time unit = year/ 2π.

At t = 1,360,000 it is clear that $1/a_{c3}$ tends to a negative value which is approximately $-15\cdot 10^{-8}$ and this undoubtedly corresponds to the escape of the body m_3 from the system.

After this case, the values $V_0 = 0.018$ and 0.019 were tried. The first of these was quickly rejected, but the second was used for calculating $1/a_{c3}$ up to the time t = 1,200,000 (Fig. 2).

By interpolation it was found that $1/a_{c3} = 0$ corresponds to approximately $V_0 = 0.0195$, or a little less. The calculations were then carried out with $V_0 = 0.0195$ and $V_0 = 0.01949$ up to t = 1,520,000. The tabulated values of $1/a_{c3}$ (Table 1) and the corresponding graphs (Fig. 3) show that the value $V_0 = 0.0195$ is closest to the limit which interests us.

In Fig. 3 the vertical scale has been increased 10 times as compared with the scale in Fig. 2.

TABLE 1

Values of $1/a_{C_3}$

t	$V_0 = 0.01949$	$V_0 = 0.0195$	t	$V_0 = 0.01949$	$V_0 = 0.0195$
0	$-18228 \cdot 10^{-9}$	$-18521 \cdot 10^{-9}$	800	-231	-526
$80 \cdot 10^3$	-7580	-7862	880	$+45$	-253
160	$+3041$	$+2754$	960	$+309$	$+11$
240	$+3014$	$+2714$	1040	$+394$	$+99$
320	-852	-1153	1120	$+334$	$+41$
400	-2564	-2865	1200	$+225$	-67
480	-1520	-1820	1280	$+144$	-150
560	-244	-542	1360	$+124$	-170
640	$+18$	-275	1440	$+166$	-130
720	-216	-506	1520	$+238$	-58

As an example we will investigate the trajectories for the case $V_0 = 0.0195$

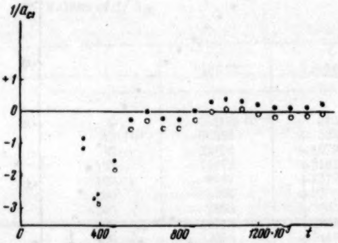

Fig. 3. The same values are plotted here as in Fig. 2 but the vertical scale has been expanded by a factor 10. The lower (open) circles give $1/a_{C_3}$ for $V_0 = 0.0195$, the upper (filled) circles for $V_0 = 0.01949$.

Fig. 4 gives the trajectories of all three bodies in an absolute coordinate system and Fig. 5 gives the trajectories in the coordinate system whose origin is placed at the center of mass of the bodies m_1 and m_2.

The calculations are not restricted to the values of the masses and separations given by (2) because similar trajectories can be obtained using other masses and initial conditions if the following law of similarity is fulfilled.

If λ is the ratio of the separations and μ is the ratio of the masses, then the ratio of the velocities ν and the ratio of the times τ (necessary to transform the system into some other similar system) are obtained from the equations

$$\nu = \frac{\lambda}{\tau} = \frac{\sqrt{\mu}}{\sqrt{\lambda}} \tag{3}$$

and

$$\tau = \frac{\lambda^{3/2}}{\sqrt{\mu}} .$$

Using Equation (3), we have calculated the values of the initial velocity V_0 for the case when the masses and initial separations are different from those used in the above example (2); these values are given in Table 2.

The values of the velocity V_0 in kilometers per second are given in brackets, since

$$1 \text{ AU/ time unit} = 29.767 \text{ km/ sec.}$$

We now proceed to the second problem:

To determine the minimum value of the initial velocity V_0 for which the system breaks up completely.

This problem is associated with an investigation of the relative motion of the bodies m_1 and m_2. The problem reduces to the determination of the minimum value of the initial velocity V_0 for which the stars m_1 and m_2 break away from each other. In other words, we have to find the value of V_0 for which

$$\frac{1}{a_{12}} = 0,$$

when the stars are sufficiently far apart.

In this case, the equation which determines $1/a_{12}$ is the following:

$$\frac{1}{a_{12}} = \frac{2}{r_{12}} - \frac{1}{2w^2}(w^2V_{12}^2),$$

where

$$w^2V_{12}^2 = (w\dot{x}_1 - w\dot{x}_2)^2 + (w\dot{y}_1 - w\dot{y}_2)^2.$$

The trial value of V_0 chosen was $V_0 = 0.025$, but it was found that this value of the velocity leads to a very positive value of $1/a_{12}$ — about $+100 \cdot 10^{-6}$. The next value of V_0 taken was 0.030 and, finally, 0.0285. The results are given in Table 3 and the corresponding graphs (Fig. 6) show that the value of the initial velocity which is of interest is about

$$V_0 = 0.0287.$$

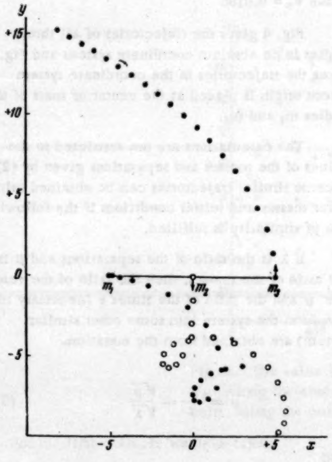

Fig. 4. The motion of the stars when the initial velocity $V_0 = 0.0195$ in an absolute coordinate system. The distances along the axes are in 1000 astronomical units. The circles represent the positions of the stars at intervals of 80,000 time units.

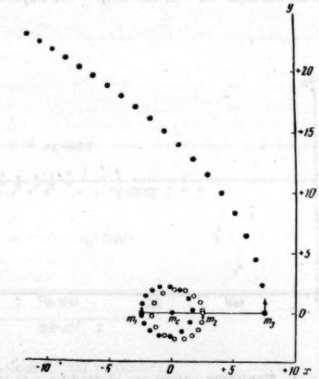

Fig. 5. The same example as in Fig. 4, but in this case the motion represented relative to the center of mass of the stars m_1 and m_2. The center of mass is situated at the point m_C.

Using Equation (3), we can obtain the values of the initial velocity for other initial conditions (Table 4). This table is analogous to Table 2. The values of the initial velocity in kilometers per second are given in brackets.

As was stated above, the system investigated can also be characterized by the value of the constant total

TABLE 2

Initial Velocity V_0 for Which the Star m_3 Escapes

Separations \ Masses	0,5	1	2	5	10	20
2000 AU	0.0218 (0.649)	0.0308 (0.918)	0.0436 (1.298)	0.0689 (2.052)	0.0975 (2.902)	0.1379 (4.104)
5000 AU	0.0138 (0.410)	0.0195 (0.580)	0.0276 (0.821)	0.0436 (1.298)	0.0617 (1.836)	0.0872 (2.596)
10000 AU	0.0097 (0.290)	0.0138 (0.410)	0.0195 (0.580)	0.0308 (0.918)	0.0436 (1.298)	0.0617 (1.836)
0.1 ps =20626.5 AU	0.0068 (0.202)	0.0096 (0.286)	0.0136 (0.404)	0.0215 (0.639)	0.0304 (0.904)	0.0429 (1.278)
0.2 ps	0.0048 (0.143)	0.0068 (0.202)	0.0096 (0.286)	0.0152 (0.452)	0.0215 (0.639)	0.0304 (0.904)
0.5 ps	0.0030 (0.090)	0.0043 (0.128)	0.0061 (0.181)	0.0096 (0.286)	0.0136 (0.404)	0.0192 (0.572)

TABLE 3

Values of $1/a_{12}$

t	$V_0 = 0.030$	$V_0 = 0.0285$	t	$V_0 = 0.030$	$V_0 = 0.0285$
0	$-50000 \cdot 10^{-9}$	$-6125 \cdot 10^{-9}$	720	−36717	+7995
$40 \cdot 10^3$	−39898	+ 3233	800	−37970	+7080
80	−22758	+19798	880	−38843	+6519
120	−11172	+31624	960	−39462	+6179
160	− 6167	+37122	1040	−39908	+5982
200	− 5706	+37992	1120	−40232	+5872
240	− 7893	+36034	1200	−40471	+5822
320	−15313	+28653	1280	−40648	+5808
400	−22652	+21193	1360	−40781	+5819
480	−28276	+15590	1440	−40881	+5844
560	−32215	+11850	1520	−40956	+5878
640	−34895	+ 9474			

TABLE 4

Initial Velocity V_0 for Which the System Breaks Up

Separations \ Masses	0,5	1	2	5	10	20
2000 AU	0.0321 (0.955)	0.0454 (1.35)	0.0642 (1.91)	0.1015 (3.02)	0.1435 (4.27)	0.2029 (6.04)
5000 AU	0.0203 (0.604)	0.0287 (0.854)	0.0406 (1.21)	0.0642 (1.91)	0.0908 (2.70)	0.1283 (3.82)
10000 AU	0.0144 (0.427)	0.0203 (0.604)	0.0287 (0.854)	0.0454 (1.35)	0.0642 (1.91)	0.0908 (2.70)
0.1 ps =20626.5 AU	0.0100 (0.297)	0.0141 (0.421)	0.0200 (0.595)	0.0316 (0.941)	0.0447 (1.33)	0.0632 (1.88)
0.2 ps	0.0071 (0.210)	0.0100 (0.297)	0.0141 (0.421)	0.0223 (0.665)	0.0316 (0.941)	0.0447 (1.33)
0.5 ps	0.0045 (0.133)	0.0063 (0.188)	0.0089 (0.266)	0.0141 (0.421)	0.0200 (0.595)	0.0283 (0.841)

energy h (1). Let us introduce the following quantities for the cases discussed above:

$$h_{c3} = \frac{1}{2}\left[(m_1 + m_2)V_c^2 + m_3V_3^2\right] - \frac{(m_1 + m_2)m_3}{r_{c3}}$$

and

$$h_{12} = \frac{1}{2}\{m_1[(\dot{x}_1 - \dot{x}_c)^2 + (y_1 - \dot{y}_c)^2] + m_2[(\dot{x}_2 - \dot{x}_c)^2 + (\dot{y}_2 - \dot{y}_c)^2]\} - \frac{m_1m_2}{r_{12}},$$

where r_{c3} is the distance between the star m_3 and m_C, the center of mass of the stars m_1 and m_2.

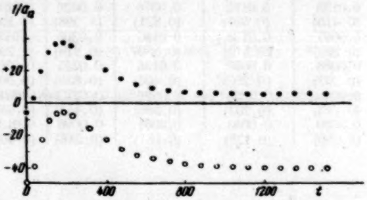

Fig. 6. The values of $1/a_{12}$ for various initial velocities V_0. Along the abscissa time is plotted in 1000 time units, along the ordinate the value of $1/a_{12} \cdot 10^6$; the open circles correspond to $V_0 = 0.030$, the filled-in circles correspond to $V_0 = 0.0285$.

V_C, the velocity of the center of mass m_C, is given by

$$V_c^2 = \dot{x}_c^2 + \dot{y}_c^2,$$

$$\dot{x}_c = \frac{m_1\dot{x}_1 + m_2\dot{x}_2}{m_1 + m_2},$$

$$\dot{y}_c = \frac{m_1\dot{y}_1 + m_2\dot{y}_2}{m_1 + m_2}.$$

In our case all the masses are equal. Let us investigate the case when the masses and separations are given by (2) at the time t = 0; $V_2 = V_3 = V_0$. Then

$$h = V_0^2 - 0.0005,$$

$$h_{c3} = \frac{3}{4}V_0^2 - \frac{2}{7500},$$

$$h_{12} = \frac{1}{4}V_0^2 - 0.0002.$$

The values of h, h_{C3}, and h_{12} are given in Table 5.

From these data, it can be seen that knowing the total energy h, or h_{C3} or h_{12}, beforehand does not help us to determine the features of the motion in the system. To determine these features it is necessary to carry out a numerical integration of the differential equations of motion. This can be easily seen from the variation of the quantities h_{C3} and h_{12} (see Tables 1 and 3), since these quantities are nothing else but

$$h_{c3} = -\frac{1}{a_{c3}}, \quad 2h_{12} = -\frac{1}{a_{12}}.$$

TABLE 5

V_0	h	h_{c3}	V_0	h	h_{c4}
0.0188562	−0.000144444	0	0.0223607	0	−0.000075
0.019	−0.000139	+0.000004083	0.0282843	+0.0003	0
0.01949	−0.0001201399	+0.000018228	0.0285	+0.00031225	+0.0000030625
0.0195	−0.00011975	+0.000018521	0.0287	+0.00032369	+0.0000059225
0.020	−0.0001	+0.000033333	0.030	+0.0004	+0.000025
0.0223607	0	+0·000108333			

In future it is necessary to investigate the cases of the three-body problem with fewer limitations, for example, the case when the stellar masses are not equal, the stellar velocities are in different directions, etc.

Astronomy Department of the Academy
of Sciences,Latvian SSR

Received February 2, 1957

LITERATURE CITED

[1] E. Strömgren, Astron. Nachr. 182, 181 (1909).

[2] C. Burrau, Astron. Nachr. 195, 113 (1913).

[3] E. Strömgren, Monthly Notices, Roy. Astron. Soc. 80, 12 (1919).

[4] K. Bohlin, Astr. Iaktt. och Undersökh. Stockholm Obs. 10, No. 11 (1923).

[5] J. Zumkley, Astron. Nachr. 272, 66 (1941).

[6] O. Iu. Shmidt, Doklady Akad Nauk SSSR 58, No. 2, 213 (1947).

[7] B. E. Markarian, Soobshchen. Biurak. Obs. No. 5 (1950); No. 9 (1951).

[8] V. A. Ambartsumian, Soobshchen. Biurak. Obs. No. 15 (1954).

[9] V. G. Fesenkov and D. A. Rozhkovskii, Astron. J. (USSR), 29, 397 (1952).

[10] P. P. Parenago, Proc. Second Conference on Cosmogony [In Russian] (Izd AN SSSR, Moscow, 1953) p. 343.

BRIEF COMMUNICATIONS

REMARKS ON THE ARTICLE BY V. F. D'IAKONOV ENTITLED "THE INFLUENCE OF DIURNAL ABERRATION ON THE ACCURACY OF DETERMINATIONS OF LATITUDE FROM OBSERVATIONS OF POLARIS"*

A. A. Mikhailov

It is shown from elementary geometrical considerations supported by an analytic proof that the influence of diurnal aberration on latitude determinations from observations of Polaris is negligible, not exceeding 0."005. The conclusion of V. F. D'iakonov to the contrary [Astr. J. 34, 3, 484 (1957)] is incorrect.**

In the article under the above title it was inferred that the influence of diurnal aberration on latitude determinations from observations of Polaris can amount to 0."5. It can easily be seen that this is entirely incorrect. It is clear from elementary geometrical considerations that the diurnal aberration does not appreciably affect latitudes determined from the zenith distance of stars close to the meridian. The diurnal aberration acts in a direction which is perpendicular to the meridian, so that its component along the zenith distance on the meridian is exactly zero and at small distances from the meridian the effect is of the second order of smallness. This would be sufficient except for the fact that the author of the article under discussion attempts an analytic derivation in which he makes his mistake; we shall give a correct derivation which confirms the geometrical argument.

D'iakonov uses the familiar formula for reducing to the meridian the zenith distance of a star at a small hour angle; by differentiation with respect to the hour angle he obtains the correct expression (4) for the variation of the latitude $\Delta\varphi_\alpha$ under the influence of the component of diurnal aberration which is in the direction of the right ascension. In order to obtain the total variation of latitude we must add the effect of the declination component of the diurnal aberration; here a fundamental error is committed by the use of the formula $\varphi = z + \delta$, which is applicable only to the meridian itself. In order to obtain a correct result we must also differentiate (2) with respect to δ, which when added to $\Delta\varphi_\alpha$ would give a vanishingly small effect on the latitude.

The second error lies in the use of a formula for reduction to the meridian which applies only to small hour angles $\underline{t}$ but which is here applied to all of the hour angles of Polaris. For this case it would be necessary to use the following formula:

$$\varphi = 90^\circ - z - p\cos t + \ldots,$$

where $\underline{p}$ is the polar distance of the star. Differentiation of this expression indicates practically zero effect of the diurnal aberration on latitude. The most exact result requires use of a series expansion with differentiation of only the first term, starting with the rigorous formula

$$\cos z = \sin\varphi\sin\delta + \cos\varphi\cos\delta\cos t.$$

Differentiating this formula with respect to the variables δ and $\underline{t}$ on the right-hand side, we obtain the dependence of dz on dδ and dt = − dα. Inserting the expressions for the diurnal aberration components parallel to the declination and right ascension, that is Eq. (1) of D'iakonov, we obtain after some transformations

---

* The editor has received letters from Prof. A. N. Deutsch and A. V. Butkevich, who also point out the error in D'iakonov's article.

** Soviet Astronomy — AJ, p. 419.

$$dz = -k \cos\varphi \cos z \sin A,$$

where $k = 0''.32$ is the coefficient of diurnal aberration and A is the azimuth of the star. In order to obtain the effect of latitude we differentiate the same formula with respect to φ and obtain

$$dz = \cos A \, d\varphi.$$

Hence by eliminating dz we finally obtain

$$\Delta\varphi = -k \cos\varphi \cos z \, \mathrm{tg}\, A.$$

This formula, which applies to all stars, is not new but is also given in the well-known manual of practical astronomy by Th. Albrecht entitled "Formeln und Hilfstafeln für geographische Ortsbestimmungen."

We can simplify this formula for Polaris, the azimuth of which is always small and very close to

$$\mathrm{tg}\, A \approx \sin A \approx \frac{p \sin t}{\sin z}.$$

Moreover, we can assume $\cos\varphi \approx \sin z$, whence

$$\Delta\varphi = -kp \sin\varphi \sin t.$$

This correction reaches its maximum value at $t = \pm 90°$, when for $p = 1°$ $\Delta\varphi$ has the following values for different latitudes:

φ	$\Delta\varphi$
0°	0″.0000
30	0.0028
60	0.0048
80	0.0055

Thus, the influence of diurnal aberration on latitude determinations from observations of Polaris is absolutely negligible and is usually disregarded. This result, as well as the formulas that have been given, has been known for a long time. We recall them here only to prevent errors which can result from D'iakonov's article that unfortunately was printed in the Astronomical Journal.

Main Astronomical Observatory,
Academy of Sciences, USSR

Received September 14, 1957

THE GRAVITATIONAL INSTABILITY OF A GAS FILAMENT

E. A. Dibai

The theory of small vibrations of a continuous medium is used to examine the instability to longitudinal perturbations of a fluid cylinder in its own gravitational field. It is shown that for certain values of the density, the cylinder is gravitationally unstable and breaks up into several condensation. The results obtained can be used to explain the origin of star chains.

1. An important property both of luminous and nonluminous nebulae is their filament-like structure. It has often been noted by Shain [1] that "the filament may be considered a universal characteristic of nebulae." The remarkably widespread occurrence of filaments has also been mentioned by Fesenkov [2]. There occur luminous and nonluminous filamented nebulae, separate elongated nebulae, isolated filaments, and finally the arms of gas and dust observed in neighboring galaxies.

Many observers have noted that such filaments and arms tend to break up as they evolve, falling apart into separated condensation. Edgeworth [3] arrived theoretically at a similar conclusion, and much observational data tending to verify this proposal has been obtained by Fesenkov and Rozhkovskii [4], Shain [5], Martynov [6], and others.

Vorontsov-Vel'iaminov [7] has discovered many cases in which the dust-filled galactic arms of M33 have broken up into chains of nebulae. He has emphasized that such phenomena do not occur by chance, and has pointed to similar objects in our Galaxy. Dark filaments which are broken up into chains of globules have also been noted by Khavtasi [8] in his catalog of nonluminous nebulae.

Further, a number of authors (Edgeworth [3], Fesenkov [9]) connect the hypothesis of filament decay to the origin of star chains, having in mind the possibility that gravitational forces may condense the decay products into stars.

In this connection it is interesting to investigate the gravitational instability of a gas filament. We shall investigate this problem, as is often done in the theory of gravitational instability, by assuming that the matter of which the filament is composed moves according to the laws of hydrodynamics.

2. In investigating the gravitational effects of density fluctuations in an unbounded homogeneous medium, Jeans [10] showed that perturbations propagate as waves with the velocity

$$V = \sqrt{c^2 - \frac{4\pi G\rho}{k^2}}, \tag{1}$$

where $c = \sqrt{\gamma RT}$ is the mean sound velocity, and k is the wave number. According to this, when

$$\lambda \geqslant \sqrt{\frac{\pi c^2}{G\rho}} \tag{2}$$

the propagation velocity becomes imaginary, which means that the condensations and rarefactions increase exponentially with time, giving rise to condensation nuclei. Thus (2) is the condition for gravitational instability, usually called the Jeans criterion.

Mathematically, the investigation of gravitational instability reduces to solving the differential equation

$$\frac{\partial^2 s}{\partial t^2} = 4\pi G\rho s + c^2 \nabla^2 s, \tag{3}$$

where $s = \delta\rho/\rho$ is the density variation ("condensation"), and ∇^2 is the Laplacian operator. This equation describes the propagation of small adiabatic oscillations in an unbounded homogeneous medium [10, 11].

Consider a filament in the form of a homogeneous infinite cylinder of radius R_0. Then in cylindrical coordinates r, z, Eq. (3) can be written

$$\frac{\partial^2 s}{\partial t^2} = 4\pi G\rho s + c^2 \left[\frac{\partial^2 s}{\partial r^2} + \frac{1}{r} \cdot \frac{\partial s}{\partial r} + \frac{\partial^2 s}{\partial z^2}\right]. \tag{4}$$

We shall attempt to find a solution of this equation in the form

$$s = \varphi(r)\, e^{i\omega t - ikz}, \tag{5}$$

representing longitudinal waves propagating along the z axis with the boundary conditions

$$\begin{aligned} &s < \infty \text{ for } r = 0 \text{ (on the axis of the cylinder)}, \\ &s = 0 \text{ for } r = R_0 \text{ (at the walls of the cylinder)}. \end{aligned} \tag{6}$$

Inserting (5) into (4), we obtain an equation for $\varphi(r)$, and finally

$$s = [C_1 I_0(qr) + C_2 H_0(qr)]\, e^{i\omega t - ikz}, \tag{7}$$

where $I_0(qr)$ and $H_0(qr)$ are Bessel and Hankel functions of zeroth order of the first kind, and q is given by

$$q^2 = \frac{4\pi G\rho + \omega^2}{c^2} - k^2. \tag{8}$$

Using the boundary conditions (6) and setting $C_1 = 1$ for simplicity, we finally obtain

$$s = J_0\left(\frac{\mu_1}{R_0}, r\right) e^{i\omega t - ikz}, \tag{9}$$

where μ_1 is the first root of the Bessel function.

Let us now establish the criterion for gravitational instability. We use Eq. (8) to find an expression for the propagation velocity of a wave along the cylindrical axis, obtaining

$$V = \sqrt{c^2 - \frac{4\pi G\rho}{k^2} + \frac{c^2}{k^2}\left(\frac{\mu_1}{R_0}\right)^2}. \tag{10}$$

With Jeans, we may assert that gravitational instability sets in when the wave velocity V becomes negative. This means that the cylinder is unstable for all perturbation wavelengths greater than the critical wavelength which causes the radical in (10) to vanish, or in other words when

$$\lambda > \lambda_0,\ \lambda_0 = \left[\frac{G\rho}{\pi c^2} - \left(\frac{\mu_1}{2\pi R_0}\right)^2\right]^{-1/2}. \tag{11}$$

Thus (11) is the criterion for gravitational instability of a cylinder, and λ_0 is approximately equal to the distance between the condensations into which the cylinder eventually decays. It is easily seen that in the limit as $R \to \infty$, this expression becomes the Jeans criterion. The case in which the expression under the radical sign in

(11) becomes negative corresponds to a stable state of the cylinder (there are no real wavelengths for the instability).

3. As an example of this theory, let us consider a filament of gas and dust whose radius is $R_0 = 0.1$ parsec at a temperature $T = 5°C$. The numerical values of the quantities entering Eq. (11) are $G = 6.68 \cdot 10^{-8}$, $R = 8.31 \cdot 10^{7}$, $\mu_1 = 2.4$. For simplicity, we shall choose the ratio of specific heats γ equal to unity.

If we use the criterion for gravitational instability given by (11), we reach the following conclusions for this case.

For densities of the order of 10^{-21} and lower, the filament is stable ($\lambda^2 < 0$). It becomes unstable when the density becomes of the order of $5 \cdot 10^{-20}$, and the wavelength of the instability is 0.4 parsec. The filament should therefore break up into a series of equally spaced condensations of equal masses. The masses of these condensations are of the order of 3 sun masses.

It would seem that these results can be used to explain the origin of dense star chains.

A later article will be devoted to the gravitational instability of an infinite cylinder in the presence of a magnetic field.

In conclusion, I take this opportunity to express my gratitude to Professor D. Ia. Martynov, who suggested the topic, for valuable remarks and discussion of the results obtained.

P. V. Shternberg State
Astronomical Institute

Received January 16, 1957

LITERATURE CITED

[1] G. A. Shain, Astron. J. (USSR) 32, 389 (1955).

[2] V. G. Fesenkov, Astron. J. (USSR) 28, 215 (1951).

[3] Edgeworth, Monthly Notices, Roy. Astron. Soc. 106, 488 (1947).

[4] V. G. Fesenkov and D. A. Rozhkovskii, Astron. J. (USSR) 29, 381 (1952).

[5] G. A. Shain, Astron. J. (USSR) 32, 392 (1955).

[6] D. Ia. Martynov, Uchenye Zapiski Kazansk. Univers. 114, vol. 8, 89 (1954).

[7] B. A. Vorontsov-Vel'iaminov, Astron. J. (USSR) 32, 404 (1955).

[8] D. Sh. Khavtasi, Biull. Abstum. obs. 18, 74 (1955).

[9] V. G. Fesenkov, Izv. Astrofiz. Inst. AN Kazakh. SSR 2, 13 (1956).

[10] Jeans, Astronomy and Cosmogony (Cambridge, 1928).

[11] A. B. Severnyi, Trudy GAISh 13, 2, 54 (1940).

THE PERIODS OF SHORT-PERIOD CEPHEIDS IN THE DIRECTION OF THE GALACTIC CENTER

E. D. Pavlovskaia

It is shown that the periods determined by S. I. Gaposchkin for eight RR Lyrae stars are not correct. They are related to the true periods by the well known relation $\frac{1}{p} = \frac{1}{p'} \pm 1$. The true periods of these stars are close to $0^d.5$, this being the most frequent value for the RR Lyrae stars in the neighborhood of the sun.

In the article by S. I. Gaposchkin entitled "285 Variable Stars in the Direction of the Galactic Center" [1] an investigation of variables in the region $18^h0^m-30^\circ.2$ is reported; in particular the periods of 108 short-period cepheids are given. The distribution of the periods of these stars differs considerably from the distribution of the periods of previsouly known RR Lyrae variables in the galaxy. The majority of short-period cepheids in the given region have periods around $0^d.3$ and, in addition, the shape of the brightness curves of these stars is unusual for their period.

This result, if correct, is of special interest for modern cosmogony. The commission for the study of variable stars kindly placed at our disposal Gaposchkin's specific data, so that we were able to test his conclusions. Gaposchkin's observations are contained in the bulletin "Variable Stars" 11, No. 4 (1957). The data used by Gaposchkin enabled us to examine the matter critically. During most nights only one or two plates were obtained and almost all of the observations pertain to approximately the same portion of the day. Table 1 gives the number of nights when 1, 2, 3,...7 plates were obtained and Table 2 gives the relative distribution for different times of observation. It can easily be seen that 77% of all times of observation fall in the interval $0^d.650-0^d.850$.

TABLE 1

Number of obs. per night	1	2	3	4	5	6	7
n	22	12	9	6	2	2	1
%	40.7	22.2	16.7	11.1	3.7	3.7	1.8

TABLE 2

Portion of day	0.551–0.650	0.651–0.750	0.751–0.850	0.851–0.950	0.951–0.050
n	1	54	43	23	5
%	0.8	42.9	34.1	18.2	4.0

This character of the data makes it possible that incorrect periods were obtained, which means that in some instances instead of the true periods we have the periods which are related to them by $1/p = 1/p' \pm 1$, where p is the true period, and p' is the related period. We undertook a check on the published periods on the basis of this hypothesis. Gaposchkin's periods for 8 short-period cepheids were found to be incorrect. The data are given in Table 3, where column 2 gives the period as determined by Gaposchkin and column 3 gives the period which was determined by the present author. For these stars instead of a period close to $0.^{d}3$ we obtain about $0^{d}.5$, which is the period most frequently found for short-period cepheids in the galaxy.

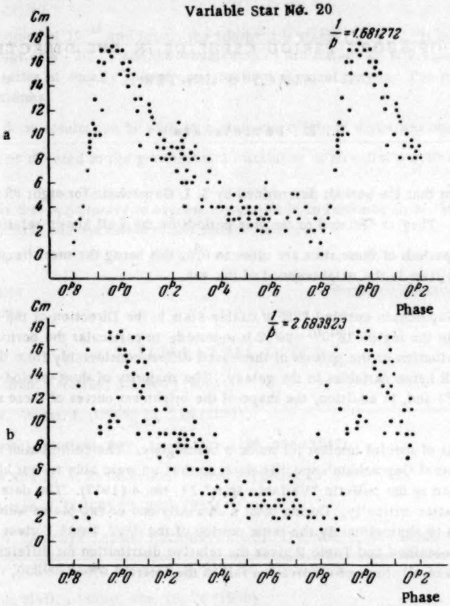

Fig. 1.

Thus, the distribution of the periods of short-period cepheids in the direction of the galactic center does not differ essentially from the distribution for previously known short-period cepheids in the galaxy.

TABLE 3

Number of stars	Gaposchkin's period	Pavlovskaia's period	Number of stars	Gaposchkin's period	Pavlovskaia's period
4	$0^{d}34139$	$0^{d}51883$	17	$0^{d}37102$	$0^{d}59084$
12	$0^{d}32341$	$0^{d}47863$	20	$0^{d}37259$	$0^{d}59479$
14	$0^{d}30744$	$0^{d}44444$	45	$0^{d}30540$	$0^{d}44023$
15	$0^{d}32111$	$0^{d}47362$	50	$0^{d}31208$	$0^{d}45423$

As an illustration we give the light curve of star No. 20. The brightness curves are given in steps since all of Gaposchkin's observations are expressed in steps and only the final average light curves are given in stellar magnitudes. Fig. 1a gives our light curve and Fig. 1b give the light curve which we calculated with the period published by Gaposchkin. The new period is in better agreement with Gaposchkin's observations.

Our reseults have induced us to continue the work of fixing the periods of short-period cepheids in the direction of the galactic center. This work is now being done at the Shternberg State Astronomical Institute.

P. K. Shternberg State Astronomical Institute

Received July 17, 1957

LITERATURE CITED

[1] S. I. Gaposchkin, Variable Stars (USSR) 10, No. 6, 337 (1956).

THREE-COLOR COLORIMETRY OF THE INTEGRAL BRIGHTNESS OF MARS, BASED ON 1956 OBSERVATIONS

E. A. Gurtovenko, Sh. G. Gordeladze

The integral brightness of Mars in three different colors (λ_{eff} = 430, 546 and 622 mμ) was studied from observations made from Sept. 1, 1956 - Jan. 2, 1957. Vega was used as a standard. The white stars of the Pleiades, which were photographed on the same negatives as the planet, were used for the calibration curves. The results of the measurements are given in a table. The great brightness of the planet during opposition, the sharp decrease in brightness with increasing phase and the considerable decrease of the color index of Mars during the period of observations should be specially noted.

During the period of the great opposition of Mars, observations of the planet were made at the State Astronomical Observatory of the Academy of Sciences of the USSR [at Pulkovo] up till the end of 1956. The observations were carried out using a three-chamber astrograph. Photographic magnitudes were determined with an "Apo-Planar" objective (D = 136 mm, F = 1700 mm) on "Ilford ordinary No. 30" plates at $\lambda_{eff} \simeq 430$ mμ. In the two remaining chambers, with identical "Apo-Tessar" objectives (D = 109 mm, F = 1200 mm), photovisual and photored magnitudes were determined. For photovisual magnitudes, "Agfa spectral gelb [yellow] rapid" plates were used in combination with a yellow filter, while "Agfa Isopan" plates with a red filter were used for the photored work. For work in these regions of the spectrum, wavelengths equal to 546 mμ and 622 mμ, respectively, were found effective.

TABLE

Plate No.	Date	Time decr. at mean moment of obs.	m_{pg}	m_{pv}	m_{pr}	CI_I	CI_{II}	Longitude of central meridian
96	1/IX—1956	1^h9	−1.66	−3.21	−3.93	+1.55	+2.27	26°5
100	2	2.6	1.70	3.30	4.25	1.60	2.55	16.5
104	3	1.7	1.65	3.16	3.96	1.51	2.31	7.9
108	4	1.9	1.60	3.34	4.17	1.74	2.57	359.1
112	5	1.6	1.59	3.35	4.28	1.76	2.69	350.4
116	7	2.6	1.78	3.48	4.24	1.70	2.46	341.2
118	26	23.1	1.51	3.17	3.95	1.66	2.44	156.7
125	1/X	0.7	1.45	2.98	3.85	1.53	2.40	120.3
128	2	23.8	1.45	3.00	3.71	1.55	2.26	102.6
133	7	23.2	1.40	2.62	3.56	1.22	2.16	57.8
136	8	23.0	1.37	2.75	3.33	1.38	1.96	48.5
140	12	23.3	1.24	2.54	3.14	1.30	1.90	11.9
141	24	21.6	1.14	2.16	2.87	1.02	1.73	262.3
143	31	21.9	0.64	1.37	2.19	0.73	1.55	196.8
147	4/XI	21.9	0.50	1.52	2.40	1.02	1.90	159.1
148	11	21.2	0.32	1.35	2.18	1.03	1.86	93.5
149	26/XII	19.3	0.41	1.27	1.94	0.86	1.53	19.6
150	28	19.3	0.49	1.30	2.20	0.81	1.71	0.1
151	29	19.2	0.27	1.08	1.98	0.81	1.71	350.3
152	2/I—1957	19.5	0.24	1.02	1.96	0.78	1.72	311.2

Images of Mars in all three chambers proved to be quite starlike in appearance. Determination of the integral brightness of the planet was carried out, for that reason, with the use of conventional methods of stellar photometery. Vega was chosen as a reference, since its spectral class (A0) allows for assuming photographic and photored magnitudes equal.

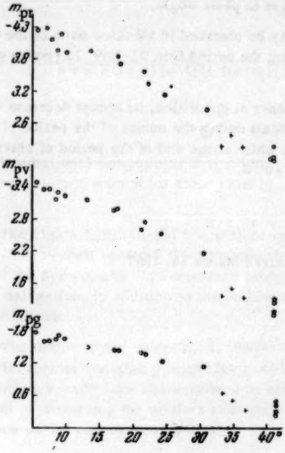

Fig. 1.

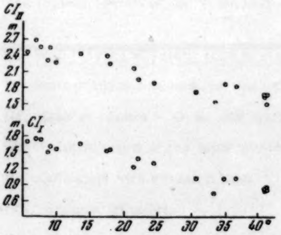

Fig. 2.

4-6 images of Mars and 2-3 images each of the reference star were obtained on each plate at identical objective apertures, but with different exposure times. The cycle of observations during each night lasted 1.5-2 hours. Prints of the Pleiades were taken on the same plates at the end of the run of observations, for calibration purposes. Since the photored magnitudes of the stars in the Plaeaides are unknown, only white stars in the Pleiades (B7 - A0) were selected in constructing calibration curves for the "Agfa Isopan" plates.

According to the Schwarzschild relation, the magnitude of the photographic effect (in the case of interest, the transmission T) may be represented in the form

$$T = f(p \log t - m/2.5),$$

where t is the time of exposure, p the Schwarzschild coefficient and m the stellar magnitude of the object. The coefficient p is determined for each lot of the emulsion by means of photometry of the stellar field of the Pleiades, taken with different exposures. As a result, we obtained

Emulsion	p
Ilford No. 30	0.831 ± 0.014
Gelb rapid	0.823 ± 0.018
Agfa Isopan	0.912 ± 0.019

Curves for $T = f(p \log t - m/2.5)$ were plotted for each plate with respect to the stars of the Pleiades, for which t = 1 was assumed. From these curves on transmission T for Mars and Vega, values of $p \log t - m/2.5$ were taken, on the basis of which the stellar magnitude of Mars was computed. The brightness of the planet so computed was corrected, in the case of each image, for differential absorption in the earth's atmosphere. Since Mars and Vega were taken at close zenith distances (the difference in air mass was of the order of 0.2-0.3), mean values of the transparency coefficient were taken from Lugin's tables in computing the correction terms. By averaging the data relating to all the images registered on a particular plate, mean values of the brightness of Mars for each set of observational data were calculated. The stellar magnitudes of Mars, referred to mean opposition ($r = 1.5237$, $\Delta = 0.5237$), are cited in the table on p. 926 .CI_I and CI_{II} are used to denote, respectively, the differences $m_{pg} - m_{pv}$ and $m_{pg} - m_{pr}$. The same results are represented graphically in Figs. 1 and 2, in their phase angle dependence.

The stellar magnitudes of Mars cited may differ slightly from the international magnitudes, as a result of the difference in the corresponding color systems. That difference, judging by the data of the effective wavelengths, should be a very insignificant one. This is also attested to by the results of a determination, in our system, of the magnitude of Capella. The mean values of 4 determinations of its photographic and photovisual magnitudes, equal to, respectively, $+0\overset{m}{.}95$ and $+0\overset{m}{.}32$, coincided, within limits of $0\overset{m}{.}1$, with the same magnitudes given in the international system ($+1\overset{m}{.}03$ and $0\overset{m}{.}21$). It may be assumed that the difference in both systems in each section of the spectrum does not exceed $\pm 0\overset{m}{.}2$.

The mean error in brightness measurements of the planet, for each date, amounts to $0\overset{m}{.}05 - 0\overset{m}{.}07$. In this connection, the spread of points in several portions of the graph (Fig. 1) should be taken as a reflection of the real measurements of the brightness of the planet, not explained by changes in phase angle.

An especially noticeable decrease in the brightness of Mars may be observed in all three parts of the spectrum on the negatives numbered 143, 147, 148, obtained successively during the period Oct. 31-Nov. 11 (points on the graph marked by crosses).

Particularly conspicuous is the appreciable brightness of the planet at opposition, its abrupt decrease with increase in phase, and a considerable lowering of the color index of Mars during the course of the period of observations. Near the opposition, the color index was equal to $+1\overset{m}{.}8$, while at the end of the period of observations (with phase angle equal to ~ 41°) its value had dropped to as low as $+0\overset{m}{.}8$.

V. I. Voroshilov took part in the observations.

Main Astronomical Observatory
Academy of Sciences of the
Ukrainian SSR, Kiev

Received March 14, 1957

CHRONICLE

SYMPOSIUM ON BRIGHT-LINE STARS HELD IN LIEGE (BELGIUM)

JULY 8-10, 1957

International symposiums devoted to the most pressing problems in astrophysics have been convened annually at Liège, Belgium, except for those years in which congresses of the International Astronomical Union are being held.

The Eighth International Symposium was devoted to a discussion of the problem of the physics of stars having bright lines in their spectra. Over 50 scientists from different countries were in attendance to participate in the work of the Symposium. In addition, a large number of Belgian astronomers took part in the Symposium. The Soviet delegation, in addition to the authors of the present article, included Prof. B. A. Vorontsov-Vel'iaminov and L. V. Mirzoian.

The theme of the Symposium, "Bright-line Stars," is a highly interesting and important topic. Although stars with spectra containing bright lines constitute only a small percentage of the total number of stars, those are nevertheless usually stars characterized by many peculiar features, features which are of great significance in the problem of unraveling the origin and evolution of stars. The study of this type of stars therefore attracts much attention on the part of astronomers.

The work of the Symposium, which was convened at Liège University, began with introductory remarks by Prof. P. Swings (Astrophysical Institute of Liège), wishing the participants at the Symposium successful and fruitful work. Prof. P. Swings and Prof. O. Struve presided in the chair at the Symposium.

The topical agenda of the Symposium breaks down into a series of sections dealing with particular problem fields:

Ia. Wolf-Rayet (WR) stars, stars of class Of and nuclei of planetary nebulae.

Ib. Stars of classes Be and Ae, and stars of P Cygni.

IIa. Stars of classes F, G, K, containing emission lines in their spectra.

IIb. Pulsating stars of the same classes.

III. Cold stars with emission lines.

IVa. Spectral binaries.

IVb. "Symbiotic" stars, i.e., stars, containing lines with sharply defined excitation and ionization levels in their spectra.

V. Discussion of interaction between different classes of variables with emission lines.

VI. Discussion of experimental and theoretical efforts underway at the present time devoted to the study of allowed and forbidden lines, of interest in the field of stars with bright lines.

Each section began with an introductory report, after which individual original communications dealing with the subject matter of the section were heard, and discussion of the topic of interest began.

An extensive introductory report devoted to emission lines in the spectra of Of and Wolf-Rayet stars was presented by Miss A. Underhill (Dominion Astrophysical Observatory, Canada) and read by P. Swings. Let us recall the fact that Of stars are O type stars exhibiting emission lines in their spectra. The most characteristic emission lines in the spectra of Of stars are the lines of He II 4686; N III 4634-4642 and C III 5696. It was disclosed, in Miss Underhill's report, that, on the basis of her investigations and those of R. Wilson (at the same observatory), Of stars and conventional O stars with absorption lines do not form any groups of stars sharply delineated from each other, but that, on the contrary, both of these groups interpenetrate into each other. Apparently, the Of with the most intense emission lines have the most extended atmospheres. The question of the difference in absolute brightnesses between Of type stars and conventional O type stars of the same classes has as yet not been solved.

In the same report, and also in a succeeding report, R. Wilson made known that the contours of the above mentioned C III, N III, He II lines in the spectra of Of stars are in their own way complex, consisting of a central relatively sharp emission "line" superimposed on a weak but very extended emission "band." The extension of these emission wings indicates Doppler speeds of the order of 1500 km/sec, which shows much in common with the properties of the spectra of Wolf-Rayet stars.

In the same report, A. Underhill proposed a new explanation for the splitting of the Wolf-Rayet group of stars into two branches, a carbon branch and a nitrogen branch. Analyzing the ionization state in the spectra of WR stars, she arrived at the conclusion that this division may be explained by introducing a hypothesis as to deviations of photospheric ionizing radiation from the radiation of an absolutely black body. WR stars, showing in the main C lines, should have a temperature of about 50,000°, and stars showing N lines for the most part should then have a temperature of about 62,000°. It is superfluous to draw up any hypotheses concerning differences in chemical composition. The explanation offered by Miss Underhill provoked a lively discussion.

The problem of the spectrophotometric temperatures of Wolf-Rayet stars was discussed by B. A. Vorontsov-Vel'iaminov (Moscow State University). New measurements taken of 10 Wolf-Rayet stars confirm the low spectrophotometric temperatures, although taking into account the new null point of the temperatures of stars of class A, and point out somewhat higher temperatures than had been found earlier. In a second report given by B. A. Vorontsov-Vel'iaminov, "Galaxies with Broad Emission Bands in the Spectra of Their Nuclei," attention was drawn to the absence of any difference between the spectra of those galaxies and radiogalaxies, and the mass of the gas contained in their nuclei was evaluated.

A number of communications were devoted to a discussion of the question of the excitation of atoms in the envelopes of the stars under consideration. V. Bappu (India) determined the excitation temperature in two Wolf-Rayet stars on the basis of SIII lines. Temperatures of 48,800° and 27,400°K were obtained.

E. R. Mustel' (of the Crimean Astrophysical Observatory) indicated, in his report, that, in the presence of sizable turbulence flows in stellar envelopes, emission may arise in the lines due to mutual collisions between individual gas clouds. As an example, the emission bands in the spectra of novae after maximum brightness were subjected to discussion.

In a report by J. Sahade (University of California, USA), results were presented of studies of a binary, one of the components of which was a WR star, its companion being an ordinary B-type star. Highly complex patterns of gas flow take place in the system.

Unfortunately, the report on the origin of the broad emission bands in the spectra of Wolf-Rayet stars was not discussed.

A large number of papers were delivered on the study of Be stars. The introductory report was delivered by V. Kourganoff (Lille Observatory, France), who briefly characterized the state of the question of Be and Ae types. He went into great detail in his report on an exposition of the theoretical work of V. V. Sobolev. The report was first read in French and then repeated in English.

The question of the radiation in L_α lines within stellar envelopes was taken up in a report by V. V. Sobolev (Astrophysical Observatory of the Leningrad State University), the report constituting a further extension and development of this theory of stellar envelopes in motion.

The report delivered by A. A. Boiarchuk (Crimean Astrophysical Observatory) dealt with a study of the envelopes of Be stars. In his report, he drew attention to the fact that, in most envelopes, the optical thickness at the center of the Balmer lines is greater than unity, beyond the Balmer series limit it is much less than unity, and beyond the Lyman series limit, it is not greater than unity. The masses of the stellar envelopes are about $10^{-10} M_\odot$. In addition, as was pointed out, a continuous outflow of matter from Be stars is evidently absent.

B. E. J. Pagel (Greenwich Observatory) reported on the results of hydrogen emission studies in stars of P Cygni and AG Pegasi. It was shown that the dimensions of the envelopes of those stars are equal, respectively, to $1.3 R_*$, and $3.3 R_*$, where R_* is the radius of the photosphere.

A new, accurate technique for reduction of spectrograms was treated in a report by H. Butler (Edinburgh Observatory). This technique consists of composing, on the basis of many records of several stars of the same spectral class (plotted in intensities), a composite record of the spectrum of stars of the particular type. This composite record then serves as a reference standard for other spectra of Be-type stars. This method proved successful in detecting weak Fe II emission lines in the spectra of Be stars and in studying changes taking place in the spectra.

Findings of studies of the Balmer emission decrement in spectra of Be stars were reported in a paper by H. Rojat and R. Herman (Meudon Observatory, Paris).

A number of papers delivered discussed the behavior of the V/R ratio in the spectra of Be stars. As is well known, one of the most characteristic features of the spectra of Be stars is the central depression (absorption) in the emission lines. This depression, brought about by absorbing atoms in the outermost parts of the envelope of Be stars, divides the emission into tow parts. That part which is situated on the violet end of the central depression of the spectrum is designated by the letter V; the opposite part is designated by the letter R. The ratio of the intensities of both those components, V/R, functions as a very excellent characteristic measure of the motion of the outer absorbing layers of the envelope relative to the inner emitting parts.

In his report, M. Johnson (Birmingham) made an attempt to explain the observed changes in the value of V/R in the spectra of some stars by the action of various mechanisms. Struve's suggestion of the rotation of the apsidal lines in a projected equatorial ring was studied, and such mechanisms as nonradial pulsations, etc., were also alluded to.

In her report, M. Hack (Merate Observatory, Italy) dealt with changes in the value of V/R in ζ Tauri during the period 1902-1956, and discussion on the materials she presented took place.

D. B. McLaughlin (University of Michigan) drew the conclusion, based on many years' study of fluctuations in the value of V/R for a number of stars, that neither the hypothesis of binary rotation nor the hypothesis of a pulsating envelope can explain the changes observed in the V/R ratio and the radial velocity of emission and absorption line components.

M. Zuckermann (Astrophysical Institute, Paris) made some preliminary remarks on observations of rapid brightness fluctuations of SS Cygni in different beams.

Three reports were given delaing with section IIa. K. Böhm (Kiel University) made an attempt to explain the presence of ultraviolet radiations in the spectra of stars of T Tauri by the overlapping of emission lines in higher terms of Balmer lines (excluding the Balmer continuum). An assumption was made as to the significant role of self-absorption in all of the lines indicated. However, as was remarked upon in the discussion, this attempt at explaining ultraviolet emission comes up against the difficulty that polarization of ultraviolet radiation of stars of T Tauri has been detected in recent studies.

L. V. Mirzoian (Burakan Observatory), in his report, discussed some of the facts characterizing stars with continuous emission, and also discussed some possible explanations for this emission. He cited a number of arguments in support of the concept that this radiation has a thermal character.

L. Rosino (Padua, Italy) reported on eight flare stars which he discovered during 1955-1956 in the cluster NGC 2264. Short-period variables have a mean visual magnitude at a minimum of around $17\overset{\mathrm{m}}{.}6$ and a mean amplitude of about $1\overset{\mathrm{m}}{.}7$. The period of brightness change from minimum to maximum brightness and back again to minimum is 38 minutes. The stars are accordingly of shorter period than the flare stars in Orion, and are easily recognized as of longer period than the flare stars in Taurus. Intense work will be continued in that area of study.

Section IIb, on pulsating stars, was initiated with an introductory report by E. Schatzman (Astrophysical Institute, Paris). C. Whitney (Smithsonian Astrophysical Observatory, USA) made a contribution on the emission of Ca II lines in classical cepheids. He considered three possible sources of Ca II emission: a) the existence of some limited region of high kinetic temperature generated by a pulsating wave; b) excess recombinations in an ascending gas in upper layers of the hydrogen ionization region; c) disturbances in the chromosphere. Whitney came to the conclusion that Ca II emission arises in the chromosphere of cepheids.

A. Delsemme (Astrophysics Institute of University of Liège) gave a report on temperature change in cepheids, based on emission in the spectrum of RU Camelopardi.

Section III was started with an introductory report delivered by K. Wurmom (Hamburg Observatory, West Germany). Individual contributions were made by W. Iwanowska (Nikolaj Kopernik Astronomical Observatory, Torun, Poland), S. Gaposchkin (Mount Stromlo, Australia) and C. Bruce (Electrical Research Laboratory, Great Britain). The first two of these reports dealt with studies of various properties of the spectra of long-period variables, and the report by C. Bruce summed up the results of a theory put forward earlier to the effect that electrical discharges play a great role in the physical phenomena characterizing the pulsations of the stars discussed.

A sizable group of reports following the introductory report by Otto Struve were made on spectral binaries whose spectra contain emission. A series of reports was devoted to studies of the eclipsing variable W Serpentis. The spectrum of this star is of interest both from the point of view of absorption and that of emission. According to remarks by J. Sahade and O. Struve, the most intense absorption lines of the star appear in the envelope surrounding the entire stellar system; the weaker and broader absorption lines have their origin in the atmosphere of the primary. This star ejects gases which form an envelope around the star and at the same time give rise to emission bands, best visible (during an entire period) in the hydrogen lines. The secondary star is also surrounded by an envelope, whose existence was detected on the basis of a broad emission appearing only during the eclipse. The outermost layers of the expanding envelope bounding the entire system give rise to forbidden Fe II lines, observable over the entire cycle of light variations. A. Beer (Observatory of Cambridge University, Great Britain) and Margherita Hack presented, in their reports, findings on spectrophotometeric studies of this star.

The spectrum of the star Plackett HD 47129 was reported on by O. Struve, J. Sahade and K. Abhyankar. The spectrum of this massive spectroscopic binary with $P = 14\overset{d}{.}4$ experiences noticeable changes. Especially interesting are the periodic variations in the structure of the H_α line, observed in the emission spectrum. These variations are correlated with the appearance of strong lines of the "envelope" type in He I 3888, 4472, 5876. The radial velocity determined on the basis of those lines comes to about 700 km/sec; this suggests the presence of a rapidly expanding flow of gas. The star must be extremely unstable and may represent an intermediate object between a normal "quiet" binary of class 0 and a binary containing a Wolf-Rayet star.

M. Plavec (Astronomical Institute, Czechoslovakia) gave a report on Lagrangian binary points in close binary systems.

K. O. Wright and R. Kisvaga (Dominion Observatory, Canada) submitted reports on interesting fluctuations of the Hα emission contour in the spectrum of ε Aurigae.

The introductory report for section IVb was given by P. Merrill (Mt. Wilson and Mt. Palomar Observatories, USA). He enumerated five groups of stars with emission lines characterized by high excitation states, which are superimposed on a spectrum characterized by low temperature. It was noted in this report, that up to the present time, there is still some question as to whether or not "symbiotic" stars are binaries, or whether we are dealing here with a single star found "inside" another. He also pointed out the fact that, according to a body of data, outflow of gas should take place from the central region of a "symbiotic" star.

J. Greenstein and W. Tifft (Mt. Wilson and Mt. Palomar, USA) discussed an interesting object, a symbiotic star situated at upper galactic latitude of + 15° and having a large velocity in space. This is the first case of that kind. The fundamental spectrum of this star is of the spectral class gM3, and the emission lines are exceptionally intense and numerous.

C. Whiting (Leuschner Observatory, USA) reported on the peculiar star 17 Leporis. The normal spectrum of 17 Leporis is composite and consists of broad diffuse lines of hydrogen and Mg II 4481, which arise in the inner stationary reversing layer, and from sharp lines of metals, arising in the expanding outer envelope. During an intense flare, the lines of the envelope double, with violet components giving expansion velocities of the order of 150 km/sec. The emission spectrum consists of the H_α line, whose structure is the same as in P Cygni. H_β sometimes has a "red" emission component. Weak emission lines on the "red" side of the envelope lines are observed, and frequently so when the envelope is active.

M. Bloch and Cheng Moa-Ling (Observatory of Lyon) reported on recent spectroscopic observations of some symbiotic stars.

C. Payne-Gaposchkin (Harvard Observatory) presented a review, for section V, dealing with the question of the interaction occurring between different classes of variables with emission lines. Finally, for the last section, R. Gastrang (University of London) reported on the state of work reached in determining various constants for atomic transitions of interest in the problem of bright-line stars. He reported that computers have been liberally employed to this end and that computers will be used in the first instance to determine atomic constants for forbidden transitions.

The Symposium came to an end with concluding remarks by Prof. Otto Struve. Participants of the Symposium expressed their acknowledgment to Prof. P. Swings and to the University of Liège for their excellent work in organizing the Symposium and for their hospitality. An excursion to the Ardennes was undertaken after the conclusion of deliberations.

During the Symposium, participants of the Soviet delegation, despite the crowded program of the sessions, held many discussions with foreign astronomers on a whole number of questions of scientific intests. The cordial atmosphere prevailing at the Symposium aided in the success of these informal discussions.

It has been proposed that the following Symposium in Liège, in 1959, take up problems of novae and supernovae.

Received Novermber 14, 1957

E. R. Mustel', A. A. Boiarchuk

of the more complex geometries between different degrees of variables with emission lines. Finally, for the last section, K. Hastings (University of London) reported on the state of work engaged in [illegible] groups [illegible] simulations of interest in the problem of bright-line stars. He reported that computers have been liberally employed on this [illegible] that [illegible] to determine [illegible] for hot [illegible] [illegible]

The symposium closes as it opened with an excellent talk by Prof. [illegible]. Participants of the Symposium expressed their appreciation to Prof. [illegible] and to the [illegible] for their excellent work in organizing the Symposium and for their hospitality. An [illegible] to the [illegible] concluded the sessions.

During the free periods, particularly at the [illegible] of the [illegible], besides the scheduled program of the sessions, held many discussions with foreign astronomers on a large number of questions of scientific nature. The cordial, friendly atmosphere at the symposium aided in the success of these informal discussions.

It has been proposed that the following symposium [illegible], in 1962, take up problems of novae and supernovae.

[illegible] E. R. Mustel [illegible]

Soviet Astronomy – AJ: Author Index for Vol. 1, 1957

(Russian Original Vol. 34, 1957, Astronomical Journal of the Academy of Sciences of the USSR)

Afanas'eva, P. M. A Catalog of Right Ascensions of 203 Stars Based on Observations with a New Photoelectric Transit Instrument - 598.
Agekian, T. A. The Theory of the Fluctuations of the Observed Number of Galaxies - 366.
Alaniia, I. F. Color Excesses in 102 RR Lyrae Stars - 205.
Alduseva, V. Ia., see Martynov, D. Ia. - 425.

Barkhatova, K. A. Open Stellar Cluster NGC 6811 - 201.
Barkhatova, K. A. The Open Stellar Clusters NGC 6823 and NGC 6830 - 822.
Boiarchuk, A. A. Some Characteristics of Shells of Be Stars - 192.
Brumberg, V. A. Permanent Configurations in the Problem of Four Bodies and Their Stability - 57.
Bugoslavskaia, E. Ia. Coronal Streamers - 228.
Butkevich, A. V. Calculation of Latitude by the Method of M. V. Pevtsov - 610.

Clemence, G. M. Tables of the Principal Planets - 432.

Dadaev, A. N. Awarding of the 1957 Lenin Prize to B. K. Ioannisiani for the Designing of Astronomical Instruments - 491.
D'iakonov, V. F. The Influence of Diurnal Aberration on the Accuracy of Determination of Latitude from Observations of Polaris - 469.
Dibai, E. A. The Gravitational Instability of a Gas Filament - 920.
Dirikis, M. A. A Special Case of the General Three-Body Problem - 909.
Dukhnovskii, P. G. On Some Peculiarities in the Motions of Comets - 80.
Dziubenko, N. I. The Distribution of Matter in the Polar Rays of the Solar Corona - 373.

Fedin, L. A. On the Utilization of a Thin Lummer-Gehrke Plate - 138.
Fedorova, N. I. The Infrared Spectrum of the Northern Night Sky in the Region 9500-11,500 A - 241.
Fesenkov, V. G. The Early Thermal History of the Earth - 112.
Fialko, E. I. Distribution of Meteoric Radio Echoes According to Their Duration - 235.
Fialko, E. I. On the Problem of Determining the Mass Distribution of Meteors - 411.
Filin, A. Ia. On the Kinematic Peculiarities of B Stars - 517.
Filin, A. Ia. The Kinematic Peculiarities of B Stars and the Rotation of the Local System - 812.
Fomenko, B. D. Variation of the Coefficient of Transparency of the Atmosphere During the Total Solar Eclipse of June 30, 1954 - 841.

Gal'perin, Iu. I. Observations of Hydrogen Emission in Aurorae - 133.
Gel'fgat, B. E., see Radzievskii, V. V. - 568.
Gnevyshev, M. N., R. S. Gnevysheva and V. G. Kurt. On the Observation of the Infrared Coronal Lines 10,747 and 10,798 A - 654.
Gnevysheva, R. S., see Gnevyshev, M. N. - 654.
Gorbatskii, V. G. On the Interpretation of the Emission Spectrum of Long-Period Variable Stars. I. - 834.
Gordeladze, Sh. G., see Gurtovenko, E. A. - 926.
Gordon, I. M. The Nonthermal Component of the Radiation of Unstable Stars and the Main Features of Their Spectra - 719.
Grushinskii, N. P. On the Errors of Interpolation and Representation in Detailed Gravimetric Surveys, the Accuracy of Charts, and the Best Distribution of Stations - 260.
Grushinskii, N. P. The Fundamental Gravimetric Station at the P. K. Shternberg State Astronomical Institute (GAISh) - 455.
Gulak, Iu. K. Photometry of the Images of Some Planetary Nebulae - 508.
Gulak, Iu. K. The Spatial Structure of Some Planetary Nebulae - 802.
Gurtovenko, E. A. and Sh. G. Gordeladze. Three-Color Colorimetry of the Integral Brightness of Mars, Based on 1956 Observations - 926.
Gurzadian, G. A. Planetary Ring Nebulae - 796.

Hsi Tse-Tsung. An New Catalog of Novae Recorded in the Chinese and Japanese Chronicles - 161.

Iavnel', A. A. The Characteristics of Chemical Composition of Meteoritic Matter and the Origin of Meteorites - 435.
Iavnel', A. A. Meteoritic Matter at the Place of Fall of the Tungus Meteorite - 769.
Iavnel', A. A. Peculiarities of the Mineral Composition and Structure of Meteoritic Matter and the Origin of Meteorites - 891.
Idlis, G. M. On the Paper by A. M. Mikisha and F. A. Tsitsin, Some Problems of the Theory of Galactic Potential - 290.
Idlis, G. M. On the Evolutionary Interpretation of the Main Sequence of Stars - 733.

Kaplan, S. A. Shock Waves in Interstellar Space. II. Ionization Discontinuities - 183.

Kaplan, S. A. Shock Waves in Interstellar Space. III. Hydromagnetic Discontinuities - 317.
Kharitonov, A. V., see Moroz, V. I. - 874.
Kipper, A. A Symposium on "Electromagnetic Phenomena in Cosmic Physics" in Stockholm on August 27-31, 1956 - 293.
Kolchinskii, I. G. Some Results of Observations of the Vibration of Images of Stars at the Main Astronomical Observatory of the Academy of Sciences of the Ukrainian SSR at Goloseevo - 624.
Kolpakov, P. E. On the Acceleration of Charged Particles in the Electromagnetic Field of Sunspots - 218.
Korchak, A. A. Electromagnetic Radiation by Cosmic-Ray Particles in the Galaxy - 360.
Koval', I. K. Results of Photographic Observations of Mars at the Kharkov Astronomical Observatory During 1954 - 404.
Kozhevnikov, N. I. Solar Limb Darkening at Wavelengths of 1-4μ - 856.
Krat, V. A. On the Observations of the Sun During the International Geophysical Year - 766.
Kruchinenko, V. G., Iu. P. Platonov and V. B. Sukhov. An Electronic-Mechanical Computer for Determining the Mean Times of Stellar Transits During the Observations - 594.
Kulikov, K. A. Review of:The Motions of the Heavenly Bodies, by Iu. A. Riabov - 488.
Kurochkin, N. E. The Distribution of Absorbing Matter and the Spiral Structure of the Galaxy - 31.
Kurt, V. G., see Shcheglov, P. V. - 474.
Kurt, V. G., see Gnevyshev, M. N. - 654.

Lidov, M. L. Automodel Motion of a Gas with Spherical Symmetry in the Field of a Gravitating Center - 588.

Makarova, E. A. A Photometric Investigation of the Energy Distribution in the Continuous Solar Spectrum in Absolute Units - 531.
Marinbakh, A. B. The Influence of the Position Error of a Ship on the Astronomically Determinable Compass Correction - 459.
Martynov, D. Ia. and V. Ia. Alduseva. Changes in the Construction of the MF-2 Microphotometer Adapting It to Measurements of High Density - 425.
Masevich, A. G. The Evolution of Stars in the X and h Persei Double Cluster - 177.
Masevich, A. G. A Meeting of the Commission for Cosmogony Devoted to the Future Development of Work on Cosmology - 306.
Masevich, A. G. A Reply to G. M. Nikol'skii's Note - 481.
Masevich, A. G., see Ruben, G. - 705.
Meshcheriakova-Babich, O. I., see Vsekhsviatskii, S. I. - 556.
Mikhailov, A. A. On the Observation of Artificial Satellites - 309.
Mikhailov, A. A. Review of:Studies in the History of Astronomy by P. G. Kulikovskii - 483.
Mikisha, A. M. and F. A. Tsitsin. On the Distribution of Mass in the Galaxy - 45.
Mikisha, A. M. and F. A. Tsitsin. The Virial Theorem as Applied to the Dynamics of Stellar Systems - 661.
Mironov, A. V. and V. S. Prokudina. On the Identification of the Emission of the Night Sky at About 5300A - 430.
Mirzoian, L. V. Opening of the Biurakan Astrophysical Observatory of the Academy of Sciences of the Armenian SSR and the Conference on Nonstationary Stars - 297.
Moroz, V. I. and A. V. Kharitonov. Photoelectric Photometry of Sections of the Surface of Mars - 874.
Muliarchik, T. M. and K. I. Petrova. Increase of the Sensitivity of Some Photographic Emulsions by Means of Preliminary Short Exposure - 108.
Mustel', E. R. The Physical Nature of the Differences Between Geomagnetic Disturbances of Sudden and Nonsudden Commencement - 124.

Nikol'skii, G. M. A Note on the Paper "Luminosity Function for Stars of the Main Sequence and its Interpretation" by A. G. Masevich - 479.

Obrezkova, E. I. Variations of the Mean Latitude of Poltava, Mizusawa, Richmond and Washington - 445.
Ogorodnikov, K. F. Statistical Mechanics of the Simplest Types of Galaxies - 748.
Ogorodnikov, K. F. On the Principles of Statistical Mechanics of Stellar Systems - 787.
Orlov, S. V. Radial Systems in the Head of the Comet 1908 III (Morehouse) - 231.

Panovkin, B. N. A Model of the Inner Corona Based on Radio Data - 497.
Pavlovskaia. E. D. The Periods of Short-Period Cepheids in the Direction of the Galactic Center - 923.
Peregudov, F. I. Effective Scattering Cross Section of a Weakened Meteor Trail - 606.
Perel', Iu. G. Plenum of the Commission on the History of Astronomy - 493.

Petit, M. On the International Cooperation for the Study of Flare Variable Stars - 783.
Petrova, K. L., see Muliarchik, T. M. - 108.
Pikel'ner, S. B. and I. S. Shklovskii. An Investigation of the Properties and Energy Dissipation of the Gaseous Galactic Corona - 149.
Pikel'ner, S. B. Energy Dissipation, Heating and Ionization in Interstellar Gas Due to Shock Waves - 310.
Pikel'ner, S. B. Third Symposium on Cosmical Gas Dynamics - 773.
Pil'nik, G. P. The Collimation of a Transit Instrument - 103.
Platonov, Iu. P., see Kruchinenko, V. G. - 594.
Potter, Kh. I. A New Method for Determining the Photographic Positions of Celestial Objects - 245.
Prokudina, V. S., see Mironov, A. V. - 430.
Pskovskii, Iu. P. The Determination of the Absolute Magnitudes of Cepheids and Supergiants and the Zero Point of the Period-Luminosity Relation - 19.

Radzievskii, V. V. and B. E. Gel'fgat. The Restricted Problem of Two Bodies of Variable Mass - 568.
Riabov, Iu. A. Some Methods of Plotting an Intermediate Orbit for Asteroids of the Trojan Group. I. - 268.
Riabov, Iu. A. Some Methods of Plotting an Intermediate Orbit for Asteroids of the Trojan Group. II. - 574.
Ridel', E. A., see V'iushkov, P. V. - 476.
Ruben, G. and A. Masevich. An Investigation of Evolutionary Paths for a Homogeneous Stellar Model with a Convective Core - 705.

Sadler, D. H. Astronomical Ephemerides - 255.
Safronov, V. S. Conference on the Physics and the Origin of Planetary Nebulae - 304.
Safronov, V. S. Reporting and Coordinating Plenum of the Astronomical Council of the USSR Academy of Sciences - 495.
Severnyi, A. B. A Spectroscopic Investigation of the Deuterium Dα Line in Active Regions on the Sun - 324.
Severnyi, A. B. Some Results of Investigations of Nonstationary Processes on the Sun - 668.
Shain, G. A. The Inclination to the Galactic Equator of the General Magnetic Field of the Galaxy in the Solar Vicinity - 1.
Sharonov, V. V. On the Role of True Absorption in the Martian Atmosphere - 547.
Sharov, A. S. A Numerical Method for Determining the Stellar Density in a Spheroidal Cluster - 142.
Shcheglov, P. V. Photographing Stars by Means of an Image Converter Tube - 472.
Shcheglov, P. V. and V. G. Kurt. High Voltage Sources for Supplying Image Converter Tubes - 474.
Shcheglov, V. P. Chardzhou International Latitude Station - 648.
Shcheglov, P. V. The Spectrum of the Crab Nebula - 658.
Shklovskii, I. S. A Possible New Type of Fluorescence of the Earth's Atmosphere - 130.
Shklovskii, I. S., see Pikel'ner, S. B. - 149.
Shklovskii, I. S. Once More on the Distances to Planetary Nebulae and the Evolution of their Nuclei - 397.
Shklovskii, I. S. On the Nature of the Optical Emission from the Crab Nebula - 690.
Shteins, K. A. The Distribution of Comets of Jupiter's Family - 92.
Sigal, M. I., see Vitkevich, V. V. - 698.
Sitnik, G. F. Application of Silver Sulfide Photoelectric Cells with a Barrier Layer to Absolute Spectrophotometry and Pyrometry. I. Measuring Apparatus Using a Silver Sulfide Photocell - 416.
Sitnik, G. F. Spectrophotometry and Pyrometry. II. Method of Using SSBL for Absolute Spectrophotometric and Pyrometric Measurements - 860.
Sobolev, V. V. The Diffusion of Radiation in a Medium of Finite Optical Thickness - 332.
Sobolev, V. V. The Diffusion of L_α Radiation in Nebulae and Stellar Envelopes - 678.
Sukhov, V. B., see Kruchinenko, V. G. - 594.
Sytinskaia, N. N. A New Value of the Light Constant of the Moon - 870.

Tsitsin, F. A., see Mikisha, A. M. - 45.
Tsitsin, F. A., see Mikisha, A. M. - 661.

Vitkevich, V. V. Investigation of the Solar Supercorona by the Reception of the Radio Emission from Jupiter - 214.
Vitkevich, V. V. Radio Stars and the Methods of Their Investigation - 346.
Vitkevich, V. V. and M. I. Sigal. On the Radio Emission of Coronal Condensations - 698.
V'iushkov, P. V. and E. A. Ridel'. A Bolometric Pyrheliometer for Absolute Measurements of Direct Solar Radiation - 476.
Vlasov, B. I. The Determination of Azimuths at Laplace Points - 462.
Vodop'ianova, T. V. A Supplement to the General Catalogue of Absolute Brightnesses of Comets. Comets of 1947-1954 - 900.
Vorontsov-Vel'iaminov, B. A. The Morphology of Galaxies. III. Diffuse Matter in Spherical Stellar Systems - 9.

Vsekhsviatskii, S. I. and O. I. Meshcheriakova-Babich. The Distribution of Orbit Elements in the Ejection Theory - 556.

Xanthakis, J. On One Classification of the Cycles of Sunspots and Faculae - 385.

Soviet Astronomy – AJ: Analytic Subject Index for Vol. 1, 1957

(Russian Original Vol. 34, 1957, Astronomical Journal of the Academy of Sciences of the USSR)

Aberration of Light
Absorption of Light
Artificial Satellites
Associations of Stars
Asteroids (Minor Planets)
Astrographic Measurements
Astronomy, History and Progress
Atomic and Molecular Spectra
Aurorae
Azimuth
Biographical Material
Book Reviews
Books on Sale
Catalogs
Celestial Mechanics
Charged Particles, Acceleration and Emission
Clusters, Globular
Clusters, Open
Colors of Stars
Color-Magnitude Diagram
Comets
Computing and Automatic Computers
Conferences and Meetings
Constants, Astronomical and Physical
Coordinates, Astronomical
Cosmic Rays
Cosmogony and Cosmology
Crab Nebula
Deuterium
Earth, Atmosphere
Earth, Figure
Earth, Interior
Earth, Magnetic Field
Earth, Movement of Poles
Earth, Origin and Development
Eclipse, Lunar
Eclipse, Solar
Eclipsing Binaries
Elements, Abundances
Elements, Origin
Emission-Line Stars
Envelopes, Stellar
Ephemerides
Errata
Extinction, Atmospheric
Extinction, Interstellar
Figure of Celestial Bodies
Flare Stars
Galaxies
Galaxy, The (Milky Way)
Gas Dynamics
Geodesy
Giant and Supergiant Stars
Gravity and Gravimetry
Helium
Hertzsprung-Russell (H-R) Diagram
Hydrodynamics
Hydrogen, Ionized; H II Regions
Hydrogen, Lyman Series
Hydrogen, Neutral, in Galaxy
Image Converter
Infrared, Observations in
Instruments and Accessories
International Astronomical Union (IAU)
International Geophysical Year (IGY)
Interplanetary Medium
Interstellar and Intergalactic Medium
Ionosphere
Latitude
Letters to the Editor
Local System
Longitude
Luminosity Classification
Luminosity Function
Magellanic Clouds
Magnetic Field, Interstellar
Magnetic Fields, Stars
Magnetic Storms (see Solar-Terrestrial Relationships)
Magnetohydrodynamics
Magnitudes, Absolute
Mass-Luminosity Relation
Meridian Circle
Meteorites
Meteors
Moon
Navigation and Nautical Astronomy
Nebulae, Diffuse
Nebulae, Emission
Nebulae, Planetary
Night Sky
Nonstable Stars
Novae and Supernovae
Nuclear Transformations
Nutation
Observatories
Occultations
Optics
Orbits, Theory and Computation

Parallax
Period-Luminosity Relation
Photographic Process and Materials
Photometry, Multicolor
Photometry, Photoelectric
Photometry, Photographic
Planets and Satellites, Observations
Planets and Satellites, Structure
Polarization and Polarimetry
Populations, Stellar
Positions of Stars
Precession
Proper Motions
Radial Velocities
Radiation and Energy Transport
Radio Astronomy, Discrete Sources
Radio Astronomy, Meteors
Radio Astronomy, Neutral Hydrogen Emission, 21 cm
Radio Astronomy, Planets and the Moon
Radio Astronomy, Sun
Radio Telescopes
Redshifts
Refraction, Atmospheric
Relativity
Rockets, Observations from
Rotation, Stellar
Seeing and Scintillation
Sequences, Stellar
Shock Waves
Solar System, Origin and Development
Solar-Terrestrial Relationships
Spectral Classification
Spectrophotometry
Spectroscopic Binaries
Spectroscopy, Stellar
Spectrum, Line Identification
Stars, Distribution in Space
Stars, Motion in Space
Stars, Formation
Stars, Structure and Evolution
Stellar Systems, Dynamics
Subdwarfs
Sun, Chromosphere
Sun, Corona
Sun, Corpuscular Emission
Sun, Flares
Sun, Magnetic Fields
Sun, Photosphere
Sun, Prominences
Sun, Radio Emission
Sun, Spectrum
Sun, Ultraviolet Emission
Sun, X-Rays
Sunspots
Symposia
Synchrotron Radiation
Telescopes
Time
Time Service and Time Signals
Transit Instrument
Turbulence
Ultraviolet, Observations in
Variable Stars (see also Eclipsing Binaries)
Visual Binaries
White Dwarfs
Zodiacal Light

Absorption of Light
  Color Excesses in 102 RR Lyrae Stars, I. F. Alaniia - 205.
  The Distribution of Absorbing Matter and the Spiral Structure of the Galaxy, N. E. Kurochkin - 31.
  The Morphology of Galaxies. III. Diffuse Matter in Spherical Stellar Systems, B. A. Vorontsov-Vel'iaminov - 9.
Artificial Satellites
  On the Observation of Artificial Satellites, A. A. Mikhailov - 309.
Asteroids (Minor Planets)
  Some Methods of Plotting an Intermediate Orbit for Asteroids of the Trojan Group. I, Iu. A. Riabov - 268.
  Some Methods of Plotting an Intermediate Orbit for Asteroids of the Trojan Group. II, Iu. A. Riabov - 574.
Astrographic Measurements
  A New Method for Determining the Photographic Positions of Celestial Objects, Kh. I. Potter - 245.
Astronomy, History and Progress
  Fortieth Anniversary of Soviet Astronomy, - 665.
  P. G. Kulikovskii (ed.), Studies in the History of Astronomy. Reviewed by A. A. Mikhailov - 483.
  Plenum of the Commission on the History of Astronomy, Iu. G. Perel', - 493.
Aurorae
  Observations of Hydrogen Emission in Aurorae, Iu. I. Gal'perin - 133.
Azimuth
  The Determination of Azimuths at Laplace Points, B. I. Vlasov - 462.
Biographical Material
  Awarding of the 1957 Lenin Prize to B. K. Ioannisiani for the Designing of Astronomical Instruments, A. N. Dadaev - 491.
Book Reviews
  Iu. A. Riabov, The Motions of the Heavenly Bodies, Reviewed by K. A. Kulikov - 488.
  P. G. Kulikovskii (ed) Studies in the History of Astronomy. Reviewed by A. A. Mikhailov - 483.
Book on Sale
  Academy of Sciences USSR Press. Books on Sale - 308.
Catalogs
  A Catalog of Right Ascensions of 203 Stars Based on Observations with a New Photoelectric Transit Instrument, P. M. Afanas'eva - 598.
  A New Catalog of Novae Recorded in the Chinese and Japanese Chronicles, Hsi Tse-Tsung - 161.
  A Supplement to the General Catalogue of Absolute Brightnesses of Comets. Comets of 1947-1954, T. V. Vodop'ianova - 900.
Celestial Mechanics
  A Special Case of the General Three-Body Problem, M. A. Dirikis - 909.
  On Some Peculiarities in the Motions of Comets, P. G Dukhnovskii - 80.
  Permanent Configurations in the Problem of Four Bodies and their Stability, V. A. Brumberg - 57.
  Some Methods of Plotting an Intermediate Orbit for Asteroids of the Trojan Group. I, Iu. A. Riabov - 268.
  The Distribution of Comets of Jupiter's Family, K. A. Shteins - 92.
  The Distribution of Orbit Elements in the Ejection Theory, S. I. Vsekhsviatskii and O. I. Meshcheriakova-Babich - 556.
  The Restricted Problem of Two Bodies of Variable Mass, V. V. Radzievskii and B. E. Gel'fgat - 568.
Charged Particles, Acceleration and Emission
  Electromagnetic Radiation by Cosmic-Ray Particles in the Galaxy, A. A. Korchak - 360.
  On the Acceleration of Charged Particles in the Electromagnetic Field of Sunspots, P. E. Kolpakov - 218.
Clusters, Globular
  A Numerical Method for Determining the Stellar Density in a Spheroidal Cluster, A. S. Sharov - 142.
Clusters, Open
  Open Stellar Cluster NGC 6811, K. A. Barkhatova - 201.
  The Evolution of Stars in the X and h Persei Double Cluster, A. G. Masevich - 177.
  The Open Stellar Clusters NGC 6823 and NGC 6830, K. A. Barkhatova - 822.
Colors of Stars
  Color Excesses in 102 RR Lyrae Stars, I. F. Alaniia - 205.
Color-Magnitude Diagram
  Open Stellar Cluster NGC 6811, K. A. Barkhatova - 201.
  The Open Stellar Clusters NGC 6823 and NGC 6830, K. A. Barkhatova - 822.
Comets
  A New Catalog of Novae Recorded in the Chinese and Japanese Chronicles, Hsi Tse-Tsung - 161.

A Supplement to the General Catalogue of Absolute Brightnesses of Comets. Comets of 1947-1954, T. V. Vodop'ianova - 900.
On Some Peculiarities in the Motions of Comets, P. G. Dukhnovskii - 80.
Radial Systems in the Head of the Comet 1908 III (Morehouse), S. V. Orlov - 231.
The Distribution of Comets of Jupiter's Family, K. A. Shteins - 92.
The Distribution of Orbit Elements in the Ejection Theory, S. I. Vsekhsviatskii and O. I. Meshcheriakova-Babich - 556.

Computing and Automatic Computers
An Electronic-Mechanical Computer for Determining the Mean Times of Stellar Transits During the Observations, V. G. Kruchinenko, Iu. P. Platonov and V. B. Sukhov - 594.

Conferences and Meetings
A Meeting of the Commission for Cosmogony Devoted to the Future Development of Work on Cosmology, A. Masevich - 306.
Conference on the Physics and the Origin of Planetary Nebulae, V. S. Safronov - 304.
Opening of the Biurakan Astrophysical Observatory of the Academy of Sciences of the Armenian SSR and the Conference on Nonstationary Stars, L. V. Mirzoian - 297.
Plenum of the Commission on the History of Astronomy, Iu. G. Perel' - 493.
Reporting and Coordinating Plenum of the Astronomical Council of the USSR Academy of Sciences, V. S. Safronov - 495.
Seventh Conference on Meteorites - 144.

Cosmic Rays
Electromagnetic Radiation by Cosmic-Ray Particles in the Galaxy, A. A. Korchak - 360.

Cosmogony and Cosmology
A Meeting of the Commission for Cosmogony Devoted to the Future Development of Work on Cosmology, A. Masevich - 306.

Crab Nebula
A New Catalog of Novae Recorded in the Chinese and Japanese Cronicles, Hsi Tse-Tsung - 161.
On the Nature of the Optical Emission from the Crab Nebula, I. S. Shklovskii - 690.
The Spectrum of the Crab Nebula, P. V. Shcheglov - 658.

Deuterium
A Spectroscopic Investigation of the Deuterium Dα Line in Active Regions on the Sun, A. B. Severnyi - 324.

Earth, Atmosphere
A Possible New Type of Fluorescence of the Earth's Atmosphere, I. S. Shklovskii - 130.
Variation of the Coefficient of Transparency of the Atmosphere During the Total Solar Eclipse of June 30, 1954, B. D. Fomenko - 841.

Earth, Magnetic Field
The Physical Nature of the Differences Between Geomagnetic Disturbances of Sudden and Nonsudden Commencement, E. R. Mustel' - 124.

Earth, Origin and Development
The Early Thermal History of the Earth, V. G. Fesenkov - 112.

Eclipse, Solar
Variation of the Coefficient of Transparency of the Atmosphere During the Total Solar Eclipse of June 30, 1954, B. D. Fomenko - 841.

Emission-Line Stars
On the Interpretation of the Emission Spectrum of Long-Period Variable Stars. I, V. G. Gorbatskii - 834.
Some Characteristics of Shells of Be Stars, A. A. Boiarchuk - 192.
Symposium on Bright-Line Stars Held in Liege (Belgium) July 8-10, 1957 - 929.

Envelopes, Stellar
Some Characteristics of Shells of Be Stars, A. A. Boiarchuk - 192.
The Diffusion of L_α Radiation in Nebulae and Stellar Envelopes, V. V. Sobolev - 678.

Ephemerides
Astronomical Ephemerides, D. H. Sadler - 255.

Extinction, Atmospheric
Variation of the Coefficient of Transparency of the Atmosphere During the Total Solar Eclipse of June 30, 1954, B. D. Fomenko - 841.

Flare Stars
On the International Cooperation for the Study of Flare Variable Stars, M. Petit - 783.

Galaxies
Statistical Mechanics of the Simplest Types of Galaxies, K. F. Ogorodnikov - 748.
The Morphology of Galaxies. III. Diffuse Matter in Spherical Stellar Systems, B. A. Vorontsov-Vel'iaminov - 9.
The Theory of the Fluctuations of the Observed Number of Galaxies, T. A. Agekian - 366.

Galaxy, The (Milky Way)
An Investigation of the Properties and Energy Dissipation of the Gaseous Galactic Corona, S. B. Pikel'ner and I. S. Shklovskii - 149.
On the Distribution of Mass in the Galaxy, A. M. Mikisha and F. A. Tsitsin - 45.

On the Paper by A. M. Mikisha and F. A. Tsitsin, Some Problems of the Theory of Galactic Potential, G. M. Idlis - 290.
The Distribution of Absorbing Matter and the Spiral Structure of the Galaxy, N. E. Kurochkin - 31.
The Inclination to the Galactic Equator of the General Magnetic Field of the Galaxy in the Solar Vicinity, G. A. Shain - 1.

Gas Dynamics
- An Investigation of the Properties and Energy Dissipation of the Gaseous Galactic Corona, S. B. Pikel'ner and I. S. Shklovskii - 149.
- Automodel Motion of a Gas with Spherical Symmetry in the Field of a Gravitating Center, M. L. Lidov - 588.
- Third Symposium on Cosmical Gas Dynamics, S. B. Pikel'ner - 773.
- The Gravitational Instability of a Gas Filament, E. A. Dibai - 920.

Geodesy
- Calculation of Latitude by the Method of M. V. Pevtsov, A. V. Butkevich - 610.
- The Determination of Azimuths at Laplace Points, B. I. Vlasov - 462.
- The Influence of Diurnal Aberration on the Accuracy of Determination of Latitude from Observations of Polaris, V. F. D'iakonov - 469.

Giant and Supergiant Stars
- The Determination of the Absolute Magnitudes of Cepheids and Supergiants and the Zero Point of the Period-Luminosity Relation, Iu. P. Pskovskii - 19.

Gravity and Gravimetry
- On the Errors of Interpolation and Representation in Detailed Gravimetric Surveys, the Accuracy of Charts, and the Best Distribution of Stations, N. P. Grushinskii - 260.
- The Fundamental Gravimetric Station at the P. K. Shternberg State Astronomical Institute (GAISh), N. P. Grushinskii - 455.

Hydrogen, Ionized; H II Regions
- Shock Waves in Interstellar Space. II. Ionization Discontinuities, S. A. Kaplan- 183.

Hydrogen, Lyman Series
- A Possible New Type of Fluorescence of the Earth's Atmosphere, I. S. Shklovskii - 130.
- The Diffusion of L_α Radiation in Nebulae and Stellar Envelopes, V. V. Sobolev - 678.

Image Converter
- High Voltage Sources for Supplying Image Converter Tubes, P. V. Shcheglov and V. G. Kurt - 474.
- Photographing Stars by Means of an Image Converter Tube, P. V. Shcheglov - 472.

Infrared, Observations in
- On the Observation of the Infrared Coronal Lines 10,747 and 10,798 A, M. N. Gnevyshev, R. S. Gnevysheva and V. G. Kurt - 654.
- Solar Limb Darkening at Wavelengths of 1-4μ, N. I. Kozhevnikov - 856.
- The Infrared Spectrum of the Northern Night Sky in the Region 9500-11,500 A, N. I. Fedorova - 241.

Instruments and Accessories
- A Bolometric Pyrheliometer for Absolute Measurements of Direct Solar Radiation, P. V. V'iushkov and E. A. Ridel' - 476.
- An Electric-Mechanical Computer for Determining the Mean Times of Stellar Transits During the Observations, V. G. Kruchinenko, Iu. P. Platonov and V. B. Sukhov - 594.
- Application of Silver Sulfide Photoelectric Cells with a Barrier Layer to Absolute Spectrophotometry and Pyrometry. I. Measuring Apparatus Using a Silver Sulfide Photocell, G. F. Sitnik - 416.
- Application of Silver Sulfide Photoelectric Cells with a Barrier Layer to Absolute Spectrophotometric and Pyrometric Measurements, G. F. Sitnik - 860.
- Astronomical Clock AChF-1 with Isochronous Pendulum, F. M. Fedchenko - 637.
- Changes in the Construction of the MF-2 Microphotometer Adapting it to Measurements of High Density, D. Ia. Martynov and V. Ia. Alduseva - 425.

International Geophysical Year (IGY)
- On the Observations of the Sun During the International Geophysical Year, V. A. Krat - 766.

Interstellar and Intergalactic Medium
- Electromagnetic Radiation by Cosmic-Ray Particles in the Galaxy, A. A. Korchak - 360.
- Energy Dissipation, Heating and Ionization in Interstellar Gas Due to Shock Waves, S. B. Pikel'ner - 310.
- Shock Waves in Interstellar Space. II. Ionization Discontinuities, S. A. Kaplan - 183.
- Shock Waves in Interstellar Space. III. Hydromagnetic Discontinuities, S. A. Kaplan - 317.
- The Morphology of Galaxies. III. Diffuse Matter in Spherical Stellar Systems, B. A. Vorontsov-Vel'iaminov - 9.

Ionosphere
- A Possible New Type of Fluorescence of the Earth's Atmosphere, I. S. Shklovskii - 130.

Latitude
- Calculation of Latitude by the Method of M. V. Pevtsov, A. V. Butkevich - 610.

Chardzhou International Latitude Station, V. P. Shcheglov - 648.
Remarks on the Article by V. F. D'iakonov Entitled "The Influence of Diurnal Aberration on the Accuracy of Determinations of Latitude from Observations of Polaris", A. A. Mikhailov - 918.
The Influence of Diurnal Aberration on the Accuracy of Determination of Latitude from Observations of Polaris, V. F. D'iakonov - 469.
Variations of the Mean Latitude of Poltava, Mizusawa, Richmond and Washington, E. I. Obrezkova - 445.

Letters to the Editor
A Note on the Paper "Luminosity Function for Stars of the Main Sequence and Its Interpretation" by A. G. Masevich, G. M. Nikol'skii - 479.
A Reply to G. M. Nikol'skii's Note, A. G. Masevich - 481.
On the Paper by A. M. Mikisha and F. A. Tsitsin, Some Problems of the Theory of Galactic Potential, G. M. Idlis - 290.

Local System
On the Kinematic Peculiarities of B Stars, A. Ia. Filin - 517.
The Inclination to the Galactic Equator of the General Magnetic Field of the Galaxy in the Solar Vicinity, G. A. Shain - 1.
The Kinematic Peculiarities of B Stars and the Rotation of the Local System, A. Ia. Filin - 812.

Luminosity Function
A Note on the Paper "Luminosity Function for Stars of the Main Sequence and Its Interpretation" by A. G. Masevich, G. M. Nikol'skii - 479.
A Reply to G. M. Nikol'skii's Note, A. G. Masevich - 481.
Open Stellar Cluster NGC 6811, K. A. Barkhatova - 201.

Magnetic Field, Interstellar
An Investigation of the Properties and Energy Dissipation of the Gaseous Galactic Corona, S. B. Pikel'ner and I. S. Shiklovskii - 149.
The Inclination to the Galactic Equator of the General Magnetic Field of the Galaxy in the Solar Vicinity, G. A. Shain - 1.

Magnetohydrodynamics
A Symposium on "Electromagnetic Phenomena in Cosmic Physics" in Stockholm on August 27-31, 1956, A. Kipper - 293.
Shock Waves in Interstellar Space. III. Hydromagnetic Discontinuities, S. A. Kaplan - 317.

Magnitudes, Absolute
The Determination of the Absolute Magnitudes of Cepheids and Supergiants and the Zero Point of the Period-Luminosity Relation, Iu. P. Pskovskii - 19.

Meteorites
Meteoritic Matter at the Place of Fall of the Tungus Meteorite, A. A. Iavnel'- 769.
Peculiarities of the Mineral Composition and Structure of Meteoritic Matter and the Origin of Meteorites, A. A. Iavnel' - 891.
Seventh Conference on Meteorites - 144.
The Characteristics of Chemical Composition of Meteoritic Matter and the Origin of Meteorites, A. A. Iavnel' - 435.

Meteors
Distribution of Meteoric Radio Echoes According to Their Duration, E. I. Fialko - 235.
On the Problem of Determining the Mass Distribution of Meteors, E. I. Fialko - 411.

Moon
A New Value of the Light Constant of the Moon, N. N. Sytinskaia - 870.

Navigation and Nautical Astronomy
The Influence of the Position Error of a Ship on the Astronomically Determinable Compass Correction, A. B. Marinbakh - 459.

Nebulae, Planetary
Conference on the Physics and the Origin of Planetary Nebulae, V. S. Safronov - 304.
Once More on the Distances to Planetary Nebulae and the Evolution of their Nuclei, I. S. Shklovskii - 397.
Planetary Ring Nebulae, G. A. Gurzadian - 796.
Photometry of the Images of Some Planetary Nebulae, Iu. K. Gulak - 508.
The Diffusion of L_α Radiation in Nebulae and Stellar Envelopes, V. V. Sobolev - 768.
The Spatial Structure of Some Planetary Nebulae, Iu. K. Gulak - 802.

Night Sky
On the Identification of the Emission of the Night Sky at About 5300 A, A. V. Mironov and V. S. Prokudina - 430.
The Infrared Spectrum of the Northern Night Sky in the Region 9500-11,500 A, N. I. Fedorova - 241.

Nonstable Stars
The Nonthermal Component of the Radiation of Unstable Stars and the Main Features of Their Spectra - 719.
Opening of the Biurakan Astrophysical Observatory of the Academy of Sciences of the Armenian SSR and the Conference on Nonstationary Stars, L. V. Mirzoian - 297.

Novae and Supernovae
  A New Catalog of Novae Recorded in the Chinese and Japanese Chronicles. Hsi Tse-Tsung - 161.
Observatories
  Opening of the Biurakan Astrophysical Observatory of the Academy of Sciences of the Armenian SSR and the Conference on Non-stationary Stars, L. V. Mirzoian - 297.
Optics
  On the Utilization of a Thin Lummer-Gehrke Plate, L. A. Fedin - 138.
Orbits, Theory and Computation
  On Some Peculiarities in the Motions of Comets, P. G. Dukhnovskii - 80.
  Some Methods of Plotting an Intermediate Orbit for Asteroids of the Trojan Group. I, Iu. A. Riabov - 268.
  Some Methods of Plotting an Intermediate Orbit for Asteroids of the Trojan Group. II, Iu. A. Riabov - 574.
Period-Luminosity Relation
  The Determination of the Absolute Magnitudes of Cepheids and Supergiants and the Zero Point of the Period-Luminosity Relation, Iu. P. Pskovskii - 19.
Photographic Process and Materials
  Increase of the Sensitivity of Some Photographic Emulsions by Means of Preliminary Short Exposure, T. M. Muliarchik and K. I. Petrova - 108.
Photometry, Photoelectric
  Application of Silver Sulfide Photoelectric Cells with a Barrier Layer to Absolute Spectrophotometry and Pyrometry. I. Measuring Apparatus Using a Silver Sulfide Photocell, G. F. Sitnik - 416.
  Application of Silver Sulfide Photoelectric Cells with a Barrier Layer to Absolute Spectrophotometry and Pyrometry. II. Method of Using FESS for Absolute Spectrophotometric and Pyrometric Measurements, G. F. Sitnik - 860.
Planets and Satellites, Observations
  On the Role of True Absorption in the Martian Atmosphere, V. V. Sharonov - 547.
  Photoelectric Photometry of Sections of the Surface of Mars, V. I. Moroz and A. V. Kharitonov - 874.
  Results of Photographic Observations of Mars at the Kharkov Astronomical Observatory During 1954, I. K. Koval' - 404.
  Tables of the Principal Planets, G. M. Clemence - 432.
  Three-Color Colorimetry of the Integral Brightness of Mars, Based on 1956 Observations, E. A. Gurtovenko, Sh. G. Gordeladze - 926.
Positions of Stars
  A Catalog of Right Ascensions of 203 Stars Based on Observations with a New Photoelectric Transit Instrument, P. M. Afanas'eva - 598.
  A New Method for Determining the Photographic Positions of Celestial Objects, Kh. I. Potter - 245.
Radiation and Energy Transport
  The Diffusion of L_α Radiation in Nebulae and Stellar Envelopes, V. V. Sobolev - 678.
  The Diffusion of Radiation in a Medium of Finite Optical Thickness, V. V. Sobolev - 332.
Radio Astronomy, Discrete Sources
  Radio Stars and the Methods of Their Investigation, V. V. Vitkevich - 346.
Radio Astronomy, Meteors
  Distribution of Meteoric Radio Echoes According to their Duration, E. I. Fialko - 235.
  Effective Scattering Cross Section of a Weakened Meteor Trial, F. I. Peregudov - 606.
  On the Problem of Determining the Mass Distribution of Meteors, E. I. Fialko - 411.
Radio Astronomy, Sun
  A Model of the Inner Corona Based on Radio Data, B. N. Panovkin - 497.
  Investigation of the Solar Supercorona by the Reception of the Radio Emission from Jupiter, V. V. Vitkevich - 214.
  On the Radio Emission of Coronal Condensations, V. V. Vitkevich and M. I. Sigal - 698.
Radio Telescopes
  Radio Stars and the Methods of their Investigation, V. V. Vitkevich - 346.
Rotation, Stellar
  Some Characteristics of Shells of Be Stars, A. A. Boiarchuk - 192.
Seeing and Scintillation
  Some Results of Observations of the Vibration of Images of Stars at the Main Astronomical Observatory of the Academy of Sciences of the Ukrainian SSR at Goloseevo, I. G. Kolchinskii - 624.
Shock Waves
  Energy Dissipation, Heating and Ionization in Interstellar Gas Due to Shock Waves, S. B. Pikel'ner - 310.
  Shock Waves in Interstellar Space. III. Hydromagnetic Discontinuities, S. A. Kaplan - 317.
  Shock Waves in Interstellar Space. II. Ionization Discontinuities, S. A. Kaplan - 183.
Solar System, Origin and Development
  The Early Thermal History of the Earth, V. G. Fesenkov - 112.

Solar-Terrestrial Relationships
- A Bolometric Pyrheliometer for Absolute Measurements of Direct Solar Radiation, P. V. V'iushkov and E. A. Ridel' - 476.
- The Physical Nature of the Differences Between Geomagnetic Disturbances of Sudden and Nonsudden Commencement, E. R. Mustel' - 124.

Spectrophotometry
- Application of Silver Sulfide Photoelectric Cells with a Barrier Layer to Absolute Spectrophotometry and Pyrometry. I. Measuring Apparatus Using a Silver Sulfide Photocell, G. F. Sitnik - 416.
- Application of Silver Sulfide Photoelectric Cells with a Barrier Layer to Absolute Spectrophotometry and Pyrometry. II. Method of Using FESS for Absolute Spectrophotometric and Pyrometric Measurements, G. F. Sitnik - 860.

Spectrum, Line Identification
- On the Identification of the Emission of the Night Sky at About 5300A, A. V. Mironov and V. S. Prokudina - 430.
- The Infrared Spectrum of the Northern Night Sky in the Region 9500-11,500 A, N. I. Fedorova - 241.

Stars, Distribution in Space
- A Numerical Method for Determining the Stellar Density in a Spheroidal Cluster, A. S. Sharov - 142.
- The Theory of the Fluctuations of the Observed Number of Galaxies, T. A. Agekian - 366.

Stars, Motion in Space
- On the Kinematic Peculiarities of B Stars, A. Ia. Filin - 517.
- The Kinematic Peculiarities of B Stars and the Rotation of the Local System, A. Ia. Filin - 812.

Stars, Structure and Evolution
- An Investigation of Evolutionary Paths of a Homogeneous Stellar Model with a Convective Core, G. Ruben and A. Masevich - 705.
- On the Evolutionary Interpretation of the Main Sequence of Stars, G. M. Idlis - 733.
- The Evolution of Stars in the X and h Persei Double Cluster, A. G. Masevich - 177.

Stellar Systems, Dynamics
- On the Principles of Statistical Mechanics of Stellar Systems, K. F. Ogorodnikov - 787.
- Statistical Mechanics of the Simplest Types of Galaxies, K. F. Ogorodnikov - 748.
- The Virial Theorem as Applied to the Dynamics of Stellar Systems, A. M. Mikisha and F. A. Tsitsin - 661.

Sun, Corona
- A Model of the Inner Corona Based on Radio Data, B. N. Panovkin - 497.
- Coronal Streamers, E. Ia. Bugoslavskaia - 228.
- Investigation of the Solar Supercorona by the Reception of the Radio Emission from Jupiter, V. V. Vitkevich - 214.
- On the Observation of the Infrared Coronal Lines 10,747 and 10,798 A, M. N. Gnevyshev, R. S. Gnevysheva and V. G. Kurt - 654.
- On the Radio Emission of Coronal Condensations, V. V. Vitkevich and M. I. Sigal - 698.
- The Distribution of Matter in the Polar Rays of the Solar Corona, N. I. Dziubenko - 373.

Sun, Flares
- Some Results of Investigations of Nonstationary Processes on the Sun, A. B. Severnyi - 668.

Sun, Magnetic Fields
- A Symposium on "Electromagnetic Phenomena in Cosmic Physics" in Stockholm on August 27-31, 1956, A. Kipper - 293.
- On the Acceleration of Charged Particles in the Electromagnetic Field of Sunspots, P. E. Kolpakov - 218.

Sun, Photosphere
- Solar Limb Darkening at Wavelengths of 1-4μ, N. I. Kozhevnikov - 856.

Sun, Radio Emission
- On the Radio Emission of Coronal Condensations, V. V. Vitkevich and M. I. Sigal - 698.

Sun, Spectrum
- A Photometric Investigation of the Energy Distribution in the Continuous Solar Spectrum in Absolute Units, E. A. Makarova - 531.
- A Spectroscopic Investigation of the Deuterium Dα Line in Active Regions on the Sun, A. B. Severnyi - 324.

Sunspots
- On One Classification of the Cycles of Sunspots and Faculae, J. Xanthakis - 385.
- On the Acceleration of Charged Particles in the Electromagnetic Field of Sunspots, P. E. Kolpakov - 218.

Symposia
- A Symposium on "Electromagnetic Phenomena in Cosmic Physics" in Stockholm on August 27-31, 1956, A. Kipper - 293.
- Symposium on Bright-Line Stars Held in Liège (Belgium) July 8-10, 1957 - 929.
- Third Symposium on Cosmical Gas Dynamics, S. B. Pikel'ner - 773.

Synchrotron Radiation
- On the Nature of the Optical Emission from the Crab Nebula, I. S. Shklovskii - 690.

Transit Instrument

- A Catalog of Right Ascensions of 203 Stars Based on Observations with a New Photoelectric Transit Instrument, P. M. Afanas'eva - 598.
- The Collimation of a Transit Instrument, G. P. Pil'nik - 103.

Variable Stars

- Color Excesses in 102 RR Lyrae Stars, I. F. Alaniia - 205.
- On the International Cooperation for the Study of Flare Variable Stars, M. Petit - 783.
- On the Interpretation of the Emission Spectrum of Long-period Variable Stars, I, V. G. Gorbatskii - 834.
- The Determination of the Absolute Magnitudes of Cepheids and Supergiants and the Zero Point of the Period-Luminosity Relation, Iu. P. Pskovskii - 19.
- The Periods of Short-Period Cepheids in the Direction of the Galactic Center, E. D. Pavlovskaia - 923.

Solar Terrestrial Studies

[illegible] Experiment for Studying Electron Concentration [illegible] - [illegible]

[illegible]

Spectrophotometry

[illegible]

Stars, [illegible]

[illegible]

Stars, [illegible]

[illegible]

Sun, Corona

Transit Instrument

A Catalog of Light Absorption of the Star Field on Observation with a [illegible] Transit Instrument, [illegible] - [illegible]

The Calibration of [illegible] Transit Instrument, [illegible] - [illegible]

Variable Stars

Color Excesses in [illegible] - [illegible]

On the International Comparison [illegible] of Light Variable Stars, [illegible] - [illegible]

On the Determination of the Number of [illegible] - [illegible]

The [illegible] of the Absolute Magnitudes [illegible] of the Period-Luminosity Relation, [illegible] P. Parenago - [illegible]

The Problem of [illegible] Parenago - [illegible]

[illegible]

Sun, Photosphere

[illegible]

Sun, Radio Emission

[illegible]

Sun, Spots

[illegible]

SOVIET ASTRONOMY – AJ

(Translation of the Astronomical Journal of the USSR, Vol. 34, No. 6,
published by the American Institute of Physics, April 1959)

Volume 1, Number 6 November-December 1957

CONTENTS

	PAGE	RUSS. PAGE
On the Principles of Statistical Mechanics of Stellar Systems. K. F. Ogorodnikov	787	809
Planetary Ring Nebulae. G. A. Gurzadian..........................	796	820
The Spatial Structure of Some Planetary Nebulae. Iu. K. Gulak	802	827
The Kinematic Peculiarities of B Stars and the Rotation of the Local System. A. Ia. Filin..	812	838
The Open Stellar Clusters NGC 6823 and NGC 6830. K. A. Barkhatova	822	848
On the Interpretation of the Emission Spectrum of Long-Period Variable Stars. I. V. G. Gorbatskii	834	860
Variation of the Coefficient of Transparency of the Atmosphere During the Total Solar Eclipse of June 30, 1954. B. D. Fomenko	841	868
Solar Limb Darkening at Wavelengths of 1-4 μ. N. I. Kozhevnikov	856	883
Spectrophotometry and Pyrometry. II. Method of Using SSBL for Absolute Spectrophotometric and Pyrometric Measurements. G. F. Sitnik....................	860	887
A New Value of the Light Constant of the Moon. N. N. Sytinskaia................	870	899
Photoelectric Photometry of Sections of the Surface of Mars. V. I. Moroz and A. V. Kharitonov..	874	903
Peculiarities of the Mineral Composition and Structure of Meteoritic Matter and the Origin of Meteorites. A. A. Iavnel'.........................	891	921
A Supplement to the General Catalogue of Absolute Brightnesses of Comets. Comets of 1947-1954. T. V. Vodop'ianova	900	932
A Special Case of the General Three-Body Problem. M. A. Dirikis	909	943

Brief Communications

	PAGE	RUSS. PAGE
Remarks on the Article by V. F. D'iakonov Entitled "The Influence of Diurnal Aberration on the Accuracy of Determinations of Latitude from Observations of Polaris" A.A.Mikhailov	918	952
The Gravitational Instability of a Gas Filament. E. A. Dibai	920	954
The Periods of Short-Period Cepheids in the Direction of the Galactic Center. E. D. Pavlovskaia	923	956
Three-Color Colorimetry of the Integral Brightness of Mars, Based on 1956 Observations. E. A. Gurtovenko, Sh. G. Gordeladze..........................	926	959

Chronicle

	PAGE	RUSS. PAGE
Symposium on Bright-Line Stars Held in Liege (Belgium). July 8-10, 1957............	929	962
Index for Volume I	935	

SIGNIFICANCE OF ABBREVIATIONS MOST FREQUENTLY ENCOUNTERED IN SOVIET ASTRONOMY PERIODICALS

AN SSSR	*Academy of Sciences, USSR*
FIAN	*Physics Institute, Academy of Sciences USSR*
GAFI	*State Astrophysical Institute*
GAISh	*P. K. Shternberg State Institute of Astronomy*
GAO	*Main Astronomical Observatory*
Gidrometizdat	*Hydrometeorological Press*
GITI	*State Scientific and Technical Press*
GITTL	*State Press for Technical and Theoretical Literature*
GOI	*State Optical Institute*
GONTI	*State United Scientific and Technical Press*
Gosfizkhimizdat	*State Physical Chemistry Press*
GOST	*All-Union State Standard*
Goztekhizdat	*State Technical Press*
GTTI	*State Technical and Theoretical Press*
IF KhI	*Institute of Physical Chemistry Research*
IFP	*Institute of Physical Problems*
IL	*Foreign Literature Press*
IPF	*Institute of Applied Physics*
IPM	*Institute of Applied Mathematics*
ISN (Izd. Sov. Nauk)	*Soviet Science Press*
IIaP	*Institute of Nuclear Studies*
Izd	*Press (publishing house)*
KISO	*Solar Research Commission*
LFTI	*Leningrad Institute of Physics and Technology*
LIM	*Leningrad Institute of Metals*
LITMiO	*Leningrad Institute of Precision Instruments and Optics*
Mashgiz	*State Scientific-Technical Press for Machine Construction Literature*
MATI	*Moscow Aviation Technology Institute*
MGU	*Moscow State University*
Metallurgizdat	*Metallurgy Press*
MOPI	*Moscow Regional Pedagogical Institute*
NIAFIZ	*Scientific Research Association for Physics*
NIFI	*Scientific Research Institute of Physics*
NIIMM	*Scientific Research Institute of Mathematics and Mechanics*
NII ZVUKSZAPIOI	*Scientific Research Institute of Sound Recording*
NIKFI	*Scientific Institute of Motion Picture Photography*
OIIaI	*Joint Institute of Nuclear Studies*
ONTI	*United Scientific and Technical Press*
OTI	*Division of Technical Information*
OTN	*Division of Technical Science*
RIAN	*Radium Institute, Academy of Sciences of the USSR*
Ts NIIGAiK	*Central Scientific Research Institute of Geodetics, Aerial Survey, and Cartography*
URALFTI	*Ural Institute of Physics and Technology*
VAGO	*All-Union Astronomic and Geodetic Society*
VNIIM	*All-Union Scientific Research Institute of Meteorology*

NOTE: Abbreviations not on this list and not explained in the translation have been transliterated, no further information about their significance being available to us.—*Publisher.*

The expanded program of the American Institute of Physics comprises translation of six leading Soviet physics journals, as listed below. These translations, by competent, qualified scientists, provide all research laboratories and libraries with accurate and up-to-date information of the results of research in the U.S.S.R.

Soviet Physics—Technical Physics

A translation of the "Journal of Technical Physics" of the Academy of Sciences of the U.S.S.R. The translation began with the 1956 issues. Twelve issues per year, approximately 3,000 Russian pages. Annually $75.00 domestic, $79.00 foreign. Libraries* $35.00 domestic, $39.00 foreign. Back numbers, all issues $8.00.

Soviet Physics—Acoustics

A translation of the "Journal of Acoustics" of the Academy of Sciences of the U.S.S.R. The translation began with the 1955 issues. Four issues per year, approximately 400 Russian pages. Annually $12.00 domestic, $14.00 foreign. (No library discounts.) Back numbers, all issues $4.00.

Soviet Physics—Doklady

A translation of all of the "Physics Sections" of the Proceedings of the Academy of Sciences of the U.S.S.R. The translation began with the 1956 issues. Six issues per year, approximately 1,500 Russian pages. Annually $35.00 domestic, $38.00 foreign. Libraries* $15.00 domestic, $18.00 foreign. Back numbers for Volumes 1 and 2, $5.00 per issue; Volume 3 and subsequent, $7.00 per issue.

Soviet Physics—JETP

A translation of the "Journal of Experimental and Theoretical Physics" of the Academy of Sciences of the U.S.S.R. The translation began with the 1955 issues. Twelve issues per year, approximately 4,000 Russian pages. Annually $75.00 domestic, $79.00 foreign. Libraries* $35.00 domestic, $39.00 foreign. Back numbers, all issues $8.00.

Soviet Physics—Crystallography

A translation of the journal "Crystallography" of the Academy of Sciences of the U.S.S.R. The translation began with the 1957 issues. Six issues per year, approximately 1,000 Russian pages. Annually $25.00 domestic, $27.00 foreign. Libraries* $10.00 domestic, $12.00 foreign. Back numbers, all issues $5.00.

Soviet Astronomy—AJ

A translation of the "Astronomical Journal" of the Academy of Sciences of the U.S.S.R. The translation began with the 1957 issues. Six issues per year, approximately 1,100 Russian pages. Annually $25.00 domestic, $27.00 foreign. Libraries* $10.00 domestic. $12.00 foreign. Back numbers, all issues $5.00.

Subscriptions should be addressed to the American Institute of Physics. 335 East 45th Street. New York 17. N. Y.

---

* For libraries of non-profit academic institutions.